Methods and limitations in defect chemistry modelling

Poulsen, Finn Willy

Publication date:
2007

Document Version
Publisher's PDF, also known as Version of record

Risø-R-1590(EN)

Methods and Limitations in Defect Chemistry Modelling

Finn Willy Poulsen

Fuel Cells and Solid State Chemistry Department
(formerly part of Materials Research Department)
Risø National Laboratory, DTU, Roskilde, Denmark
April 2007

Denne afhandling er af Danmarks Tekniske Universitet antaget til forsvar for den tekniske doktorgrad. Antagelsen er sket efter bedømmelse af den foreliggende afhandling.

Kgs. Lyngby, den 18. januar 2007

Lars Pallesen
Rektor

/Kristian Stubkjær
Forskningsdekan

This thesis has been accepted by the Technical University of Denmark for public defence in fulfilment of the requirements for the degree of Doctor Technices. The acceptance is based on this dissertation.

Kgs. Lyngby, 18 January 2007

Lars Pallesen
Rector

/Kristian Stubkjær
Dean of Research

ISBN 978-87-550-3576-8
ISSN 0106-2840
Risø-R-1590(EN)
Electronic version of thesis can be downloaded from
http://www.risoe.dk/rispubl/reports/ris-r-1590.pdf

Schultz Grafisk, April 2007

List of content 3

ERRATA

Methods and Limitations in Defect Chemistry Modelling
By Finn Willy Poulsen
April 2007
ISBN 978-87-550-3576-8

General comments

During conversion of text to the thesis format A5S subscripts and superscripts written with a small font often have lost a "-" = "minus" in chemical formulas and in exponents of 10, i.e. where a low pO_2 value is given.
Text written in *italics* below are the new text replacing the old erratic ones.

Page#

8 paragraph 3) replace ref. to paper A2 by paper *A3*.
12 and 65: Reference to paper A161 is wrong. Paper on a new oxyhydride NdHO is being finalised by *Wiederøe, Poulsen, Fjällvåg and Berg 2007.*
15 line 10 :… Sc have shown *different populations on the O1 and O2 sites.*
39 last line, delete "but".
49 paragraph 6.3 line 3: *five* oxidation states (not four).
53 next to last line: The point *defect* model …..
55 last line: constants, out *of* the two …..
57 third to last line: distinguish between the penta- or hexavalent U model- *actually the numerical solution for U = +5.5 i.e. p =1.5 is better…..*
64 line 9: see eq 7.6 etc… replace by *Table 7.3*
65 ref A161, 2005: see comment to page 12 and 65
66 line 8 from bottom, replace (Glerup, 2002) by *A144*
93 Corrections equation (3): replace K_U by $1/K_U$. Line 6 from bottom remove soft left side bracket in K_U /([U_A…. K_U /[U_A…. In equation (5) use $U_A^{\bullet p}$ as U-variable
95 equation in line 8: bracket with (8/3) should read *(3/8)*
97 line 8: Insert *Donor* doped Ba-titanates
99 Since the titanate can exolute Sr, whereby the A/B ratio in the perovskite will be <1, one should write the Sr content as $Sr_{1-\varepsilon}$ …… and not as Sr_{1-y}
A1 p 566 next to last line: Seebeck coefficient *decreases* with decreasing oxygen partial pressure
P 567 next to last paragraph: slang 1/4 and –1/4 slopes talked about without specifying logarithmic axes.
A3 p116 Table 1: Negative charge missing on Y**'**.
P119 Figure caption 1 and 2: $K_i = \boldsymbol{10^{-11}}$.
A5 p151 and Figure 2: minuses in exponents are missing.
A6 p1833 last paragraph before section 4 Conclusions. It is unclear how the uncertainty here Combine with the certainty of data, model and conclusion of Figure 7.
A7 missing minus in supercripts
A8 p 388 missing minus in 10^{-5} *Å*.

A bit of history

Brief introduction to non-stoichiometric oxides and defects in solids

To perceive chemical compounds as being stoichiometric[1], is a main message of the Daltonian atomic theory (John Dalton, 1808)[2]. Dalton and first-year chemistry courses teach that the molar ratios of the elements' in compounds can only adopt discrete values, which can be deduced from the elements position in the periodic table. Molecules obey this rule- but it is now realised that solids seldom do, i.e. the ratio between the molar content of the elements in the solid can vary continuously in a range and adopt rational and irrational values. The real world is therefore defective. The defect chemistry issues treated in the present thesis reflect important phenomena in the real world: why and how metals corrode (Hansson, 2004), the function of chemical sensors, diffusion and intercalation in battery materials and electrochromics (A59,1992), why solid oxide fuel cells, SOFC's, (Möbius,1997) and SOEC electrolysers work or don't work and so forth. The concepts and methods of defect chemistry are also finding their way into heterogeneous catalysis and in explaining the oxygen stoichiometry in H_{TC} ceramic superconductors. These and future technologies based on oxygen- and hydrogen separation membranes (A115, A120, A121, A126, A135) can be analysed and often explained by solid-state defect chemistry concepts. Very little will be said about these practical aspects in the remainder of the thesis– sufficient number of reviews are available. Most cases discussed in the submitted papers A1-A10, and in the bulk text of the thesis are, nonetheless, oxides of relevance to the SOFC-technology, since the author has spent more than 18 years on these materials. But the specific materials properties as such, are not the issue here. The subject of the thesis is targeted on defect chemistry modelling as a discipline, and its foundations and limitations are scrutinized.

The defect chemistry methods and their limitations are of course equally applicable to nitrides, halides, carbides, sulphides etc. Areas I have not explored. For my self and others the present thesis may serve as the first few paragraphs of the not yet written book "A Hitchhikers guide to defect space".

A few cornerstones in the development of solid state defect chemistry will be quoted. For a thorough review consult (Schmalzried, 2004) " Advent of solid-state thermodynamics, kinetics and electrochemistry in the 20th century". Werner Nernst noticed in 1899 that a DC current could be passed through a redhot ceramic rod containing zirconium oxide, later on called "Nernst mass", and the heating and light emission continued as long as the current was passed. Nernst himself believed that the current was carried by metal ions, (Nernst, 1899). Ascribing the movement to oxygen ions or oxygen ion vacancies, $V_O^{\bullet\bullet}$, was discussed much later by Carl Wagner in his classical paper " Über den Mechanismus der elektrischen Stromleitung in Nernststift " (Wagner, 1943). The birth of the oxygen ion vacancy possibly dates further to back to 1939 in the work of Zintl and Croatto on solid solutions of CeO_2 and La_2O_3, where the concept of "Leerstellen im Sauerstoffionenteilgitter"[3] was introduced (Zintl, 1939). However it was not until the x-ray and density study of

[1] From Greek *"stoicheioin" = component* and *"metria" = process of measuring*
[2] 1766 - †1844.
[3] Empty places in the oxygen-ion sublattice

Hund that the final direct proof[4] of vacant oxygen sites in the lattice of YSZ was presented (Hund, 1951). Cation vacancies and interstitial metal ions, $V_{Ag}^{|}$ and $Ag_i^{\bullet}$, were suggested the major defects in AgBr by Yakov Ilich Frenkel (Frenkel, 1926).

The Schottky mechanism for simultaneous formation of defects on both the cation and anion sublattices[5] was advanced in 1930 by Wagner and Schottky (Wagner, 1930). Werner Heisenberg was probably the first to treat an electron missing in the valence band in solids as a virtual particle, an electron hole (Heisenberg, 1931). Holstein described localisation of excess or deficit electronic charge on specific ions, associated with a local disturbance of the lattice as a "small polaron" (Holstein,1959). The polaron movement is assisted by the phonons of the lattice leading to a temperature activated "hopping". According to Chambers small and large polarons may co-exist in solids, and their contribution to collective properties such as the conductivity and Seebeck effect is obtained using transport numbers as weighing factors (Chambers,1952; A75).

The two foremost tools, still in use in defect chemistry, were developed 50 years ago: i) the Brouwer approximation technique for predicting concentration versus chemical activity (partial pressure of gas) relationships (Brouwer, 1954) and ii) the Kröger-Vink notation, which provides a unique description of a chemical species, and where it is located in the crystal lattice (Kröger,Vink, 1956).

Several textbooks address the topic of defect chemistry and non-stoichiometry, many of them emphasising oxides, cf. (Kofstad,1972), (Kröger,1974), (Sørensen, 1981), (Kosuge, 1994). Smyth's monograph mostly deals with halides in spite of the title (Smyth, 2000). These books all teach the Brouwer-approximation technique, but with no mentioning of how one in practice would determine the precise concentrations at equilibrium by analytical or numerical methods. The Brouwer-approach has definitely pedagogical qualities, since it forces the user to distinguish between important species and less important ones, i.e. those of insignificant concentration are omitted from the electroneutrality condition. Software packages for solving sets of defect equations do exist. Schober and Wenzl (1995) used the SEQS code, from CET, Norman Oklahoma, to model proton uptake in perovskites. In mineralogy, homemade software has been in use, possibly even earlier than this (Hirsch, 1991), though is has not spread to the solid state ionics academia. Completely new software packages will soon be available from T. Norby[6], Oslo University and J. Abrantes[7] in Portugal. While the latter number-crunching algorithms lack the clarity of the Brouwer-approach, they will eventually dominate defect chemistry science and teaching in a few years time. The sequential way of solving the set of defect equations from a given model, as described in the present thesis and the submitted papers, has virtues, but also inherent drawbacks of both worlds: the operator has to do some initial thinking and algebraic manipulations, before the non-linear set of equations yield and lead to an exact numerical solution; furthermore – there is no guaranty that a route leading to a solution can be found, e.g. see paper A8; but in most of the cases, where a route once has indeed been found, one will have a very fast algorithm at hand, which needs nothing more than a spreadsheet program to produce correct and instant Brouwer-diagrams.

---

[4] Allowing to discriminate between substitutional versus interstitial solution of dopant.
[5] Correctly speaking a crystal structure is described by only one lattice.
[6] Truls Norby [t.e.norby@kjemi.uio.no]
[7] DefChem program; João C.C. Abrantes [jabrantes@estg.ipvc.pt]

Acknowledgements

My employment at Risø National Laboratory since March 1978 resulted from the Materials Research Departments role in Danish energy research programmes supported by Handelsministeriet, later on by Energiministeriet /Energistyrelsen, EU, the Nordic Energy program, and the Japanese NEDO. These projects had well defined goals related to advanced batteries and fuel cells. Several of the early research projects dealing with solid electrolytes for all solid state Li-batteries, tape casting of zirconia for solid oxide fuel cells (SOFC), and a CEC-project on stress measurements in SOFC components by neutron diffraction were cast by myself. All the projects were in a pre-competitive stage, and relied much on innovation, i.e. fabrication of new materials by new techniques and implementation of characterisation methods for these materials by (at least to us) "new" methods. A large degree of academic freedom was at hand in the past. I am grateful in this respect to the heads of the Materials Research Department at Risø, Dr. techn. Niels Hansen, Robert Feidenhansl´ and Allan Schrøder Pedersen for letting me play the role of a *libero* in many of these energy research projects.

In my daily work I have benefited from constructive collaboration with several local colleagues. I mention the important ones: Erik O. Ahlgren, Janet J. Bentzen, Marianne Glerup, Jesper Rømer Hansen, Shin-ichi Hashimoto, Knud Jensen, Bruno Kindl, Jørgen Kjems, Dorthe Lybye, Kjeld Larsen, Bjørn Malmgren-Hansen, Peter Vang Hendriksen, Mogens Mogensen, Henrik Paulsen, Henning Friis Poulsen, Jens Ranløv, Torben Strauss, Martin Søgård, and Ole Toft Sørensen. All the co-authors of the submitted papers A1-A10 are thanked for excellent collaboration. Two scientists at Risø have made an effort to influence me in the past. Niels Hessel Andersen tried in vain, in our younger days, to make me adopt a solid state *physicists* approach to problems, which I felt were better treated by solid state *chemistry* concepts. In later years Nicholas Bonanos has tried to teach me how to think, measure and analyse systematically. When it came to understanding fundamental issues of physico-chemical nature, I appreciated learning from my colleagues at the Danish universities and Reader John R. Owen, University of Southampton.

Starting December 1991, I acted for a 1½ year as Nordic research professor under the Energy Research Programme for Fuel Cells. The NEFP-programme, sponsored by Nordisk Ministerråd (Council of the Nordic Ministers), is thanked for giving me that opportunity. The interaction with the research groups under late Per Kofstad and his successor Truls Norby at the University of Oslo, and Kjell Wiik, Reidar Tunold and Kemal Nisancioglu at NTNU in Trondheim amplified my thinking. The sequential way of solving defect equations was actually conceived during my stay at NTNU. Notably, on the ski slopes in Bymarka, where I hesitated to get close to anything like " steepest descend" methods.

Finally, I thank my wife Anne-Britt Foosnæs, my daughters Eva Louise and Ida Maria, and colleagues and friends in Denmark, Norway and elsewhere. Perpetually, they have reminded me about my commitment to finish at least one major enterprise, the present thesis, before I got too old. Keld West and N. Bonanos are thanked for valuable comments on the manuscript.

Virum, July 2005

1. Subject and layout of the thesis

1.1 Subject

The thesis concerns the purposes, means and several limitations encountered in defect chemistry modelling (simulation). This discipline is frequently exercised in solid state (high temperature) chemistry, catalysis, photochemistry and semiconductor science. More specifically the thesis will address six problems:

1) Purpose and limitations in defect chemistry modelling: What should a defect model explain? How is a model defined? What a defect model can possibly not explain/concern.

2) Where and why does the Brouwer approximation technique fail? Brouwer's first diagram for Ga^{3+} doped CdS is recalculated by the sequential method. (Brouwer, 1954).

3) How we can solve the set of non-linear equations in concentrations arising from a "chemical equilibrium description" for a given defect model. A surprisingly simple, though efficient and transparent algorithm was developed by the author starting April 1992. This numerical approach was demonstrated in the submitted papers A1,2,5,7-10 and also applied in the authors papers A63, A99, A104, A109, A113, A122, A145. Other numerical recipes are briefly listed.

4) Why ideal-mixture behaviour apparently apply very often. In the ideal approach we equate the thermodynamic activity a_i of a host ion/ionic defect/vacancy/electron *i*, with a measure of the molar content, $a_i = [i]$ in mass action law expressions.

5) Three ways of treating apparent deviations from ideality are dealt with: i) the regular solution model; ii) introduction of activity coefficients in mass action law expressions; and iii) thirdly expansion of defect models by adding more species and equilibria.

6) Coincidental resemblance of two or more defect models. Large versus small polaron descriptions, association reactions and protonic defects are dealt with.

The models to be discussed and tested are considered at constant temperature, and with the partial pressure of oxygen, or partial pressure of water or dopant concentration as variable. This is necessarily the first task in any defect modelling. In a next phase, not treated in this dissertation, comes testing and verification of models on data obtained at several temperatures. In order to deconvolute the temperature dependence of the total electrical conductivity into contributions from i) bulk – and grain-boundary effects, and ii) majority and minority carriers, one needs to carry out a

vast number of transport number and Seebeck coefficient measurements, as for instance done by the group of Norby (Norby,2004; Widerøe,2004; Stensvik,2001).

1.2 Outline of the thesis

Before writing this thesis several choices as to the style, message and depth of argumentation were considered. Starting with a completely virgin canvas- it was not easy to forecast how the final painting came out- and if it would sell. During the writing it became clear that the main message turned out quite pessimistic, in the sense that I happened to demonstrate that little can be proven,- that several models may describe the same experimental data, - that others may have over-interpreted their data and so forth. The title and message of the thesis therefore changed gradually underway – from an optimistic sort of "A universal procedure for solving defect equilibria….." , via more modest versions – into the present quite conservative one.

Readers, who are not familiar with defect chemistry should stop here and read paragraph 2.1 and papers A2-A5 first. Papers A3 and A5, and any of Appendices 1,2,3 or 5 should also be read by scholars, who are not familiar with the authors way of solving sets of defect equations[8]. Paragraphs 4.1 and 4.2 should be accessible to readers with a general understanding of chemical equilibria.

At a first glance, the dissertation looks quite theoretical. It is not. The mathematics is simple, when attacked by the authors method. The main hurdle to non-solid state chemists will be the use of the Kröger-Vink nomenclature for the defect species. An additional confusion may arise when handling the schism between a chemical description- here called the small polaron model- or the physicist delocalised electron or electron hole description, cf. the discussion in paragraph 7.3.

Items no. 1 to 6, listed under 1.1, are dealt with chapter by chapter. A number of statements are presented in the form of *conjectures*, i.e. a full mathematical proof is usually not presented- either because the postulate is evident- alternatively too difficult- or at present seemingly impossible to prove for the author- as well as for others? Descriptions of four, not yet published defect models, each having an additional new feature and their algorithms are presented in Appendices 1,2,3 and 5.

It is attempted to arrive at conclusion(s) at the end of each chapter, but several chapters/discussions are left open. This is especially true for the discussion of association equilibria in reduced Ceria in paragraph 6.3. A procedure for handling five different types of defect associates has been established and is presented in App. 5, but it is not put into use in the present thesis due to the uncertainty of the data.

A summary of the submitted papers A1-A10 is given in paragraph 1.3. Since it is only since 1999 that the more essential papers A3, A5 and A8 appeared in the literature, relatively few references to these papers, and applications made by others have appeared so far in the open literature. Specific cases, where other researchers have used or expanded a sequential method[9], are cited in paragraph 4.3. This includes one instance of an independent suggestion of a sequential like method (Spinolo,1995).

---

[8] The author has coined the name "sequential method" out of lack of mathematical knowledge.
[9] Song et al. were so kind as to employ the name " Poulsen's method" in (Song,2003).

The reference list is split in two: Part 1 gives publications of the author *not* submitted with this thesis,- these are written as A11- etc.; Part 2 gives references used in the body text. The author has taken the liberty, for brevity, not list all author names, when referencing the papers in the bulk of the text.

Finally the papers A1-A10 are included as reprints.

1.3 Summary of the submitted papers A1-A10

A1. A. Holt, E.O. Ahlgren and F.W. Poulsen,
Synthesis, electrical properties and defect chemistry of Ti-doped $NdCrO_3$,
Proc. 3rd Int. Symp. Solid Oxide Fuel Cells, (Eds. S.C. Singhal and H. Iwahara), Honolulu, USA, May 16-21, 1993. Proc. vol. **93-4,** 562-571. (1993)

Paper A1 is the first presentation in the open literature of the use of the sequential mathematical method for solving a chemical defect system, in the present case a set of nine equations (6 linear + 3 nonlinear). The algorithm was not shown explicitly in the paper. Simulated concentration curves were calculated by a GWBASIC code, approximately 1½ A4 page long, similar to the one shown in Figure 4.2. The title compounds, $NdCr_{1-x}Ti_xO_3$ display many properties typical of non-stoichiometric perovskite oxides, including a shift from p-type to n-type majority carrier conduction around 10^{-6} atm. of oxygen.

A2. F.W.Poulsen, G. Ø. Lauvstad and R. Tunold,
Conductivity and Seebeck measurements on strontium ferrates.
Solid State Ionics **72,** 47-53. (1994)

The slope of logσ versus log pO_2 at low pO_2 $-1/6$, and $\approx 1/4$ at high pO_2 are rationalized via a conventional defect chemistry model. The stoichiometry will saturate at $[O_{tot}]/[Fe] = 3$ at high pO_2. This is taken into account in the mass action law for equilibration with O_2. A cubic equation in the hole concentration is obtained, which fits well with the observations.

A3. F.W. Poulsen,
Method for calculating ionic and electronic defect concentrations in proton containing perovskites. J. Solid State Chem. **143**, 115-121. (1999)

Paper A3 is the first example of how to solve defect equations for an oxygen non-stoichiometric perovskite, archetype of $SrCeO_3$, which can accommodate protons in the structure. The protonic defects are described as sitting on a lattice oxygen, $OH_O^{\bullet}$. The defect description includes a Schottky equilibrium: $nil = V_A^{||} + V_B^{||||} + 3\ V_O^{\bullet\bullet}$. The solid is in equilibrium with two gasses, water vapour and oxygen. A sequential solution could only be obtained at fixed p_{water}. Protonic defects are discussed further in paragraph 7.4.

A4. Bonanos, N.; Poulsen, F.W., ***Considerations of defect equilibria in high temperature proton-conducting cerates***. J. Mater. Chem. **9**, 431-434. (1999)

The paper deals with chemical modelling of the proton uptake in perovskites. No site limitation for protons is assumed,- they are treated chemically as interstitial ions $H_i^{\bullet}$,

and not as a proton attached to lattice oxygen $OH_O^{\bullet}$. In order to obtain an analytical solution to the defect equations we had to refrain from including the Schottky equilibrium. An analytical expression in 4th power of the variable $(3-[V_O^{\bullet\bullet}])/[V_O^{\bullet\bullet}]$ was obtained. Although this has an analytical solution, it turned out to be much easier to find the solution by iteration. A literature survey revealed that very limited stoichiometry and conductivity data at $pO_2 > 0.21$ atm. is available. 3D- Brouwer diagrams were calculated using representative equilibrium constants. The calculations were confirmed using the method of paper A3.

A5. F. W. Poulsen, ***Defect chemistry modelling of oxygen-stoichiometric, vacancy concentrations and conductivity of*** $(La_{1-x}Sr_x)_yMnO_{3+d}$**.** Solid State Ionics **129,** 145-162. (2000)

Paper A5 is a demonstration of the applicability of two different defect models: a small polaron description, i.e. Mn^{2+}, Mn^{3+} and Mn^{4+} ; and a large polaron[10] description, i.e. Mn^{3+}, $e^{\prime}$, $h^{\bullet}$) for Sr-doped La(Sr)MnO_3. Nowotny and Rekas (1998) were only able to model LSM by developing two sets of equations, describing the sub-, respectively over stoichiometric range, whereas the sequential solution covers the entire pO_2 domain. LSM is the most widely used cathode material (oxygen electrode) in SOFC technology. The improvement of SOFC cathode performance upon cathodic polarisation can be rationalised from the calculated increase of the oxygen vacancy concentration. The sequential method allowed also the consequences of deviations from unity of the A/B ratio to be analysed.

A6. ShanwenTao, Finn Willy Poulsen, Guangyao Meng and Ole Toft Sørensen,
High-temperature stability of the oxygen-ion conductor $La_{0.9}Sr_{0.1}Ga_{0.8}Mg_{0.2}O_{3-x}$**.**
J. Materials Chemistry **10**, 1829-1833. (2000)

Paper A6 utilises the analytical procedure of Bonanos and Poulsen (1999), A4, to predict the possible content of protonic and oxide defects in $La_{0.9}Sr_{0.1}Ga_{0.8}Mg_{0.2}O_{3-x}$. The main conclusion, obtained by comparison of modelled data with experimental data is that the material was not stable at 1000 ^{O}C in a humid atmosphere.

A7. F.W. Poulsen, M. Glerup and P. Holtappels,
Structure, Raman spectra and defect chemistry modelling of conductive pyrochlore oxides, Solid State Ionics **135**, 595-602. (2000)

Pyrochlore structure oxides, $A_2B_{2-x}Mf_{2-x}O_7$, can be doped both by aliovalent and homovalent dopants, Mf. This will influence ionic, electronic and structural properties. A mixed defect model was constructed, which included electronic defects both as localised $Ce^{\prime}$ ions and delocalised electrons. Model simulations are illustrated for $Pr_2Zr_{2-x}Ce_xO_{7\pm\delta}$.

[10] In the remainder of this thesis we use the term "large polaron" simply meaning an electronic defect not associated with a specific site, but without it's quantum mechanical connotations.

A8. Finn. W. Poulsen**,**
Speculations on the existence of hydride ions in Proton Conducting oxides, Solid State Ionics, **145**, 387-397 (2001)

The first part of this paper speculates on the existence of fluorite and perovskite structure oxides with a partial replacement of oxide ions by hydride ions. The coexistence of substitutional hydride ion defects, $H_O^{\bullet}$ and protonic defects $OH_O^{\bullet}$ in perovskite structure oxides is then modelled. The competition of four different species: O_O^X, $V_O^{\bullet\bullet}$, $OH_O^{\bullet}$ and $H_O^{\bullet}$ for the oxygen site results in a complex pO_2 dependence. Hydride ions as stable constituents in oxides are further discussed in paragraph 7.4 and in paper A161.

A9. Marianne Glerup, Ole Faurskov Nielsen and Finn W. Poulsen
The structural transformation from the Pyrochlore structure, $A_2B_2O_7$, to the Fluorite structure AB_2, studied by Raman Spectroscopy and Defect Chemistry Modelling,
J. Solid State Chem. **160** (1): 25-32 (2001)

The defect model in this work is an expansion of the one presented in paper A7 including a description of cation anti-site disorder. It is an experimental study of pyrochlore structure oxides, discussing both vibration spectra and defect chemistry. It is demonstrated that one defect model, at fixed pO_2, can describe both a pyrochlore and a fluorite structure oxide and a smooth transition between the two. The statistical value of the anti-Frenkel equilibrium constant for distribution of oxygens on two sites is deduced. The statistical distribution on the oxygen sites matches with the oxygen occupancies determined by Rietveld refinement on x-ray diffraction data.

A10. Finn W. Poulsen and Martin Søgård,
Defect chemistry modelling of complex SOFC materials,
Proc. 5th European SOFC Forum, Lucerne 2002, Ed. Joop Huijsmans, 687-694. (2002)

Two different systems are modelled:1) over-stoichiometric and sub-stoichiometric $La_{2-x}Sr_xNiO_{4\pm\delta}$ with interstitial oxygens both in the sub- and the over-stoichiometric region; and 2) La(Sr)Fe(Co)O_3, where in total four different oxidation states of the transition metals are handled. The sequential method was designed such for the latter system that two pO_2 solutions are obtained for each guess of one value of the Co^{+3} concentration.

2. Purpose and limitations of defect chemistry modelling

Two main hypotheses underlie the *quasi*[11] *chemical* approach employed in solid state defect chemistry, in the present thesis as well as in the literature:

i) Ions, atoms, vacancies and electrons in a solid behave as if they were in a solvent-free solution, i.e. all species can in principle diffuse over all the crystallographic positions and interstitial voids of the crystal, where they participate in equilibration via electron exchange or association with other species.[12] There is therefore an obvious analogy between ionic liquids, such as molten salts and defect chemistry of ionic solids. With the reservation that solid materials may have difficulties to reach thermodynamic equilibrium due to the much lower diffusion coefficients in solids compared to liquids.

ii) Chemical and electrical interactions between the entities mentioned under i) inside the solid, as well as interactions between the solid and the surrounding atmosphere containing at least one common element with the solid obey thermodynamics and electrostatics. Single ion and vacancy activities can be defined but not measured individually, see (Jacobsen,1975). Phrased differently- following (Rickert,1973) – only the chemical potential of a pair of structure elements = one building unit is a measurable well-defined quantity. The mass action law will in the following, as in most literature, be applied using virtual chemical potentials for the structure elements, i.e. the individual point defects including electrons and/or holes (Wagner and Schottky,1930). As such, any model can be uniquely described mathematically.

In what follows, we will exclusively deal with crystalline solids. The analogy between solution chemistry and solid state chemistry manifests itself in identical ways of describing mass- and electrical charge conservation and in using the mass action law, but with the extension that electrons, electron holes, vacancies and interstitial sites are considered on equal terms with ionic species.[13] It is conceivable that vacancies can be treated just as any other physical chemical species, since their number needs to be taken into account; - it takes energy to create them,- and their distribution over the lattice adds to the configurational entropy. Keeping track of the population on the various crystallographical sites in the crystal, i.e. defining the linear site conservation equations, can to some extent be compared to bookkeeping central atoms and ligands in complexes in a solution.

The space charge regions in crystals, found at surfaces, junctions and grain boundaries and dislocations are not treated in this thesis. It requires solving the

[11] quasi = resembling, as it were
[12] Frozen-in equilibria are treated in (Sasaki,1999abcd) and (Maier,2004) and further in Chapter 6.3.
[13] Electrons may be stable also in ionic melts, and be longlived in non-aqueous solvents, such as solvated electrons obtained by dissolution of Na metal in liquid ammonia, NH_3.

chemical equilibrium and the Poison equation[14] simultaneously. The classical work of Kliever and Kohler on space charge layers in NaCl, and recent work by (Hagenbeck,1996;1999) on acceptor doped $SrTiO_3$, Waser (2000) on grain boundaries and (Hendriks,2002) and (Guo,2003) on YSZ should be consulted.

2.1 On definitions in a defect model

A defect model defines the host lattice- and the defect species, i.e. their charge, position in the lattice and the maximum possible concentration. The Kröger-Vink notation (1956) has been followed in the published papers and in this thesis, with the exception of Chapter 3, dealing with Brouwer's original work on Ga^{+3} doped CdS (Brouwer 1954)**.**

In the present dissertation and the enclosed papers we use the following definition of the nature of the electronic states, especially those of transition metal and rare earth cations:

Small polarons are discrete oxidation states, which in a chemical notation are denoted as for instance Fe^{+2}, Fe^{+3} and Fe^{+4}, and Ce^{+4} and Ce^{+3}, etc. In Kröger-Vink notation these species are assigned relative charges, which usually adopt discrete and integral values,[15] depending on the choice of reference compound, see below. The lattice is perturbed around a small polaron, because of the different size of the ion compared to the host ion, for which it substitutes- and also if the charge of the species deviates from that of the host ion[16]. The electronic charge transport via small polarons is thermally activated as in a semiconductor, and can usually be described by an Arrhenius type of relation $\sigma \propto T^{-1}\exp(-\Delta E/kT)$. Other modified Arrhenius relations have also been suggested, such as $\sigma \propto T^{-3/2}\exp(-\Delta E/kT)$, see (Naik,1978).

Large polarons are here denoted $e^{\prime}$ for electrons in the conduction band, and $h^{\bullet}$ for holes in the valence band. The charges are then *not* associated with any particular element. We use the traditional symbols "n" and "p" for the concentrations of electrons and holes, respectively. The main difference from small polarons is then that large polarons are not counted in site conservation relations. Under the bracket of *large polarons* we also include more metallic-like electrons. The electrical conduction may or may not be described by a simple Arrhenius relation. It should be stressed that the observation of a shift from a positive Arrhenius type of behaviour to a negative temperature dependence at high temperature is *not* in itself a proof of metallic-like behaviour. The main reason for the decrease in conductivity at high temperature is the loos of oxygen, which results in a decrease in the concentration of electron holes (Sitte,2002). Small – and large polaron descriptions are compared further in paragraph 7.3.

In order to obtain the *formal charge* of a species in the K-V notation, one has to make a choice of a reference compound. Experiences with a multitude of defect models have exposed a number of common features of defect models, as used in the literature and the authors work:

---

[14] $\nabla^2\phi = -\rho/\varepsilon$, where ϕ is the electrical potential; ρ is charge density and ε the permittivity, cf. p 224 (Maier,2000)

[15] Models based on non-integral charges are also treated below and in Appendix 2.

[16] One might as well also consider redox-stable aliovalent dopants as small polarons, but with a low or negligible mobility.

i) Usually a cubic- sort of average approach is assumed. That is, all ions of the same element in a given oxidation state are treated as having identical energy, although from a crystallograpical point of view there may be more than one type of site for anions or cations of that element. Two types of oxygen are, for instance, present in orthorhombic perovskites, and three types of oxygen positions are available in pyrochlores, cf. paper A7, A9. Also all oxygen vacancies are therefore, for convenience, assumed to have the same probability to form. Reality is more complex, as shown in the structural studies by Knight & Bonanos on Y-doped $BaCeO_3$ (1994), Ranløv on Y-doped $SrCeO_3$ (1995) and (Lybye,2004) on Sr-doped $LaMO_3$, where M=Al, Ga, Sc have shown. The above simplifications are made, in order to reduce the number of unknown concentrations, and thereby the number of equations, which one has to handle. The protonic models treated in paragraph 7.4 do handle two different types of sites for protons.

ii) One is free to choose the charges in the reference compound. $SrTiO_3$ for instance, could equally well be described with reference to a hypothetical $A^{1+}B^{+5}O_3$, $A^{2+}B^{+4}O_3$, or $A^{3+}B^{+3}O_3$ state. Site- and mass conservation will read the same,- only the electroneutrality condition, ENC, will look differently, see the example on the following pages.

Paper A9 illustrates the usefulness of describing fluorites and pyrochlores using a common frame: an ordered pyrochlore structure with a potential to go disordered.

Likewise can Bi_2O_3 in its high temperature, superionic δ-phase be described as a fluorite structure using, say cubic CeO_2 or any hypothetically cubic AO_2 compound as reference. The main species will then be $Bi_{Zr}^{|}$, O_O^X and $V_O^{\bullet\bullet}$. If the low temperature α-phase of Bi_2O_3 itself is used as reference, then all host species will formally be neutral: Bi_{Zr}^X, O_O^X and the neutral, structural oxygen vacancies V_O^X. However, this is leading to a dilemma, when additional oxygen vacancies are formed by doping with divalent oxides - these will not be neutral, but have a charge of +2, $V_O^{\bullet\bullet}$. There are thus two types of oxygen vacancies in the latter model. Norby has advocated a new "defect notation in inherently deficient systems", where anion sites with a partial anion occupation is considered the normal state (Norby,2001): in the perovskite related structure $Sr_4(Sr_2Nb_2)O_{11}$ the average occupancy on the oxygen site is 11/12, with the real charge –2 * 11/12 = -11/6. An oxygen vacancy thus carries the K.-V. charge + 11/6, and a fully occupied oxygen site (which is now considered a defect) has the K.-V. charge -2 -(-11/6) = -1/6. However, at the end of his discussion, Norby comforts the reader by assuring that the usual slope of the log σ versus $\log(pO_2)$ plot come out anyhow.

We will illustrate the consequences for the algebraic formulation of the electroneutrality condition by changing the reference state for a nonstoichiometric bronze $(La_{1-x}Sr_y)Ti_{1-z}Nb_zO_{3-\delta}$.[17] In the first model we use a hypothetical WO_3 compound, $V(0)_AW(+6)_BO(-2)_3$, as the reference lattice. The physical charges in a 100% ionic formulation are shown in parentheses. The ENC reads as eq (2.1). Note that cation vacancies on the A-site are neutral in this description.

[17] Unpublished analysis from 1999, by the author and John Bradley, St. Andrews University, Scotland.

Table 2.1. "Large polaron" defect description of an A- and B-site acceptor doped bronze structure $(La_{1-x}Sr_y)Ti_{1-z}Nb_zO_{3-\delta}$ with delocalised electrons and electron holes. The reference state is chosen as a hypothetical WO_3 structure with vacant A-site positions.

A-site	B-site	O-site	Delocalized
$La_A^{\bullet\bullet\bullet}$	$Nb_B^{\vert}$	O_O^x	$h^{\bullet}$
$Sr_A^{\bullet\bullet}$	$Ti_B^{\vert\vert}$	$V_O^{\bullet\bullet}$	$e^{\vert}$
V_A^x			

.

Tungsten type bronzes are often tetragonal, but will be treated as if they were cubic perovskites: all oxygens are identical, - likewise we assume that all oxygen vacancies have the same properties. For $(La_{1-x}Sr_y)Ti_{1-z}Nb_zO_{3-\delta}$ using $V(0)_AW(+6)_BO(-2)_3$ as reference the condition of ENC reads:

$$3[La_A^{\bullet\bullet\bullet}] + 2[V_O^{\bullet\bullet}] + 2[Sr_A^{\bullet\bullet}] + p = 2[Ti_B^{\vert\vert}] + [Nb_B^{\vert}] + n \quad (2.1)$$

where the following is valid

A-site balance: $$[La_A^{\bullet\bullet\bullet}] + [Sr_A^{\bullet\bullet}] + [V_A^x] = 1 \quad (2.2)$$

B-site balance: $$[Nb_B^{\vert}] + [Ti_B^{\vert\vert}] = 1 \quad (2.3)$$

O-site balance: $$[O_O^x] + [V_O^{\bullet\bullet}] = 3 \quad (2.4)$$

If one alternatively chooses $M(+1)_AM'(+5)_BO(-2)_3$ as the reference state, then the corresponding ENC would read

$$2[La_A^{\bullet\bullet}] + 2[V_O^{\bullet\bullet}] + 1[Sr_A^{\bullet}] + p = [Ti_B^{\vert}] + [V_A^{\vert}] + n \quad (2.5)$$

Now note that eqs. (2.1) and (2.5) appear quite different, not only that the charge multipliers in front of each concentration differ, but also $[Nb_B^{\vert}]$ is "missing" in eq (2.5) and $[V_A^{\vert}]$ appears in stead. Do the two different analytical expressions really reflect the same reality, or is one correct - the other in error?

Answer: Since the rewritten site conservation relations: $[La] + [Sr] + [V_A] - 1 = 0$ and $[Ti] + [Nb] - 1 = 0$ are valid in both descriptions,[18] it follows that

$$[La] + [Sr] + [V_A] - 1 = 0 = [Ti] + [Nb] - 1 \quad (2.6)$$

or $$[La] + [Sr] = [Ti] + [Nb] - [V_A] \quad (2.7)$$

[18] Written without charges- but this doesn't invalidate the argument in the present context.

which holds true in both descriptions. One can obtain eq. (2.7) by subtracting eq. (2.5) from eq (2.1). The two choices are therefore leading to the same mathematics, but expressed in different linear combinations of the respective linear relations. Q.E.D.

iii) The concept of average oxidation states appears to work well, see App. 2. Spinel structures derive from the mineral $Mg(II)Al(III)_2O_4$. The divalent and trivalent ions may in the case of 3d-transition metal spinels change place, the so-called inverse spinels. For magnetite, $Fe(II)Fe(III)_2O_4$, it will be proven in Appendix 2 that there is no reason to distinguish between the two oxidation states of iron, when modeling the oxygen content. Also if the material is doped with another transition metal such as Co or Cr, there seems to be no need to specify to what degree the metal ions are distributed on tetrahedral- or octahedral sites as in a spinel or inverse spinel. If we assume that one formula unit of the reference compound Magnetite contains three identical iron ions, then these will have the average oxidation state +8/3 = +2.666, which is then also the K.-V- charge of an interstitial metal ion. Excess and deficit of oxygen can be accounted for by hole, respectively electron formation at unspecified positions in the lattice, where all cations are assumed to have the same formal average charge. Such a model mimics the observed stoichiometry curves of Lu et al. (1993) just as well as the much more complex models applied by them, cf. App. 2. The spinel model in Appendix 2 for M_3O_4 compounds, is an analogy to the average anion-situation discussed under point ii). However, in the spinel case a simplification rather than an increase in confusion is obtained by applying fractional charges!

iu) Ions in interstitial positions carry their own charge, irrespective of the choice of reference compound. Stated in a different manner: the lattice has no opinion or influence on the charge of ions, which do not form a part of the lattice. If no restrictions are imposed on the possible upper concentration of interstitials, then solving the defect model is rather easy. If a restriction is imposed on the maximum concentration of interstitial sites, then a new, virtual species, an empty, uncharged interstitial, V_i^X, has to be added, and the degree of complexity of the model increases one step as one more site-balance and species is present. Sr-doped $La_2NiO_{4\pm\delta}$ is an example of such a model with a tuneable concentration of interstitials, cf. paper A10.

u) Finally, defect models have nothing to do with structure, but exclusively deal with chemistry and book-keeping of the population of sites according to the stoichiometric ratios of the elements in the reference compound. This has the implication that a model developed for e.g. an ABO_3 perovskite compound can directly be transferred to all other compounds observing the same 1:1:3 ratio of the elements, i.e. for $M_\delta M'O_3$ bronzes, $LiNbO_3$-type structures, carbonates MCO_3, nitrates $M'NO_3$ etc. However, it is not thereby implied that an identical chemistry can be realised in the respective compounds- the only point made here is that one at least theoretically *possible* chemistry in say a nitrate would result in the same mathematics as for a perovskite.

2.2 Purpose: what can be modelled?

Common sense tells us: An operational model should be able to describe as many experimental data sets as possible, using a minimum of adjustable parameters. It means that interpolated, estimated values should fall as close as possible on the trace of the experimental values. If the model is able also to forecast, i.e. extrapolate

reliably outside the present experimental range, then additional credibility and functionality is ascribed to the model. Ultimately- if a model can describe *all* experimental data, one may start to believe that these materials are behaving ideally, as the model it is founded on some idealised laws of nature, cf. Chapter 5.

A defect model should primarily output the concentrations of all the species, as function of temperature, partial pressure in the surrounding of one or more of the constituent elements in the solid and the content and nature of impurities and dopants. The input for the model calculation is the known impurity and dopant levels, and the thermodynamic properties of the mass action laws involved, specified as entropy and enthalpy of reaction[19]. The total, calculated oxygen content as function of pO_2, can then be compared to the content measured by TG, and equilibrium constants can be adjusted to improve the fit. A major concern of the present work is that the experimental oxygen stoichiometry curve vs. pO_2 may be explained equally well by several defect models, since the models have 2,3,4 or more adjustable equilibrium constants.

A model calculation automatically outputs data for the regions in partial pressures, at which a change of majority carrier occurs, be it from n to p, ionic to electronic, protonic to oxide ion conduction, or otherwise. The major obstacle here is that before a comparison to experimental total conductivity data can be established, one must first find the electrical mobilities of the species involved. Performing thermoelectric measurements to establish the concentration and sign of the major carrier in a given partial pressure range is invaluable in this respect, and has been the subject of several studies by Erik Ahlgren (1997a,b) and the author (A1, A2, A75, A79, A85, A86, A87, A89). Hall effect measurements are usually not applicable,- due to the relatively low conductivities of non-stoichiometric oxides compared to metals and also due to the mixed nature of conduction (electronic/ionic or mixed ionic). Also the combination of magnetic fields and high temperatures raises practical problems.

When Schottky reactions are important, one can calculate the increase or decrease in number of unit cells, when the sample is equilibrated at a certain partial pressure, leading to a macroscopic length change as observed in over-stoichiometric $LaMnO_{3+\delta}$ (Miyoshi,2002). Models can also treat a Schottky reactions proceeding with exolution or consumption of a secondary phase, cf. Appendix 3. The defect model of La-doped $SrTiO_3$ described in App. 3 establishes such a link between defect chemistry and dilatometry.

Finally, by means of various ways of numerical differentiations of the concentration curves in the Brouwer diagram one gets "for free" the enhancement factor, W, for diffusion in a chemical gradient, see Chapter 3, as well as the predicted slopes of the various $\log(c_i)$ vs. $\log pO_2$ curves, to compare with the limiting slopes observed in conductivity and TG measurements.

[19] T. Norby, Oslo University, Norway, is in the process of establishing a large data base for defect chemistry calculations.

2.3 What is not modelled?

Needless to say, kinetic aspects are not among the issues to be answered. There is no guarantee that the calculated equilibrium state will ever be reached. The consensus is that electronic equilibria equilibrate faster than ionic ones, and in the latter class diffusion of highly charged or voluminous cations are the slowest. No structural aspects are answered either, although 1000's of defect chemistry papers in the literature by tradition include the phrase "*on the defect structure* of ..Balonium doped Kryptonite" in their title, abstract or the bulk of the text.

The equilibration reactions with the ambient gas at the surfaces are formulated as overall reactions involving only species as found in the bulk plus one or two gas species, with the full knowledge that different surface states species may be present and kinetically play a major role. However from a thermodynamic point of view we need not worry, since we only need to specify start and end state, but not the route taken for a given reaction.

In a model calculation, solutions can be obtained even at very high and very low partial pressures. These solutions obey all the site-, mass-, electroneutrality- and mass action law constraints – but they correspond to unrealistic situations with very high cation vacancy concentrations, see Chapter 3, respectively a large amount of oxygen being removed, which corresponds to reduction of cations to unrealistic low states. The calculations thus give no warning as to the phase limits. This deficiency of certain models can partly be remedied by using a small polaron description - with a fixed lowest possible oxidation state at the reducing or oxidising end.

2.4 What can be measured ?

The oxygen content is usually not known on an absolute scale. Often one assigns a value derived from defect chemistry considerations to an observed plateau in the stoichiometry curve. For protonic materials it is critical to be able to strip the material completely from hydrogen;- furthermore very small weight changes are encountered, of the order of 0.1 %, even when a full uptake is met. Most classical chemical assay methods (titration, ICP, atomic absorption, etc) determine the oxygen as a difference after analysing for the metal contents. Special titration methods can differentiate between, say Mn^{3+} and Mn^{4+}, as required in analysis of $La/SrMnO_{3\pm\delta}$ cathode materials, - still the oxygen content is only determined indirectly (Krogh Andersen,1994). Modern spectroscopic methods installed in SEM and TEM, eg. EELS, EDX etc., can be calibrated to give also the oxygen content within some %. The oxygen content can alternatively be determined as a weight difference after reducing a complex oxide in hydrogen, as done for instance with the Balachandran – type compounds $Sr_4Fe_{6-x}Co_xO_{13\pm\delta}$ (A121, A135). After reduction only FeO, Co and SrO remains as certified by x-ray powder diffraction. An absolute method for oxygen analysis exists: it is based on a complete reduction of an oxide with excess carbon at temperatures over $2000^{O}C$.[20] All oxygen ends up as CO, which is analysed quantitatively. The method is however optimal for samples with low oxide content (traces). Finally, crystallographers and physicists have faith in their occupation numbers, being output from their Rietveld refinement on diffraction data, preferentially made by neutrons. In paper A9 we show that meaningful oxygen occupancies can indeed also be extracted from x-ray data and match with theoretical

[20] See LECO company making such equipment on www.leco.com

predictions. The distribution of dopant ions in the first few coordination spheres around a host ion can be analysed from EXAFS-data, as for instance done for doped ZrO_2 (Ishizawa,1999) and Ho- and Mg co-doped $BaTiO_3$ (Ohsato,2004). The site, at which a dopant substitutes, can be found by the TEM channelling method ALCHEMI invented by Spence and Taftø (1983). It is based on an analysis of the correlation of the various elements characteristic x-ray fluorescence and it was employed quite early on Yb-doped $CaZrTi_2O_7$ by Turner (1991). The ALCHEMI method has, regrettably only been tested once at Risø, where it was shown directly that the Ca-dopant substitutes at the La-site in $La_{1-x}Ca_xCrO_{3-\delta}$ (Bilde-Sørensen & Poulsen,1992). Since many oxygen separation membrane materials and SOFC cathode candidates have doping on both cation sites this method ought to be more popular and fruitful to pursue.

3. Shortcomings and virtues of the Brouwer approximation procedure

Graphical representations of chemical systems showing all concentrations as log c_k's versus some activity log c_i are widespread. To mention two: Hägg-diagrams, where the concentration of acidic and basic molecules/ions are shown as function of the acidity, pH; and distribution/predominance diagrams, which are used to show the consecutive formation of complexes $M(H_2O)_{6-n}X_n$– here the log(ligand concentration) = log(C_X) is used for the abscissa. In solid state chemistry such log c_j 's versus log (activity) plots are called Brouwer diagrams.[21] The activity may be that of oxygen pressure in the case of an oxide, pO_2; pCl_2 in the case of a chloride or p_{water} in the case of proton containing oxides etc,- it may also be the electrical potential, or the dopant concentration.

We will see how well the Brouwer approximation works, using G. Brouwer's first example on Ga-doped CdS[22], from his classical paper (1954). The species considered are shown in Brouwer's notation[23] and translated to Kröger-Vink notation in Table 3.1. The approximated Brouwer diagram is shown in Figure 3.1.

Table 3.1 Species in Brouwer's model for Ga^{3+}–doped CdS.

Cd-site		S-site	
Brouwer notation	K-V notation	Brouwer notation	K-V notation
Cd^+ (or electron)	$Cd_{Cd}^{\cdot}$	S^- (or electron hole)	$S_S^{\bullet}$
V_C^+	$V_{Cd}^{\cdot}$	V_A^-	$V_S^{\bullet}$
V_C^{2+}	V_{Cd}^{x}	V_A	$V_S^{\bullet\bullet}$
$[Cd^{2+}(Ga^{3+})]$	$Ga_{Cd}^{\bullet}$		
Cd^{2+}	Cd_{Cd}^{x}	S^{2-}	S_S^{x}

Equations (3.1)-(3.7) describe the model, maintaining Brouwer's notation:

Equilibration with Cd vapor: $K_R * p_{Cd} = [V_A][Cd^+]^2$ (3.1)

Schottky reaction: $K_S = [V_A^-][V_C^+]$ (3.2)

Hole + electron ionization: $K_i = [Cd^+][S^-]$ (3.3)

Transition of electron to form Cd^+: $K_5 = [Cd^+][V_A]/[V_A^-]$ (3.4)

[21] Many publications use incorrectly the term "Kröger-Vink" diagram

[22] Normal CdS has the hexagonal ZnO-wurtzite structure.

[23] For masochists only, expression borrowed from N. Bonanos, when mathematics gets too hairy.

Further hole formation: $K_3 = [Cd^{+}][V_C^{2+}]/[V_C^{+}]$ (3.5)

ENC: $[Cd^{+}] + [V_C^{+}] = [S^{-}] + [V_A^{-}] + 2[V_A] + [Ga^{3+}]$ (3.6)

$[Ga^{3+}] \equiv [Cd^{2+}(Ga^{3+})]$ = known dopant concentration (3.7)

The result is 7 equations with 7 variables, out of which one, the dopant concentration $[Ga^{3+}]$, is already known. Note that there is no site conservation on the Cd- and S-site in Brouwer's treatment, ie $[Cd^{2+}]$ and $[S^{2-}]$ are set constant. If a variation of the host Cadmium ion concentration is taken into account via the equilibration reaction with Cd vapor (3.1), one has to rewrite the reaction as

$$Cd(gas) + [Cd^{2+}] \Leftrightarrow [V_A] + 2[Cd^{+}] \quad (3.8)$$

and the mass action law then expands in the denominator

$$K_R^{'} * p_{Cd} = [V_A][Cd^{+}]^2/[Cd^{2+}] \quad (3.9)$$

The sample is increased in size by one Cd-site and one S-site, when reaction (3.8) proceeds from left to right. This of course also applies, when writing the mass action law as in eq. (3.1). $K_R^{'}$ and K_R in (3.1) and (3.9) will now differ. The other equilibria also have to be rewritten, if consumption of $[Cd^{2+}]$ and $[S^{2-}]$ is taken into account (not shown here). Solving that set of equations will be much more difficult, as there now will be 9 unknowns in 9 equations and the mass action law expressions will contain more terms.[24]

In the Brouwer procedure equations (3.1)-(3.5) are used and combined after taking their logarithm. The linear electroneutrality equation ENC in eq. (3.6), must be truncated so only one freely varying positive and one negative species dominate in a given region. The following guidelines in establishing the Brouwer approximations apply: i) majority defects should be identified and handled first - high concentrations are set constant in mass action law expressions; ii) low concentrations can be omitted from the ENC, especially if the impurity or dopant concentrations are higher , and known. In short, the Brouwer technique will only produce linear relations in the log(concentration) versus log(activity) plane.

Brouwer decided to divide the p_{Cd} range into four regions and found the four corresponding approximated ENC's, cf. the original paper. The Brouwer diagram was then calculated using the following equilibrium constants: $\log K_i = 34.0$; $\log K_S = 32.3$; $\log K_5 = 17.5$ and $\log K_3 = 15.0$. The concentrations were measured in particles per cm^3, thus the large values for the equilibrium constants. Also, in Figure 3.1 is shown his numerical solution. The numerical method is unfortunately not specified in the paper. The concentration of one of the species, $[V_A] \equiv$ the doubly charged positive sulphur vacancy, passes through a minimum around $K_R * p_{Cd} = 10^{50}$ atm. This is because a singly charged sulphur vacancy, V_A^{-}, is also included in the model. The errors of the approximated solution occur in the transition regions 12, 23, and 34, marked by vertical lines. It is seen that the deviations in the concentrations between the log-linear approximation and the precise one are between one half to a full decade.

[24] Solution will be presented in a forthcoming paper

Brouwer still claims: " *it is seen that the approximation is satisfactory in wide ranges, only a slight smoothing of the sharp bends being required to get the exact answer to the problem".*

The solution presented by Brouwer was checked using the authors sequential method. The algorithm was easy to establish:

- Guess a value for $[S^-]$, then $[Cd^+]$ can be found from $[Cd^+] = K_i / [S^-]$;
- Substitute in ENC to create a quadratic equation in the variable $[V_A^-]$: $[V_A^-]^2 * (1+2K_5/[Cd^+]) + [V_A^-] ([S^-] - [Cd^+] + [Ga^{3+}]) - K_S = 0$,
- Solve this quadratic analytically, choose positive root,
- Then calculate remaining concentrations from eqs. (3.2-3.7),
- Insert finally calculated concentrations in eq. (3.1) to find the Cd partial pressure in equilibrium with these concentrations, or as in Brouwer's paper the product $K_R * p_{Cd}$, which is used as the plotting parameter for the abscissa.

The result is shown in Figure 3.2. There is a perfect match with Brouwer's calculation. It is noticed that the approximation method as well as the numerical solution extend to very high concentrations, far exceeding what is physically possible in terms of permissible number of particles/ cm^3. From the molar weight and density of CdS ie.144.477 g/mole and 4.83 g cm^{-3}, respectively, we find that the maximum number of Cd or S-sites is $2.01*10^{22}$ /cm^3. Thus the calculations below $K_R * p_{Cd} \approx 10^{43}$ atm. have no physical meaning. A similar limitation applies in the high end.

Having established the algorithm for the CdS-case allows us to see the impact of changing the equilibrium constants (one will do). When K_i is increased a factor of 10000 we get a simpler Brouwer diagram as shown in Figure 3.3. Only three regions are observed instead of four, and the hole and electron concentrations are comparable (and ≈ 100 x higher) over the middle region, a situation the Brouwer approximation technique can not cope with.[25]

[25] LSM as a case with coexistence (comparable concentrations) of more than two defect species (divalent, trivalent and tetravalent Mn) is discussed in paper A4.

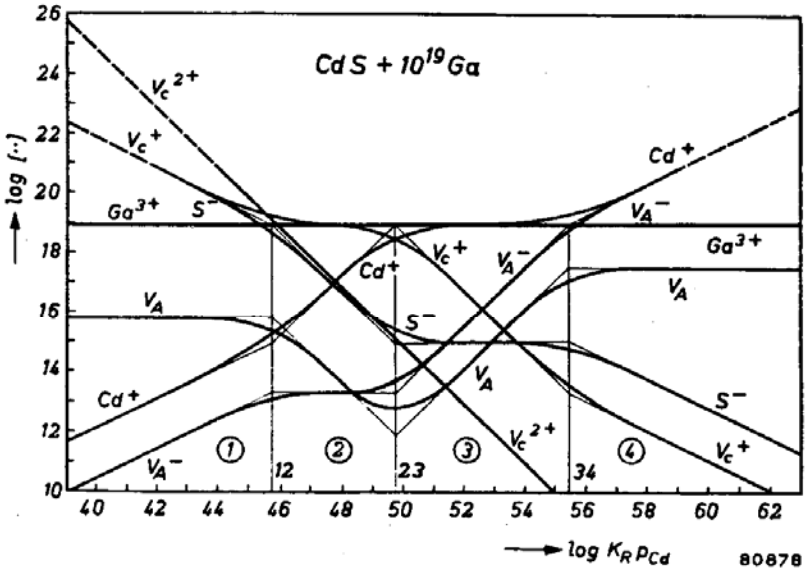

Fig. 2. Exact solution of the system CdS + 10^{19} Ga drawn in full, the approximate solution being indicated by minor lines. Note the close agreement.

Figure 3.1 Scanned version of the original figure from Brouwer's paper

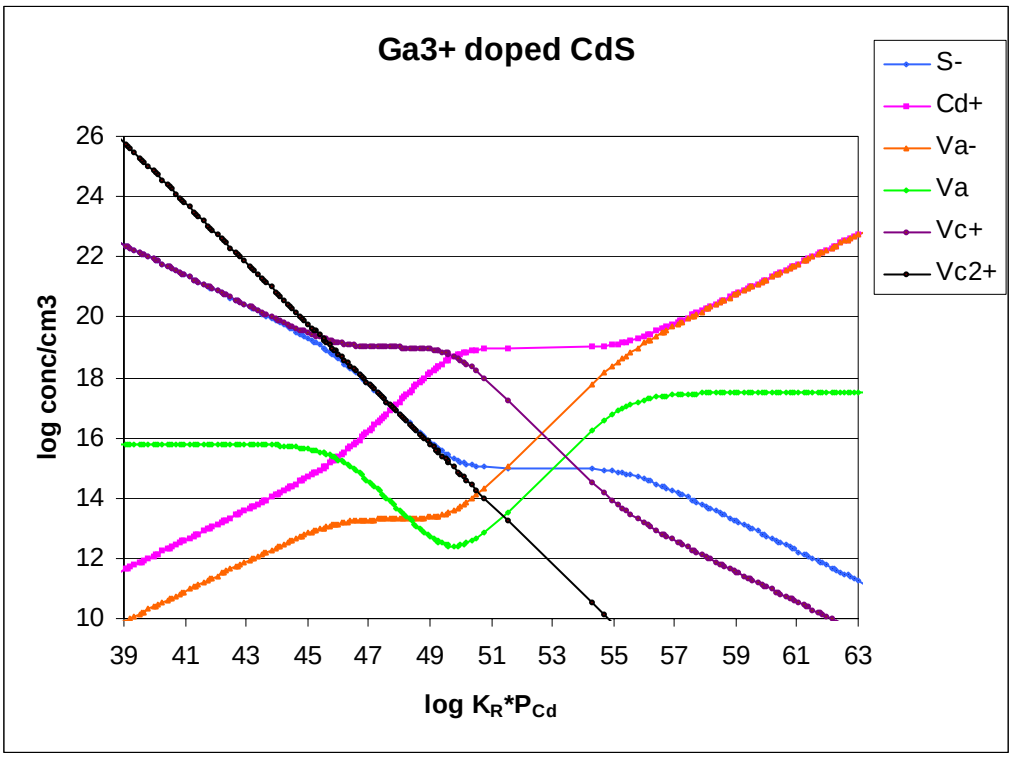

Figure 3.2 Reconstruction of Brouwer's diagram, see Figure 3.1. : $\log K_i = 34.0$; $\log K_S = 32.3$; $\log K_5 = 17.5$ and $\log K_3 = 15.0$.

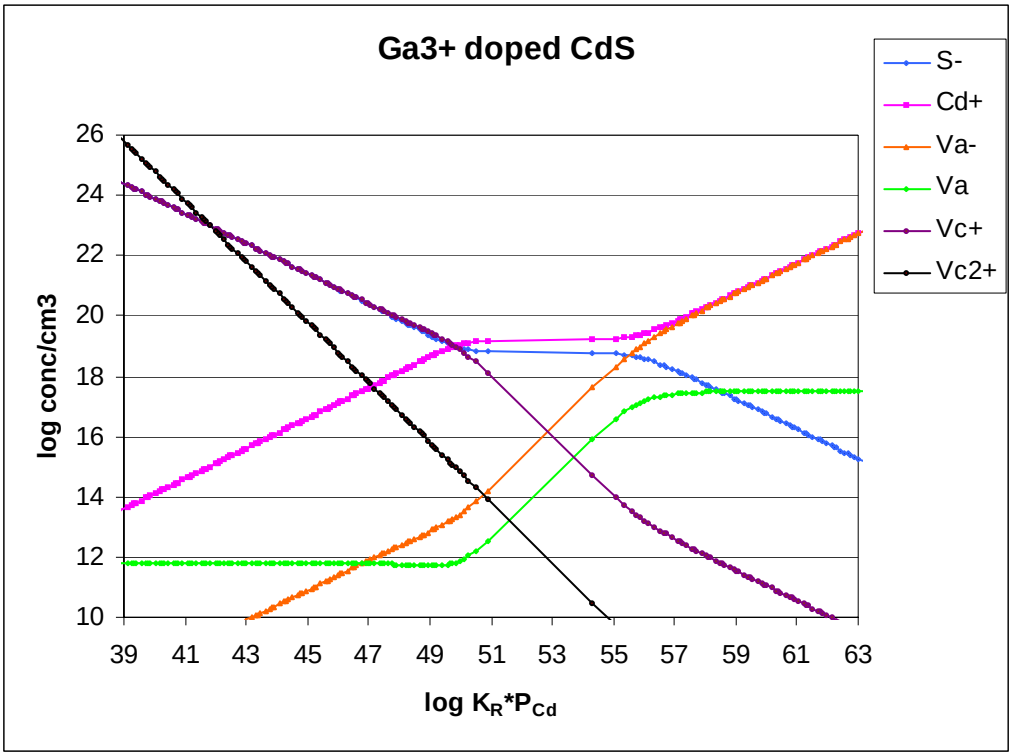

Figure 3.3 . Same defect model as in Figure 3.2, but with new value of $\log K_i = 38.0$. Figure 3.2 and 3.3 illustrates one further problem with the Brouwer approach, namely that a diagram apparently can reflect a simpler chemistry than the one actually in play.

A further limitation of the Brouwer approximation approach is connected to the assumption of constant defect concentrations in certain partial pressure ranges. This leads to problems with theoretical prediction of the thermodynamic enhancement factor, W, as will be shown below. We will take a perovskite, $La_{0.9}Mg_{0.1}BO_{3-\delta}$, as an example, where the B-metal can exist in the oxidation states+2, +3 and +4. The oxygen content will at high pO_2 saturate at three oxygen per B, i.e. $\delta \Rightarrow 0$, assuming that formation of cation vacancies is not possible in this material. In some intermediate pO_2 range the oxygen content will be nearly constant, corresponding to $\delta = 0.05$. The more stable the +3 state is corresponding to the two other oxidation states- the wider will be the pO_2 range, where $\delta \approx 0.05$, cf. Figure 4.3.

The so-called thermodynamic enhancement factor, W, links the real diffusion coefficient for oxygen, $D_{selfdiffusion}$, to that observed experimentally in a gradient in the oxygen potential, the chemical diffusion coefficient:

$$D_{chem} = W * D_{selfdiffusion} \qquad (3.10)$$

where

$$W = -\tfrac{1}{2}\, \delta \ln(P_{O2}) / \delta \ln(C_O) \qquad (3.11)$$

and C_O is the concentration of oxygen in the given interval (Mikkelsen, 2001). W is obtained by differentiating the stoichiometry data as in eq. (3.11). If the oxygen stoichiometry curve is assumed to be flat in certain regions, as in the Brouwer approximation, then both $[V_O^{\bullet\bullet}]$ and $[O_O^X]$ are constant, and consequently the theoretical prediction for W will reach infinity, which has no physical meaning.

The sequential method and other numerical methods thus offers obvious advantages over the Brouwer technique: correct concentrations are obtained, and differentiation to obtain limiting log(conc) versus log(activity) slopes and the enhancement factor W are obtained in the same instance. Papers A3, A5 and A8 show these kind of differentiations.

Simple is safe

4. Solving a set of non-linear defect equations

4.1 General comments

It is supposed that the following conjecture is valid:

> *The mathematical formulation of quasi-chemical defect chemistry models always results in a set of linear and non-linear equations. The latter ones come from the mass action law expressions. The linear ones come from mass-, charge- and site conservation. By substitution/elimination of variables one can in principle obtain an algebraic equation in one of the variables. This will always take the form of a polynomial, i.e. no transcendental or implicit expressions will result. This polynomial[26] will easily reach a higher degree than 4. Then, according to the Norwegian mathematician Niels Henrik Abel[27], there is in general no analytical solution.*
> *The conclusion that there is in general no analytical solution to the mathematical formulation of a defect model can also be arrived at from a different argument: Only in special cases will non-linear sets of equations have an analytical solution[28].*

The solid state chemistry literature does contain statements going against the above postulate. However, in such cases, the mass action law has been replaced by more complex functional relationships. The group of Hempelmann in Saarbrücken, for instance, introduced a Fermi-Dirac statistics in their description of proton uptake in doped Ba-zirconates and in the more complex BCN18 perovskites, - they point out that the resulting expression for the [$OH^{\bullet}$] concentration is an implicit function in [$OH^{\bullet}$], their equation (2) in (Groβ, 2000). This will be discussed further in paragraph 7.4.

Irrespective of, how we solve the set of equations numerically, we are faced with the problem of how to discriminate all solutions but the *one and only* physical solution. This is easily done for those solutions, which contain negative or complex roots for the concentrations, i.e. those referring to non-physical concentrations.

> Conjecture: *There is only one physical solution to the chemical equilibrium problem in a single phase solid, and all other solutions to the set of equations contain either negative[29] or complex roots.*

---

[26] The analytical expression for an over-stoichiometric perovskite involving a Schottky equilibrium will be 12^{th} to 18^{th} degree in the concentration variable, cf. paper A5 .
[27] 1802 - †1829.
[28] Conclusion arrived at after superficial consultation with modern math books.
[29] When one or more concentrations in a solution come out negative, then one or more of the other concentrations will usually exceed the maximum concentration for a given site in order to satisfy mass conservation. Assuming a negative concentration of an acceptor dopant can be considered as a positive concentration of a donor dopant, but only with regard to its influence in the ENC.

The complexity of defect models, and thereby the complexity of the mathematics to be solved, will increase dramatically as the number of species and number of non-linear relationships increase. Below is listed a number of features, which add to the complexity of the set of equations describing a given defect model:

i) The more atomic elements that are present, the more cumbersome the mathematics will get.

ii) The more small polaron states we include, the higher the complexity: small polaron descriptions turn out to be more difficult than n-p type descriptions, since three variable concentrations are at play, e.g. $[M^{\bullet}]$, $[M^{x}]$ and $[M^{/}]$, whereas in the n-p description only two variable concentrations, n and p, are at play, whereas all element M is assumed present as M^{x}.
A model for a perovskite including three oxidation state for the B-cation, but in addition also a redox labile dopant showing two oxidation states (a total of 10 species) has been solved in analogy with the method used in A3 and A5, but due to the extra equilibrium for the dopant one now has to solve a cubic equation underway in the sequential algorithm. [30]

iii) The more gases, with which the sample equilibrates, - external equilibria are with one or typically at most two gases.

iu) Number of species competing for the same site. The oxygen site can for instance be occupied by O_O, V_O in various oxidation states,, protons $OH_O^{\bullet}$ or hydride ions as, $H_O^{\bullet}$, see paper A8 dealing with hydride ions in perovskites, or foreign atoms with similar ionic radius to the oxide ion, e.g. $F_O^{\bullet}$.

u) When a site is involved in association of defects, embracing one or more neighbouring sites, cf. the case of association in fluorite structure oxides treated in paragraph 6.3. Appendix 5 demonstrates that a case with possible co-existence of five different associates can be handled. This is probably the most complex defect model treated by the sequential method so far, as it involves 6 non-linear equations and four linear ones.

ui) Number of defect equilibria in the solid (internal equilibria), especially Schottky or anti site equilibria adds to the complexity.

4.2 History and applications of the sequential method

Starting around 1991, the author was trying to solve sets of defect equations, with the ambition *not* to apply Brouwer approximations. The case under study was that of reduced ceria including one or two associates between the dopant ion and the oxygen vacancy or between reduced cerium (trivalent) and the oxygen vacancy. However, the authors limited skills in mathematics combined with even more limited skills in programming did not allow to solve the problem applying Newton-Rahpson-, simplex-, Gauss-pivot, or other library routines. The only tool at hand was the simple

[30] Internal note, F.W. Poulsen, 1995, Allpero-Excel code..

GWBasic language, which the author mastered at beginners level. Root finding was done by a slow dissection trial- and error method, but calculations often crashed or diverged. As a last desperate resort I decided to plug in known concentrations and the corresponding partial pressure of oxygen to check the reliability of my primitive algorithm. Surprisingly, it was realised that the problem had been solved quite easily by inverting it. The conventional approach is asking the question: "What are the calculated concentrations of the species in a model at a specified partial pressure and for known values of the equilibrium constants and dopant concentrations"? Instead one could ask the question: "Assume, that we fix[31] one of the concentrations, and we can calculate the remaining ones, what is then the partial pressure corresponding to this set of concentrations – and is it indeed the one and only solution we are looking for"? Table 4.1 summarises the two ways of thinking.

Table 4.1. The main difference between a conventional and the author's sequential procedure for solving defect equations for a system with N different species.

	Conventional	Sequential method
Number of equations	N	N
Independent variable	pO_2	$[C_1]$
Dependent variables	$[C_i]$, i = 1,N	$[C_i]$, i = 2,N; pO_2

Inverting the problem, in order to make it easier to solve, formally corresponds to a shift in choice of independent/dependent variable. One might actually question, whether the partial pressure of an experiment is known to a higher precision than the measured property, be it the sample weight, conductivity or other pO_2 dependent property. The pO_2 is often measured up-stream or down-stream to the sample, but seldom right at the sample position. Coulometric titration data of Ceria in a closed cell (Zachau-Christiansen et al., 1993,1996), (Riess, 1987) and $SrFeO_3$ (Bakken et al, 2004) are among the exceptions.

The sequential solution method was presented in public for the first time on October 26th in 1992 at a Nordisk Ministerråds workshop on high temperature electrode materials, at Risø (A63), under the title *Exact solutions to Kröger-Vink diagrams for perovskites.* A 1992 version of the GWBasic code is shown in Table 4.2. The code generated a file, which was imported into the spread sheet Supercalc4/ or 5 for visualisation of the Brouwer diagram. An illustration of an output from the 1992 proceedings paper (A63) is shown in Figure 4.3 for nostalgic reasons. Details are given in the figure caption.

In 1993 the author and colleagues (paper A1) used the sequential method to visualise a theoretical Brouwer diagram for the pO_2 dependence of stoichiometry and conductivity of Ti-doped $NdCr_{1-x}Ti_xO_3$.

[31] Fix, meaning choose as independent variable statistically speaking. In simpler terms: we just assign a numerical value to one of the variable concentrations and calculate the consequences of this choice.

In 1995 the technique was presented at the Ambleside, UK Conference on ceramic oxygen ion conductors and their technological applications in the talk " *Defect equilibrium calculations in high temperature proton conductors*.

An unpublished talk in Uppsala University , Sweden, *Defect chemistry in perovskites* was given on October 16th 1996.

In the following years several presentations of the technique were made at international meetings, (A63, A99, A104, A109, A113, A122, A145) .The paper *Method for calculating ionic and electronic defect concentrations in fluorite structure oxides* (A109) dealt with protonic defects in zirconia and thoria. During the printing process of the proceedings of the 3. International symposium on " Ionic and mixed conducting ceramics", Paris (FR), 31 Aug - 5 Sep 1997, the Editor/printer unfortunately left out all the illustrations.

Finally, full papers on proton containing perovskites and on the large and small polaron modelling of Sr-doped lanthanum manganite were published in 1999 (A3) and in 2000 (A5). The latter paper was a contribution to the memorial issue of Solid State Ionics in honour of late professor Per Kofstad, Oslo University. Kofstad died in the age of 67 in 1997. His book (Kofstad,1972) inspired more than one generation of scientists.

Since then, the sequential approach has been applied in a number of papers to describe pyrochlores (A7,A9), La-nickelates (A10), spinels (App.2) and $SrTiO_3$ with exclusion of a SrO rich phase , see App. 3 and the upcoming paper A151. Most of the cases dealt with in chapters 5-7 and the appendices are in the process of being published.

```
1 REM 28 august ITEK
2 REM (the new principle from 24 apr. 92)
3 REM Delocalised electron model
4 REM La1-xSrxMnyO3+-delta, 9 species perov8.bas
6 GOSUB 10000
10 PRINT " PROGRAMME PEROV8.bas SIMULATES La1-xSrxMnyO3+d PEROVSKITES"
15 GOTO 50
16 REM lines 20-40 for testing
20 F$="slam."
21 QS#=2.5E-12
22 QR#=4800000!
23 QI#=.008125
24 X=.1
25 Y=1
26 VS#=6
27 VE#=0
28 ST#=50
40 GOTO 100
41 REM end of test lines
50 PRINT" INPUT NAME OF DATAFILE:"
55 INPUT F$
56 PRINT" input your initials and the date ( no commas!!!)"
57 INPUT SLAM$
60 PRINT" input equilibrium constants KS, KR, Ki"
62 INPUT QS#,QR#,QI#
70 PRINT" input x and y in La1-xSrxMnyO3+d"
74 INPUT X,Y
100 GOSUB 1000
120 STOMI=4
122 STOMA =1
124 PMIN=2
126 PMAX=1E-25
150 REM branch for testing: goto 300
200 PRINT " input -log(value of vacancy concentration):min,max"
210 INPUT VS#,VE#
220 PRINT " input number of steps in Vox ( 50-200)"
240 INPUT ST#
300 I=0
309 V = 10^(-VS#+I*(VS#-VE#)/ST#)
310 O=3-V
311 IF V>10^(-VE#) GOTO 900
320 REM calculate Va and Vb from quadratic equation
325 GOSUB 4000
330 REM calculate [n] from quadratic equation
350 GOSUB 5000
360 REM calculate remaining concentrations
362 GOSUB 6000
375 STO=O/MN
376 REM TEST criteria on concentrations
377 IF STO>3.5 OR VA>1! GOTO 500
378 IF STO<2.5 GOTO 500
380 IF N<0! OR MN<0! OR VA<0! OR VB<0! GOTO 430
390 IF N=0! OR MN=0! OR VA=0! OR VB=0! GOTO 430
400 PO2# = (O/(N*N*V*QR#))^2#
402 IF STO<STOMI THEN STOMI=STO
404 IF STO>STOMA THEN STOMA=STO
406 IF PO2<PMIN THEN PMIN=PO2
408 IF PO2>PMAX THEN PMAX=PO2
409 GOSUB 12000
410 PRINT#1,ILT,STO!,VAK!,VAA!,VAB!,NEG!,HOLE!,MAA!
412 REM PRINT#1,pO2#,",",STO,",",V,",",VA#,",",VB#,",",N,",",P,",",MN
415 PRINT" solution found in step#:   ",I
420 GOTO 700
430 PRINT" no solution, negative concentrations!!!!"
432 GOTO 700
500 PRINT" calculation outside limits"
700 I=I+1
805 GOTO 309
900 CLOSE#1
902 PRINT" "
910 PRINT" END OF SIMULATION, DATA HAS BEEN STORED UNDER"
912 PRINT F$
920 PRINT" "
950 PRINT" solutions were found in pO2 range:"
952 PRINT "pO2   =  "PMIN," to  ",PMAX
954 PRINT " corr. to stoich.", STOMI," to  ",STOMA
999 STOP
1000 REM file manipulation
1010 OPEN "o",#1,F$
1020 PRINT#1,"filename: ",F$,SLAM$
1025 PRINT#1,QS#,QR#,QI#,X,Y
1030 PRINT#1,"  pO2            stoich            V          Va      Vb    n
  p   Mn"
1100 RETURN
4000 REM solution to quadratic eq. in Va
4010 A=1#
4020 B= (1#-Y)/Y
4030 C=-QS#/(V*V*V)
4040 VA#=-B/(2#*A)+ SQR(B*B/(4#*A*A)-C/A)
4054 VB#=1#-Y+Y*VA#
4056 SR=X*(1#-VA#)
4060 RETURN
5000 REM solution to quadratic eq. in [n]
5010 A=1#
5020 B=X*(1#-VA#)+3#*VB#+3#*VA#-2#*V
5030 C=-QI#
5040 N=-B/(2#*A) + SQR(B*B/(4#*A*A)-C/A)
5100 RETURN
6000 REM calculate remaining concentrations
6010 P=QI#/N
6012 IF X=0 THEN LA=1-VA
6014 IF X=0! GOTO 6030
6020 LA=SR*(1/X-1)
6030 MN = 1-VB
6100 RETURN
10000 DEFDBL V,N,P,A,B,C,X,Y
10100 RETURN
12000 REM change in format before print out
12010 ILT!=PO2#
12020 VAK!=V
12030 VAA!=VA#
12040 VAB!=VB#
12050 NEG!=N
12060 HOLE!=P
12070 MAA!=MN
13000 RETURN
20000 STOP
```

Figure 4.2. One of the first Basic-codes for defect chemistry modelling using the sequential method, written Summer 1992. Size of a GWBASIC interpreter at the time: 83 kB, size of the PEROV.BAS program: 2780 bites.

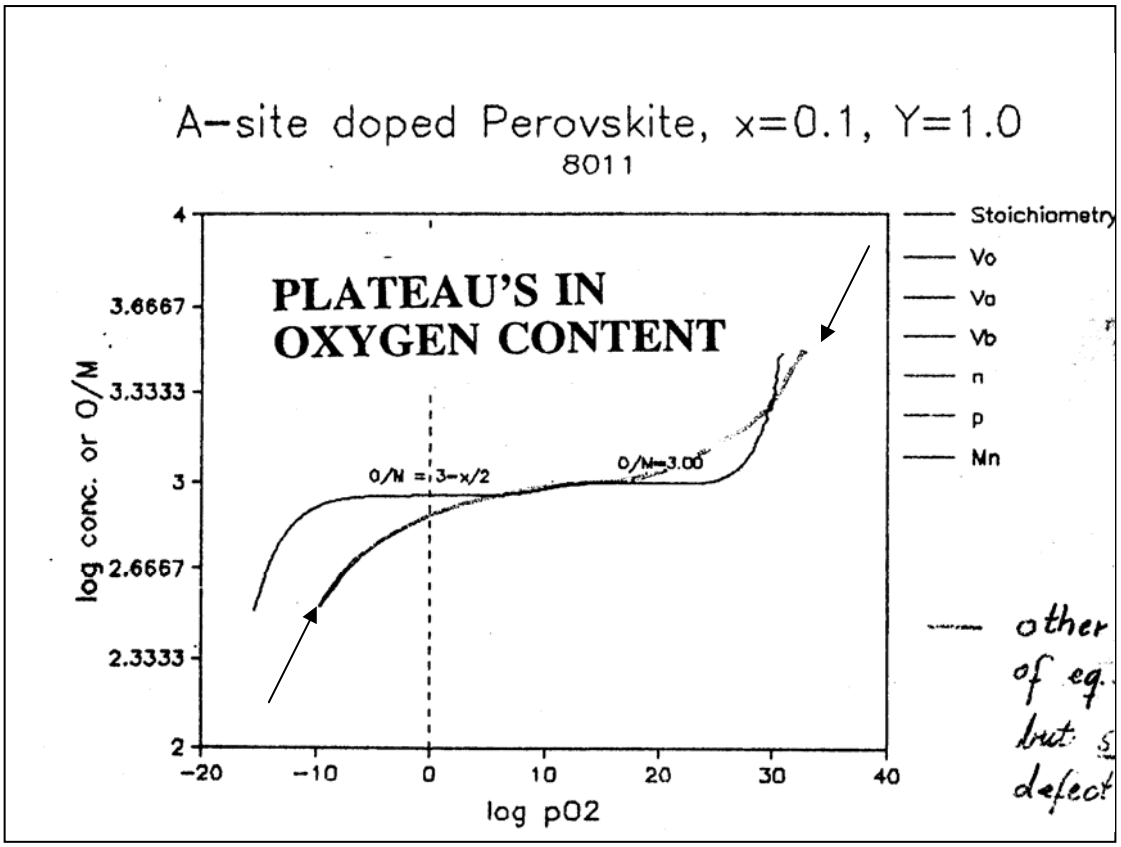

Figure 4.3. Simulated oxygen stoichiometry curves for a perovskite $A_{0.9}B_{0.1}MO_3$. Often two plateaus are observed experimentally, but if the three oxidation states of M have comparable energies the plateaus merge, as for curve marked with arrows. (Note added in proof). From the 1992 Proceedings paper (A63).

The salient features of the sequential method are as follows:

Mathematical foundation of the "Sequential" technique

Spinolo and Anselmi-Tamburini (1995) justifies the method with reference to the "implicit function theorem", see paragraph 4.3. Qualitative, hand-waving, arguments by the present author are found above, in 4.2, and in papers A3, A5.

Physico-chemical foundation of the "Sequential" technique

In case one chooses the oxygen vacancy concentration or the hole or electron concentration as independent variable, it is clear that these relate to the chemical activity of oxygen in the gas phase in a monotonic manner. Stated alternatively: the Fermi level varies monotonically with pO_2.

Advantages of the "Sequential" technique

High computational speed, transparency of mathematics and easy to do yourself.

Disadvantages of the "Sequential" technique

i) A solution of the equations, giving directly the equilibrium concentrations at a pO_2 matching that of an experiment is not obtained; by adding a simple macro/subroutine one can obtain this, see (Song, 2003).

ii) Sometimes a sequential solution is seemingly impossible to achieve. A few examples will be given. In the study of protons in perovskites (A3) no solution was possible for fixed pO_2; The solution for fixed pO_2 was therefore obtained by interpolation, which is safe but tedious. Likewise, at fixed pO_2, concentrations as function of temperature can not be found by the sequential method.

Unsolved cases: Mixed proton -Hydride case and protonic conductors at fixed pO_2.

4.3 Studies published by others using similar sequential type of method

Under this heading we will, among other things, try to clarify the problem of, who "invented" the sequential method.

Henny Bouwmeester[32] of Twente University, NL informs that he and van Hassel used a similar numerical procedure around 1992, but explicit statements in the open literature has not been found. Bart van Hassel et al. did employ a similar "inverse" thinking by using the oxygen nonstoichiometry as the integrating variable in their flux-equation, their eq (11), in stead of using the pO_2 in their work on oxygen permeation in Ca- doped $LaCrO_3$ (1993a). Hassel et al's subsequent work on ferrite-, manganite and cobaltite perovskites (1993b), however, does not explain how the defect equations were solved. Neither is van Hassel specific on this point in a earlier proceedings paper (1992).

Ofer Porat wrote a Ph.D. thesis in 1994[33] and published a paper a year later with Riess, where a sequential type of method is used (Porat, 1994,1995). In a subsequent paper with Harry Tuller, Porat applied a sequential solution to pyrochlores and U-doped ceria. (Porat,1997). He arrived at a master equation to be solved after substitution into the ENC of 6th degree in the electron concentration, *n*, but the expression was only second order in the "variable" pO_2. In other words, by guessing a value for *n*, pO_2 can be found, where-after the remaining defect concentrations are then calculated easily. It should be stressed that Porat & Tuller were only able to derive this algorithm by assuming the host lattice oxygen concentration to be constant (i.e. applying a Brouwer approximation)[34].

Two papers, advocating the sequential method, have appeared from the group of Giorgio Mario Spinolo in Milan (Spinolo,1995,1997). Spinolo et al state that " it becomes impossible to obtain an exact analytical solution"[35] of the form $c_i = F_i(\ldots, pO_2)$, as the number of defect equilibria increases. This is only partly correct- insofar as the polynomial may be higher order than 4th. In the 1995 paper they deal with a generic oxide MO_2 under reducing conditions. The oxide lattice is assumed perfect, as is the cation lattice- the defects are interstitial metal ions, of which 5 charge states are specified. This set of equations is only easily solved due to the assumptions that the chemical activities of the host ions are unity. All species can then be formed by reaction with oxygen or electrons. By assuming that the electron concentration is a "strictly monotonically decreasing function" they solved the concentrations one by one for a chosen value of n. The underlying mathematical principle is described as the "implicit function theorem", which expresses that if the function $n = F(\text{constants}, pO_2)$ exists, then the function $pO_2 = F'(\text{constants}, n)$ also exists, and expresses the same relationship. The simulated concentrations, on a mole fraction basis, are in the ranges $10^{-9}<n<10^{-4}$ and for the interstitial metal ions with charges $0\leq z\leq+4$, they find $10^{-18}<[M_i^{z\bullet}]<10^{-2}$. Their choice of equilibrium constants thus leads to a system in the dilute regime.

---

[32] Private communication from Henny Bouwmeester 2004.
[33] Not available to the author.
[34] The general solution for oxides described by Sasaki & Maier (1999b), could only be obtained via the same assumption that [Oo] is either constant or do not enter the equilibria at all. Sasaki& Maier did however not solve for pO_2, but for the hole concentration by iteration.
[35] Possibly they meant *expression* and not *solution*.

The success of the sequential technique is, however, not restricted to selecting a variable, the concentration of which varies monotonically as function of partial pressure of oxygen (or other gas, or electron concentration), as claimed in (Spinolo,1995a). In case a variable is chosen that goes through a maximum or a minimum in the pO_2 range of interest, eg. the Mn^{3+} concentration in a small polaron description of doped LSM, then, for each test value of the variable $[Mn^{3+}]$ we assume, there will be two valid solutions for pO_2. We are thus generating two branches of the concentration versus pO_2 curve in one go. This is for instance employed in the paper of Poulsen and Søgård (A10) on La(Sr)Fe(Co)O_3.

Spinolo et al, anyhow, do not seem to have used their approach a lot, - it is applied in a paper on the defects in $BaCuO_2$ (Spinolo, 1995b). By the way, (Poupon,1999) appears to be one of the few, except for the present author, who refer to Spinolo's work in their work on the defects in Al- and Nb-doped SnO_2.

In conclusion, the sequential method seems to have been developed independently in several groups during the early and mid 1990-ties. The systems treated in the present authors' papers, especially those being able to handle a Schottky equilibrium papers A3, A5, are of higher complexity than the cases treated by Spinolo and Porat.

The author's paper and algorithm for proton conducting perovskites, A3, is the basis of the paper from Balachandran's group at Argonne Nat. Labs, where they calculate the flux of protons over a membrane exposed to a gradient in pH_2 (Song, 2003). The model is coded and solved in C-language.

Tsur & Randall includes the authors algorithm in their papers on $BaTiO_3$ (Tsur,2001) and in their more general paper with the title "A universal analytical approach to defect chemistry of $A^{2+}B^{4+}O_3$ perovskites" (Tsur,2000).

The authors small polaron algorithm for perovskites, A5 is currently in use by N. Grundy, ETH, Zürich, Wærnhuus, NTNU Trondheim (Wærnhuus,2004), and by R. Glöckner IFE, NO. The author's $La_{2-x}Sr_xNiO_{4\pm\delta}$ algorithm, A10, is also being used by groups at Imperial College, London and the University of Barcelona.

4.4 Other methods for solving mathematics of defect models

As mentioned in the introduction, the days of using Brouwer approximations, iteration methods on high order polynomials, or homemade algorithm's such as the authors, soon belong to antiquity. Complete software packages from T. Norby, Oslo, Norway and J. Abrantes, Aveiro, Portugal will overtake the field in a few years time. The solid state chemistry literature does show some attempts to present such more complete codes already. A few examples will be given – the mathematical foundations of the respective methods are not always accounted for in the respective papers. General equation solvers can nowadays cope with non-linear cases – most of them are based on minimisation of the sum of squared errors of the N equations, which are typed in without rearrangement. The problem encountered is that of weighing the various equations: conservation equations are differences between numbers of comparable magnitude, whereas the mass-law equations deal with either

very small or excessively large numbers, depending on the choice of concentration unit. This opens a way to possible errors and/or numerical instabilities. Kevane, treated analytical expressions for oxygen vacancies and electrical conduction in metal oxides, with focus on Ceria , and included three stages of ionisation of the oxygen vacancy: $V_O^{\bullet\bullet}$, $V_O^{\bullet}$ and V_O^{x}. A cubic equation in the electron concentration resulted, and was solved via the trigonometric solution (Kevane, 1968)[36]. Schober & Wenzl (1995) made use of the commercial SEQS computer program in their work on protons in perovskites. Stone describes how to handle complex chemical equilibria, using the Newton-Raphson iteration method (Stone,1966). Ling took a statistical thermodynamic approach, to modelling reduced Ceria, 5 mol% Ca-doped Ceria (Ling,1994a) and $LaCrO_3$ (Ling,1994b)). The mathematical method used was a conjugate gradient method. Nobody has really commented or tested Ling's approach, which seems to be forgotten also by himself. Treating the corundum case, α-Al_2O_3, Lagerlöf & Grimes handled a model with 27 species and 24 mass action law expressions (Lagerlöf,1998), but again the reader is has no chance to verify the computations.

A paper by Estonian Lott and Turn (1999) presented a code, which was able to handle systems of equal or higher complexity, but the software appears not to have been employed further. They illustrated the method by simulating Cu-, Al-, Bi- and Cl codoped ZnO. One of the most thoroughly described defect chemistry cases appears to be that of doped $SrTiO_3$ by Moss & Härdtl (Moos,1997), who estimated numerical values to all energies and entropies for the equilibria and transport properties. But the numerical code for calculating concentrations was not disclosed.

In common to the above mentioned approaches, is the lack of transparency of the software,- and the fact that it is extremely difficult for other researchers to test the sensitivity of the model and validity of the results, unless they are in procession of the named software and a competing software. In chapters 5,6 and 7 we will address the problem of testing various defect models, since the sequential method provides us with a manageable way.

Starting 2002 with the study of Grundy et al. on the La_2O_3-SrO system (Grundy,2002), we will begin to see more applications of the "The compound energy formalism" to defect chemistry problems, which can be handled by the Chalphad-software (Hillert, 2001). Recently a paper on the defect chemistry of $LaMnO_3$ is in the press (Grundy 2004). A collaboration between the author and N. Grundy was agreed late 2004 to investigate to what extent our different model tools describe the same reality and result in comparable output.

[36] Several interpretations, eg the log pO_2 log sigma 1/5 dependence, were in error, cf. Chapter 7.

No-one is perfect

5. Why ideality often appears to apply in defect chemistry modelling

5.1 General comments

Numerous oxygen stoichiometry data sets are in literature analysed as obeying ideality, meaning that the mass action law is found to be fulfilled, when representing (unknown) chemical activities by mole fractions or site occupancies[37], see for instance (Bakken et al, 2002) on chromite- and manganites- perovskites, Mizusaki et al. (1984) on manganites, and (Kuo,1989) on chromites. The applicability of the mass action law to the chemistry inside and/or on the surface of a solid can be arrived at by definition of virtual chemical potentials (Kröger et al, 1956,1959, 1974) or by kinetic arguments. For a general, treatment of thermodynamic modeling of solid solutions, but not highlighting defect aspects, see (Ganguly, 2001).

The good apparent agreement between experimental data and the calculated stoichiometry is usually displayed in oxygen stoichiometry or deficiency δ versus log pO_2 diagrams – both quantities may however be subject to experimental errors. A special concern is the following fact: often the oxygen content is not known on an absolute scale, but is assigned a limiting value at some high or low pO_2 – for perovskites such as acceptor doped $La_{1-x}Ca_xCrO_{3-\delta}$, δ is often defined equal to zero for materials equilibrated in air (Larsen, 1997), (Boroomand, 2000). When data obtained at different temperatures are analyzed, the authors often succeed to represent the temperature dependence of the equilibrium constant by one enthalpy and one entropy of reaction as extracted from van't Hoff plots. However, very seldom these thermodynamic quantities are compared with integral heats and entropies of formation obtainable from calorimetry (Bakken,2004). It is indeed fascinating, that ideality by and large is obeyed for so many solid systems, in contrast to the non-ideal behavior observed in most concentrated liquid electrolytes. The absence of a solvent probably plays an important role here.

In a zero'th approximation, it is tempting to rationalise ideality by the high ionic strength in solids, since all host ions are present in high content, equivalent of many moles/liter; - defect concentrations may on the other hand be low, but the defects often have a high self-diffusion coefficient. The defects thereby experience an average field from the other ions most of the time. Finally one may choose not to speculate on assigning activity coefficients to virtual species, such as vacancies or electron holes, thus taking the pragmatic decision of treating everything on an equal and most simple basis.

[37] Activity of component i : $a_i = \gamma_i X_i$. X_i is some concentration measure. Activity coefficient $\gamma_i = 1$ in an ideal solution.

5.2 Regular solution analysis of non-stoichiometric $SrFeO_{3-\delta}$

The dilemma of deciding if a non-stoichiometric oxide is indeed behaving ideal or not, will be addressed using precision data taken[38] from a new coulometric and calorimetric study of non-stoichiometric $SrFeO_{3-\delta}$ (Bakken,2004). The conductivity and Seebeck effect of mildly doped strontium ferrate has also been studied by the author (A2).

For an archetype oxide $ABO_{3-\delta}$, where A is divalent and redox stable, we have in the simplest approach the following equilibrium controlling the oxygen deficiency:

$$O_O^X + 2B^X \Leftrightarrow V_O^{\bullet\bullet} + 2B^{|} + 1/2\ O_2(gas) \qquad (5.1)$$

$$K_{redox} = \frac{[V_O^{\bullet\bullet}]\,[B^{|}]^2\,P_{O2}^{1/2}}{[O_O^X]\,[B^X]^2} \qquad (5.2)$$

This small polaron model is further described by the relations

Oxygen site: $[V_O^{\bullet\bullet}] = \delta \Rightarrow [O_O^X] = 3-\delta$;
ENC: $2[V_O^{\bullet\bullet}] = [B^{|}]$;
B-Site occupancy: $[B^X] + [B^{|}] = 1$

This leads to an expression for K_{redox} involving only one variable, the deficiency δ

$$K_{redox} = \frac{4\delta^3 P_{O2}^{1/2}}{(3-\delta)\,(1-2\delta)^2} \qquad (5.3)$$

The above treatment follows the traditional, ideal formulation of the mass action law, where a concentration independent equilibrium constant K_{redox} should apply.

Since an experiment delivers values of δ as function of partial pressure of oxygen at a given temperature, one measurement will in principle be sufficient in order to establish a value of K_{redox}. More stoichiometry data are of course usually available. Equation (5.3) is cubic in δ, and thus has analytical roots. A test of the validity of the simple, ideal description can either be done by making a least squares fit, and then plot measured and calculated stoichiometry as function of log pO_2, see Figure 5.2 – or one can calculate the value of K_{redox} straight from eq. (5.3), point by point from each pair of (δ, pO_2) data, and then inspect if a constant value of K_{redox} is obtained, irrespective the value of δ, conversely the partial pressure. The latter method is here suggested to be more sensitive, and is illustrated in Figure 5.1 below, and further discussed in 5.3.

[38] Data was digitised from a gif-picture of Figure 12 of (Bakken ,2004) using the shareware *Data Thief II*-software.

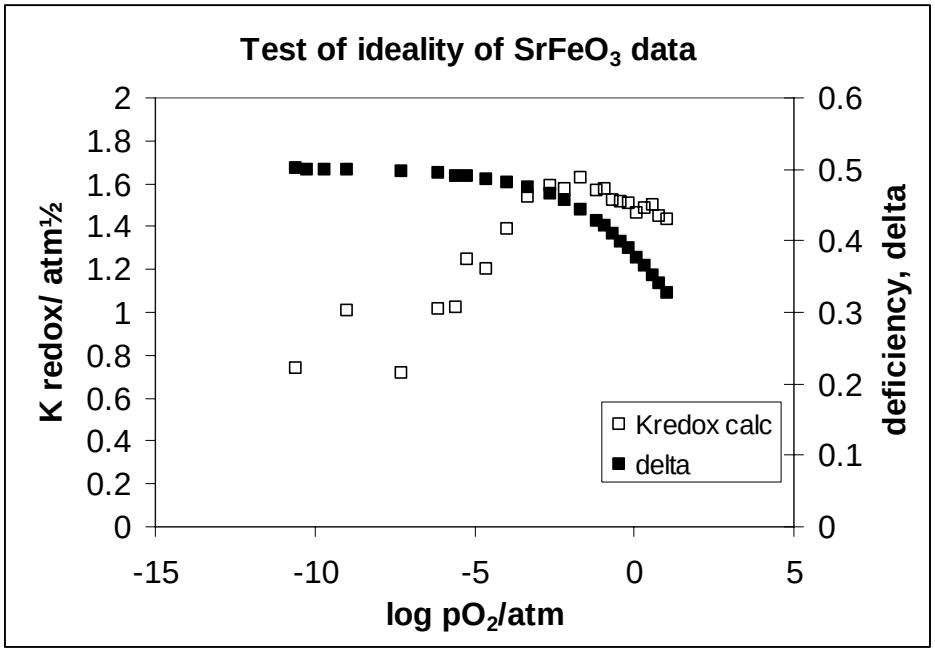

Figure 5.1. Stoichiometry data and calculated "ideal" equilibrium constant K_{redox} of $SrFeO_{3-\delta}$ at 1223K. Data digitized from (Bakken,2004).

The following is observed from Figure 5.1: i) for $pO_2 > 10^{-2}$ atm. one equilibrium constant $K_{redox} = 1.5 \pm 0.1$ $atm^{½}$ can represent all data. A larger scatter of K_{redox} is seen at low pO_2, when δ approaches or gets below 0.5. This is unavoidable due to the term $(1-2\delta)$ in the denominator of eq. (5.3). It should be stressed that this simple model is *not applicable at all* to stoichiometries with $\delta>0.5$, as no divalent B nor electrons are included in the simple model. Bakken (2004) also find that their data can be modeled by *one* constant, as shown in Bakken's original Figure 10.

The data could as well be modeled by the general small polaron algorithm LSM234, as described in paper A5. This model can however also handle reduction beyond the plateau, where $\delta > 0.5$.

Table 5.1. Input for modeling of $SrFeO_{3-\delta}$ at 1223K, with the general perovskite code LSM234 (ref A5).

Sr- Doping level	A/B-ratio	$K_{schottky}$	K_{redox} /$atm^{½}$	K_i
1	1	$<10^{-30}$	1.4	$< 10^{-6}$

The choice of constants shown in Table 5.1, i.e. the very low $K_{schottky}$, ensures that cation vacancies are completely negligible, i.e. $[V_{Sr}^{||}]$ and $[V_{Fe}^{||||}]$ are below 10^{-12} mole fraction. The charge disproportionation, $K_i = 10^{-6}$ for

$$2\ Fe^{|} = Fe^{||} + Fe^{X}; \qquad K_i = [Fe^{||}] * [Fe^{X}]/ [Fe^{|}]^2 \qquad (5.4)$$

is set low and gives at most 0.1 at % divalent iron, Fe^{II}, even at the most reducing conditions, 10^{-11} atm. The influence of the magnitude of the charge disproportionation constant, K_i, is further visualized in Figure 5.2. It is seen that the upper pO_2 branch is left unchanged, even when K_i varies 2 orders of magnitude. It can be concluded that the measurement range down to $pO_2 = 10^{-11}$ atm. contains no information on the possible magnitude of K_i. It should be noted that $SrFeO_3$ at subambient to very low temperatures displays a completely different chemistry with charge disproportionation of Fe(IV) into Fe(III) and the unusual state Fe(V), as shown by numerous ^{57}Fe Mössbauer studies (Demazeau,1995).

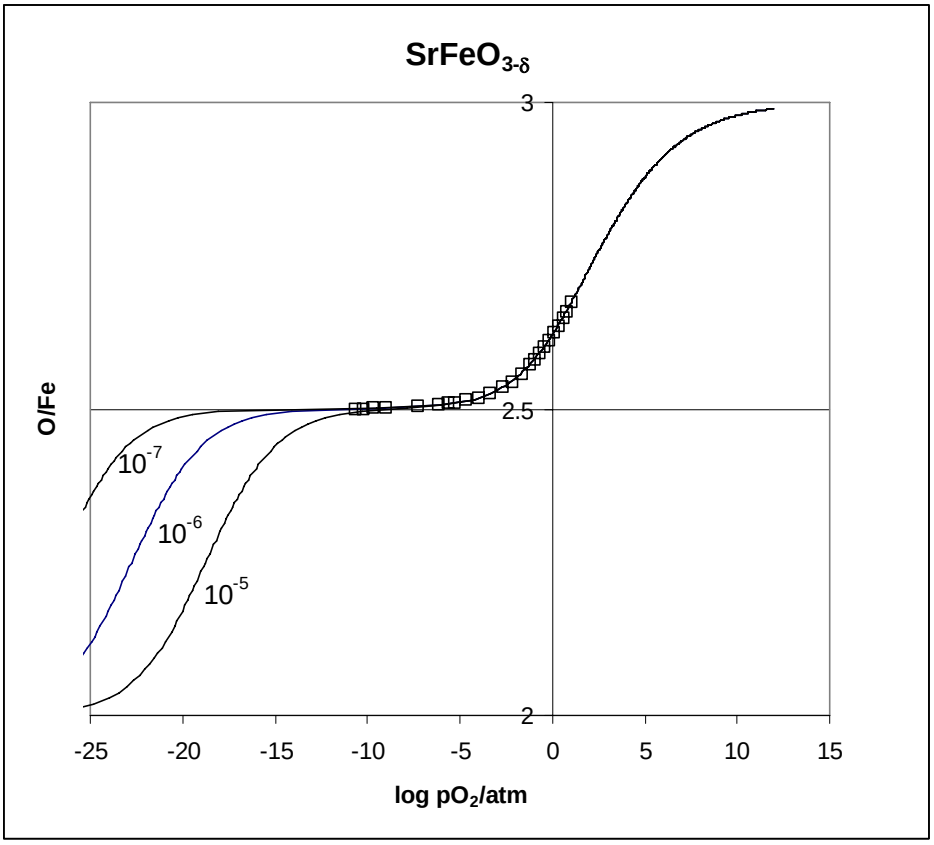

Figure 5.2. Calculated (LSM234)-code, paper A5, and observed oxygen stoichiometry in $SrFeO_{3-\delta}$ at 1223K. Input as in Table 5.1, but for three different cases of K_i , the charge disproportionation constant. Data digitised from (Bakken, 2004).

Now, the problem encountered by Bakken et al. (2004), is that the value of K_{redox} is not the one expected from calorimetry. They therefore developed a regular solution model for $SrFeO_{3-\delta}$. A regular solution between the two end members $SrFeO_{2.5}$ and $SrFeO_3$ is obeying the relations $\Delta S_{excess,mix} = 0$, i.e. $S_{mix} \equiv S_{ideal,mix}$, and $\Delta H_{excess} \neq 0$; whereas but $\Delta H_{excess,ideal} \equiv 0$.

.

The authors arrived at a partial pressure versus δ relationship, their equation (11), looking as follows:

$$\log pO_2 = 1/(RT\ln(10))\{4\Delta_f G_m^{O}(ABO_3) - 4\,\Delta_f G_m^{O}(ABO_{2.5}) + (16\delta-4)\Omega_B\} +$$

$$4\{\log(1-2\delta)-\log(2\delta)\}-2\log(\delta/(3-\delta) \qquad (5.5)$$

Here the term $(16\delta-4)\Omega_B$ relates to the excess enthalpy of mixing of Fe3+ and Fe4+ ions, and the $\Delta_f G_m^{O}$ - terms give the non-configurational Gibbs energies of formation.[39]

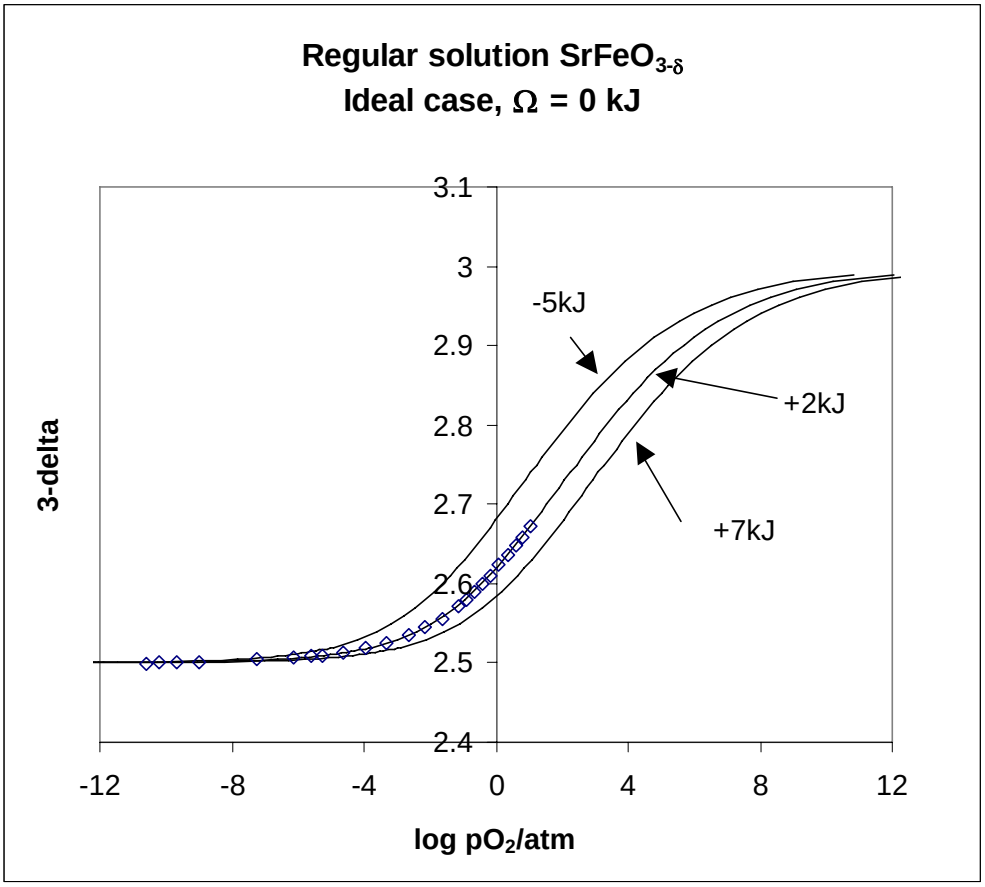

Figure 5.3. Simulation of oxygen deficiency for three different equilibrium constants, expressed as $\Delta_f G_m^{O}(ABO_3) - \Delta_f G_m^{O}(ABO_{2.5})$. The interaction constant, Ω_B, in eq. (5.5) is set to zero, in which case eq. (5.5) mimics ideality.

From Figure 5.3 it appears that the ideal solution model *produces a curve shape*- which matches the data and different values of the equilibrium constant for reduction

[39] The two end members are assumed to have no disorder on the O-sites.

will just translate the curve towards higher pO_2, the more unfavorable , i.e. the more positive Δ G for reduction becomes.

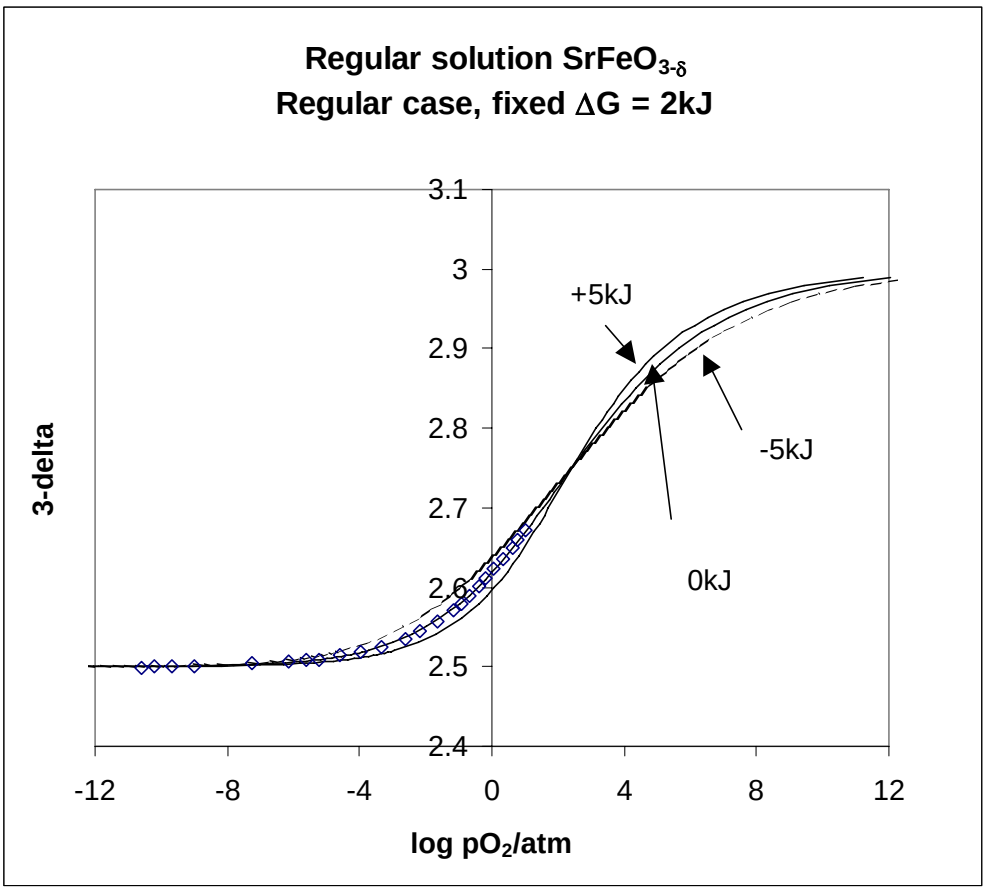

Figure 5.4. Regular solution modelling of $SrFeO_{3-\delta}$ at 1223K. Various values of the interaction parameter Ω_B , in eq. (5.5) are tested.

From Figure 5.4, as well as from the original Figure 12 of (Bakken et al, 2004), it appears that when $\Omega_B \neq 0$, i.e. the solid solution is assumed non-ideal, but precisely a regular solution, *then a different curve shape* will result, which do not match the observations. The present author summarises that $SrFeO_{3-\delta}$, at least from a practical point of view, behaves and can better be described as an ideal, than as a regular solution. This is so, since the data set can be described better with just one parameter, K, than with two parameters, K and a non-zero value for Ω_B. The author is not exactly an expert in thermodynamics and has no answer to the dilemma. It is likely that many data sets, hitherto considered as obeying an ideal mass action law formulation would not pass as ideal, if subjected to the way of analysis underlying Figure 5.1, i.e. the equilibrium constant is calculated point by point and compared.

An answer to the title question of this chapter “Why ideality often appears to

apply in defect chemistry modelling" could be: Many data are indeed satisfactorily described as ideal, - the limited precision and amount of data do not allow us to sort out if true, systematic deviations or random ones are present.[40]

Kröger (1977) suggested the idea that two opposing phenomena for electronic defects are at play: that of Debue-Hückel screening and that of Fermi degeneracy of the electronic levels (Rosenberg,1960). This should have the effect that the chemical potential of electronic defects can be described well by the ideal relationship $\mu_e = \mu^O_e + k\ln(n_e)$ up to much higher electron concentrations, n_e, than one would initially expect. The current author can not understand this thinking.

Next chapter will deal with deviations from ideality, and other means of handling them.

[40] A situation in analogy to the saying " *Healthy* people are *sick* people, who have not been checked carefully enough".

Viel Geschrei und wenig Wolle

6. Handling deviations from ideality

6.1 General remarks

When data and model calculations don't match, there may be shortcomings on both sides. The model may even be in error or self-contradictory. We will assume that the latter category has been eliminated. The data may be corrupt or contain systematic or random errors, or data are not representing a true chemical equilibrium. For the reduction of undoped CeO_2, for instance, Kevane (1963) and Riess (1987) reported the slope of logδ vs. log pO_2 close to -1/5 in their respective studies. Wang et al. observed a slope of –1/4.6 for doped Ceria $Ce_{0.9}Gd_{0.1}O_{2-\delta}$ at 700 ^{O}C (Wang,1998). For a thorough review on Ceria consult the paper by Mogensen, (2000). Standard defect theory predicts a slope of -1/6 for undoped ceria at low degrees of reduction, and -1/4 for doped ceria, but no model discussed so far[41] for ceria have resulted in a -1/5 slope, extending over several decades of partial pressure of oxygen. This paradox stems from lack of imagination. If one studies the defect chemistry literature on the reduction of rutile TiO_2, a defect mechanism has indeed been suggested, which involves interstitial titanium, $Ti_i^{\bullet\bullet\bullet\bullet}$, and results in that "magic" slope of -1/5 (Gautron,1981). An argument for a -1/5 slope goes as follows:

Table 6.1. Defect model leading to an "unusual" partial pressure dependence

Reduced $TiO_{2-\delta}$, understood as $[(1- 5/2\delta)\ Ti_{Ti}^{X}\ (2\delta)Ti_{Ti}'\ (\delta/2)Ti_i^{\bullet\bullet\bullet\bullet}]O_{2-\delta}$

where $\delta = [Ti_{Ti}']/2$

$5\ Ti_{Ti}^{X} + 2O_O^{X} \Leftrightarrow Ti_i^{\bullet\bullet\bullet\bullet} + 4Ti_{Ti}' + O_2$ (gas)

$$K_{reduction} = \frac{[Ti_i^{\bullet\bullet\bullet\bullet}][Ti_{Ti}']^4\, pO_2}{[Ti_{Ti}^{X}]^5\ [O_O^{X}]^2}$$

$[O_O^{X}]$ is constant in this model and $[Ti_{Ti}^{X}] \approx$ constant at low degrees of reduction and the ENC reads

$[Ti_i^{\bullet\bullet\bullet\bullet}] = 4[Ti_{Ti}']$, and we therefore obtain

$K_{reduction} \propto [Ti_i^{\bullet\bullet\bullet\bullet}][Ti_{Ti}']^4\, pO_2 = 4[Ti_{Ti}']\,[Ti_{Ti}']^4\, pO_2 = 4[Ti_{Ti}']^5\, pO_2$

leading to $\log([Ti_{Ti}']) \propto \log pO_2^{-1/5}$ q.e.d.

[41] With the exception of (Kofstad,1967), who however operates with mysterious *singly* and *doubly* charged Ce in interstitial positions.

The fluorite structure does in principle have room for interstitial cations, but the interstitial model sketched above would lead to a shrinkage of the sample upon reduction due to elimination of unit cells – which is against reality. We do not argue here that the rutile model of Table 6.1 applies to Ceria,- the only point made is that, contrary to categorical statements in literature[42], defect models do exist, which results in –1/5 slopes.

Obviously, utmost care in data collection, and selection of model(s) should be observed, before one jumps to the conclusion that a non-ideal model is required for the interpretation of the data. The core of the problem is exactly the following: how to recognise, when non-ideality is at play, or alternatively, a new and more complex , but still ideal, defect chemistry than initially assumed, should be applied?

True deviations from ideality should *primarily* be treated using non-ideal solution theory, such as the regular solution model dealt with in paragraph 5.2 (Bakken, 2004). Recent high temperature solution calorimetry on YSZ and Y-doped HfO_2 showed a strong negative interaction parameter Ω of –93.7, and –155 kJ/mole, respectively, (Lee,2004a,b) indicative of non-ideality. Recent EXAFS-studies also clearly demonstrates that the assumption that the oxygen coordination around the host cations (Zr or Hf) and that of the dopant, Y, on the average should be identical, is not a valid one (Ishizawa,1999). A recent factor group analysis of the Raman active vibrational modes of YSZ by Glerup, Nielsen and the author (Glerup,2004) corroborates the EXAFS conclusion that YSZ is not a simple solid solution- there are different preferred local arrangements around host and dopant cations with occupation on split atom positions.

Disagreement between model and experiment can in a *second* approach be removed by introduction of activity coefficients as discussed in 6.2.

A *third* option for treating apparent deviations from ideality will also be commented on: that of inclusion of more defect species/equilibria into the model as discussed in 6.3. Whether on chooses 1) the non-ideal solution-, or 2) the activity coefficient-expansion, or 3) inclusion of more equilibria in describing the data - they all add more adjustable parameters in their models. Many would, incorrectly, claim that the credibility of the model thereby decreases. However, do we have a guarantee that Nature is simple?

6.2 Invoking activity coefficients in defect chemistry

The thermodynamic activity of species i, a_i, is traditionally defined via

$$a_i = \gamma_i \bullet c_i, \qquad (6.1)$$

where c_i is a concentration measure, and the activity coefficient, γ_i, for an ideal solution is unity by definition throughout a concentration range. In "real" solution chemistry γ_i can be greater or smaller than unity.

[42] Statements in literature

The equilibrium constant based on activities can be split into two components, as defined in eq. (6.2). A test of a given defect model to see, whether experimental data can be described by an ideal model, i.e. a constant $K(c_i)$, was outlined in paragraph 5.2, notably in Figure 5.1.

$$K_{red}(a_i) \equiv F(T) = K(\gamma_i) \bullet K(c_i) \qquad (6.2)$$

If $K(c_i)$ turns out to vary with the degree of non-stoichiometry, but one insists that this model be correct, then $K(\gamma_i)$ should display an exact reciprocal variation in order that the product of the two, $K(a_i)$, stays constant.

We will perform such a test on oxygen stoichiometry data of undoped and Gd-doped Ceria obtained by TGA by (Wang,1998) and (Bevan,1964). Also included in this analysis are coulometric titration data at $1000^{O}C$ of $Ce_{.82}Gd_{0.18}O_{2-\delta}$ (Zachau-Christiansen, 1996). The latter data set is exceptional, in that it contains more than 500 data points in the pO_2 range from 10^{-3} atm – 10^{-20} atm. The data sets are shown in Fig 6.1 and 6.2.

The reduction reaction will read the same as for the perovskite case in eq. (5.1).

$$K_{red} = \frac{a(V_O^{\bullet\bullet})\ a^2(Ce_{Ce}^{|})\ pO_2^{1/2}}{a(O_O^{x})\ a^2(Ce_{Ce}^{x})} = \frac{\gamma(V_O^{\bullet\bullet})\ \gamma^2(Ce_{Ce}^{|})}{\gamma(O_O^{x})\ \gamma^2(Ce_{Ce}^{x})} \frac{[V_O^{\bullet\bullet}]\ [Ce_{Ce}']^2\ pO_2^{1/2}}{[O_O^{x}][Ce_{Ce}^{x}]^2} = K_\gamma \bullet K_x \qquad (6.3)$$

Writing the composition as $Ce_{1-x}Gd_xO_{2-\delta}$ then K_x reads

$$K_{x,sp} = \frac{\delta(2\delta-x)^2\ pO_2^{1/2}}{(2-\delta)\ (1-2\delta)^2} \qquad (6.4)$$

Full reduction to Ce^{3+} corresponds to $\delta = 0.5$. Since we know δ in each point we can calculate K_x in each point based on mole fractions.

The reduction may also be written as a large polaron reaction

$$O_O^{X} \Leftrightarrow V_O^{\bullet\bullet} + 2e^{|} + 1/2\ O_2(gas) \qquad (6.5)$$

The mass action law then takes the slightly simpler form:

$$K_{x,lp} = \frac{\delta(2\delta-x)^2\ pO_2^{1/2}}{(2-\delta)} \qquad (6.6)$$

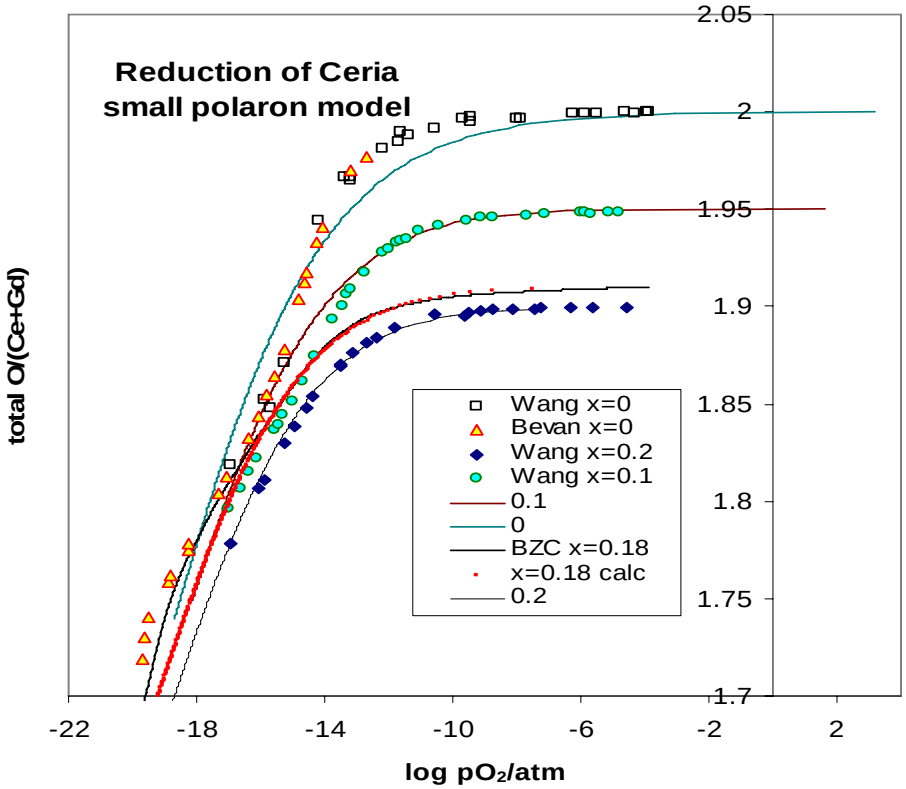

Figure 6.1. Oxygen stoichiometry data for $CeO_{2-\delta}$, $Ce_{0.9}Gd_{0.1}O_{2-\delta}$, $Ce_{0.82}Gd_{0.18}O_{2-\delta}$ and $Ce_{0.8}Gd_{0.2}O_{2-\delta}$ at around $1000^{O}C$, cf point iii) on page 48. Full curves are calculated using a small polaron model, eq.(6.4) with $K_{x,sp} = 8 \bullet 10^{-11} atm^{½}$, except for x = 0.18, where $K_{x,sp} = 5 \bullet 10^{-11} atm^{½}$.

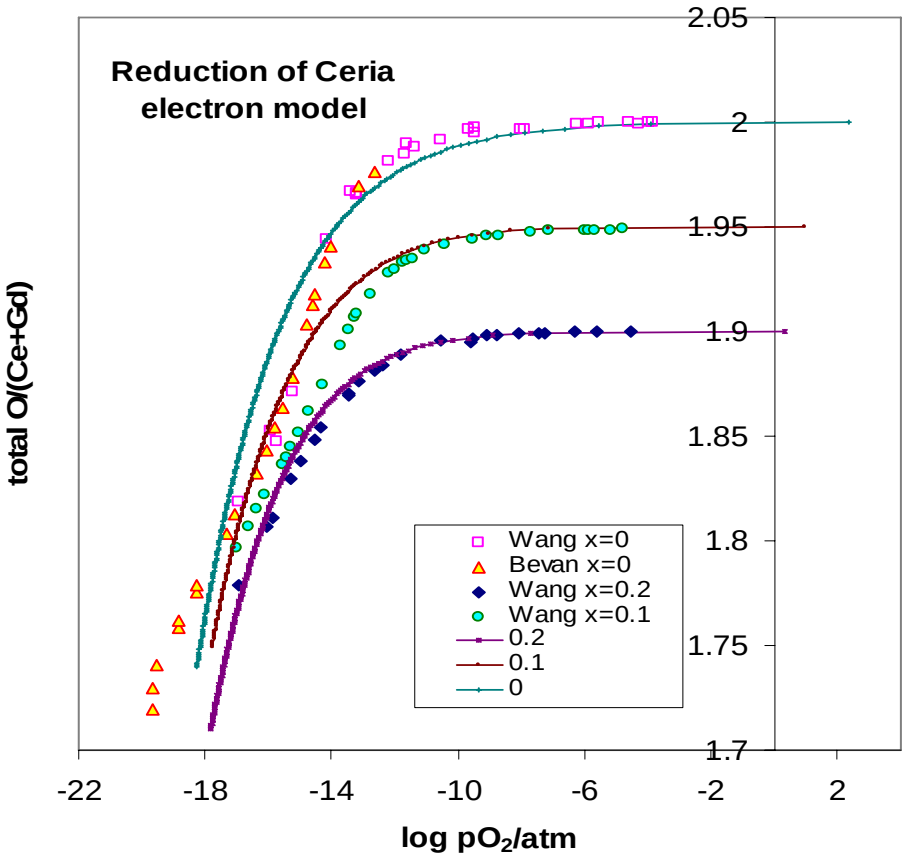

Figure 6.2. Oxygen stoichiometry data for $CeO_{2-\delta}$, $Ce_{0.9}Gd_{0.1}O_{2-\delta}$ and $Ce_{0.8}Gd_{0.2}O_{2-\delta}$ at around $1000^{O}C$ (see text). Full curves are calculated using a large polaron model, eq.(6.6) with $K_{x,lp} = 3 \bullet 10^{-11}$ $atm^{½}$.

The theoretical curves in Figures 6.1 and 6.2 were generated by tuning the value of K_x to reproduce the x = 0.2 data set as well as possible. The following observations and conclusions can be drawn from the Figures:

i) Deviations from the ideal curves are most severe at low pO_2. The large model polaron, Fig. 6.2, furthermore generates a somewhat steeper curve shape at low pO_2, than does the small polaron model, Figure 6.1.

ii) The deviations get more and more pronounced the lower the Gd- content. We therefore conclude that association of oxygen vacancies, $V_O^{\bullet\bullet}$ and the aliovalent dopant $Gd^{|}$ is not an important issue here. Wang et al arrives at the same conclusion (Wang,1998). The good oxygen ion conduction in Gd-doped Ceria is another indication that association = trapping of oxygen vacancies by the dopant is unimportant.

iii) The data obtained by the three research groups are not internally consistent. The Wang data for x = 0 were collected at 1000 ^{O}C but superimpose well on the Bevan data recorded at 1023 ^{O}C, as if there was no temperature dependence. The Zachau-Christiansen data for x = 0.18 were obtained at 1000^{O}C but required a value of K_x = 5 •10^{-11}atm^{½}, whereas Wang's data for x=0.2 requires $K_{x,sp}$ =8 •10^{-11}atm^{½}. This is a problematic fact, since the ideal mass action law obviously fits quite good, the higher the Gd-concentration, and we would expect close to the same numerical value of K_x to apply both to the x=0.18 and x= 0.20 data sets. We conclude that some of the data sets , if not all, are biased by experimental errors- and we are left with the very unsatisfactory situation that we do not know, which is the more reliable data set!

Now we will return to the main issue of the current paragraph- how do we interpret an apparent variation of K_x with the degree of non-stoichiometry? Figure 6.3 shows the variation of the concentration equilibrium constant K_x for the five data sets also displayed in Figure 6.1.

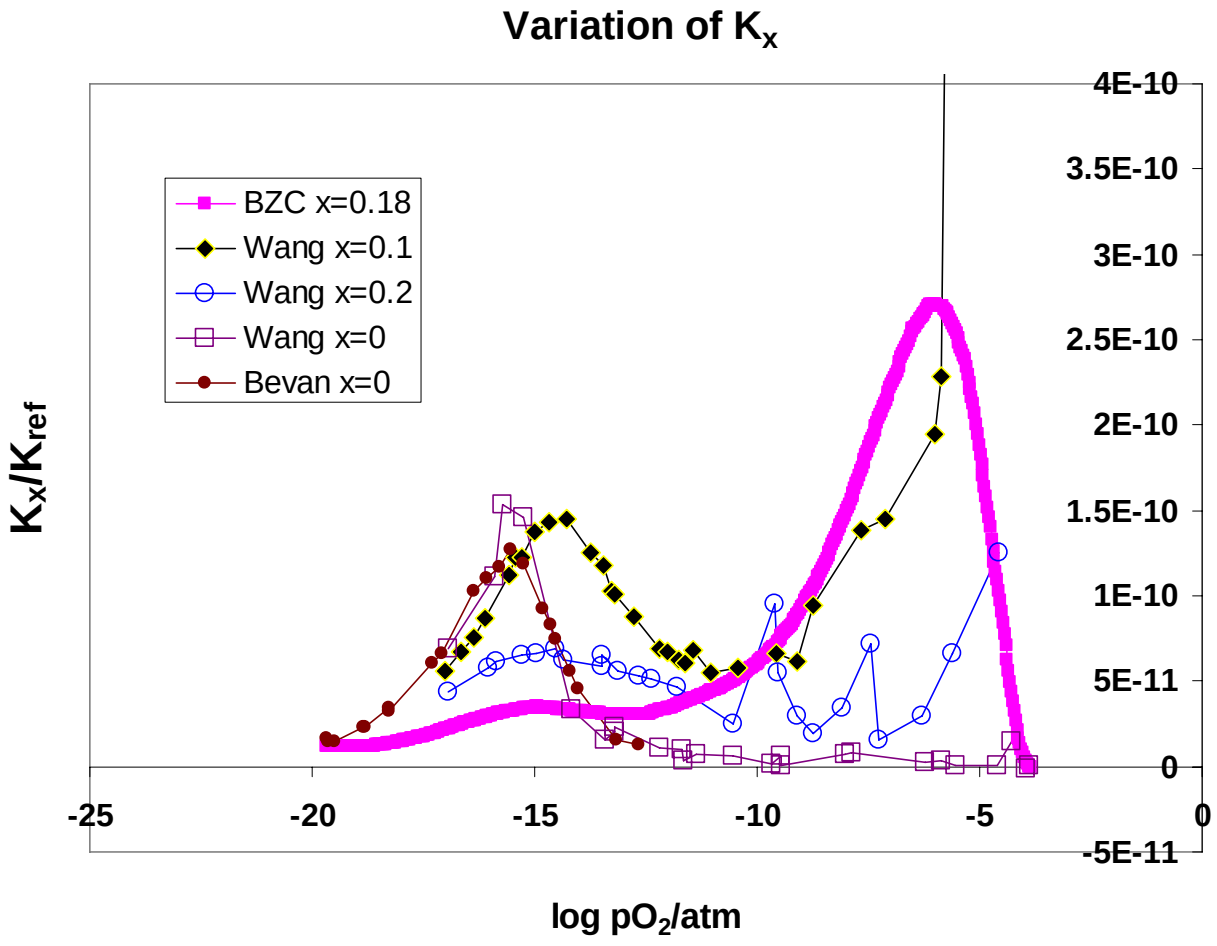

Figure 6.3. Oxygen stoichiometry data for reduction of $Ce_{1-x}Gd_xO_{2-x/2}$ compounds at around 1000 ^{O}C. The calculated value of K_x from equation (6.4), normalized to the value of K_x at the third highest oxygen pressure.

The plot of calculated K_x values from eq. (6.4) as function of pO_2 , Figure 6.3, reveals very large variations from constant K_x behaviour. For comparison, each curve of K_x-values were normalized with respect to the K_x at the third to the highest oxygen pressure. The values of K_x are peaking at $pO_2 \approx 10^{-15}$ atm. for all compositions and possibly also around 10^{-5} atm. The latter data range show large scatter, except for the x = 0.18 series. This is likely to be due to small systematic errors influencing the calculation of K_x, since the term (2δ-x) is close to zero in eq. (6.4); the peaks around10^{-15} atm. however, are for sure a reality. If one still insists that the data were error-free, and the simple reduction reaction was in control, then in order for K(activity) to be constant we would have to demand $1/K_\gamma$ to vary in exactly this manner. We don't know how the activity coefficients of the individual ionic species should vary with concentration. For the activity coefficients for electrons in a solid Rosenberg (1960) has made an estimate. He found that the activity coefficient increases dramatically (monotonically), 2 orders of magnitude, going from the dilute regime to the situation, where the electron concentration approaches the number of available sites/cm^3. The only comforting thing in Rosenberg's treatment may be that the concentration, at which deviations from ideality take off, scales with $T^{3/2}$. This implies that this limit at 1200K is crossed at a concentration 8 x larger than it would be at 300K. It is doubtful if this extrapolation is permissible and if Rosenberg's treatment is applicable to solids of predominantly ionic nature.

Anyhow, we do certainly not expect K_γ to display a minimum and two maxima in the oxygen vacancy range 0.05 to 0.1 mole fraction, and that it should vary over more than two orders of magnitude. The conclusion we are forced to draw is that introduction of activity coefficients is not likely to be the answer in explaining the present data sets. It remains then to decide if the data are corrupted in some way – or alternatively that they reflect that a more complex defect model applies. Future will show.

6.3 Comment on adding more equilibria, maintaining ideality

Additional small polaron states can be introduced in cases, where the oxygen stoichiometry versus pO_2 data can not be modelled by two or three oxidation states. Paper A10 presents a case, where we deal with four oxidation states of Co and Fe. The stoichiometry curve can in principle show several plateaus, corresponding to stepwise well separated reduction reactions. One recent example is $Gd_{0.9}Sr_{0.1}Co_{0.2}Fe_{0.8}O_{3-\delta}$, which show three, possibly four, plateau's in the oxygen stoichiometry curve (Søgård,2005a). Battery materials operating at ambient temperature, on the other hand, quite often show this characteristic as protons or alkali ions are intercalated during discharge and when the material is investigated to the extremes of their stability range. This is the case for $Li_xMn_2O_4$,, when cycled in the full range $O \leq x \leq 4$ (Koksbang,1996).

There are substantial evidences that oppositely charged defects interact, i.e. are attracted to each other (Fergus,2003). Minervini (1999) recently published an atomistic computer simulation of clusters in M_2O_3 - doped ceria. Association of defects happens for electrostatic reasons – but the higher the temperature gets, this is counteracted for entropic reasons. The evidence stems primarily from spectroscopic-, conductometric- and structural experiments (EXAFS). Two or more nearest neighbour defects can behave like a electrical dipole, which can reorient by ions jumping in an electrical field as seen in thermally stimulated depolarisation current experiments on

fluoride ion conductors (Schoonman,1986). The association phenomenon is analogous to ion-pair formation in concentrated solutions and in polymeric Li-electrolytes (Yang,1995). It can be described in terms of additional chemical equilibria. The associate is thus defined as a new species, which occupies more than one lattice site. It has been realised that the main reason for the difference in oxygen ion conduction in otherwise similar structures, and for the same nominal concentration of potentially mobile oxygen vacancies, can be ascribed to association (trapping) of the oxygen vacancy by the lower valence dopant. Taking Gd-doped reduced Ceria as an example one might anticipate two 1:1 associates between Gd', respectively reduced Ce' and the oxygen vacancy; and three neutral 2:1 associates of the type Gd'- $V_O^{\bullet\bullet}$ -Gd', Ce'- $V_O^{\bullet\bullet}$-Ce', Gd'- $V_O^{\bullet\bullet}$ - Ce' and higher order clusters. The sequential solution technique can cope with such a myriad of equilibria[43] – where most other techniques fail.

Inclusion of more equilibria gives *a priori* a greater ability in adjusting a model to the experimental data. However, the shape of the calculated oxygen stoichiometry curve does not change dramatically, when associates are included: the main effect of postulating significant formation of associates between reduced host ions and oxygen vacancies is to translate the stoichiometry curve towards higher pO_2, compared to the case with no association.

One *principal* problem with inclusion of association equilibria is the underlying assumption that the involved cations should be free to rearrange as the oxygen vacancy concentration changes. Thus, a necessary shift must take place from cationic defects being predominantly involved in 2:1 associates at low [$Vo^{\bullet\bullet}$] to more 1:1 associates being formed at higher vacancy concentrations. In the definition of a 2:1 associate one must assume that the two cations are nearest neighbours on the cation sublattice; for the 1:1 associates to make sense we must require that there is *no* other cation of that sort in the nearest cation coordination shell. Since cations[44] usually have diffusion coefficients 10^6 times lower than for the oxygen vacancies and electrons, such a rearrangement is only possible at very high temperature or if equilibration time at lower temperatures approaches geological time spans. An early paper of the author, (A21, 1981) was an attempt to design a counting system for defects, which allows to handle defects and their first coordination sphere. Dissociation of defect associates in YSZ is believed to take place above some 700-800 ^OC , where the Arrhenius-type conductivity curves have a bend-over to a lower apparent activation energy around 0.6 eV. It is questionable if the Y-dopant distribution does rearrange over the time span of a few days, over which a typical conductivity experiment will run. Other ordering/segregation phenomena in YSZ, even at 1000^OC lead to a decrease of the ionic conductivity over the time span of months.

The gradual shift in concentration of 1:1 and 2:1 associates with reduction degree of Gd-doped Ceria is illustrated in Figure 6.4, using the parameters in Table 6.2. Note that there is no association assumed with reduced cerium ions in this simulation. Redistribution of Ce^{+3} should be much easier than that of Gd^{+3}, since the former process needs only transport of electrons, but no jump of cations.

---

[43] Se Appendix 5.

[44] Argument valid for fluorite and perovskite structures- not necessarily for other structures such as rock salt and spinel.

In conclusion it is found that association equilibria should be modeled under the heading of a frozen-in distribution of dopants. That is to say, one has to assume that the dopant is present in a frozen-in distribution of isolated defects, ready to form 1:1 associates and distant pairs of dopants able to form 2:1 associates.

Table 6.2. Input values for a simulation of reduced Ceria, used to generate Figure 6.4.

Dopant level	K_{redox}(atm-½)	K_1	K_2
Gd: x = 0.18	$5 \cdot 10^{11}$	$2.95 \cdot 10^{2}$	5.0

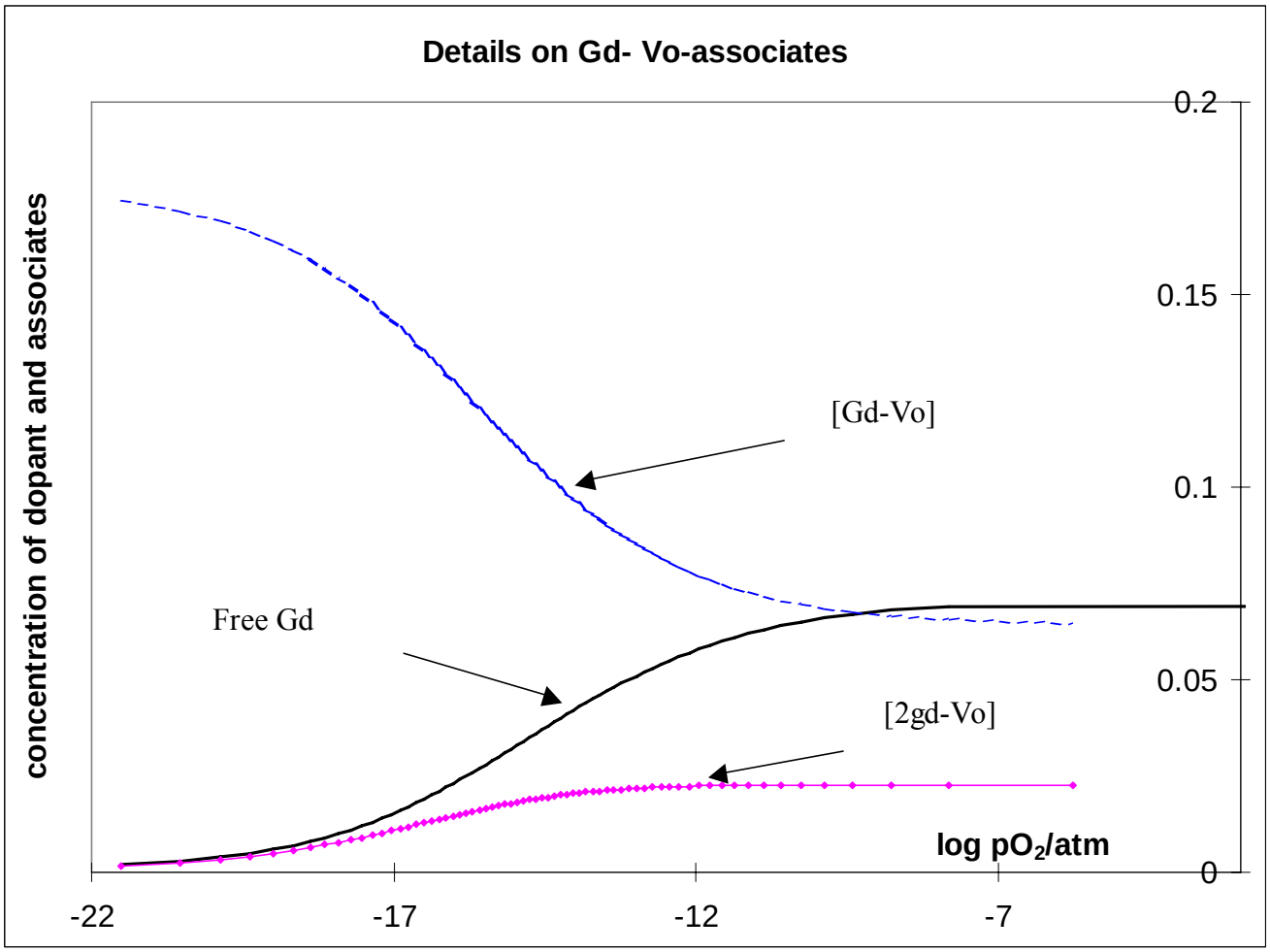

Figure 6.4. Simulated associate and free dopant concentration for CGO, using the equilibrium constants of Table 6.2.

All cats are grey in the dark

7. Coincidental resemblance of various defect models

This chapter will deal with comparison of defect models. In contrast to the cases discussed in the previous chapters, we will here concentrate on data sets, which follow theoretical model calculations nicely- but the dilemma is now that alternative model(s) fit equally well. The aim is thus to show that two or more models may describe equally well the same pO_2-dependent property, typically the oxygen stoichiometry curve. The models will be based on different definitions and species, leading to different mathematical relations. Several ways of comparison of models are employed:

i) Test of models on the same experimental data.
This path may be hampered by noisy data, systematic errors, or limited pO_2 and /or pH_2O ranges or a low number of data point. Three cases will be used: $SmMnO_3$, $NdMnO_3$ and $U_{0.8}Er_{0.2}O_{2\pm\delta}$.

ii). Test models on synthetic data.
One can generate data with one model and test if other models can describe the data. The problem of how to calculate "ideal" data is treated in Chapter 4 and in the enclosed papers. Large- and small polaron descriptions of perovskites a la $La/SrMO_3$. are investigated. Also the Lankhorst rigid band/itinerant electron model for highly non-stoichiometric doped La-cobaltites (Lankhorst,1997a,b) is commented on.

iii) Proving by algebra, the identity or difference of two models. We will not be able to prove the equivalence of two models in the true sense of the definition of *equivalence ≡ two mathematical or logical statements, linked so, that one is true, if and only if the other one is true*. This is because the leading idea of the present thesis is that of handling mathematical relations, which are **not** present in a *closed form*.
Two charge models for an oxidised fluorite structure oxide will be compared semi-analytically in Appendix 4.

The final paragraph, 7.4, deals with protonic defects in oxides and how to model them. Let the first element be the last one.

7.1 Test on real data, reduction of $SmMnO_3$ and $NdMnO_3$

It has been claimed for a long time that lanthanide manganite perovskites do *not* follow an ideal point defect model when reduced to $LnMnO_{3-\delta}$ following:

$$O_O^X + \mathbf{2}Mn_{Mn}^X \Leftrightarrow V_O^{\bullet\bullet} + \mathbf{2}Mn_{Mn}^{|} + 1/2\ O_2(gas) \qquad (7.1)$$

$$K = \frac{[V_O^{\bullet\bullet}][Mn_{Mn}^{|}]^2 P_{O2}^{1/2}}{[O_O^X]\,[Mn_{Mn}^X]^2} = \frac{4\delta^3 P_{O2}^{1/2}}{(3-\delta)(1-2\delta)^2} \qquad (7.2)$$

In order to repair on this one could invoke other ways of describing the state of charge on the Mn, see paragraph 7.3 for the full Monty, or one could i) assume that formation of associates between oxide ion vacancies and reduced manganese species takes place or ii) assume that arrangement of defects in superstructures or domains takes place. The association mechanism has been suggested for fluorite structure oxides, see previous chapter, and it was also the main conclusion in the work of van Roosmalen and Cordfunke (1991a,b) on $LaMnO_3$. They assumed that *all* created oxygen ion vacancies are tied up in forming a neutral simple cluster with two divalent manganese ions. The reduction will then have to be written

$$O_O^X + 2Mn_{Mn}^X \Leftrightarrow [Mn_{Mn}^{|} - V_O^{\bullet\bullet} - Mn_{Mn}^{|}] + 1/2\ O_2(gas) \qquad (7.3)$$

where the three species in [ ] on the RHS of equation (7.3) behaves like one structural and thermodynamic entity. The mass action law now takes a different form

$$K' = \frac{[Mn_{Mn}^{|} - V_O^{\bullet\bullet} - Mn_{Mn}^{|}]P_{O2}^{1/2}}{[O_O^X]\,[Mn_{Mn}^X]^2} = \frac{\delta P_{O2}^{1/2}}{(3-\delta)\,(1-2\delta)^2} \qquad (7.4)$$

Atsumi (1997) followed the procedure of van Roosmalen & Cordfunke(1991a,b), when analyzing all their data on the series $LnMnO_3$, where Ln = La, Pr, Nd, Sm and Y. It should be emphasized that the two models described above can not cope with the overstoichiometric cases, since no cation vacancies are included in the models. We will now show, by means of the small polaron code described in paper A5, that the above model is not the only one, which describe the TG data satisfactorily. The TG data of Atsumi et al are shown in Figure 7.1, replotted by the author. In order to simulate the substoichiometric range we suppress formation of cation vacancies by setting $K_{Schottky}$ to a very low number, see Table 7.1. The cation vacancy concentrations are thereby suppressed to a level below 10^{-13} mole%. Two major conclusions can be drawn from Figure 7.1:

i) The simple point defect model with only Mn2+ and Mn+3 can be simulated by the generalized code by assigning a low value to $K_i = [Mn_{Mn}^X]^2/([Mn_{Mn}^{|}][\,Mn_{Mn}^{\bullet}])$. The dashed curves in Figure 7.1 are *neither* here, *nor* in the article of Atsumi based on a least squares fit, - the K is chosen such that the curves pass through the experimental point at the lowest pO_2. The point model creates a wrong curve form, irrespective of the value of K in eq. (7.2) and fits very badly!

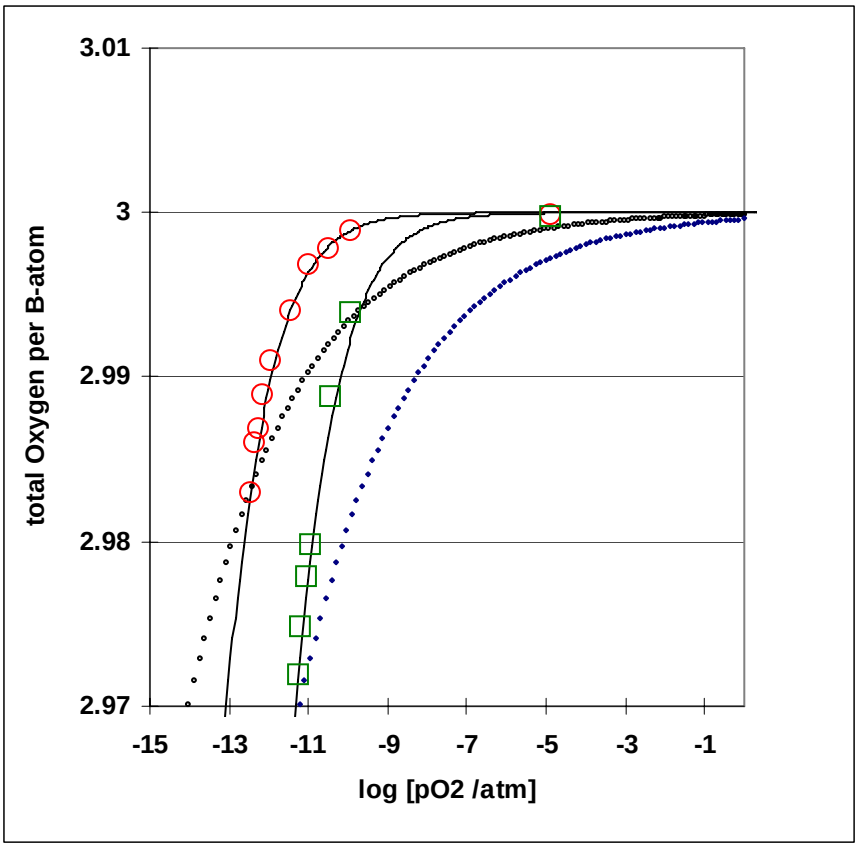

Figure 7.1 Comparison of two point-defect models for reduction of $SmMnO_3$ (□) and $NdMnO_3$ (O). TG data from Atsumi et al (1997). Dashed curves: simple model with only tri- and divalent Mn; Full curves: charge redistribution via the reaction $2Mn_{Mn}^{x} \Leftrightarrow Mn_{Mn}^{'} + Mn_{Mn}^{\bullet}$ included. Equilibrium constants are given in Table 7.1.

ii) The small polaron model of paper A5, where one more charged manganese species, $Mn_{Mn}^{\bullet}$, is included produces a proper curve shape – and with a suitable adjustment of K_{re}, see model 1 in paragraph 7.2, it can be shifted along the pO_2 axis to cover the observed data just as well as the cluster model of vanRoosmalen (1994).

Now, it may be objected that the 2:1 association model only makes use of one equilibrium constant to describe the data, whereas the present model, including a charge disproportionation, uses two constants. Therefore in the calculations underlying Figure 7.1 and 7.2, it is imposed that one of the equilibrium constants is set equal for both simulations, since they are closely related compounds.
Setting $K_{re}(SmMnO_3) = K_{re}(NdMnO_3)$ as in Figure 7.2 implies that the energy required for creating an oxygen vacancy and a reduced manganese species is identical in the two materials, but the internal charge redistribution on the Mn-site is influenced by the nature of the A-ion. Alternatively, setting $K_i(SmMnO_3) = K_i(NdMnO_3)$ as in Figure 7.1 implies that the energy of forming an oxygen vacancy is dependent on the type of A-ion. Since the effectiveness of packing of the larger A- and oxygen ions of comparable size is the governing principle in perovskites, we favour the latter formulation.

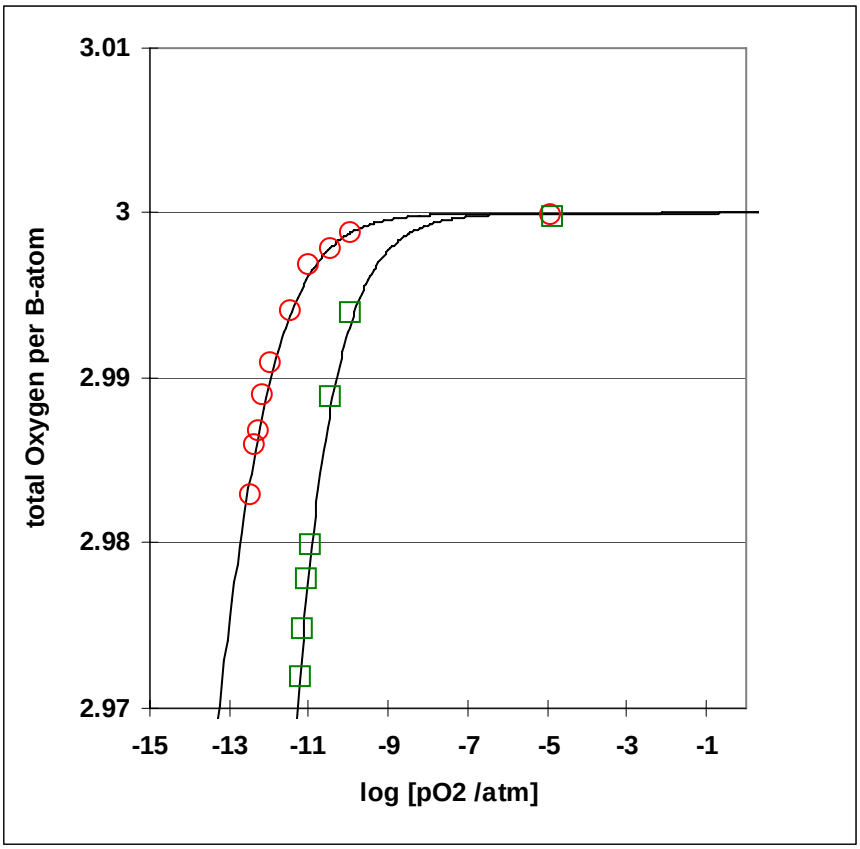

Figure 7.2 Reduction of $SmMnO_3$ (□) and $NdMnO_3$ (O). TG data from Atsumi et al (1997). Full curves are calculated with an alternative combination of equilibrium constants compared to Figure 7.1, see Table 7.1.

Finally, when comparing Fig 7.1 and 7.2 we arrive at the conclusion that within experimental errors, we are not able to distinguish which combination of equilibrium constants, out the two we have tested is the better one.[45]

[45] The author is aware of the recursive nature of this conclusion: proving that we can not prove anything. It is believed though that it can be fruitful to point out, where such recursive arguments are at stake, see (Hofstadter,1980).

Compound	$K_{schottky}$	$K_{redox}/atm.^{½}$	K_i	Figure	Type
$SmMnO_3$	10^{-35}	$3*10^{-7}$	0.1	Fig 7.1	CD
	10^{-35}	$4*10^{-8}$	0.6	Fig 7.2	CD
	10^{-40}	$1*10^{4}$	$1*10^{-7}$	Fig 7.1	Simple
$NdMnO_3$	10^{-35}	$4*10^{-8}$	0.1	Fig 7.1	CD
	10^{-35}	$3*10^{-7}$	0.0145	Fig 7.2	CD
	10^{-40}	$4*10^{2}$	$1*10^{-7}$	Fig 7.1	Simple

Table 7.1. Input values of equilibrium constants for generating the stoichiometry curves in Figure 7.1 and 7.2. Over-stoichiometry, i.e. formation of cation vacancies is suppressed completely by choosing very low values for $K_{schottky}$.
Key: CD = charge disproportionation on three Mn states plays a role; Simple = only tri- and divalent Mn are important.

7.2 Test on real data for over- and substoichiometric $U_{0.8}Er_{0.2}O_{2\pm\delta}$

Uranium dioxide maintains the cubic fluorite structure up to an oxygen content of approximately $UO_{2.25}$. This could in principle be explained by cation vacancies, i.e. the high oxygen content limit understood as $U_{0.888}\,\square_{\,0.112}\,O_{2.0}$, where $\square$ symbolises vacant cation sites. Overwhelming evidence, including the measured density>x-ray density points to a defect structure including interstitial oxygens of some form (Naito,1990). Interstitial oxygens may be viewed upon as being formed via uptake form the gas phase during oxidation, see eq. (1) in App. 1. Interstitial oxygens may equally well be present in sub-stoichiometric urania solutions, delivered through displacement of the reaction:

$$O_O^x \leftrightarrow V_o^{\bullet\bullet} + O_i'' \Rightarrow K_{Oi} = [V_o^{\bullet\bullet}]\,[O_i'']/\,[O_O^x] \qquad (7.5)$$

The stoichiometry data for $U_{0.8}Er_{0.2}O_{2+\delta}$, obtained at $1500^{O}C$ by Kim(1995) are shown in Figure 7.3. The data cover the stoichiometry range, O/(U+Er), from 1.977 to 2.034, so even for the lowest oxygen content the samples are on the average oxidised,- the stoichiometry, at which U is on the average +4, is $U_{0.8}Er_{0.2}O_{1.90}$. Kim et al found it necessary to divide the data treatment in two parts, corresponding to O/(U+Er) smaller or larger than 2.00. It is noticed from the original Figure 9 of the Kim's paper that the two model calculations applied do **not** meet at O/(U+Er) = 2.00, a fact which is not commented on in the paper.

The main problem of formulating a defect model for Urania valid at high temperature, i.e. 1200-1500 ^{O}C is that most inspiration leading to assumption of quite

complicated clusters of defects comes from structural studies by diffraction and electron microscopy carried out at room temperature (Willis,1987), or even as low as 80 K as in (Conradson,2004), in any case much lower than $1500^{O}C$. In this paragraph we show that a much simpler model gives an equally good description.

The essentials of Kim's model are: a Willis type of $[2:1:2]^{m-}$ cluster embracing 2 lattice and 3 interstitial oxygen sites, and a neutral associate involving pentavalent U i.e. $[Er'U^{\cdot}]^{x}$ exist in the over-stoichiometric region; Er' and neutral associate $[2Er'V_O^{\cdot\cdot}]^{x}$ are postulated in the sub-stoichiometric region. $U^{\cdot}$ and U^{x} are present in various concentration in both regimes.

The algorithm for solving two Urania models by the sequential procedure is given in Appendix I. No associates or clusters are involved, but both a one- and a two-electron oxidation of U^{+4} are investigated. The adjusted equilibrium constants of the two models are given in Table 7.2, and the resulting calculated stoichiometry curves are displayed in Figure 7.3. The general behaviour of the models are as follows: as K'_{ox} or K_U increases, the stoichiometry curve will move towards lower pO_2. As K_{Oi} increases one will observe that the hyper-stoichiometric branch will lift towards larger over-stoichiometry, whereas the hypo-stoichiometric branch will move only little. It is seen from Figure 7.3 that the two models fit well within the experimental range of oxygen stoichiometries. Figure 7.4 shows the corresponding Brouwer diagram for the U^{+4}/U^{+5} model of $U_{0.8}Er_{0.2}O_{2\pm d}$, at $1500^{O}C$.

Conclusions: i) a much simpler defect mechanism than the one "proven" by Kim et al. can explain both the low- and high pO_2 branches of the stoichiometry data; ii) within the experimental range of O/(U+Er), from 1.977 to 2.034 one can not easily distinguish between the penta- or hexavalent U model; iii) the hexavalent model extrapolates at high pO_2 to unrealistically high over-stoichiometries – therefore this model can possibly be discarded on this basis.

Table 7.2. Adjusted equilibrium constants for two defect descriptions of non-stoichiometric Er-doped Urania, x = 0.2.

Input for simulation in Figure 7.3	p=1 U^{+5}	p=2 U^{+6}
K'_{ox} [atm.$^{-½}$]	$1.1*10^{12}$	$1.3*10^{9}$
K_{Oi}	$5*10^{-7}$	$3*10^{-7}$
K_U	$8*10^{-4}$	$1.2*10^{-3}$

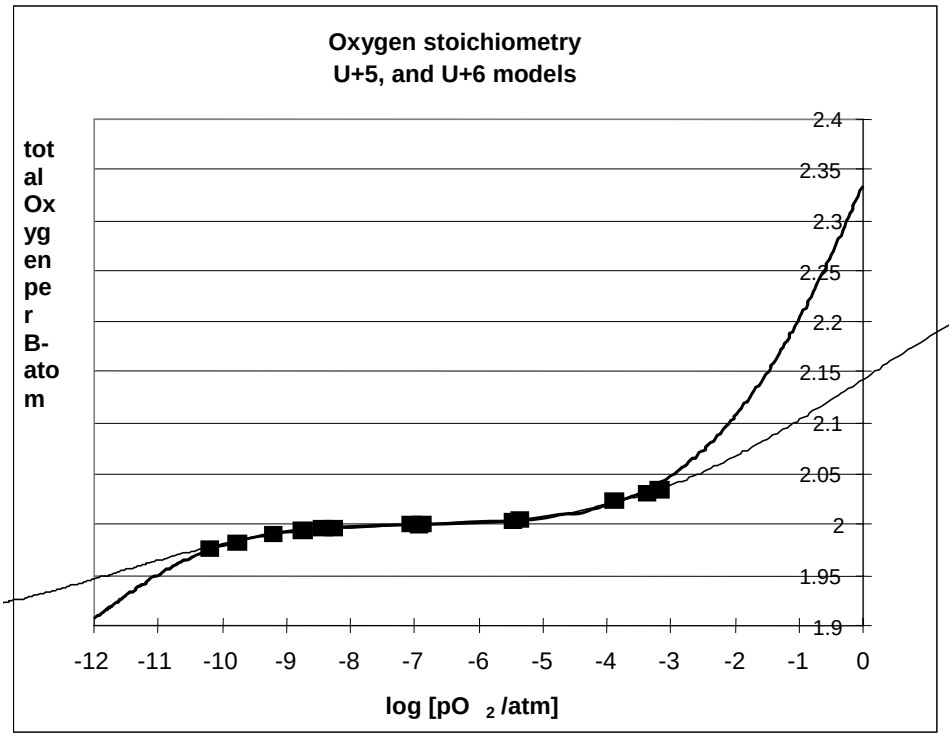

Figure 7.3. Observed (symbols) and calculated stoichiometry of $U_{0.8}Er_{0.2}O_{2\pm\delta}$, at 1500 ^{O}C (Kim,1995). Key: Thin line is U^{+5} model; thick line is U^{+6} model. Equilibrium constants as in Table 7.2.

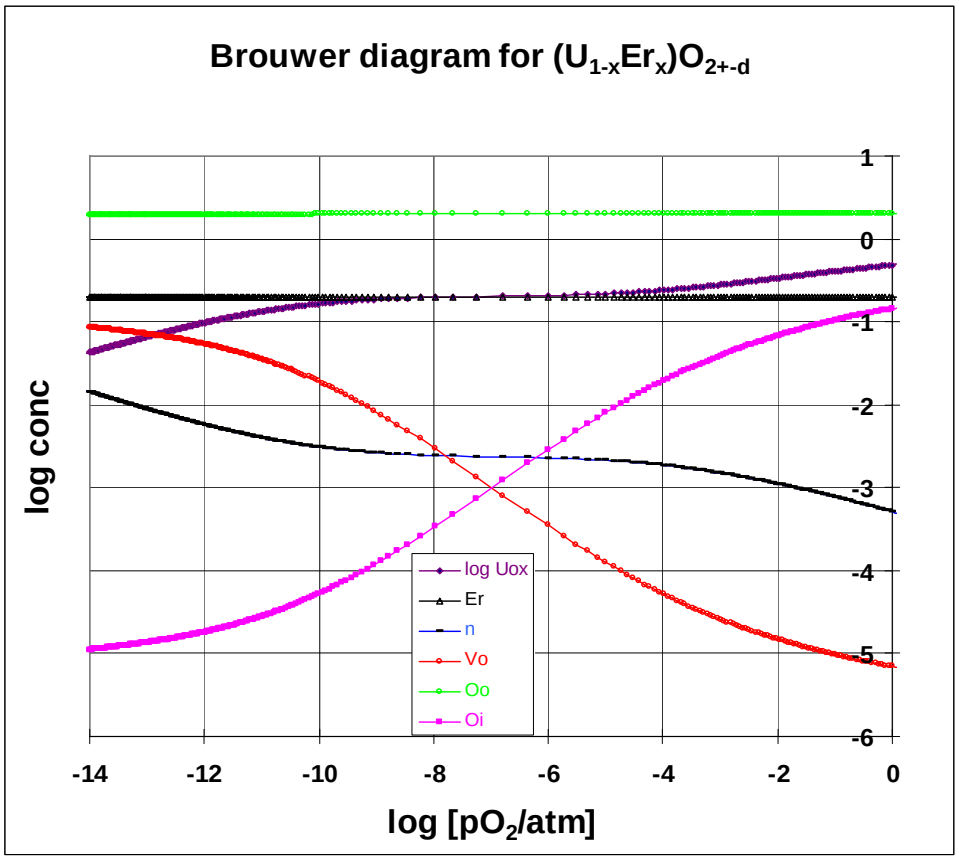

Figure 7.4 Brouwer diagram for the U+4/U+5 model of $U_{0.8}Er_{0.2}O_{2\pm d}$, at 1500 ^{O}C from the equilibrium constants of Table 7.2, case p=1.

7.3 Test of different valence state descriptions on synthetic data.

Chemists, like the author, will prefer to operate within the chemical- small polaron description- until proven wrong, whereas physicists and semi conductor people will as first choice operate with holes in the valence band and electrons in the conduction band when describing the conductivity, thermoelectric and other properties of a non-stoichiometric oxide. Strong evidence for one or the other may change ones point of view. Models can however be formulated, where the two types of view are mixed. There will arise *no* inconsistency in the mathematical description in such *mixed* models.

We will limit the discussion to cases of oxides, where there is only one type of reducible cation, typically a 3d-transition metal such as Fe, Mn, Ni or Co. The metal ion can be both reduced and oxidised, but will stay on the same crystallographic site - and the structure is preserved, with minor changes of the lattice parameters. The reduced state can then be represented either by an electron, e', or by a reduced cation $M_M^{'}$ = a small polaron. The oxidised state can be described as 1) an oxidized metal ion, $M_M^{\bullet}$ 2) a hole in a band, $h^{\bullet}$ or 3) as a small polaron on a partly oxidized lattice oxygen, $O^{\bullet}_O$. The latter species has resemblance to the peroxide ion O^{-}**.** Thus 2 x 3 ways of formulating a defect model for the system are possible even at this elementary level. These are outlined in Table 7.4. For each model two redox reactions must be specified, since *two* redox equilibria define *three* oxidation states.

Models #1, #4 and #6 will be compared in the following by simulation of a hypothetical perovskite. Equilibrium constants were chosen such that a very large variation in stoichiometry results, i.e. the O/M ratio is 2.5< O/M<3.5 in the pressure range 10^{-20} to 10^{2} atm of oxygen. The region 3<O/M<3.5 is possible via extensive formation of cation vacancies by a Schottky reaction. The lower limit O/M = 2.5 is the phase border to a Brownmillerite structure. The synthetic data were generated applying the sequential approach to the mathematics of the mixed e', $O^{\bullet}_O$ model #4.

From Figure 7.5 we observe that the "pure" small polaron model #1 can indeed reproduce the error-free synthetic data from model 4 down to a pO_2 of 10^{-16} atm. The "pure" electronic large polaron model #6 can reproduce the data generated by model 4 over the entire range.

It is concluded that the stoichiometry versus pO_2 relationship at high pO_2 can *not* tell us if a hole-description or a small polaron description $O^{\bullet}_O$ is the correct one. ESR and/or other spectroscopic evidence would probably give the answer for a given material. Appendix 4 gives further proof that although the definition of the mass law expressions are different, one may in practice observe that the two models coalesce.

A Rigid Band Formalism has been applied by Lankhorst et al. for the non-stoichiometry of La/Sr-cobaltites upon reduction (Lankhorst, 1997a,b). It is based on the assumption that itinerant ("metal like") electrons are donated to a rigid band formed between Co 3d-orbitals and O 2p-orbitals as the material is reduced and oxygen vacancies are formed. This raises the Fermi level (~chemical potential of electrons). The following expression for the relationship between stoichiometry, temperature and partial pressure of oxygen was derived:

$$\mu_{O2}^{oxide} = \mu_{O2}^{gas} = E_{ox} - (4(2\,[V_O^{\bullet\bullet}] - [Sr_{La}^{|}])/g(\varepsilon_F) \quad -TS_{ox} - 2RT\ln([V_O^{\bullet\bullet}]/(3 - V_O^{\bullet\bullet}]) \tag{7.6}$$

The partial pressure of oxygen is "hidden" in the μ_{O2}^{gas} parameter, which, at a given temperature, is obtained from standard thermodynamic tables. $[Sr_{La}^{|}]$ is the doping level. One virtue of the model is that it has only *three* adjustable parameters:[46] $g(\varepsilon_F)$ is the density of states of the Fermi level and E_{ox} and S_{ox} are energy and entropy terms associated with the oxidation written as

$$V_O^{\bullet\bullet} + 2e^{|} + 1/2\ O_2(gas) \Leftrightarrow O_O^X \qquad (7.7)$$

Søgaard et al. (2005) have recently applied the same analysis to cobaltite stoichiometry data obtained at Risø, and observed that the model only fitted well for temperatures higher than 800 ^{O}C. The same trend was also observed by Lankhorst. The energy, E_{ox}, was found to be in the range –200 to –300 kJ/mole in Søgaard's study study for dopant level $[Sr_{La}^{|}] = 0.15$ and 0.4. It should be independent on the dopant concentration. Lankhorst' data for $[Sr_{La}^{|}] = 0.2$; 0.4 show better consistency. The density of state $g(\varepsilon_F)$ showed a smaller variation in the two studies, i.e. 0.0147-0.019 mol/kJ. It is felt that the above treatment is a better description in the present case than a small or large polaron description: La-cobaltites are an exception, they show a true negative, metallic like temperature dependence- and the electrical conductivity is also exceptionally high- in excess of 2000 S/cm at 650 ^{O}C in air.

[46] Any of the models in Table 7.4 will require 4 constants to be known: two enthalpies and two entropies.

Table 7.4 Six choices for describing oxidation and reduction of a transition metal oxide, such as $La_{1-x}Sr_xMnO_3$, where the transition element shows ability to valence fluctuations. Key: sp= small polaron;
m= mixed; lp= delocalised large polaron or unspecified band type; * = compared analytically in Appendix 4.

Model	Reduced state	Middle state	Oxidised state	Type
1	$Mn_{Mn}^{\prime}$	Mn_{Mn}^{x}	$Mn_{Mn}^{\bullet}$	sp
	$O_O^x + \mathbf{2}Mn_{Mn}^x \Leftrightarrow V_O^{\bullet\bullet} + \mathbf{2}Mn_{Mn}^{\prime} + 1/2\ O_2(gas)$ $2Mn_{Mn}^x \Leftrightarrow Mn_{Mn}^{\prime} + Mn_{Mn}^{\bullet}$			
2	$e^{\prime}$	Mn_{Mn}^{x}	$Mn_{Mn}^{\bullet}$	m
	$O_O^x \Leftrightarrow V_O^{\bullet\bullet} + \mathbf{2}e^{\prime} + 1/2\ O_2(gas)$ $Mn_{Mn}^x \Leftrightarrow Mn_{Mn}^{\bullet} + \mathbf{e}^{\prime}$			
3	$Mn_{Mn}^{\prime}$	Mn_{Mn}^{x}	$O_O^{\bullet}$	sp
	$O_O^x + \mathbf{2}Mn_{Mn}^x \Leftrightarrow V_O^{\bullet\bullet} + \mathbf{2}Mn_{Mn}^{\prime} + 1/2\ O_2(gas)$ $Mn_{Mn}^x + O_O^x \Leftrightarrow Mn_{Mn}^{\prime} + O_O^{\bullet}$			
4	$e^{\prime}$	Mn_{Mn}^{x}	$O_O^{\bullet}$	m
	$O_O^x \Leftrightarrow V_O^{\bullet\bullet} + \mathbf{2}e^{\prime} + 1/2\ O_2(gas)$ $O_O^x \Leftrightarrow O_O^{\bullet} + \mathbf{e}^{\prime}$			*
5	$Mn_{Mn}^{\prime}$	Mn_{Mn}^{x}	$h^{\bullet}$	m
	$O_O^x + \mathbf{2}Mn_{Mn}^x \Leftrightarrow V_O^{\bullet\bullet} + \mathbf{2}Mn_{Mn}^{\prime} + 1/2\ O_2(gas)$ $Mn_{Mn}^x \Leftrightarrow Mn_{Mn}^{\prime} + h^{\bullet}$			
6	$e^{\prime}$	Mn_{Mn}^{x}	$h^{\bullet}$	lp
	$O_O^x \Leftrightarrow V_O^{\bullet\bullet} + \mathbf{2}e^{\prime} + 1/2\ O_2(gas)$ $nill \Leftrightarrow e^{\prime} + h^{\bullet}$			*

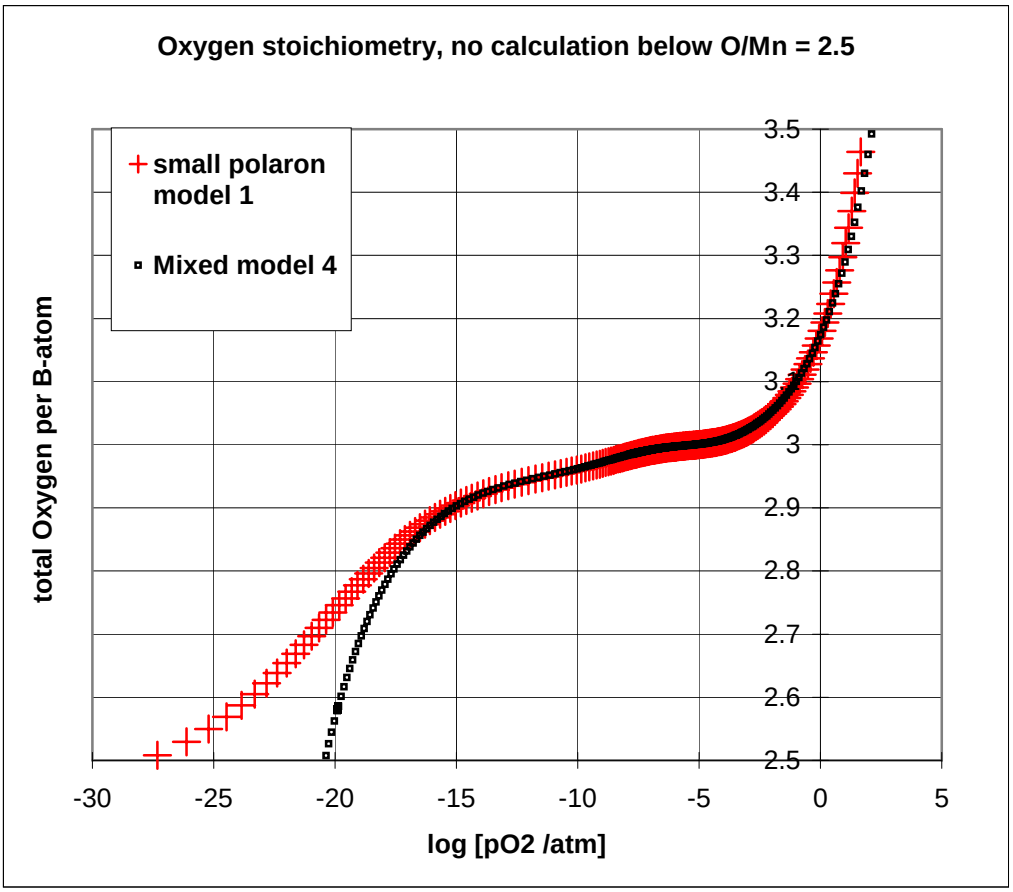

Figure 7.5 . Defect modelling of a Schottky-defect dominated acceptor doped perovskite $La_{0.9}Sr_{0.1}MO_{3\pm\delta}$. Synthetic data were generated by model 4, see Table 7.4. Equilibrium constants in model 1 were then adjusted, such that a perfect match occurs over some 16 decades in partial pressure of oxygen.

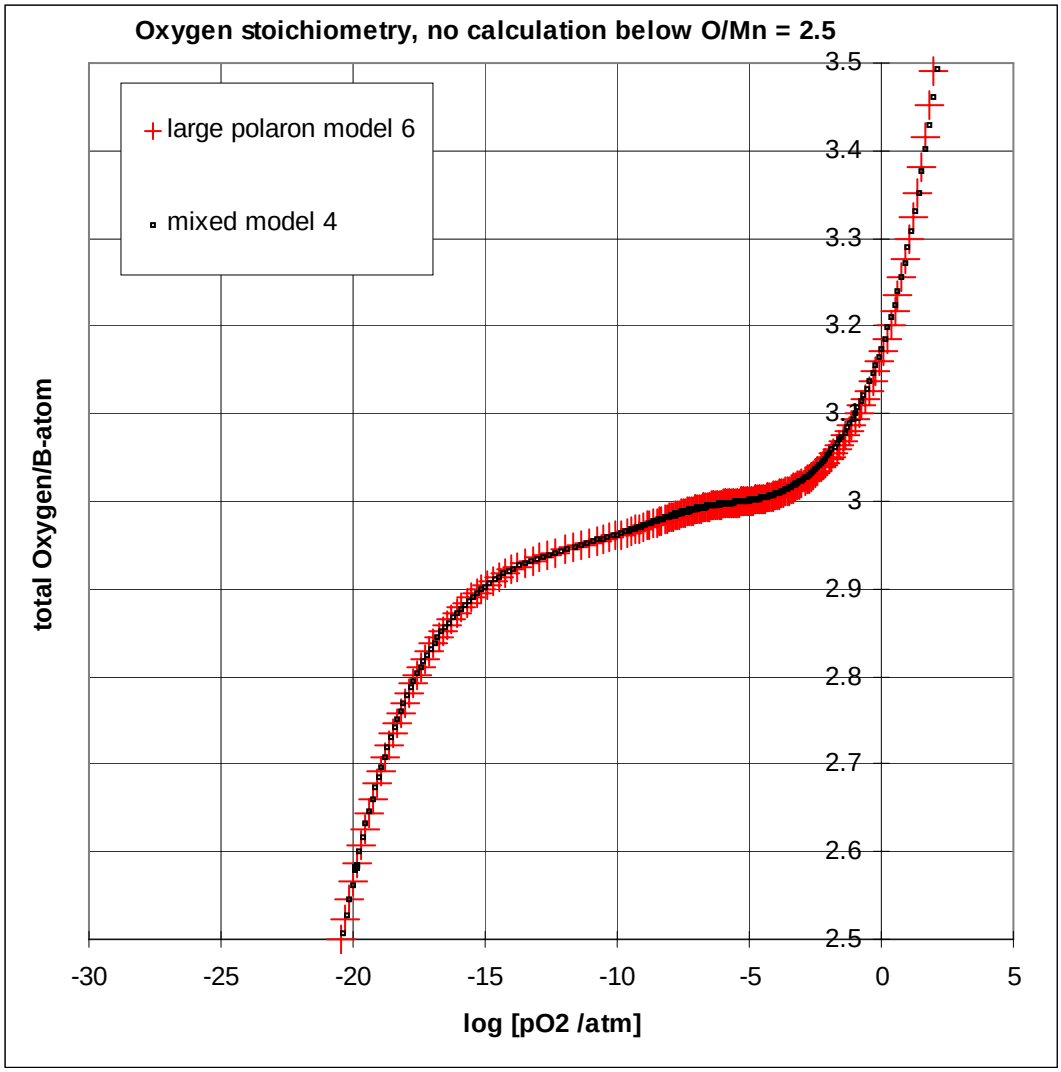

Figure 7.6. Defect modelling of a Schottky-defect dominated acceptor doped perovskite $La_{0.9}Sr_{0.1}MO_{3\pm\delta}$. Synthetic data were generated by model 4, see Table 7.4. Equilibrium constants in model 6 were then adjusted, such that a perfect match occurs over some 22 decades in partial pressure of oxygen.

7.4 Various descriptions of hydrogen defects in oxides

In this final paragraph we will address protons and other charge states of hydrogen as defects in oxides. Protons are important since they are mobile, and can be present in concentrations of tens of atomic %. Proton conducting materials have potentials as electrolytes in medium temperature SOFC's (Coors,2003,2004) or in hydrogen sensors for instance in molten Aluminium metal (Yajima,1995). Furthermore, protons are different from most other cationic defects[47] in that they may be transient species, who choose to leave the compound at high temperature or low partial pressure of water, removing thereby also lattice oxygen and leaving as water molecules, see eq. 7.6 etc. and text below.

The research field related to protons in oxides at high temperature, primarily in perovskites, was first explored by Hiroyasu Iwahara in Tottori/Nagoya (Takahashi & Iwahara,1979), (Iwahara,1981) and (Matsumoto,2004). In USA Arthur S. Nowick et al. have contributed to protonic conductors, starting approximately 1986 on $KTaO_3$ (Lee,1986). In 1993 the group announced a new class of more complex perovskites $A_2B_{1+x}B'_{1-x}O_{6-\delta}$, where the doping is achieved not by adding a new element, but by synthesising ceramics with a B/B' ratio deviating from unity. A is typically Sr^{+2} or Ba^{+2}, B can be trivalent ions and B' can be Nb^{+5} or Ta^{+5} (Liang, 1993). The foremost material of the latter category is that of BCN18 meaning $Ba_3Ca_{1.18}Nb_{1.82}O_{8.73}$ (Groβ, 1998). In Europe the leading groups have been those of Truls Norby et al in Oslo (Norby,2001,2004) , Klaus-Dieter Kreuer et al in Stuttgart (Kreuer,2003) , Tilman Schober et al in Jülich (Schober,1995,2005), Ralf Hempelmann et al. in Saarbrücken (Hempelmann ,1997,1998); (Groβ,1998,2000) and Nicholaos Bonanos et al in UK/Risø (Bonanos, 1989, 2001). A legend has developed over the past decades: if there is just one proton present in an oxide, then Truls Norby et al. of Oslo University will for sure spot it!

The present author's role in protonic conductors was for the first many years 1980-1989, merely that of a reader and reviewer of protonic literature (A15,A16, A22, A42). The author acquired experience with hydrated/ion-exchanged Na- and K-β-alumina's, via contact with the founder of the Energy Research Laboratory in Odense, the late Johs Jensen. The author collaborated later with Magnar Ottøy on Nafion membranes in Trondheim. The first concrete involvement in proton conducting perovskites stems from daily interaction with Dr. Bonanos, starting with a study of fabrication and electrical characterisation of $SrCe_{0.95}Y_{0.05}O_{3-\delta}$ (A93, A123). The author and N. Bonanos acted later as coordinating agents for the EU-INTAS project 99-0636: *Hydrogen in oxide systems, fundamentals and promising applications* (A149, 2003). Four western teams, three Russian (Y.M. Baikov, A. Neiman, V. P. Gorelov) and one Kazahk (T. Aksenova) teams worked in the three year project on protons in oxides. One joint study on the phase transitions of $BaCeO_3$ has resulted sofar (A150) in addition to various, not easily traceable Russian conference presentations.

After the authors involvement in numerical calculations on defect equilibria had materialised, protons in YSZ were modelled (A99, A109). A general algorithm for calculating Brouwer diagram's for an oxide (perovskite) in equilibrium with two gases, oxygen and water was published in 1999 (A4). To some extent this paper was a

[47] Typically of metal type

show–off or over-kill, in the sense that no perovskite case is known sofar, where both a Schottky equilibrium controlling the oxygen over-stoichiometry and proton uptake are at play simultaneously. A more realistic and tractable path was devised in the 1999-paper with Bonanos (A5), where an analytical solution of 4th degree was presented, omitting the Schottky equilibrium. This analytical methodology was used in the study of the possible proton uptake in $La_{0.9}Sr_{0.1}Ga_{0.8}Mg_{0.2}O_{3-\delta}$ (A7, 2000).

A speculative paper was written recently on hydride ions in oxides (A9,2001). It was motivated by discussions with Norby (2004) and Steinsvik about their paper on B-site Al-doped $SrTiO_3$ (Steinsvik,2001) , where they observed a shift in the sign of the EMF of water concentration cells around $pO_2 = 10^{-12}$ atm, and $p_{water} = 0.02$ atm/1000^{O}C. One possibility, discussed in their paper, is that the charge state of hydrogen in the solid changes from proton-like at high pO_2 to hydride like at low pO_2. Both their paper and paper A9 agree that such a shift to the hydride state should occur at a pO_2 at least 20 orders of magnitude lower than the pressure concluded on basis of the concentration cell experiment. Stated in chemical terms (A9,2000): tetravalent and trivalent Ti should not be stable, when a very reducing species like the hydride ion H^- sits next to it in a crystal lattice. The stable state of Ti in equilibrium with hydride ions would rather be Ti^{+2} or lower.

However, recent electrical transport studies by Widerøe (2004) and Norby et al. (2004) on acceptor doped $CaTiO_3$ $BaCeO_3$ and ZrO_2 and nominally undoped $BaTiO_3$ show the same apparent sign-shift in transport number measurements- but the interpretation is still not certain according to the authors. One possibility is that protons and electrons at reducing conditions behave like neutral hydrogen and permeates through the solid electrolyte, thereby interfering with the potential measurement.

Coexistence of hydride ions and transition metal ions has been verified in the crystallographic study of $LaSrCoO_3H_{0.7}$ by Hayward (2002). The formal oxidation state of Co in this compound is only +1.7, which indeed is low. The intuitive thinking that very reducing circumstances are required in order to stabilise hydride ions in oxides, has on the other hand proved successful. Widerøe and the author have synthesised the hitherto non-existent compound NdHO by reaction of Nd_2O_3 with CaH_2 or LiH under 8% H_2/92%Ar at 700 ^{O}C (A161,2005). The structure of NdHO was studied by neutron diffraction and derives from the fluorite structure, cf the structure of LaHO (Malaman,1984), since the ionic radii of the hydride ion and the oxide ion are comparable. Hydride ion conductivity in oxides can possibly be inferred from studies of slightly off-stoichiometric compounds such as $LaH_{1+2x}O_{1-x}$, where $y<2x$ (Brice,1982).

The remaining part of this paragraph will deal with *positively* charged protonic defects. The first element in the Periodic Table, hydrogen, offers a unique possibility to study isotope effects. Exchange of protons with deuterons is easily achieved using heavy water vapor. Even tritium exchanged samples have been studied (Mukundan, 1999). Tritium removal from radioactive gases via electrolysis through a ceramic membrane has been suggested and studied (Kawamura, 2002). A Raman and IR study of protons and deuterons in perovskites was part of the Ph.D. study of Marianne Glerup (A142, 2002). The recorded spectra are clearly indicative of more than one type of protons/ OH groups in many perovskites.

The conductivity isotope effect is a mixed one – it results from the different mobility and concentration of H^+ respectively D^+. In order to sort out these two contributions we have recently completed a study of the thermodynamic (H/D)

isotope effect in BCN18 and $SrCe_{0.95}Y_{0.05}O_{3-\delta}$ (Huijser, 2005). A genuine thermodynamic isotope effect was observed at 800 ^{O}C: at identical partial pressures of H_2O, respectively D_2O, the two compounds do uptake more heavy water than light water.

Two central issues relating to protons as defects are addressed below: i) Shall we describe protons as interstitial species, $H_i^{\bullet}$, or is it required to describe them as being attached to an oxygen as the species $OH_O^{\bullet}$? ii) Are there more than one type of protons in certain oxides? In case the answer is yes, how do we model this situation?

Ad i) Description of protonic defects in the Kröger-Vink notation:

The two, equally widespread, ways of describing protons in oxides are shown in Table 7.3. Although the protons do not enter the site conservation equation on the oxygen site using the interstitial description,- their uptake is anyhow limited just as in the other model by the amount of available oxygen vacancies defined by the remaining constraints in the model. The analytical solution to perovskites is much easier found and handled for the interstitial formalism, as shown in paper A5. At low uptake of protons/water both models will converge into Sieverts law showing a $p_{water}^{½}$ dependence of the proton concentration in the solid. Evidence from extensive conductivity studies by Norby et al (2001,2004) point towards individual jumps of protons from one oxygen ion to the neighbour oxygen ion – the $OH_O^{\bullet}$ does not jump as an entity to a neighbouring vacant oxygen site. Oxide ion conduction is considered to occur independently, with a different attempt frequency and activation energy. Proton conduction increases as the proton content raise, and as a consequence the vacancy concentration and oxide ion conduction goes down[48] as we approach saturation. IR- and Raman spectroscopy (Glerup, A144, 2002) give clear evidence that protons spend time corresponding to many vibrational periods attached to an oxide ion, where it lives the life of a hydroxyl ion, OH^-. The essential difference to OH^- as found in alkaline substances such as NaOH, is that the proton in perovskites is surrounded by many oxide ions, which are capable of accepting the proton, whereas in NaOH and alike, all oxide ions already have at least one proton attached to them. The sharpness of the IR OH-stretching peak around 3200-3500 cm^{-1} correlate with a low mobility of protons as in $La_{.9}Ca_{.1}ErO_{3-\delta}H_{\varepsilon}$, whereas good protonic conductors of the Sr/Ba-cerate family display much broader absorption peaks extending over some 500 cm^{-1} centred around 3300 cm^{-1}(Glerup,2002). The author favours the $OH_O^{\bullet}$ description over the interstitial $H_i^{\bullet}$ description due to observation of the characteristic stretching frequency.

Ad ii) Are there more than one type of protons in certain oxides?

A complexity of the IR absorption bands signalises that several different $OH_O^{\bullet}$ species may be present simultaneously,. This is the case for the spectra of partly D_2O exchanged $La_{.9}Sr_{.1}Sc_{.9}Mg_{.1}O_{3-\delta}H/D_{\varepsilon}$, and $SrCe_{.59}Y_{.05}O_{3-\delta}H/D_{\varepsilon}$ (Glerup,2002), where all OD- spectral features are a replica of the OH-spectral region, but displaced

[48] Fixed pO_2 is assumed in this argument.

towards lower frequencies by a factor of approximately $1/\sqrt{2}$. The interpretation is that the IR and Raman spectral features we see are probing the individual environments of protons, whereas the average environment of the lattice is probed by diffraction techniques.

There are two types of oxygen positions in orthorhombic perovskites, such as those mentioned above. The oxygen sites furthermore have different populations of cations, host lattice and dopant ones, in their first coordination sphere. This raises the second question, whether there are physically different protons in oxides[49] at high temperature? The answer is clearly a yes, although all papers, except for the papers of the Hempelmann group (see below), treat them as only one sort, this includes the author. Muon spin rotation experiments, μSR, have indicated a trapping site near the Sc dopant in $SrZr_{1-x}Sc_xO_3$ (Hempelmann, Soetratmo,1998), but neutron powder diffraction (Sosnowska,2001) and QENS (Quasi elastic neutron scattering) studies of BCN18 and alike have been less conclusive (Pionke,1997).

[49] We are not considering hydroxide-hydrates with recognisable water molecules or other low T compounds here.

Table 7.3 Two alternative models for describing proton uptake in an acceptor doped fluorite structure oxide (q= 2) or perovskite (q =3). The top equation is the oxygen site conservation equation.

$H_i^{\bullet}$ interstitial model	$OH_O^{\bullet}$ hydroxide model
$[O_O^x] + [V_O^{\cdot\cdot}] = q;$	$[O_O^x] + [V_O^{\cdot\cdot}] + [OH_O^{\cdot}] = q;$
$[A_A^x] = 1-x; \quad [M_A'] = x;$	$[A_A^x] = 1-x; \quad [M_A'] = x;$
ENC: $p + 2[V_O^{\cdot\cdot}] + [H_i^{\cdot}] = x + n$	ENC: $p + 2[V_O^{\cdot\cdot}] + [OH_O^{\cdot}] = x + n$
$H_2O(gas) + V_O^{\cdot\cdot} \Leftrightarrow 2H_i^{\cdot} + O_O^x \Rightarrow$	$H_2O(gas) + V_O^{\cdot\cdot} + O_O^x \Leftrightarrow 2OH_O^{\cdot} \Rightarrow$
$K'_W = [H_i^{\cdot}]^2 \times [O_O^x])/(pH_2O \times [V_O^{\cdot\cdot}])$	$K_W = [OH_O^{\cdot}]^2/(pH_2O \times [V_O^{\cdot\cdot}] \times [O_O^x])$

Hempelmann et al. measured the proton uptake in the perovskites $SrYb_{.05}Zr_{.95}O_{2.975}$ (Hempelmann, 1997) and $Ba_3Ca_{1.18}Nb_{1.82}O_{8.73}$ (Groβ, 1998) and analysed the data using a two site defect model based on Fermi-Dirac statistics. The rational for doing so was partly in error, namely their finding that Sieverts type plots produced straight lines, but the linear behaviour did not extrapolate through the origin, cf. insert in Figure 7 of (Groβ, 1998) and Figure 5 of (Groβ,2000),- NB! the latter graph has a typing error for the x-axis, where the square root of pressure does not appear. This deviation from Sievert's law they took as evidence for a two site model with reference to studies on hydrogen in metals (Kirchheim, 1982). The square root dependence of Sievert's law is however *only* approached in the low concentration limit but is *not* valid 1/3 to halfway towards saturation, as for the data in question. At higher protonic concentrations the damping effect of a decreasing $[V_O^{\cdot\cdot}]$ will set in, cf. mass law expressions in Table 7.3.

The Fermi-Dirac model is interesting in any case, and has surprising properties, not fully exposed in the quoted papers. The development of their model is not repeated here. Equation (7.6) was obtained by Hempelmann et al:

$$[OH_O^{\bullet}] = \frac{(1-c_t)}{(1-\exp[\Delta G_O - RT\ln\{(p_w/p_{ref}) \cdot 1/2 \cdot (3x - [OH_O^{\bullet}])\}/(2RT)]} + \frac{c_t}{(1-\exp[\Delta G_t - RT\ln\{(p_w/p_{ref})) \cdot 1/2 \cdot (3x - [OH_O^{\bullet}])\}/(2RT)]} \quad (7.6)$$

i.e. for the total content $[OH_O^{\bullet}] = [OH_O^{\bullet}]_{ordinary} + [OH_O^{\bullet}]_{trap\ site}$ (7.7)

where:

c_t is the fraction of available proton sites called "trapped"
x is the mole fraction of excess Ca in BCN18 i.e. x = 0.18
ΔG_O is the Gibbs energy for water absorption in ordinary sites
ΔG_t is the Gibbs energy for water absorption in trapped sites
p_{ref} is 1 atm of water vapor pressure

Equation (7.6) is a transcendental function in the total proton concentration $[OH_O^{\bullet}]$, but it can be solved easily with p_w as the variable, assuming a numerical value for $[OH_O^{\bullet}]$. The algorithm for doing so is as follows:

Find a value of p_w for which $[OH_O^{\bullet}] - [OH_O^{\bullet}]_{ordinary} - [OH_O^{\bullet}]_{trap\ site} = 0$.
The *Solver* or *Goal seek* functions in Excel can do this job.

The proton content distributes between the trap site and an ordinary site. The energy of formation was estimated to be 30-35 kJ/mol more favourable for the trap site in BCN18, and the partition of sites are 8.5% trap sites, the remainder 91.5% of sites are ordinary. For the zirconate $SrZr_{.95}\ Yb_{.05}O_{2.975}$ only 3-5 % of the protons are estimated to reside on traps. The maximum amount of protons that can be taken up in the Fermi-Dirac model at high p_{water} is still dictated by the amount of dopant, as in the conventional case, since the parentheses $(3x - [OH_O^{\bullet}])$ in eq. (7.6) can not assume a negative value.

The two terms $[OH_O^{\bullet}]_{ordinary}$ and $[OH_O^{\bullet}]_{trap\ site}$ can be evaluated individually. Surprisingly- the trap sites do not fill up first – there will always be a higher concentration of protons residing on the ordinary site for $c_t < 0.5$. The trap site does however come to saturation at a lower water partial pressure than does the ordinary site, see Figure 7.7.

A conventional *quasi chemical* description with two protonic sites is easy to develop and analyse with the sequential method. The uptake of protons will proceed in parallel, but to different levels depending on the magnitudes of the two equilibrium constants:

ordinary sites $K_{wo} = [OH_O^{\cdot}]^2_{ordinary}/(pH_2O \times [V_O^{\cdot\cdot}] \times [O_O^x])$ (7.8)
trap sites $K_{wt} = [OH_O^{\cdot}]^2_{trap\ site}/(pH_2O \times [V_O^{\cdot\cdot}] \times [O_O^x])$ (7.9)

From these two expressions we deduce that

$$[OH_O^{\cdot}]_{ordinary}/[OH_O^{\cdot}]_{trap\ site} = (K_{wo}/K_{wt})^{1/2} = \text{constant} \quad (7.10)$$

which will be valid at *any* partial pressure of water or total proton content, i.e. one site does not saturate before the other, since their concentration ratio is a constant number. When we in this model associate a more negative Gibbs energy of reaction for the trap site, i.e. $K_{wt} > K_{wo}$, then the trap site will achieve the highest population of protons

in contrast to the situation in the Fermi-Dirac description, which has the built in restriction of a small c_t.

The conventional two-site model, as described above, is also depicted in Figure 7.7. The equilibrium constants of the two models have been scaled such that they obey the relationship

$$[OH_O^{\cdot}]_{ordinary}/[OH_O^{\cdot}]_{trap\ site} = c_t/(1-c_t) = 0.085\ /0.915 = (\ K_{WO}/K_{WT}\ )^{½}$$
$$\Rightarrow\ K_{WT}/K_{WO} \approx\ 115$$

We notice from the graph that the total proton content calculated by the Fermi-Dirac model[50], and the conventional two-site model give a not too good description of the experimental data at 600 ^{O}C. The experimentally determined proton uptake levels off starting around $p_{water} > 0.5$ atm, which should not occur in neither model. However, the steeper start-uptake at lower p_{water} is better accounted for by the Fermi-Dirac model.

In conclusion: Proton uptake, even in cubic perovskites, appears to be a challenging situation to model, and we must await the answer on the details from further theoretical progress and higher quality of the data.

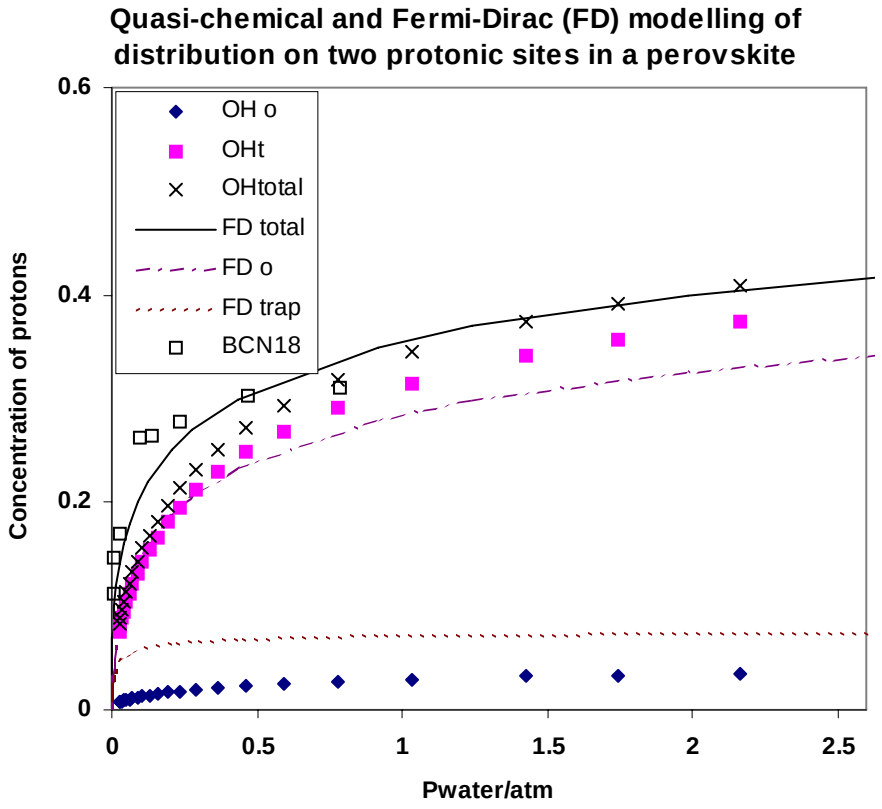

Figure 7.7. Modeling of proton uptake in a perovskite of the BCN18 type. Key: Open symbols are experimental data at 600 ^{O}C from (Groβ,1998); subscript o = ordinary site, subscript t = trap site; curves are calculated from the Fermi-Dirac model, eq. (7.6).

[50] ΔH_{trap} = -115kJ/mole, $\Delta H_{ordinary}$ = - 80kJ/mole, ΔS for both sites = -85J/mole/K

8. Dansk resume

Denne afhandling beskriver og undersøger defektkemiske modeller for ikke-støkiometriske oxider med ABO_3 - (perovskit), K_2NiF_4-, wolfram-bronze-, MO_2 - (fluorit-CaF_2), $A_2B_2O_7$ - (pyrochlor) og MM'_2O_3 - (spinel) strukturer. Defektmodellerne er en kemikers valg. En kemisk formulering af massevirkningsloven danner basis for modellerne. Såvel små polaron-modeller med lokaliserede ladninger, såvel som modeller med ikke-lokaliserede elektroner og elektronhuller som konstituenter i gitteret, og blandede modeller tages i betragtning. Også en gennemsnitsladnings-model, med brudne oxidationstrin for metalionerne i en spinel præsenteres.

En sekventiel måde til løsning af defektmodellers tilhørende ikke-lineære ligningssystemer er udforsket som den primære metodologi. Denne metode er udviklet siden 1992 og beskrevet af forfatteren i 7 af de 10 inkluderede publikationer. Med denne metode er der ikke noget behov for at reducere ligningssystemet ved substitution, således at et analytisk udtryk i een af de typisk 7-12 ubekendte koncentrationer i en defektmodel opnås. Med den sekventielle matematiske metode kan én og samme algoritme bruges over hele støkiometriområdet, hvilket har store fordele frem for publicerede metoder, der baserer sig på Brouwer- approksimationer. Sidstnævnte har været den fremherskende metode i de sidste 50 år, hvor forskere – for at kunne håndtere ligningssystemerne, har måttet opdele deres beregninger i to eller flere regioner, f.eks. i et under- og overstøkiometrisk område. Tre af publikationerne omhandler mindre komplicerede defektmodeller, hvor analytiske løsninger er anvendt.

Fire af publikationerne omhandler oxider, der står i ligevægt med både oxygen og vanddamp, og hvor der optages protoner og oxygen i strukturen. To-site modeller for sådanne protoniske materialer sammenlignes - en Fermi-Dirac formulering og en konventionel quasi-kemisk beskrivelse med to krystallografisk og energetisk forskellige positioner for protonen. Ingen af modellerne beskriver data godt.

Hovedvægten i afhandlingen er sammenligning og undersøgelse af forskellige modeller, der tilsyneladende kan beskrive den samme relation mellem oxygen indhold og partialtryk af oxygen i den omgivende atmosfære. Oxygen-støkiometri data er ofte behæftet med fejl, og/eller måleserierne består af forholdsvis få datapunkter, hvilket vanskeliggør analysen.

Data for en række SOFC-relevante materialer bliver undersøgt indgående, men det er ikke de konkrete materialeegenskaber, der diskuteres, derimod er målet for undersøgelsen, hvordan defektkemiske modeller fungerer og kan tilpasses til virkeligheden. Adskillige tilfælde behandles, hvor det er fundet, at der er en tilfælding ækvivalens mellem stor- eller lille polaron modeller, eller mellem tilfælde, hvor ingen, respektivt fuld association antages mellem dopant og oxygen-vakancer. I sådanne tilfælde kan der ikke på basis af oxygen-støkiometri data træffes noget valg mellem modellerne.

9. English summary

This thesis investigates defect chemistry models for non-stoichiometric oxides of the ABO_3- (perovskit), K_2NiF_4-, tungsten-bronze-, MO_2 - (fluorite) , $A_2B_2O_7$ - (pyrochlor) and MM'_2O_3 - (spinel) structures. The approach taken in defining the defect models is that of a chemist. The chemical formulation of the mass action law is underlying the models. Both small polaron models with localized charges, large polaron models with inclusion of electrons and electron holes as constituents in the lattice, and mixed models are considered. Also an example of an average model assigning a non-integral oxidation state to the metal ions in a spinel is presented.

The main methodology applied is a sequential way of solving sets of non-linear equations defining various defect models. This method, developed by the author since 1992, is described in 7 of the enclosed 10 published papers. Using this method, there is no need to search for an analytical expression on a closed form in one of the 7-12 unknown concentrations in a given model. The sequential method allows one to use the same numerical recipe throughout the stoichiometry range,- in contrast to published procedures based on Brouwer approximations, where - for reasons of complexity of the mathematics- authors have been forced to divide their computations into two or more regions- for instance the sub- and over stoichiometric ones. Three of the papers give examples on how to obtain and apply analytical expressions for less complicated models. Four of the submitted papers treat oxygen non-stoichiometry with the additional complexity due to proton uptake by oxides in a water or hydrogen containing atmosphere. Two-site models for such protonics are discussed- a Fermi-Dirac formulation and a more conventional two-site quasi chemical description. None of the models are especially good in describing data.

The main emphasis in the bulk of the text of the thesis is on comparison and investigations of defect models, which apparently describe the same reality, i.e. the relationship of measured oxygen content as function of partial pressure of oxygen. The analysis of oxygen stoichiometry is in general plagued by the rather low precision of the data, and the scarcity of data points at a given temperature.

Specific data sets from SOFC-relevant compounds are scrutinized, but the message of the thesis is not a discussion of materials properties of specific compounds, rather the target is the methods, and the conditions under which defect chemical models operates. Several cases of coincidental resemblance of defect models have been encountered, where discrimination between small- and large polaron models, or models with or without defect association can not be done at present on basis of oxygen stoichiometry data alone.

List of scientific and technical publications by Finn Willy Poulsen relevant to the topics of this thesis

(referred to in the text as Axx)

A12. F.W. Poulsen, Behaviour of Hard and Soft ions in solid electrolytes, NATO advanced study institute on materials for advanced batteries. Ed. J. Broadhead. Plenum Press. (1980) p. 229-234.

A13. U.v. Alpen, S.B. Brummer, Ph. Colomban, R. Collongues, L. Cot, A. Howe, R.A. Huggins, A. Levasseur, F.W. Poulsen, J.M. Reau and J. Schoonman, Solid Electrolytes, NATO advanced study institute on materials for advanced batteries. Ed. J. Broadhead. Plenum Press. (1980) p. 331-342.

A15. F.W. Poulsen, An introduction to proton conduction in solids, Risø-M-2244 (1980), 20 pp.

A16. F.W. Poulsen, Protonledende faste stoffer. Litteraturoversigt. Risø-I-43, (1980).

A17. F.W. Poulsen, Ionic conductivity of solid Lithium Iodide and its Monohydrate, Solid State Ionics (1981), 2, 53-57.

A19. F.W. Poulsen, Raman spectra from sodium ion conducting glasses. Risø-I-58, (1981) 9 pp.

A21. F.W. Poulsen, Configurational model for conductivity of stabilized fluorite structure oxides, Solid State Ionics (1981), 5, 535-538.

A22. F.W. Poulsen, Limitations on the performance of solid state proton conductors, I: Solid State Protonic Conductors I, (ed. J. Jensen and M. Kleitz) Odense University Press (1982), 21-26.

A23. N. Hessel Andersen, J.K. Kjems and F.W. Poulsen, Neutron Scattering Studies of the Ionic Conductor LiI,D_2O, Physica Scripta (1982), 25, 780-784.

A24. N. Hessel Andersen, F.W. Poulsen and G. Eichinger, Conductivity, structure, and specific heat of $LiBiO_2$, Studies in Inorganic Chemistry (1983), 3, 287-290.

A25. F.W. Poulsen, N. Hessel Andersen, B. Kindl, and J. Schoonman, Properties of LiI-Alumina Composite Electrolytes, Solid State Ionics (1983), 9/10, 119-122.

A26. R. Dupree, J.R. Howells, A. Hooper, and F.W. Poulsen, NMR- Studies of Lithium Iodide based Solid Electrolytes, Solid State Ionics (1983), 9/10, 131-133.

A27. F.W. Poulsen, Ionic Conductivity of Solid and Molten Lithium thiocynate and its hydrate, Acta Chem. Scan. (1985), A39, 119-122.

A28. N.H. Andersen, J.K. Kjems and F.W. Poulsen, Fremstilling og karakterisering af faststofionledere (Fabrication and characterisation of solid electrolytes), Final Report to Ministry of Energy, Risø-M-2489 (1985), 201 pp.

A29. F.W. Poulsen, N. H. Andersen, K. Clausen, S. Skaarup and O. Toft Sørensen (editors), Transport-Structure Relations in Fast Ion and Mixed Conductors. Proc. 6th Risø International Symposium on Metallurgy and Materials Science 9-13 September 1985. (Risø, 1985) 491 pp.

A30. F.W. Poulsen, Composite Electrolytes. I: Proc. 6th Risø International Symposium on Metallurgy and Materials Science 9-13 September 1985. Edited by F.W. Poulsen, N. Hessel Andersen, K. Clausen, S. Skaarup, O. Toft Sørensen (Risø, 1985) 67-78.

A31. F.W. Poulsen, P.J. Møller. Conductivity Dependence of Alumina Surface Area for LiI-Alumina Composites. I: Proc. 6th Risø International Symposium on Metallurgy and Materials Science 9-13 September 1985. (Eds F.W. Poulsen, N. Hessel Andersen, K. Clausen, S. Skaarup, O.T. Sørensen), Risø, 1985 159-164.

A32. F.W. Poulsen, Raman Spectrum of the solid electrolytes LiI,H_2O and LiI,D_2O, J. of Raman Spectrosc. (1986), 17, 189- 191.

A33. F.W. Poulsen, Searching for new Solid Electrolytes for Li, I: Proceedings of Symposium on "Generel og anvendt elektrokemi i Danmark". April 9, 1986, Technical University of Denmark. (Publ. by Dansk Elektrokemisk Forening, Selskabet for analytisk Kemi, Lyngby) (1986) 14-15.

A34. N.H. Andersen, J.J. Bentzen, M. Mogensen, F.W. Poulsen and O.T. Sørensen, Solid Electrolyte Research at Risø National Laboratory, I: Proceedings of Symposium on "Generel og anvendt elektrokemi i Danmark". April 9, 1986, Technical University of Denmark. (Publ. by Dansk Elektrokemisk Forening, Selskabet for analytisk Kemi, Lyngby) (1986) 16- 17.

A35. M. Mogensen and F.W. Poulsen, Thin Solid Electrolyte layers on Lithium Electrodes, I: Proceedings of Symposium on "Generel og anvendt elektrokemi i Danmark". April 9, 1986, Technical University of Denmark. (Publ. by Dansk Elektrokemisk Forening, Selskabet for analytisk Kemi, Lyngby) (1986) 26-27.

A36. F.W. Poulsen, Composite Li-conducting Solid Electrolytes (1986), Risø-M-2540, 94 pp.

A37. F.W. Poulsen, The Effect of Different Internal Surfaces in Composite Lithium Electrolytes, J. Power Sources 20 (1987) 317-325.

A38. F.W. Poulsen, "Resultater fra iltionleder forskningen" (Results from the oxygen ion conductor research), (1987), Risø-I-286. 18 pp.

A39. F.W. Poulsen, N.H. Andersen, K.N. Clausen, D.R. Sadoway and L. Øgendal, Super Ionic Conduction in Alkali Metal Hexachloro Niobates and Tantalates. Solid State Ionics (1988) 28/30, 271-275.

A40. J.J. Bentzen, N.H. Andersen, F.W. Poulsen, O.T. Sørensen, R. Schram, Evaluation of 2- and 4-Point Conductivity Measurements on Oxide Ion Conductors. Solid State Ionics (1988) 28/30, 550-559.

A42. F.W. Poulsen, Proton Conduction in Solids, I: "High Conductivity Solid Ionic Conductors, Recent trends and Applications", Ed. T. Takahashi. World Scientific Publ. Co., Singapore, (1989), 166-200.

A45. J.J. Bentzen, J.B. Bilde-Sørensen, B. Kindl, H. Paulsen and F.W. Poulsen, Thin tape cast Zirconia for solid oxide fuel cells, Proceedings of the 5'th Scandinavian Symposium on Materials Science, May 22-25, 1989, Ed.: I. Hansson and H. Lilholt, 1989, 149-157.

A46. F.W. Poulsen, Techniques for the Danish Solid Oxide Fuel Cell project, Risø-M-2778 (1989), pp. 57.

A48. F.W. Poulsen, J.J. Bentzen and J.B. Bilde-Sørensen, Conductivity of thin YSZ-materials, Proc. of SOFC-Nagoya, International Symposium on Solid Oxide Fuel Cells, 13-14 November 1989 (Publ. by SOFC Society of Japan) (1989), 93- 100.

A49. F.W. Poulsen, J.B. Bilde-Sørensen, K. Ghanbari-Ahari, G.G. Knab and M. Hartmanova, Oxygen Ion Conduction in Ternary Zirconia Mixtures: Effect of SrO on MgSZ. Solid State Ionics (1990) 40/41, 947-951.

A51. B. Kindl, M. Mogensen and F.W. Poulsen, First Danish Solid Oxide Fuel Cell tests, Proc. of SCAN-ELCHEM-90, Copenhagen 7-10 Oct, 1990, Eds. O. Hammerich, O, Jensen and J. Ulstrup, Publ. Danish Electrochem. Soc.) SC03, 2pp.

A53. F.W.Poulsen, P. Buitink and B. Malmgren-Hansen, Van der Pauw- and conventional 2-point conductivity measurements on YSZ-plates.(1991). Proc.2' Int. Symp. on SOFC, Athens (Publ. CEC, EUR 13564 EN) 755-765.

A54. K. West, B. Zachau-Christiansen, S. Skaarup, F. W. Poulsen and K. Jensen, Electrochemical Investigations of Sputtered Oxide Electrodes, Final Report to Ministry of Energy, Contract # 1443/87-3, Oct 1991, 45 pp.

A55. F.W. Poulsen, Admittance spectroscopy on SOFC materials, Proceedings of Nordic Symposium of High Temperature Fuel Cells, December 9-10, 1991, Oslo, ed. B.Bergman, 10 pp.

A56. F.W. Poulsen, Electrical characterisation of mixed conduction in oxides, Proceedings of Nordic Symposium of High Temperature Fuel Cells, December 9-10, 1991, Oslo, ed. B.Bergman, 4 pp.

A57. H. Toftegaard, F.W. Poulsen, and B. Malmgren-Hansen, 4-point ac and dc conductivity measurements on SOFC materials,Proceedings of Nordic Symposium of High Temperature Fuel Cells, December 9-10, 1991, Oslo, ed. B.Bergman, 2 pp.

A58. F.W. Poulsen and N. van der Puil, Phase relations and conductivity of Sr- and La-zirconates, Solid State Ionics (1992) 53-56, 777-783.

A59. K. West, B. Zachau-Christiansen, S.V. Skaarup and F.W. Poulsen, Lithium insertion in Sputtered Vanadium Oxide Films. Solid State Ionics (1992) 57, 41-47.

A60. F.W. Poulsen, Aspects of fuel cells, Proc. of Nordic conference on Polymeric electrolytes for Fuel Cells, Helsinki 24-25 August 1992, Ed. F. Sundholm. 8pp.

A61. M. Mogensen, C. Bagger, B. Kindl, F.W. Poulsen and P. Knudsen, Results from the Danish SOFC programme, Abstracts of 1992 Fuel Cell Seminar, Tucson, AX (US), Washington, DC, (1992) 399-402.

A62. F.W. Poulsen, E. Ahlgren and A. Holt (Eds), Proc. of Nordic Workshop on High Temperature Electrode Materials, Oct 26-27, Roskilde, Denmark,1992, (1992) 194 pp.

A63. F. W. Poulsen, Exact solutions to Kröger-Vink diagrams for perovskites, Proc. of Nordic Workshop on High Temperature Electrode Materials, Oct 26-27, Roskilde, Denmark,1992, Ed. F.W. Poulsen, E. Ahlgren and A. Holt, (1992) 6-26.

A64. J. Ranløv, F.W. Poulsen and M. Mogensen, Comment on " The characterization of doped CeO2 electrodes in solid oxide fuel cells" by B.G. Pound, Solid St.I., 52 (1992) 183-188. Solid State Ionics 61 (1993) 277-279.

A65. EFP-88 slutrapport brændselscelleprojekt, F.W. Poulsen, J.J. Bentzen, B. Kindl, H. Paulsen, January 1993, Risø-I-288(DA). 62pp.

A66. A.1, E.O. Ahlgren and F.W. Poulsen, Synthesis, electrical properties and defect chemistry of Ti-doped $NdCrO_3$, Proc. 3rd Int. Symp. Solid Oxide Fuel Cells, (Eds. S.C. Singhal and H. Iwahara), Honolulu, USA, May 16-21, 1993. Proc. vol. 93-4 (1993) 562-571.

A67. High Temperature Electrochemical Behaviour of Fast Ion and mixed Conductors. Proc. of 14'th International Symposium on Materials Science, Eds. F. W. Poulsen, J.J. Bentzen, T. Jacobsen, E. Skou and M.J.L. Østergård. (1993) 518 pp.

A68. E.O. Ahlgren and F.W. Poulsen, Review of thermoelectric power of doped chromites and manganites, ibid. (1993) 193.

A69. J. Ranløv, M. Mogensen and F.W. Poulsen, Mixed ionic and electronic conductivity of rare earth aluminates, ibid. (1993) 389.

A70. M.J.L. Østergård, T. Lindegaard, M. Mogensen, F. W. Poulsen, and B. Malmgren-Hansen, Control of electrical and electrochemical measurements on SOFC materials, ibid (1993) 507.

A71. F.W. Poulsen, G. Lauvstad and R. Tunold, Conductivity and Seebeck measurements on strontium ferrates, Solid State Ionics 72 (1994) 47-53.

A72. E.O. Ahlgren and F.W. Poulsen, Thermoelectric power of YSZ. Solid State Ionics (1994), 70/71 528-532.

A73. M. Hartmanova, F.W. Poulsen, F. Hanic, K. Putyera, D. Tunega, A.A.Urusovskaya, and T.V. Oreshnikova, Influence of copper- and iron doping on cubic yttria-stabilised zirconia, J. Mater. Sci. 29, (1994) 2152-2158.

A74. Proc. of 2nd Nordic conference on High Temperature Electrochemistry, March 1994, Geilo, Norway (1994). Eds. T. Norby and F.W. Poulsen, 120 pp

A75. E. O. Ahlgren, J. Ranløv and F.W. Poulsen, On the thermoelectric power of a mixed ionic-electronic conductor, Proc. of 2nd Nordic conference on High Temperature Electrochemistry, March 1994, Geilo, Norway (1994). Eds. T. Norby and F.W. Poulsen, 221-226.

A76. G. Ø. Lauvstad, R. Tunold, K. Wiik, K. Engvoll and F.W. Poulsen, Electrical properties of La-doped Strontium Ferrate, $La_ySr_{1-y}FeO_{3-x}$, ibid, (1994) 227-234.

A77. F.W. Poulsen, New experiments in fuel cell research, ibid (1994) 15-20.

A78. F.W. Poulsen and M. Ottøy, 2- and 4-point measurements of conductivity in proton conducting membranes, Proc. of Nordic conference on " Test methods in fuel cell research", Helsinki May 19-20, Ed. F. Sundholm. (1994) 51-58.

A79. E.O. Ahlgren, J. Ranløv and F.W. Poulsen, Thermoelectric power of doped rare earth aluminates, Proc. 2nd International Symposium on Ionic and Mixed Conducting Ceramics, Eds. T.A. Ramanurayanan, W.L. Worrell and H.L. Tuller, San Francisco, May 22-27 (1994), Abstract no. 695. Proc. vol 94-12 (1994) 598-607.

A80. Ranløv, J.; Bonanos, N.; Poulsen, F.W.; Mogensen, M., Criteria for prediction of high oxide ion conductivity in perovskite oxides. Diffus. Defect Data. Solid State Data B: Solid State Phenom. 39/40 (1994) 219-222.

A81. H. Nabielek, K. Nisancioglu, E. Aschenbach, J. Huijsmans, M. Brocco, F. Poulsen, M. Harada, A. McEvoy, and H. Haydock, IEA Agreement for a Programme of Research, Development and Demonstration on Solid Oxide Fuel Cells, Proc. of First European SOFC Forum, Lucerne, Oct 3-7, 1994. Ed. U. Bossel, 93-102.

A82. F. W. Poulsen and B. Gaudernack, Fuel cell activities under the Council of the Nordic Ministers, Proc. of First European SOFC Forum, Lucerne, Oct 3-7, 1994. (Ed. U. Bossel), 103-106.

A83. K. Engvoll, T.L. Rutlin, K. Wiik and F.W. Poulsen, Faseforhold og elektriske egenskaper til La-dopet strontiumferrat, June 1994, Institutt for uorganisk kjemi, NTH, 19pp (+41 pp Appendix).

A85. Ahlgren, E.O.; Poulsen, F.W. , Thermoelectric power of stabilized zirconia. Solid State Ionics (1995) 82, 193-201

A86. Ahlgren, E.O.; Ranløv, J.; Poulsen, F.W. , Thermoelectric power of $ErAl(Mg)O_{3-\delta}$ and $LaAl(Mg)O_{3-\delta}$. J. Electrochem. Soc. (1995) v. 142, 4230-4234.

A87. E.O. Ahlgren and F.W. Poulsen, Thermoelectric power of doped Cerium oxide,

J. Phys. Chem. Solids 57 (1996) 589-599.

A88. L. Kindermann, D, Das, R. Weiß. H. Nickel, K. Hilpert, and F.W. Poulsen, Chemical compatibility of $(La_{0.6}Ca_{0.4})_x$ $Fe_{0.8}M_{0.2}O_3$ (x=1,0.9; M= Cr,Mn,Co,Ni) with YSZ (1995) 4'th International Symposium on SOFC, June 18-23, 1995, Yokohama, Japan).

A89. Ahlgren, E.O.; Poulsen, F.W. , Thermoelectric power and electrical conductivity of strontium-doped lanthanum manganite. Solid State Ionics (1996) v. 86/88 p. 1173-1178.

A90. R.J. Aaberg, R. Tunold, F.W. Poulsen and N. Bonanos, Short term structural changes in NiO/YSZ electrodes upon reduction, Proc. 2'nd European SOFC Forum, Oslo 1996, Ed. B. Thorstensen, 363-372.

A91. N. Kjerulf-Jensen, R.W. Berg and F.W. Poulsen, Raman spectroscopic characterisation of ZrO_2 and yttrium stabilised zirconias, Proc. 2'nd European SOFC Forum, Oslo 1996, Ed. B. Thorstensen, 647-656.

A92. Poulsen, F.W.; Bonanos, N.; Linderoth, S.; Mogensen, M.; Zachau-Christiansen, B. (editors.), High temperature electrochemistry: Ceramics and metals. Proceedings. 17. Risø International Symposium on Materials science, Risø (DK), 2-6 Sep 1996. (Risø National Laboratory, Roskilde, 1996) 520 p.

A93. Ahlgren, E.O.; Hansen, J.R.; Bonanos, N.; Poulsen, F.W.; Mogensen, M., Electrical characterisation of $SrCe_{0.95}Y_{0.05}O_{3-\delta}$. In: High temperature electrochemistry: Ceramics and metals. Proceedings. 17. Risø Int. Symposium on Materials Science, Risø (DK), 2-6 Sep 1996. F.W. Poulsen, N. Bonanos, S. Linderoth, M. Mogensen, B. Zachau-Christiansen, (eds.), Risø National Laboratory, Roskilde, (1996) p. 161-166

A94. Gordes, P.; Christiansen, N.; Poulsen, F.W.; Bouakaz, L.; Thomsen, K., Electric conductivity of $La_{1-x}Sr_xFe_{1-y}Mn_yO_3$ materials. Ibid (1996) 247-252.

A99. Poulsen, F.W. , Method for calculating ionic and electronic defect concentrations in Y-stabilised zirconia. In: Nordic ceramics '97. Structural ceramics. Functional ceramics. Extended abstracts. Nordic ceramics '97, Risø (DK), 26-27 May 1997. Sørensen, B.F. (ed.), (Risø National Lab., Roskilde, 1997) p. 75-77

A101. F.W. Poulsen, L. Sörby, H.F.Poulsen, S. Garbe, In-situ studies of air electrodes in solid oxide fuel cells at 850(C using synchrotron diffraction. , Proceedings of IEA-workshop: Materials and Processes. Annex VII: SOFC under Real Operating Conditions, Jan. 28-31, 1997. les Diablerets , CH. (Ed. A.J. McEvoy and K. Nisancioglu) p 84-87.

A103. Poulsen, F.W.; Bruaset, U. (eds.), Experimental and theoretical methods in fuel cell research. Nordic NEFP workshop on experimental and theoretical methods in fuel cell research, Geilo (NO), 5-7 Mar ts 1997. (NEFP-Secretariat, Ås, 1997) 118 p.

A104. F.W. Poulsen, Multi equilibria calculations in ionic and mixed conducting electrolytes. Proc. of NEFP workshop" Experimental and theoretical methods in fuel cell research", Geilo 5-7 March 1997.(Ed. F.W. Poulsen and U. Bruaset). 4pp.

A105. L. Kindermann, D. Das, H. Nickel, K. Hilpert, C.C. Appel, F.W. Poulsen, Chemical compatibility of $(La_{0.6}Ca_{0.4})_x Fe_{0.8}M_{0.2}O_3$ with yttria-stabilized zirconia. J. Electrochem. Soc. (1997) 144 717-720.

A107. L. Sörby, F.W. Poulsen, H.F.Poulsen, S. Garbe, and J. Thomas, An in-situ (synchrotron) diffraction study of a solid oxide fuel cell system, Proceedings of EPDIC V, Parma 1997. Materials Science Forum 278-281 (1998) 408-413.

A108. Dorthe Larsen, F.W. Poulsen and M. Mogensen, Conductivity of A- and B-site doped $LaAlO_3$, $LaGaO_3$, $LaScO_3$. Proceedings of Third International Symposium on Ionic and mixed Conducting Ceramics. Paris, August 31- September 5, 1997 Eds. T.A. Ramanarayanan and M. Mogensen, PV 97-24 (1998) 293-303.

A109. F. W. Poulsen, Method for calculating ionic and electronic defect concentrations in fluorite structure oxides. Proceedings of Third International Symposium on Ionic and mixed Conducting Ceramics. Paris, August 31- September 5, 1997 Ed. T.A. Ramanarayanan, Proc. vol 97-24 (1998) 448-452.

A110. L. Kindermann, F. W. Poulsen, P.H. Larsen, H. Nickel and K. Hilpert, Synthesis and properties of La-Sr-Mn-Fe-O based perovskites. Proc. 3'rd European SOFC Forum, Nantes 2-5 June 1998, Ed. P. Stevens,123-132 (1998)

A111. L. Kindermann, F.W. Poulsen and C. Bagger, In plane conductivity of improved Ni-cermet anodes, Proc. 3'rd European SOFC Forum, Nantes 2-5 June 1998, Ed. P. Stevens,133-144 (1998)

A113. F.W. Poulsen and P. Holtappels, Modelling of defect chemistry in SOFC materials, Proc.11'th IEA SOFC Workshop. 12-13 Oct. 1998, Arnhem, The Netherlands, 10 pp.

A114. P. Holtappels, F.W. Poulsen and M. Mogensen, Conductivity of pyrochlore anode materials, Proc. 11'th IEA SOFC Workshop. 12-13 Oct. 1998, Arnhem, The Netherlands, 4 pp.

A115. Hendriksen, P.V.; Larsen, P.H.; Mogensen, M.; Poulsen, F.W., Prospects and problems of dense oxygen permeable ceramic membranes. In: 3. International conference on catalysis in membrane reactors. bstracts. ICCMR '98, Copenhagen (DK), 8-10 Sep 1998. (Society of Danish Engineers, Copenhagen, 1998) 2 p.

A116. .Z. Jiang, F.W. Poulsen and S. Mørup, Structure and thermal stability of nanostructures iron-doped zirconia prepared by high-energy ball milling, J. Mater. Res., 14 (1999) 1343-1352.

A117. N. Bonanos and F.W. Poulsen, Considerations on the defect chemistry of proton-conducting cerates, J. Mater. Chem., 9 (1999), 431-434.

A118. F.W.Poulsen, Method for calculating ionic and electronic defect concentrations in proton containing perovskites, J. Solid State Chem., 143 (1999) 115-121.

A119. P. Holtappels, F.W. Poulsen and M. Mogensen, Preparation of mixed conducting pyrochlores as SOFC anodes, Solid State Ionics 135 (2000) 675-679.

A120. P.V. Hendriksen, P.H. Larsen, F.W. Poulsen and M. Mogensen, Problems of limited dimensional and thermodynamic stability in oxygen permeable membranes, Proc. 12th SOFC Workshop, Wadahl January 10-13, 1999, Ed. K. Nisancioglu, 137-148 (1999).

A121. F.W. Poulsen and K. Wiik, Oxygen transport in Co-substituted Sr4Fe6O13, Proc. 12th SOFC Workshop, Wadahl January 10-13, 1999, Ed. K. Nisancioglu, 153-156 (1999).

A122. F.W. Poulsen, On-line demonstration of defect chemistry calculations on SOFC materials,
Proc. 12th SOFC Workshop, Wadahl January 10-13, 1999, Ed. K. Nisancioglu, 189-198 (1999).

A123. R. J. Phillips, N. Bonanos, F.W. Poulsen, and E.O. Ahlgren, Structural and electrical characterisation of SrCe1-xYxOw, Solid State Ionics 125 (1999) 389-395.

A124. Bagger, C.; Linderoth, S.; Mogensen, M.; Hendriksen, P.V.; Kindl, B.; Primdahl, S.; Larsen, P.H.; Bonanos, N.; Poulsen, F.W.; Juhl Jørgensen, M., Status of Danish solid oxide fuel cell R and D. In: Proceedings. 6. International symposium on solid oxide fuel cells (SOFC 6), Honolulu, HI (US), 17-22 Oct 1999. Singhal, S.C.; Dokiya, M. (eds.), (Electrochemical Society, Pennington, NJ, 1999) (Proceedings volume PV 99-19) p. 28-35

A125. Lybye, D.; Poulsen, F.W.; Mogensen, M., Conductivity of A- and B-site doped $LaAlO_3$, $LaGaO_3$, $LaScO_3$ and $LaInO_3$ perovskites. Solid State Ionics (2000) 128 , 91-103

A126. Hendriksen, P.V.; Larsen, P.H.; Mogensen, M.; Poulsen, F.W.; Wiik, K., Prospects and problems of dense oxygen permeable membranes. Catal. Today (2000) 56 , 283-295

A127. F.W. Poulsen, M. Glerup and P. Holtappels, Structure, Raman spectra and defect chemistry modelling of conductive pyrochlore oxides, Solid State Ionics 135 (2000), 595-602.

A128. Åberg, R.J.; Poulsen, F.W.; Norby, T. (eds.), Proceedings. Nordic workshop on materials for electrochemical energy conversion, Geilo (NO), 8-10 Mar 2000. (Nordisk Energiforskningsprogram, 2000) 153 p.

A129. F.W. Poulsen, Defect chemistry modelling of oxygen-stoichiometry, vacancy concentrations and conductivity of $(La_{1-x}Sr_x)_yMnO_3$, Solid State Ionics (2000) 129 , 145-16

A131. ShanwenTao, Finn Willy Poulsen, Guangyao Meng and Ole Toft Sørensen, High-temperature stability of the oxygen-ion conductor $La_{0.9}Sr_{0.1}Ga_{0.8}Mg_{0.2}O_{3-x}$, J. Materials Chemistry (2000), **10**, 1829-1833.

A132. M.J. Jørgensen, S. Linderoth, C. Bagger, M.Mogensen, P.V. Hendriksen, B. Kindl, P.H. Larsen, S. Primdahl, N. Bonanos, F.W. Poulsen, Development and Scale-up of Anode-Supported SOFC, Proceedings of Materialsweek 2000 (Werkstoffwoche-Partnerschaft München 25-28 Sept. 2000, 8 pp.

A133. Holtappels, P.; Poulsen, F.W.; Mogensen, M., Electrical conductivities and chemical stabilities of mixed conducting pyrochlores for SOFC applications. Solid State Ionics (2000) **135** , 675-679.

A134. Ringgaard, E.; Poulsen, F.W.; Mercurio, J.-P.; Wolny, W.W.; Høj, J.W., Impedance spectroscopy of piezoceramic multilayer components (poster). 7. International conference on electronic ceramics and their applications (Electroceramics VII), Portoroz (SI), 3-6 Sep 2000. Poster available

A135. Fossdal A, Sagdahl LT, Einarsrud MA, Wiik, K.; Grande, T.; Larsen, P.H.; Poulsen, F.W.,Phase equilibria and microstructure in $Sr_4Fe_{6-x}Co_xO_{13-\delta}$, $0 < x < 4$ mixed conductors, Solid State Ionics (2001) **143** 367-377

A137. Finn. W. Poulsen, Speculations on the existence of hydride ions in Proton Conducting oxides,
Solid State Ionics, **145**, 387-397 (2001)

A138. Marianne Glerup, Ole Faurskov Nielsen and Finn W. Poulsen,
The structural transformation from the Pyrochlore structure, $A_2B_2O_7$, to the Fluorite structure AO_2 , studied by Raman Spectroscopy and Defect Chemistry Modelling , J SOLID STATE CHEM **160** (1): 25-32 (2001)

A140. Poulsen, F.W. (ed.), Danish Solid Oxide Fuel Cell project: DK-SOFC 1997-1999. (2001) 30 p.

A141. M.Mogensen, D. Lybye, N. Bonanos, P.V. Hendriksen, and F.W. Poulsen, The effect of lattice stress in ion conducting fluorites and perovskites, Proc. IV Int. Symp. on Ionic and Mixed conducting ceramics, Ed. T. A. Ramanrayanan, The Electrochem. Soc., Pennington, NJ, PV-2001-28 15-26 (2001)

A142. Larsen, P.H.; Bagger, C.; Linderoth, S.; Mogensen, M.; Primdahl, S.; Jørgensen, M.J.; Hendriksen, P.V.; Kindl, B.; Bonanos, N.; Poulsen, F.W.; Maegaard, K.A., Status of the Danish SOFC program. In: Proceedings. 7. International symposium on solid oxide fuel cells (SOFC 7), Tsukuba (JP), 5-8 Jun 2001. Singhal, S.C. Yokokawa, H. (eds.), (Electrochemical Society, Pennington, NJ, 2001) (Proceedings volume PV 2001-16) p. 28-37

A143. Poulsen, F.W.; Søgård, M., Defect chemistry modelling of complex SOFC materials. In: Proceedings. Vol. 2. 5. European solid oxide fuel cell forum, Lucerne

(CH), 1-5 Jul 2002. Huijsmans, J. (ed.), (European Fuel Cell Forum, Oberrohrdorf (CH), 2002) p. 687-694

A144. Glerup, M.; Poulsen, F.W.; Berg, R.W., Vibrational spectroscopy on protons and deuterons in proton conducting perovskites. Solid State Ionics (2002) **148** , 83-92

A145. Poulsen, F.W., Tautology of defect chemistry models?. In: 3. Petite workshop on the defect chemical nature of advanced materials, Geilo (NO), 17-21 Apr 2002. (2002) 1 p.

A146. Poulsen, F.W., Crystallographical aspects of high temperature fuel cell materials. In: Abstracts. 32. Danske krystallografmøde; Dansync's 4. Årsmøde, Lund (SE), 30-31 May 2002. Ståhl, K. (ed.), (Technical University of Denmark, Lyngby, 2002) F12

A147Ståhl, K.; Nielsen, E.R.; Ringgaard, E.; Poulsen, F.W., The ferroelectric to paraelectric phase transition in $Pb(Zr,TI)O_3$ (PZT). In: Abstracts. 32. Danske krystallografmøde; Dansync's 4. Årsmøde, Lund (SE), 30-31 May 2002. Ståhl, K. (ed.), (Technical University of Denmark, Lyngby, 2002) P16

A148. Mogensen, M.; Lybye, D.; Bonanos, N.; Hendriksen, P.V.; Poulsen, F.W., The effect of lattice stress in ion conducting fluorites and perovskites. In: Proceedings. 4. International conference on ionic and mixed conducting ceramics, San Francisco, CA (US), 2-7 Sep 2001. Ramanarayanan, T.A.; Worrell, W.L.; Mogensen, M. (eds.), (Electrochemical Society, Pennington, NJ, 2002) (Proceedings volume PV 2001-28) p. 15-26

A149. Poulsen, F.W., Intas open call 99-0636: Hydrogen in oxide systems, fundamentals and promising applications. Final report, June 2003. Summary of results and key references. (2003) 32 p.

A150. Kuzmin, A.V.; Gorelov, V.P.; Melekh, B.T.; Glerup, M.; Poulsen, F.W., Phase transitions in undoped $BaCeO_3$. Solid State Ionics (2003) **162** , 13-22

A151. Hashimoto, S.; Kindermann, L.; Larsen, P.H.; Poulsen, F.W.; Mogensen, M., A study on the properties of $SrTiO_3$ based oxides at high temperature. In: Extended abstracts. 29. Symposium on solid state ionics in Japan, Matsushima (JP), 26-28 Nov 2003. (Solid State Ionics Society of Japan, Tokyo, 2003) p. 146-147

A152. Hashimoto, S.; Kammer Hansen, K.; Larsen, P.H.; Poulsen, F.W.; Mogensen, M., A study of as an SOFC cathode material. In: Extended abstracts. 29. Symposium on solid state ionics in Japan, Matsushima (JP), 26-28 Nov 2003. (Solid State Ionics Society of Japan, Tokyo, 2003) p. 42-43

A153. Hashimoto, S.; Kammer Hansen, K.; Larsen, P.H.; Poulsen, F.W.; Mogensen, M., A study of $Pr_{0.7}Sr_{0.3}Fe_{1-x}Ni_xO_{3-\delta}$ as a cathode material for intermediate temperature operating SOFCs. In: Extended abstracts. 12. Symposium on solid oxide fuel cells in Japan, Tokyo (JP), 11-12 Dec 2003. (Solid Oxide Fuel Cell Society of Japan, Tokyo, 2003) p. 118-121

A154. M. Glerup, O.F. Nielsen and F.W. Poulsen, Determination of local structures in cubic stabilized zirconia using Raman spectroscopy, Asian J. Phys. 13, 25-31 (2004).

A155. Søgaard M, Hendriksen PV, Poulsen FW, Mogensen M A/B-ratio and transport properties of $(La_{0.85}Sr_{0.15})_sCoO_{3-delta}$ perovskites J. Electroceram. .13: 811-816 (2004)

A156. Hendriksen, P.V.; Høgh, J.; Hansen, J.R.; Larsen, P.H.; Mogensen, M.; Poulsen, F.W., Electrical conductivity and dimensional stability of co-doped lanthanum chromites. 2004 Joint international meeting: 206. Meeting of the Electrochemical Society (ECS), 2004 Fall meeting of the Electrochemical Society of Japan (ECSJ), Honolulu (US), 3-8 Oct 2004. Abstract available

A157. Nielsen, K.A.; Solvang, M.; Poulsen, F.W.; Larsen, P.H., Evaluation of sodium aluminosilicate glass composite seal with magnesia filler. In: Proceedings. 28. International Cocoa Beach conference and exposition on advanced ceramics and composites, Cocoa Beach, FL (US), 25-30 Jan 2004. (American Ceramic Society) , Westerville, OH (US), 2004) (Ceram. Eng. Sci. Proc., v. 25, iss. 3) p. 309-314

A158. Mogensen, M.; Lybye, D.; Bonanos, N.; Hendriksen, P.V.; Poulsen, F.W., Factors controlling the oxide ion conductivity of fluorite and perovskite structured oxides. Dokiya memorial international symposium on solid oxide fuel cells, Tokyo (JP), 24-25 Jun 2004. Solid State Ionics (2004) **174** , 279-286.

A159. Dinesen, A.R.; Nielsen, K.A.; Poulsen, F.W.; Mikkelsen, L.; Hendriksen, P.V., Testing of Ni-plated ferritic steel interconnect in SOFC stacks. In: Proceedings. Vol. 2. 6. European solid oxide fuel cell forum, Lucerne (CH), 28 Jun - 2 Jul 2004. Mogensen, M. (ed.), (European Fuel Cell Forum, Oberrohrdorf, 2004) p. 940-949

A160. M.Glerup, Knight K.S. and Poulsen F.W., High temperature structural phase transitions in $SrSnO_3$ perovskite, Mat. Res. Bull.**40**, 507-520 (2005)

A161. M. Søgaard, Hendriksen, P.V.; Poulsen, F.W., Determination of transport and catalytic properties of mixed ionic and electronic conductors using transient responses. In: Solid state electrochemistry. Proceedings. 26. Risø international symposium on materials science, Risø (DK), 4-8 Sep 2005. Linderoth, S. et al; (eds.), (Risø National Laboratory, Roskilde, 2005) p. 355-362

A162. S.I. Hashimoto, Kindermann, L.; Poulsen, F.W.; Mogensen, M., A study on the structural and electrical properties of lanthanum-doped strontium titanate prepared in air. J. Alloys Compounds (2005) 397 , 245-249

A163. S.I. Hashimoto; Kammer Hansen, K.; Larsen, P.H.; Poulsen, F.W.; Mogensen, M., A study of $Pr_{0.7}Sr_{0.3}Fe_{1-x}Ni_xO_{3-delta}$ as a cathode material for SOFCs with intermediate operating temperature. Solid State Ionics (2005) 176 , 1013-1020

A164. M. Søgaard, Hendriksen, P.V.; Mogensen, M.; Poulsen, F.W.; Skou, E., Oxygen nonstoichiometry and transport properties of strontium substituted lanthanum cobaltite. Solid State Ionics (2006) 37-38 , 3285-3296

A165. K.A. Nielsen, A.R. Dinesen, A.R.; Korcakova, L.; Mikkelsen, L.; Hendriksen, P.V.; Poulsen, F.W., Testing of Ni-plated ferritic steel interconnect in SOFC stacks. Fuel Cells (2006) 6 , 100-106

A166. S. Hashimoto, L. Kindermann, Larsen, P.H.; Poulsen, F.W.; Mogensen, M., Conductivity and expansion at high temperature in $Sr_{0.7}La_{0.3}TiO_{3-\alpha}$ prepared under reducing atmosphere. J. Electroceram. (2006) 16 , 103-107

A167. S. Hashimoto, K. Kammer Hansen, Poulsen, F.W, Mogensen, M., Conductivity and electrochemical characterization of $PrFe_{1-x}Ni_xO_{3-delta}$ at high temperature. J. Alloys Compounds (2007) 428 , 256-261

General references

Ahlgren E.O., J. Phys. Chem. Solids **58**, 1475 (1997a)

Ahlgren E.O., Solid State Ionics **97,** 489 (1997b)

Atsumi T., Ohgushi T., Namikata H. and Kamegashira N.,
J. Alloys and Comp. **252**, 67 (1997)

Bakken E., Norby T., Stolen S., J. Mater. Chem., **12,** 317 (2002)

Bakken E. Stølen S., Norby T., Glenne R. and Budd M., Solid State Ionics **167,** 367 (2004)

Bevan D.J.M. and Kordis J., J. Inorg. Nucl. Chem., 26, 1509 (1964)

Bilde-Sørensen J.B. and Poulsen F.W., Internal Risø note, BC-83 ,(1992)

Bonanos N., Ellis B., Knight K.S. and Mahmood M.N., Solid State Ionics **35**, 179 (1989)

Bonanos N., Solid State Ionics **145,** 265 (2001)

Boroomand F, Wessel E, Bausinger H., and Hilpert K., Solid State Ionics **129**, 251 (2000)

Brice J.F. and Moreau A., Ann. de Chimie-Science des Materiaux **7**, 623 (1982)

Brouwer G., Philips Res. Rep. **9**, 366 (1954)

Canales-Vázques J.S., Irvine J.T.S. and Zhou W.Z., J. Solid State Chem., **177**, 2039 (2004)

Chambers R.G., Proc. Phys. Soc. **65** 903 (1952)

Chang E.K., and Blumenthal R.N., J. Solid State Chemistry, **72** 330 (1988)

Conradson S.D., Manara D., Wastin F., Clark D.L, Lander G.H., Morales L.A., Rebizant J. and Rondinella V.V., Inorg. Chem. **43**, 6922 (2004)

Coors W. G., J. Power Sources, **118**, 150 (2003)

Coors W.G., J. Electrochem.Soc. **151**, A994 (2004)

Dalton J., *A New System of Chemical Philosophy*. 3 vols. Manchester, 1808, 1810, 1827.

Demazeau G., Fabritchnyi P.,Fournes l., Darracq S., Presniakov I. A., Pokholok K. V., Gorkov V. P. and Etourneaua J., J. Mat. Chem., **5**, 553 (1995)

Dieckmann R., Ber. Bunsen-Gesellsch.-Phys. Chem, Chem Phys., **86**, 112 (1982)

Dieckmann R., J. Phys.Chem Solids **59,** 507 (1998)

Etsell T.H. and Flengas S.N., Chem. Rev. **70** 339 (1970)

Fergus J.W., J. Mat- Sci., **38** , 5259 (2003)

Flandermeyer B.F., Agarwal A.K., Anderson H.U. and Nashrallah M.M., J. Mater, Sci., **91**, 2593 (1984)

Frenkel Y., Z. Physik **53,** 652 (1926)

Ganguly J., Thermodynamic modeling of solid solutions, EMU Notes in Mineralogy, **3** Chapter 3, 37 (2001)

Gautron J., Marucco J.F. and Lemasson P., Mat. Res. Bull. **16**, 575 (1981)

Groβ B., Marion St., Hempelmann R., Grambole D., and Herrmann F., Solid State Ionics **109**, 13 (1998)

Groβ B., Engeldinger J., Grambole D., Herrmann F. and Hempelmann R., Phys. Chem. Chem. Phys., **2** 297-301. (2000)

Grundy A.N., Hallstedt B. and Gauckler L.J., Acta Mat. **50**, 2209 (2002)

Grundy A.N., Hallstedt B. and Gauckler L.J. Solid State Ionics **173,** 17 (2004)

Guo X., Sigle W. and Maier J., J. Amer. Ceram. Soc. **86**, 77 (2003)

Hashimoto, S-I., Mogensen M.. Kindermann L. and Poulsen F.W. (paper on La-doped $SrTiO_3$ in progress) (2004)

Hagenbeck R., Schneider-Stormann L., Vollmann M. and Waser R.
Mat. Sci. & Eng.-Solid State Mat. Adv. Techn., **B39**, 179 (1996)

Hagenbeck R. and Waser R., J. Eur. Ceram. Soc. **19**, 683 (1999)

Hansson A.N., Oxides in the Co-Cr-Fe-O system and oxidation behaviour of coated Fe-22Cr Steel, Ph.D. Thesis, DTU, April 2004.

van Hassel B.A., Kawada T., Sakai N., Yokokawa H., Dokiya M. and Bouwmeester H.J.M., Proceedings of the 1st Annual meeting of the Solid Oxide Fuel Cell society of Japan, Tokyo, 15-16 December 1992, pp. 111-116.(1992)

van Hassel B. A, Kawada T., Sakai N., Yokokawa, M. Dokiya, and Bouwmeester H.J. M., Solid State Ionics **66,** 295 (1993a)

van Hassel B.A., Kawada T., Sakai N., Yokokawa H., Dokiya M. and Bouwmeester H.J.M., Solid State Ionics **66** 295 (1993b)

Hayward M.A. Cussen E.J., Claridge J.B., Bieringer M., Rosseinsky M.J., Kiely C.J., Blundell S.J., Marshall I.M. and Pratt F.L., Science **295**, 1882 (2002)

Heisenberg W., Ann. Phys. **5** 888 (1931)

Hempelmann R., Eschenbaum J., Altmayer M., Groβ B., Grambole D., Herrmann F., Nagengast D., Krauser J., and Weidinger A., Ber. Bunsenges. Phys. Chem. **101**, 985 (1997)

Hempelmann R., Soetratmo M., Hartmann O., and Wäppling R., Solid State Ionics **107**, 269 (1998)

Hendriks M.G.H.M., ten Elshof J.E., Bouwmeester H.J.M. and Verweij H. Solis State Ionics **154**, 467 (2002)

Hillert M., J. Alloys and Comp., **320,** 161 (2001)

Hirsch L.M. and Shankland T.J., J. Geophys. Res. -Solid Earth and Planets **96,** 377 (1991)

Hofstadter D. R., "Gödel, Escher, Bach: an eternal golden braid" Vintage Books USA (1980).

Holstein T., Ann. Phys. (N.Y.) **8,** 343 (1959).

Huijser A, Bonanos N. and Poulsen F.W. (in press, Solid State Ionics) (2005)

Hund F., Z. Elektrochem., angew. Physik. Chem., **55,** 363 (1951)

Hägg Gunnar, Kemisk Reaktionslära, Stockholm, 1954

Ishizawa N., Matsushima Y., Hayashi M. and Ueki M., Acta Cryst., **B55**, 726 (1999)

Iwahara H., Esaka T., Uchida H., and Maeda N., Solid State Ionics **3-4**, 359 (1981)

Matsumoto H., Hayashi H., Shimura T., Amezawa K., Otake T., Yashiro K., Nigara Y., Kaimai A., Kawada T., Iwahara H. and Mizusaki J., Solid State Ionics **175**, 491 (2004)

Jacobsen T., Skou E.M. and Atlung S., Electrochimica Acta **30**, 423 (1975)

Kawamura Y., Konishi S., Nishi M. and Kakuta T., Fusion Science and Technology **41,** 1035 (2002)

Kevane C.J., Phys. Rev. **133,** A1431 (1963)

Kirchheim R., Acta Metall., **30**, 1069 (1982)

Kim H.S, Yoon Y.K and Lee Y.W., J.Nucl. Mat. **226,** 206 (1995)

Kliewer K.L. and Koehler J.S., Physical Review **140**, 1226(1965)

Knight , N. Bonanos, J. Mat. Chem.., **4**, 899 (1994)

Kofstad P., Nonstoichiometry, Diffusion and Electrical Conductivity in Binary Metal Oxides, Wiley-Interscience (1972)

Koksbang R., Barker J., Saidi M.Y., West K., Zachau-Christiansen B. and Skaarup S. Solid State Ionics **83**, 151 (1996)

Kosuge K, Chemistry of Non-stoichiometric Compounds, Oxford Press, USA (1994)

Kofstad P. and Hed A.Z., J. Amer. Ceram. Soc., **50** 681 (1967)

Kreuer K.-D., Ann. Rev. Mat. Res. **33**, 333 (2003)

Krogh Andersen I.G., Krogh Andersen E., Norby P. and Skou E. J. Solid State Chem. **113,** 320 (1994)

Kröger F.A., and Vink H.J., in Solid State Physics, edited by F. Sietz and D. Turnbull, Academic Press, Inc., San Diego, CA, 307-435 (1956)

Kröger F.A., Stieltjes F.H. and Vink H.J., Philips Res. Rep., **14**, 557 (1959)

Kröger F.A. Chemistry of Imperfect Crystals, North-Holland, Amsterdam, (1974)

Kuo J.H., Anderson H.U. and Sparlin D.M., J. Solid State Chem., **83**, 52 (1989)

Lagerlöf K.P.D. and Grimes R.W., Acta Mater. **46**,5689 (1998)

Lankhorst M.H.R., Bouwmeester H.J.M. and Verweij H., J. Solid State Chem., **133**, 555 (1997a)

Lankhorst M.H.R., Bouwmeester H.J.M. and Verweij H., J. Am. Ceram. Soc., **80**, 2175 (1997b)

Larsen P.H., Hendriksen P.V. and Mogensen M., J. Thermal Analysis **49**, 1263 (1997)

Lee, T.A. , Navrotsky A. and Molodetsky I., J. Mater. Res. **18,** 908 (2004a)

Lee, T.A. and Navrotsky A., J. Mater. Res. **19**,1855 (2004b)

Lee W.K. and Nowick A.S., Solid State Ionics **18-19**, (1986)

Liang K.C. , Nowick A.S., Solid State Ionics **61,** 77 (1993)

Ling S., Solid State Ionics **70**, 686 (1994a)

Ling S., J. Phys. Chem. Solids **55**, 1445 (1994b)

Lott K. and Turn L., J. Cryst. Growth **197**, 493 (1999)

Lu F-H., Tinkler S. and Dieckmann R., Solid State Ionics **62**, 39 (1993)

Lybye D. and Nielsen K., Solid State Ionics **167**, 55 (2004)

Maier J., Solid State Ionics **173**, 1 (2004)

Maier J., Festkörper- Fehler und Funktion, B.G. Teubner, Stuttgart-Leipzig (2000)

Malaman B. and Brice J.F., J. Solid State Chem. **53**, 44 (1984)

Mikkelsen L. and Skou E., J. Thermal Analysis and Calorimetry **64**, 873 (2001)

Minervini L., Zacate M.O. and Grimes R.W.Solid State Ionics **116**, 339 (1999)

Miyoshi S., Hong J-O., Yashiro K., Kamai A., Nigara Y., Kawamura K., Kawada T., and Mizusaki J., Solid State Ionics, **154-155,** 257 (2002)

Mizusaki J., Yamauchi S., Fueki K. and Ishikawa A., Solid State Ionics **12**, 119 (1984)

Mogensen M., Sammes N.M. and Tompsett G.A., Solid State Ionics **129**, 63 (2000)

Moos R. and Härdtl K.H., J.Am. Ceram. Soc., **80**, 2549 (1997)

Mukundan R., Brosha E.L., Birdsell S.A., Costello A.L., Garzon F.H. and Williams R.S., J. Electrochem. Soc. **146**, 2184 (1999)

Möbius H.-H., J. Solid State Electrochem., **1**, 2 (1997)

Naik I.K. and Tien T.Y., J. Phys.Chem. Solids **39**, 311 (1978)

Naito K., Tsuji T., and Matsui T., J. Rad. Nucl. Chem. **143**, 221 (1990)

Nernst W., Elektrotechnische Zeitschrift. **20**, 355, (1899)

Norby T., J. Mater. Chem., **11**, 11 (2001)

Norby T., Wideroe M., Glockner R. and Larring Y., Dalton Transactions **19**, 3012 (2004)

Nowotny J. and Rekas M., J. Am. Ceram. Soc. **81**, 67 (1998)

Ohsato H., Ozaki N., Ohnuma K., Mizuno Y., Hagiwara T., Kakimoto K. and Kishi H., Ferroelectrics **302**, 511 (2004)

Pionke M., Mono T., Schweika W., Springer T., and Schober H/T., Solid State Ionics **97**, 497 (1997)

Porat O. and Riess I., Solid State Ionics **81** , 29 (1995)

Porat O. and Tuller H.L.,,J. Electroceramics **1**, 41 (1997)

Poupon L., Iacconi P. and Pijolat C., J. Eur. Ceram. Soc. **6-7**, 747 (1999)

Ranløv J., Lebech B. and Nielsen K., J. Mat. Chem. **5**, 743 (1995)

Press W. H., Flannery B.P., Teukolsky S.A. and Vetterling W.T., I: Numerical Recipes, Cambridge Univ. Press, New York, 1986, p 274

Rickert H., Einführung in die Elektrochemie fester Stoffe, Springer-Verlag, Berlin, (1973)

Riess I., Janczikowski H., and Nölting J., J. Appl. Phys., **61** 4931. (1987)

Rosenberg A.J., J. Chem. Phys. **33**, 665 (1960)

Sasaki K. and Maier J., J. Appl. Phys., **86** 5422 (1999a)

Sasaki K. and Maier J., J. Appl. Phys. **86**, 5434 (1999b)

Sasaki K., Claus J. and Maier J. Solid State Ionics **121**, 51 (1999c)

Sasaki K. and Maier J., J. Eur. Ceram. Soc., **19**, 741 (1999d)

Schmalzried H., Z. Phys. Chem., **218**, 1385 (2004)

Schober T. and Wenzl H., Ionics **1**, 311 (1995)

Schober T. and Coors W.G., Solid State Ionics **176**, 357 (2005)

Schoonman J., Rev. Chimie Miner. **23**, 4647 (1986)

Schottky W., Z. Elektrochem., 45 (1939), 33

SEQS computer program, CET, Norman, Oklahoma

Sitte W., Bucher E. and Preis W., Solid State Ionics **154**, 517 (2002)

Smyth D. M., The Defect Chemistry of Metal Oxides, Oxford University Press, USA (2000)

Smyth D.M., J. Electroceram. **9,** 179 (2003)

Song S.J., Wachsman E.D., Rhodes J., Dorris S.E.and Balachandran U.,

Solid State Ionics **164,** 107 (2003)

Sosnowska I., Przenioslo R., Schäfer W., Kockelmann W., Hempelmann R., and Wysocki K., J. Alloy. Comp., **328,** 226 (2001)

Spence J.C.H. and Taftø J., J. Microscopy **130**, 147 (1983)

Spinolo G., AnselmiTamburini U. and Ghigna P., Z. Naturforschung A-A J. of Phys. Sci. **52**, 629 (1997)

Spinolo G. and Anselmi-Tamburini U., Ber. Bunsenges. Phys. Chem. **99,** 87-90 (1995)

Spinolo G., AnselmiTamburini U., Arimondi M., Ghigna P. and Flor G., Z. Naturforsch. A-A J.Phys. Sci. **50**, 1050 (1995b)

Steinsvik S., Larring Y. and Norby T. Solid State Ionics **143**,103 (2001)

Stone E.E., , J. Chem. Education **43,** 241 (1966)

Søgaard M., Hendriksen P.V., Lybye D., Mogensen M. and Jacobsen T., Effects of A/B-ratio in strontium doped lanthanum cobaltite, to be submitted to J. Electrochem. Soc., (2005)

Søgaard M.., Results from ongoing Ph.D. project at Risø. To be published. (2005a)

Søgaard M., Hendriksen P.V., Lybye D., Mogensen M. and Poulsen F.W. and Skou E., Oxygen non-stoichiometry and transport properties of strontium doped lanthanum cobaltite, to be submitted to Solid State Ionics (2005b)

Sørensen O.T., Editor " Non-stoichiometric oxides", Academic Press (1981)

Takahashi T., Iwahara H., Abstr. The Amer. Chem. Soc. April Meeting, 207 (1979)

Tsur Y. and Randall C.A., In proc: High temperature corrosion and materials chemistry, ed. P.Y. Hou et al, Electrochem. Soc. **2000**, 502 (2000)

Tsur Y. and Randall C.A., J. Amer. Ceram. Soc., **84**, 2147 (2001)

Turner P.S., White T.J., O'Connor A.J. and Rossouw C.J. ,J. Microscopy **162**, 369 (1991)

vanRoosmalen J.A.M. and Cordfunke E. H. P.,Solid State Chem. **110**, 109 (1994)

Wagner C. and Schottky W., Z. Phys. Chem., **B11**, 163 (1930)

Wagner C., Naturwissenschaften **31,** 265(1943)

Wang S., Inaba H., Tagawa H., Dokiya M., and Hashimoto T., Solid State Ionics **107**, 73 (1998)

Waser R. and Hagenbeck R., Acta Mater. **48**, 797 (2000)

Widerøe M., Kochetova N. and Norby T., Dalton Transactions **19**, 3147 (2004)

Willis B.T.M., J. Chem. Soc-Faraday Trans. **II 83**, 1073 (1987)

Wærnhus I., Sakai N., Yokokawa H., Grande T. and Wiik K., Solid State Ionics **175**, 69 (2004)

Wærnhus I., Vullum P.E., Holmestad R.,Grande T and Wiik K., Electronic properties of polycrystalline $LaFeO_{3-\delta}$. Part I; Qualitative Role of Schottky Defects, in press (2004)

Wærnhus I., Grande T. and Wiik K., Electronic properties of polycrystalline $LaFeO_{3-\delta}$. Part II; Defect modeling including Schottky defects in press (2004)

Yajima T., Koide K., Takai H., Fukatsu N., and Iwahara H., Solid State Ionics **79**, 333 (1995)

Yang X.Q., Lee H.S., Hanson L., McBreen J. and OkamotoY., J. Power Sources **54**, 198 (1995)

Zachau-Christiansen B., Jacobsen T., West K. and Skaarup S., in:Proc. 3rd Int. Symp. on SOFC,eds. S.C. Singhal and H. Iwahara, Electrochemical Soc. Proc. Vol. **93 - 5** p.104. (1993)

Zachau-Christiansen B., Jacobsen T. and Skaarup S., Solid State Ionics, **86 - 88**, 725 (1996)

Zintl E. and Croatto U., Z. anorg. u. allg. Chem., **242** 79 (1939)

Appendix 1.

Defect models for acceptor doped fluorite structure oxide with an oxidizable cation, and oxygen overstoichiometry made possible by formation of interstitial oxygens, examplified by $U_{1-x}Mf_xO_{2\pm\delta}$

Reference phase: $M(IV)O_2$

A-site Sum 1 mole	O-site sum 2 moles	Delocalised (no site conservation)
U_A^x (U+4)	O_O^x	O_i''
$U_A^\bullet$ (U+5) or $U_A^{\bullet\bullet}$ (U+6)	$V_O^{\bullet\bullet}$	e'
Mf_A' (Mf+3)		

Two models are defined with only one set of equations, which can deal with either the redox couple U^{+5}/U^{+4} (p=1) or U^{+6}/U^{+4} (p=2). Electrons are added to the model, such that also oxygen sub-stoichiometry at low pO_2 can be modelled. Reduction is thus described using electrons and not by trivalent U. The model is then a mixed small/large polaron description. Both redox cases can fit the experimental data of Kim et al. (1995) fairly well, as shown in paragraph 7.2, disqualifying the claim that the existence of Willis type giant clusters (Willis,1987) can be proven from Kim's high temperature TG data.

Definitions of mass law expressions and electro-neutrality, specific to this model:

Equilibration with oxygen gas, described as in eq. (1) or by

$$\tfrac{1}{2}O_2\,(gas) + V_O^{\bullet\bullet} + 2\,e' \leftrightarrow O_O^x \quad \Rightarrow \quad K'_{ox} = [O_O^x]/(pO_2^{1/2}\cdot[V_O^{\bullet\bullet}]n^2) \tag{1}$$

$$O_O^x \leftrightarrow V_O^{\bullet\bullet} + O_i'' \Rightarrow K_{Oi} = [V_O^{\bullet\bullet}]\,[O_i'']/\,[O_O^x] \tag{2}$$

$$U_A^x \leftrightarrow U_A^{\bullet p} + p\,e' \Rightarrow K_U = [U_A^x]\,/\,([U_A^{\bullet p}]n^p) \tag{3}$$

$$\text{ENC:}\quad p[U_A^{\bullet p}] + 2[V_o^{\bullet\bullet}] = [Mf_A'] + 2[O_i''] + n \tag{4}$$

Sequential solution

Triviality: $x = [Mf_A']$; guess $[U_A^{\bullet p}]$; then $[U_A^x] = 1 - x - [U_A^{\bullet p}]$; and $n = ([U_A^x]\,K_U / ([U_A^{\bullet p}])^{1/p}$; Suitable substitions and insertion in eq. (4) leads to a quadratic in $[V_O^{\bullet\bullet}]$, which is solved analytically

$$[V_O^{\bullet\bullet}]^2 + [V_O^{\bullet\bullet}]((p/2[U_A^{\bullet\bullet}] - x/2 - n/2 + K_{Oi}) - 2\,K_{Oi} = 0 \tag{5}$$

Then $[O_O^x] = 2 - [V_O^{\bullet\bullet}]$; $[O_i''] = K_{Oi}\,[O_O^x]/\,[V_O^{\bullet\bullet}]$; and total oxygen content/total amount of cations = $[O_O^x] + [O_i'']$; finally we calculate pO_2 from eq. (1)

$$pO_2 = \{\,[O_O^x]\,/(\,K'_{ox}\,)\cdot[V_O^{\bullet\bullet}]n^2)\}^2 \tag{1'}$$

Appendix 2.
Average valence defect model for a $(Co_xFe_{1-x})_3O_4$ spinel and Magnetite $Fe_{3\pm\delta}O_4$

The model was developed on request of Ph.D. student Anette Hansson, AFM Risø, who studied spinel formation and coatings on high Cr-steels (Hansson,2004).
The model ascribes an average charge to all cations of +8/3 = +2.666 and assumes a full occupation on the oxygen site at any pO_2. Reduction/oxidation is then taken care of by electrons, respectively holes. This model is able to describe Lu et al.'s stoichiometry data at 1200 ^{O}C for $(Co_{0.2}Fe_{0.8})_3O_4$ (Lu,1993). They used a complicated magnetite $Fe_{3\pm\delta}O_4$ model with two types of metal vacancies (octahedral and tetrahedral surroundings) and Fe^{+2}/Fe^{+3} distributed on one type of octahedral and on two types of tetrahedral interstitial positions,- a total of 8 cationic species. That model (Dieckmann,1982) can anyhow only be solved using a number of approximations and additional information on the distribution ratios over the tetrahedral/octahedral sites.

Reference phase: M_3O_4 with average oxidation state of metal M = + 8/3 = + 2.6667

M-site	interstitial-site	O-site	delocalised
M_M^X	$M_i^{2.6667\bullet}$	Oo^X	e'
$V_M^{2.6667\prime}$			h·

For brevity we leave out the fractional charges in the equations below, but they are clearly in operation, cf. for instance the ENC, eq. (3).

Site-conservation:

M $[M_M^X]+ [V_M] = 3$ (1)

O $[Oo^X] = 4$ (2)

Electroneutrality (ENC): Sum negative = Sum positive

$$8/3[V_M] + n = p + 8/3\,[M_i] \quad (3)$$

Mass action laws: $nill = e' + h\cdot$ $K_i = n \cdot p$ (4)

Frenkel: $M_M^X = V_M + M_i$ $K_{Frenkel} = [M_i] \cdot [V_M] / [M_M^X]$ (5)

Equilibrium with gas and forming one new formula unit of M_3O_4:

$$2O_2 = 4Oo^X + 8h^\bullet + 3\,V_M$$
$$K_{ox} = [Oo^X]^4 \cdot [V_M]^3 \cdot p^8/pO_2^2 \quad (6)$$

Sequential solution

Triviality: [Oo]=4; assume a value for $[V_M]$ in the interval 10^{-8} to .5;
then $[M_M^X] = 3-[V_M]$ and $[M_i] = K_{Frenkel} \cdot [M_M^X]/[V_M]$.

Insert $[V_M]$ and $[M_i]$ and $n = K_i/p$ in ENC, to obtain a quadratic in p

$$p^2 - 8/3([V_M] - [M_i]) \cdot p - K_i = 0 \qquad (7)$$

This is solved, where-after n is found from $n = K_i/p$. Finally the pO_2 in equilibrium with the above concentrations is calculated from eq. (6).

The p-type conductivity and non-stoichiometry parameter has a somewhat unusual log-log slope of 0.18181818.. = 2/11 at high pO_2. It can be arrived at by assuming that n and $[M_i]$ can be neglected in the ENC leading to $p \approx 8/3[V_M]$. If this Brouwer approximation is inserted in the mass action expression eq. (6) we get

$$K_{ox} = [Oo^X]^4 [V_M]^3 p^8/pO_2^2 = [Oo^X]^4 \cdot (8/3)^3 \cdot p^3 \cdot p^8/pO_2^2 \propto p^{11}/pO_2^2$$

The limiting 2/11 slope could be verified by the above algorithm.

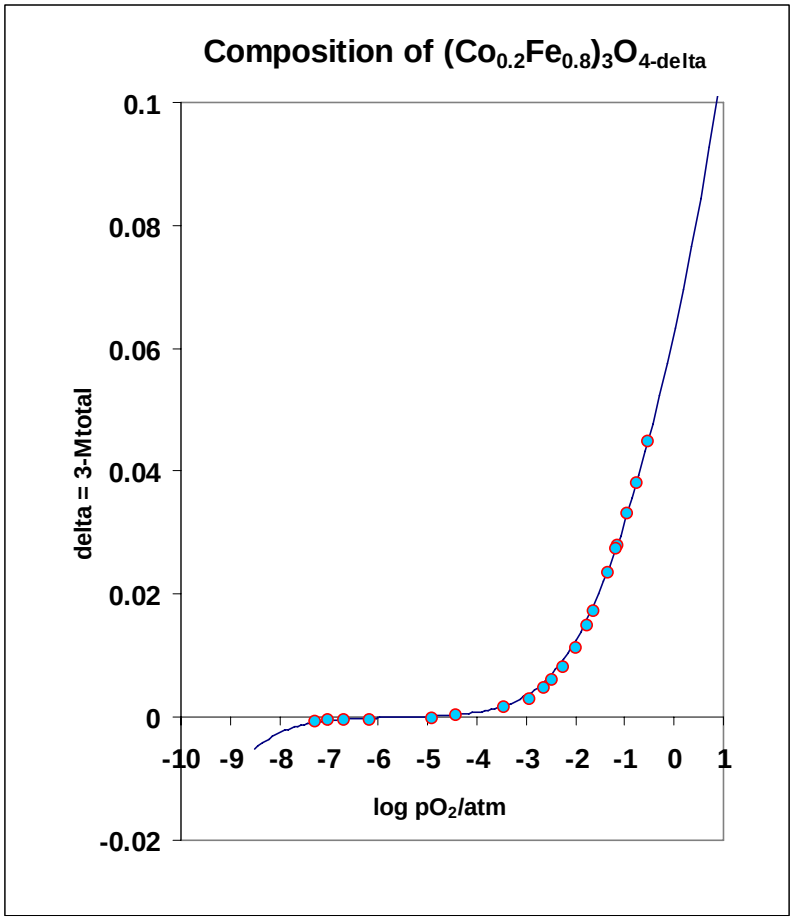

Figure App 2.1. Stoichiometry data at 1200 ^{O}C of $(Co_{0.2}Fe_{0.8})_3O_4$ (Lu,1993).
The material transforms into hematite at high pO_2 and into wüstite at low pO_2.
The calculated curve is based on an average valence model, where no distinction is made between the oxidation states of Co and Fe.

The stoichiometry data from Table 1 of Lu et al. (1993), are shown in Figure App. 2.1, together with calculated model data from the above model, using the equilibrium constants $K_{ox} = 1.5 \cdot 10^{-9}$ atm^{-2}, $K_i = 1.25 \cdot 10^{-2}$ and $K_{Frenkel} = 1.7 \cdot 10^{-9}$. Included in this model calculation, as well as in the paper of Lu et al., is an adjustable zero shift for the stoichiometry at the plateau. The zero shift was here estimated to be -0.003, compared to –0.00168 (Lu et al,1993). It is concluded that the average valence model gives just as good a description of the data as the much more complicated model described by Lu and Dieckmann.

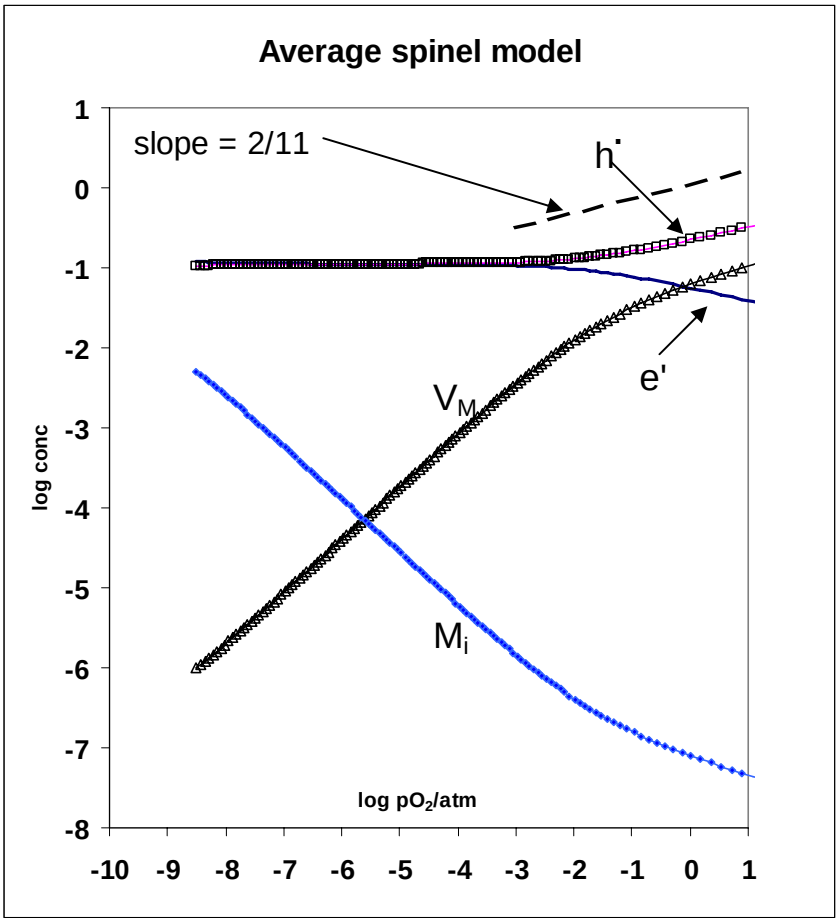

Figure App 2.2. Brouwer diagram for $(Co_{0.2}Fe_{0.8})_3O_4$ at 1200 ^{O}C using an average valence model and equilibrium constants given in the text.

The stoichiometric point, where $\delta = 0$, is located at the point, where the $[V_M]$ and $[M_i]$ concentration curves intersect, i.e. around $pO_2 = 10^{-5.5}$ atm. From Figure App 2.2 we see that $[V_M] \approx [M_i] \approx 10^{-4}$ mole/mole of M_3O_4. The crystal is then very close to the ideal spinel structure, where the Frenkel reaction, eq. (5) in the cation lattice by and large can be neglected. The value of $[V_{Fe}] = 1.4 \cdot 10^{-4}$ extracted from Figure 6 of (Dieckmann, 1982) for Fe_3O_4, also at 1200^{O}C, is quite close to the present model estimate. The high concentrations of holes and electrons, ≈ 0.1, obtained as output from the average valence model are actually not high numbers, when compared to the total amount of electrons in one formula unit of M_3O_4: they correspond to a part of 0.1/3 = 3.3% of the cations having exchanged electrons from Fe^{2+} to Fe^{3+} or vice versa.

Appendix 3.

Defect model for acceptor- and donor doped $SrTiO_3$.
Expansion upon oxidation predicted from a defect model

Reference phases: Sr(II)Ti(IV)O_3-perovskite + exoluted SrO

A-site	B-site	O-site	delocalised
Sr_{Sr}^{X}	Ti_{Ti}^{X}	Oo^{X}	e'
$La_{Sr}^{\bullet}$	Fe_{Ti}'	$V_O^{\bullet\bullet}$	
V_{Sr}''	$Nb_{Ti}^{\bullet}$		$h^{\bullet}$

The above model is utilised in a submitted paper by the author with Hashimoto et al. (2004), which presents conductivity and dilatometric data as function of pO_2 for La doped $SrTiO_3$. The model is basically that of Flandermeier et al (1984), which was more widely broadcasted by the work of Moos and Härdtl (1997). The expansion made by the present author deals with i) inclusion of simultaneous acceptor- and donor doping; and ii) a quantitative link is created to describe the macroscopic expansion upon oxidation due to exolution of Sr-rich interlayers or of a secondary Sr-rich phase. Doped Ba-titanates, on the other hand, are believed to exolute Ti-rich phases upon oxidation, cf. references in (Smyth,2003).

The main feature of defect models, which include a Schottky reaction involving only one site in a ternary or multinary oxide, such as the above mentioned cases for Sr- and Ba-titanates, is that a second phase has to be involved in order that mass conservation for the given element involved in the Schottky reaction be observed.

Perovskite structure oxides usually expand upon reduction and not the opposite as observed here. The unit cell of the main perovskite phase of $Sr_{0.7}La_{0.3}TiO_3$ contracts 0.086% upon oxidation as shown by x-ray diffraction. Still a macroscopic expansion up to 0.51 % of the sample is observed upon oxidation. The perovskite structure can not accommodate interstitial, extra oxygen ions. The extra oxygen can be placed in rock salt structure intergrowth layers (Sr/La)O as in the Ruddlesden-Popper series $(Sr/La)_{n+1}Ti_nO_{3n+1}$ of which Sr_2TiO_4 and $SrTiO_3$ are the two end members, for n = 1, respectively n = ∞. The extra oxygen uptake can alternatively be accounted for by free SrO, as has been observed by J. Maier et al (private communication,2004). Charge balance is in both cases obtained by having Sr vacancies, V_{Sr}'', in the perovskite layers. A continuous $La_2Sr_{n-2}Ti_nO_{3n+1}$ model of Canales-Vázquez et al [2004] has also been presented, which was substantiated by HREM observations.

We will illustrate the R-P type model using formation of the end member of the R-P-series as an example. Further oxidation of a $Sr_{1-y}La_yTiO_3$ perovskite, starting from a near to fully occupied oxygen "sub-lattice" can be formulated as

$$Sr_{1-y}La_yTiO_3 + xO_2(gas) = (1-2x)\ Sr_{(1-y-4x)/(1-2x)}La_{y/(1-2x)}TiO_3 \ + \ 2x\ Sr_2TiO_4 \quad (1)$$

A-site stoich perovskite	A-site non-stoich perovskite	R-P-phase
FOX[51] of Ti: +(4-y)	+ (4-4x-y)/(1-2x)	+4
molar volume		
59.7 Å^3	≈60 Å^3	95 Å^3

The upper limit for x in eq(1) is obtained, when all Ti in the A-site deficient perovskite is +4. It can be seen that this occurs for x = y/4. The change in volume, based on the change in molar volume, will be

$$\Delta V(x) = 60\,(1-2x) + 2x\,95 - 59.7 \approx 2\,(95-60)x = 70x \qquad (2)$$

The corresponding linear expansion will be

$$\Delta L/L = (\sqrt[3]{V(x)} - \sqrt[3]{60})/\sqrt[3]{V(60)}; \qquad (3)$$

If reaction (1) runs to completion for y = 0.3, we would get the maximum expansion upon oxidation as $\Delta L/L_{max} = 2.84\%$.

As two separate phases are formed on oxidation in the above reaction (1) diffusion of cations is required. Diffusion needs only to be over one or a few atomic distances,- i.e. it could potentially be a fast mechanism if the Sr-rich second phase does not precipitate immediately, but only when a solubility limit is exceeded . The overall oxygen content is $O_{tot}/Ti = 3+2x$. The mole fraction of V_{Sr}'' in the non-stoichiometric perovskite is $[V_{Sr}''] = 2x/(1-2x)$. The average oxidation state of Ti increases in the A-site deficient perovskite as the oxidation proceeds, although less and less of the perovskite phase is formed. It becomes more simple if we model the phase separation by a precipitation of pure SrO:

$$Sr_{1-y}La_yTiO_3 + xO_2(gas) = 1\ Sr_{(1-y-2x)}La_yTiO_3 + 2x\ SrO \qquad (4)$$

A-site stoich perovskite	A-site non-stoich perovskite	"R-P-phase"
FOX of Ti: +4-y	+4-y+4x	
molar volume		
59.7 Å^3	≈60 Å^3	33.75 Å^3

The change in volume will then be $\Delta V(x) = 60 + 2x\ 33.75 - 59.7 \approx 2\,(33.75)x = 67.5x$ and $\Delta L/L = (\sqrt[3]{V(x)} - \sqrt[3]{60})/\sqrt[3]{V(60)}$; for y = 0.3 we obtain $\Delta L/L_{max} = 2.74\%$ We observe that there is only a marginal difference in the prediction for the length change in the two models. The observed expansion of 0.51% indicates that the oxidation is only at its beginning in the achievable p_{O2} range or has not reached the interior of the grains in the time allowed for equilibration.

[51] FOX here meaning: formal oxidation state of Titanium

Equations governing the defect model of $Sr_{1-y}La_yTi_{1-w-z}Fe_wNb_zO_{3\pm\delta}$

Site-conservation:		***Mass:***
A	$[La_{Sr}^{\bullet}]+[Sr_{Sr}^{X}]+[V_{Sr}'']=1$	$[La_{Sr}^{\bullet}]=y$
O	$[Oo^{X}]+[V_{O}^{\bullet\bullet}]=3$	$[Fe_{Ti}']=w$
B	$[Ti_{Ti}^{X}]+[Fe_{Ti}']+[Nb_{Ti}^{\bullet}]=1$	$[Nb_{Ti}^{\bullet}]=z$

Electroneutrality (ENC): Sum negative = Sum positive

$$2[V_{Sr}''] + [Fe_{Ti}'] + n = [La_{Sr}^{\bullet}] + [Nb_{Ti}^{\bullet}] + 2[V_{O}^{\bullet\bullet}] + p \qquad (5)$$

Mass action laws: $nill = e' + h^{\cdot}$ $\qquad Ki = n \cdot p \qquad (6)$

Schottky: $Sr_{Sr}^{X} + Oo^{X} = V_{Sr}'' + V_{O}^{\bullet\bullet} + SrO(\text{new phase}) \qquad (7)$

$$[V_{Sr}''] \cdot [V_{O}^{\bullet\bullet}] \;/([Sr_{Sr}^{X}] \cdot [Oo^{X}]) = K_s$$

Eq. with gas: $\tfrac{1}{2}O_2(g) + V_{O}^{\bullet\bullet} = Oo^{X} + 2h^{\bullet} \qquad (8)$

$$K_{ox} = [Oo^{X}] \cdot p^2 / (pO_2(g)^{1/2} \cdot [V_{O}^{\bullet\bullet}])$$

Exoluted amount of SrO = $[V_{Sr}'']$, as number of moles of perovskite is constant.

Sequential solution

Trivialities: $[La_{Sr}^{\bullet}] = y$; $[Fe_{Ti}'] = w$; $[Nb_{Ti}^{\bullet}] = z$; $[Ti_{Ti}^{X}] = 1-w-z$

Assume a value for $[V_{O}^{\bullet\bullet}]$ in the interval 10^{-8} to .5 . The lower limit can be lower; the upper limit is Brownmillerite; then $[Oo^{X}] = 3 - [V_{O}^{\bullet\bullet}]$, use these two values in eq. (7) and solve for $[Sr_{Sr}^{X}]$

$$[Sr_{Sr}^{X}] = (1-y)/(1+K_s*[Oo^{X}] /[V_{O}^{\bullet\bullet}]), \qquad (9)$$

then $[V_{Sr}'']$ can be found from either

$[V_{Sr}''] = 1-y- [Sr_{Sr}^{X}]$ or $[V_{Sr}''] = K_s \cdot [Oo^{X}] \cdot [Sr_{Sr}^{X}]/[V_{O}^{\bullet\bullet}]$

In eq (5), the ENC, we now know the five ionic concentrations and only have n and p as unknowns:

$n - p + (2[V_{Sr}''] - [La_{Sr}^{\bullet}] + [Fe_{Ti}'] - [Nb_{Ti}^{\bullet}] -2[V_{O}^{\bullet\bullet}]) = 0$; insert $p=K_i/n$ gives

$n^2 + n(2[V_{Sr}''] - [La_{Sr}^{\bullet}] + [Fe_{Ti}'] - [Nb_{Ti}^{\bullet}] -2[V_{O}^{\bullet\bullet}]) - K_i = 0$

p is calculated from $p = K_i/n$. Finally the pO_2 in equilibrium with the above concentrations is calculated from eq.(10).

Appendix 4.

Analytical difference of $O_O^{\bullet}$ or $h^{\bullet}$ as the oxidized species in a fluorite oxide.

The treatment relates to the models shown in Table 7.4. It will be proven algebraically that the two descriptions in principle differ, but in practice may coincide.

Large polaron model 6	**Small polaron model 4**
$nil = h^{\bullet} + e' \Rightarrow K_{i6} = n \times p$	$O_O^x \leftrightarrow O_O^{\bullet} + e' \Rightarrow K_{i4} = [O_O^{\bullet}] \cdot n/[O_O^x]$, $[O_O^{\bullet}]$ enters ENC and the O-site conservation
Equilibration with oxygen gas $\frac{1}{2}O_2(gas) + V_O^{\bullet\bullet} \leftrightarrow O_O^x + 2h^{\bullet} \Rightarrow$ $K_{ox} = [O_O^x] \cdot p^2/(pO_2^{1/2} \cdot [V_O^{\bullet\bullet}])$	Equilibration with oxygen gas $\frac{1}{2}O_2(gas) + V_O^{\bullet\bullet} + O_O^x \leftrightarrow 2O_O^{\bullet} \Rightarrow$ $K_{ox} = [O_O^{\bullet}]^2/(pO_2^{1/2} \cdot [V_O^{\bullet\bullet}] \cdot [O_O^x])$

We impose the condition that the electron concentrations following from the two models be identical: $n_{model\ 6} = n_{model\ 4}$, and also that the positive charge concentrations should be equal at all pO_2 's

$$[O_O^{\bullet}]_{model\ 6} = [h^{\bullet}]_{model\ 4} \qquad (1)$$

forcing the two models to be identical in these two respects (but no further constraints are imposed). Then we find by of substitution of the ENC and the O-site condition into the definition of K_{i4},

$$p \equiv \frac{K_{i6}}{n} \stackrel{?}{=} [O_O^{\bullet}] \equiv \frac{K_{i4}(4-x-n)}{n(2+K_{i4}/n)} \qquad (2)$$

here x is the acceptor dopant concentration. The two models can therefore not describe the same reality, since K_{i6} will have to change continuously with varying pO_2 or n-concentration in order that the two models numerically output the same concentrations. If $K_{i4} << 1$, (then also $K_{i6} << 1$) and $n << 1$, then the above can be approximated by

$$K_{i6} \approx K_{i4} \cdot (2-x/2) \qquad (3)$$

By similar arguments one can also find the approximate relation between K_{ox6} and K_{ox4}

$$K_{ox6} \approx K_{ox4} \cdot (2-x/2)^2 \qquad (4)$$

So from a practical point of view the two models may be indistinguishable under the named conditions.

Appendix 5

Defect model for a reducible, acceptor doped fluorite structure oxide with 5 different defect associates.

Reduction of the host cation, in a one-electron step, formulated in a small polaron description, reads

$$2A_A^x + O_O^x \leftrightarrow 2\,A_A' + V_O^{\bullet\bullet} + \tfrac{1}{2}O_2\,(\text{gas}) \qquad (1)$$

$$K_{red} = \frac{[V_O^{\bullet\bullet}] \cdot [A_A']^2 \cdot pO_2^{1/2}}{[O_O^x] \cdot [A_A^x]^2} \qquad (2)$$

The simplest associates are 1:1 associates between the lower valent dopant or the reduced host ion,- these 1:1 associates carry in the K-V.-notation one positive charge. They are here called g1 and c1 for brevity, see Table 1. The next simplest associates are the uncharged 2:1 complexes, of which we include all three possible ones, including a mixed one $cg \equiv [A_A', M_A', V_O^{\bullet\bullet}]^x$. The association model thereby includes 10 species, see Table 1. The mathematical complexity of this model stems from the fact that 5 out of 10 species are defined in terms of non-linear mass law expressions, in addition to the 6th equilibrium reaction with gaseous oxygen, eq. (2). Oxygen over-stoichiometry is not included in this model, precluding p-type conduction. Likewise can the model not cope with cases, where the A-cation is reduced below the +3 stage. The last two limitations were necessary, otherwise it proved impossible to develop a sequential algorithm for finding the concentrations. Care must be taken in counting correctly in the site conservation equations (4) and (5) and the mass equation, eq. (6), since the associate species occupy more than one crystallographic site.

Table 1. Defect model for a reducible, acceptor doped fluorite type oxide with 5 different oxygen vacancy associates. Key: a short-hand notation for the associates, g1,g2,c1,c2,and cg is introduced.

Metal-site	O-site	Short name for species, associated equilibrium constant, (defined in equation #)
A_A^x	O_O^x	K_{red} (1,2)
A_A', reduced host cation, unassociated	$V_O^{\bullet\bullet}$	
M_A', unassociated dopant ion		
Associates involving both metal and O-sites $[M_A', V_O^{\bullet\bullet}]^{\bullet}$		g_1, K_{g1}, (7)
$[2M_A', V_O^{\bullet\bullet}]^x$		g_2, K_{g2}, (8)
$[A_A', V_O^{\bullet\bullet}]^{\bullet}$		c_1, K_{c1}
$[2A_A', V_O^{\bullet\bullet}]^x$		c_2, K_{c2}
$[A_A', M_A', V_O^{\bullet\bullet}]^x$		cg, K_{cg} (9)

Definitions of site- and mass- conservation:

$$\text{O-site: } [O_O^x] + [V_O^{\bullet\bullet}] + g_1 + g_2 + c_1 + c_2 + cg = 2 \quad (4)$$

$$\text{Metal-site: } [A_A^x] + [A_A'] + [M_A'] + g_1 + 2g_2 + c_1 + 2c_2 + 2cg = 1 \quad (5)$$

$$\text{Mass of the dopant: } x = [M_A'] + g_1 + 2g_2 + cg \quad (6)$$

Definitions of mass law expressions:

$$K_{g1} \equiv [M_A', V_O^{\bullet\bullet}]^{\bullet} / \{[M_A'][V_O^{\bullet\bullet}]\} \equiv g1/\{[M_A'] \cdot [V_O^{\bullet\bullet}]\} \quad (7)$$

$$K_{g2} \equiv [2M_A', V_O^{\bullet\bullet}]/\{[M_A']^2 [V_O^{\bullet\bullet}]\} \equiv g2/\{[M_A']^2 \cdot [V_O^{\bullet\bullet}]\} \quad (8)$$

$$K_{cg} \equiv [A_A', M_A', V_O^{\bullet\bullet}]/\{[A_A'] \cdot [M_A'] \cdot [V_O^{\bullet\bullet}]\} \equiv cg/\{[A_A'] \cdot [[M_A'] \cdot [V_O^{\bullet\bullet}]\} \quad (9)$$

The remaining two association equilibria are defined in an analogous manner. The electro-neutrality condition reads:

$$\text{ENC: } [A_A'] + [M_A'] = 2[V_O^{\bullet\bullet}] + g_1 + c_1 \quad (10)$$

Solution of the system of equations by the sequential method:

All concentrations can be expressed by the free $[V_O^{\bullet\bullet}]$ or the free $[M_A']$ concentration from the definitions of the equilibrium constants and the mass conservation equation for the dopant (6). After proper substitutions, these expressions are inserted in the ENC, whereby quadratics in either $[V_O^{\bullet\bullet}]$ or $[M_A']$ are obtained. After factorisation, these are

$$a[V_O^{\bullet\bullet}]^2 + b\,[V_O^{\bullet\bullet}] + c = 0 \quad (11)$$
$$d[M_A']^2 + e\,[M_A'] + f = 0 \quad (12)$$

with a, b and c having the following definitions

$$a = 2 + [M_A']\,K_{g1} - K_{c1}(K_{g1} + 2[M_A']\,K_{g2})/K_{cg} \quad (13)$$
$$b = K_{g1}/K_{cg} + 2\,[M_A']K_{g2}/K_{cg} - [M_A'] + xK_{c1}/([M_A']K_{cg}) - K_{c1}/K_{cg} \quad (14)$$
$$c = 1/K_{cg} - x/([M_A']K_{cg}) \quad (15)$$

For the converse relationship in eq. (12), d, e and f are defined as

$$d = [V_O^{\bullet\bullet}]^2\,\{K_{g1} - 2\,K_{c1}K_{g2}/K_{cg}\} + [V_O^{\bullet\bullet}]\,\{2\,K_{g2} - 1\} \quad (16)$$
$$e = 1/K_{cg} + [V_O^{\bullet\bullet}]\{K_{g1} + 2[V_O^{\bullet\bullet}] - 1 - [V_O^{\bullet\bullet}]K_{g1}\} \quad (17)$$
$$f = x/K_{cg}\,\{[V_O^{\bullet\bullet}]K_{c1} - 1\} \quad (18)$$

Searching for a sequential solution, we now have two alternatives: i) we can solve the equations from a guess of the concentration of free dopant, $[M_A']$, in the range 0 to x and solve for $[V_O^{\bullet\bullet}]$ using eqs. (11,13,14,15); alternatively ii) we guess the concentration of free oxygen vacancies $[V_O^{\bullet\bullet}]$, in the range 0 to x/2 and solve for $[M_A']$ using eqs. (12,16,17,18). Both routes are feasible, but route 1) is in practice prove more difficult to handle numerically, since for cases both of very weak and very strong association, the $[M_A']$ as function of pO_2 will be a very flat function, and the concentration interval of relevance may be difficult to locate.
Now, for a given value of $[V_O^{\bullet\bullet}]$, all the d-,e- and f-terms will assume a known numerical value. $[M_A']$ is found from the quadratic equation using the positive root. The remaining 8 concentrations then follows

$$[A_A'] = (x - [M_A'] - [M_A']\,[V_O^{\bullet\bullet}]K_{g1} - 2[M_A']^2[V_O^{\bullet\bullet}]\,K_{g2})/([V_O^{\bullet\bullet}]\,[M_A']\,K_{cg}) \quad (19)$$
$$g_1 = [M_A'][V_O^{\bullet\bullet}]\,K_{g1} \quad (20)$$
$$g_2 = [M_A']^2\,[V_O^{\bullet\bullet}]\,K_{g2} \quad (21)$$
$$c_1 = [A_A']\,[V_O^{\bullet\bullet}]K_{c1} \quad (22)$$
$$c_2 = [A_A']^2\,[V_O^{\bullet\bullet}]K_{c2} \quad (23)$$
$$cg = [M_A']\,[A_A']\,[V_O^{\bullet\bullet}]K_{cg} \quad (24)$$
$$[A_A^x] = 1 - ([A_A'] + [M_A'] + g_1 + 2g_2 + c_1 + 2c_2 + 2cg) \quad (25)$$
$$[O_O^x] = 2 - ([V_O^{\bullet\bullet}] + g_1 + g_2 + c_1 + c_2 + cg) \quad (26)$$

Note that this algorithm does not allow one to put $K_{cg} = 0$, cf eqs. (13)-(18). However, for any practical purposes, where one wants to simulate absence of the mixed cg-associate ($K_{cg} \approx 0$) one can put K_{cg} equal to some very small number, i.e. 10^{-10}. Finally, the pO_2 corresponding to the 10 equilibrium concentrations is found from the definition of the reduction equilibrium, eq. (2).

Reprints of submitted papers A1-A10

A1.

A. Holt, E.O. Ahlgren and F.W. Poulsen,
Synthesis, electrical properties and defect chemistry of Ti-doped $NdCrO_3$,
Proc. 3rd Int. Symp. Solid Oxide Fuel Cells, (Eds. S.C. Singhal and H. Iwahara), Honolulu, USA, May 16-21, 1993. Proc. vol. **93-4** 562-574. (1993)

SYNTHESIS, ELECTRICAL PROPERTIES AND DEFECT CHEMISTRY OF Ti-DOPED $NdCrO_3$

A. Holt, E. Ahlgren* and F. W. Poulsen*
Center for Materials Research, University of Oslo
Gaustadalleen 21, N-0371 Oslo, Norway

* Materials Department, Risø National Laboratory
P.O. box 49, DK-4000 Roskilde, Denmark

ABSTRACT

Synthesis, defect chemistry and electrical properties of Ti-doped $NdCrO_3$ have been studied at different oxygen partial pressures at 1000 and 1200 °C. Both the citric acid and glycine/nitrate method have been used for preparation of the specimens. The electrical conductivity has been measured by a four probe measurement technique and the Seebeck coefficient by a two point technique. The specimens used for measuring the electrical properties have been characterised by X-ray diffraction and scanning electron microscopy. The solubility of titanium in $NdCr_{1-x}Ti_xO_3$ is found to be about 20 atom %. The results from the electrical conductivity and Seebeck coefficient measurements showed a p-type conductivity at high p_{O_2} and an n-type conductivity at low p_{O_2}. At low oxygen partial pressures the concentration of electrons decreased by a slope of - 1/4 with increasing oxygen partial pressure and at high oxygen partial pressure the electron holes increased by a slope of 1/4 with increasing oxygen partial pressure. The concentration and the mobility of the electronic defects have been calculated at 1000 °C as function of oxygen partial pressure. A model calculation of the defect concentration in $NdCr_{1-x}Ti_xO_3$ is presented.

INTRODUCTION

There is today an intensive research in developing new anode materials for use in solid oxide fuel cells (SOFC) to increase the performance and the life time. Recent research on nickel-cermet anodes has shown promising results in uses where hydrogen serves as fuel. A problem with the nickel-cermet anode when methane is used as fuel, is that the nickel metal catalyses the dehydrogenation reaction of methane to form a layer of carbon between the zirconia and the nickel and thereby inhibits the anode reaction and a good performance of the SOFC. It is therefore necessary to develop new anode materials if methane is to be used directly as fuel in the SOFC. This work has investigated possible candidates in the $NdCrO_3$ - $NdTiO_3$ system.

Thermodynamic data are not available for the $NdCrO_3$ - $NdTiO_3$ system, but it is suggested that these ternary oxides are at least as stable as the most unstable binary component oxides. Cr_2O_3 is calculated to be stable down to an oxygen partial pressure of about 10^{-22} atm and for TiO_2 down to about 10^{-20} atm at 1000 °C (1,2).

Palguev et al.(3) have measured the thermal expansion coefficient of $NdCrO_3$ to be 7.8 10^{-6} K^{-1}. Previously, electrical conductivity of $NdCrO_3$ has been measured by Tripathi (4) and Palguev et al. to be in the range of 0.1 to 0.2 S/cm at 1000 °C in air. Palguev et al. also measured the electrical conductivity as function of oxygen partial pressure at 1000 °C to be constant down to 10^{-15} atmospheres, below which it decreases with decreasing oxygen partial pressures. The observed constant electrical conductivity at high oxygen partial pressure indicates that the main defect situation is controlled by lower valent impurities and electron holes, $p = [Mf_{Cr}^{'}]$.

The idea for the present work was to substitute chromium with titanium in $NdCrO_3$ to obtain high electrical conductivity at oxygen pressures equal to the operation conditions of the anode. This idea is clarified in a Kröger Vink diagram which shows the different concentrations of defects in $NdCr_{1-x}Ti_xO_3$ at different oxygen partial pressures, shown in figure 1. $[V_M^{'''}]$ denotes chromium and neodymium vacancies, $[V_O^{\cdot\cdot}]$ oxygen vacancies, $[Ti_{Cr}^{\cdot}]$ titanium on chromium sites, p electron holes and n electrons, respectively. A desirable defect situation is in the region where the free electron concentration is equal to the doping concentration, $[Ti_{Cr}^{\cdot}] = n$.

The Kröger Vink diagram in figure 1 has been calculated by combining the equations for site- and mass-balances, electroneutrality condition and the equilibrium expressions of formation for the different defects by a computer program (5). The electroneutrality condition is described by

$$3[V_{Nd}^{'''}] + 3[V_{Cr}^{'''}] + n = p + 2[V_O^{\cdot\cdot}] + [Ti_{Cr}^{\cdot}] \qquad [1]$$

The equilibrium expressions of formation for the different defects are given by equations 2, 3 and 4,

$$1/2\ O_2\ (g) + V_O^{\cdot\cdot} = O_O^x + 2\ h^{\cdot} \quad => \quad K_{Vo} = \frac{[O_o^*]\ p^2}{[V_O^{\cdot\cdot}]\ pO_2^{1/2}} \qquad [2]$$

$$0 = V_{Nd}^{'''} + V_{Cr}^{'''} + 3\ V_O^{\cdot\cdot} \quad => \quad K_s = [V_{Nd}^{'''}]\ [V_{Cr}^{'''}]\ [V_O^{\cdot\cdot}]^3 \qquad [3]$$

$$0 = e' + h^{\cdot} \quad => \quad K_i = np \qquad [4]$$

where K_{Vo} and K_i are equilibrium constants for formation of oxygen vacancies and the electronic defects and K_s is the equilibrium constants for formation of Schottky defects.

MATERIALS AND METHODS

Both the citric acid and glycine/nitrate method have been successfully used in the preparation of $NdCr_{1-x}Ti_xO_3$ and $Nd_2Ti_2O_7$ powders.

Synthesis by the citric acid method

Four different specimens of $NdCr_{1-x}Ti_xO_3$ with composition x=0, x=0.1, x=0.2, x=0.4 and one specimen of $Nd_2Ti_2O_7$ have been prepared by the citric acid method (6). $C_{15}H_{21}O_6Cr$, $C_{10}H_{14}O_5Ti$, Nd_2O_3, HNO_3 and $C_6H_8O_7$ H_2O were used as precursor materials. Nd_2O_3 dissolves in HNO_3. $C_{15}H_{21}O_6Cr$ and $C_{10}H_{14}O_5Ti$ dissolved slowly under evaporation of water from the solution. After decomposition in the temperature range 100-130 °C the powders were calcined at 1000 °C for 4 hours. The colour of the oxide powders that contained both chromium and titanium was mainly green with a taste of a yellow. The $NdCrO_3$ powder had a green colour and $Nd_2Ti_2O_7$ was light blue with a red tint under certain light conditions. The size of the particles after calcining was approximately 0.1 μm, but mainly agglomerated into larger particles.

Synthesis by the glycine/nitrate method

Three different specimens of $NdCr_{1-x}Ti_xO_3$ with composition x=0, x=0.3 and x=0.6 have been prepared by the glycine/nitrate method (7). $Cr(NO_3)_3{\cdot}9H_2O$, $Ti[OCH(CH_3)_2]_4$, Nd_2O_3 and HNO_3 were used as precursor materials.

Under addition of $Ti[OCH(CH_3)_2]_4$ a polymerisation occurred immediately and solid transparent flakes on the surface of the solution were formed. These flakes dissolved again under heating. The powder formed after the glycine-nitrate reaction was examined by X-ray diffraction and showed crystalline structures for all specimens. After calcination at 1300 °C in air the specimens were again examined by X-ray diffraction. Table I lists the colour and the crystal structure before and after calcination of the formed oxide powders.

From table I it can be seen that the $NdCr_{1-x}Ti_xO_3$ powders changed from single phase materials to two phase materials after calcination at 1300 °C in air. The formation of a single phase material directly from the glycine/nitrate syntheses at high titanium concentrations may indicate a higher solubility of titanium at lower temperatures. The results also indicate a change from orthorhombic to cubic crystal structure of $NdCr_{1-x}Ti_xO_3$ above a certain titanium concentration. The powders formed glycine-nitrate reaction were very airy and were easily broken down to smaller particles in a mortar.

Electrical conductivity measurements

The specimens used for electrical conductivity and Seebeck measurements were prepared by cold pressing $NdCr_{1-x}Ti_xO_3$ powder synthesised from the citric acid method to pellets at a pressure of 550 atmospheres with a diameter of 28 mm. The specimens were sintered at a temperature of 1500 °C for 10 hour in air after cold pressing. The porosity of the specimens, as determined by the weight and the geometrical size, was about 60% except for $Nd_2Ti_2O_7$ where the porosity was only about 6 %.

The specimens were formed to dimensions of 2-3 mm in thickness, 7-9 mm in width and about 28 mm in length with four notches on each side to attach the electrodes. Platinum wire was used as electrodes. The specific conductivity of the specimens was corrected for porosity by the equation

$$\sigma_s = \frac{\sigma_m}{(1-v_p)^2} \qquad [5]$$

where σ_s is the specific electrical conductivity, σ_m is the measured electrical conductivity and v_p is the volume fraction of pores. The error due to uncertainties in the corrections for porosity is estimated to be about 20 %.

The electrical conductivity measurements were done by a Solartron 1260 impedance/gain phase analyser. The bulk conductivity was investigated by using four probe arrangements. Controlling and data acquisition was done by a HP BASIC compatible computer running the IS program (8). The electrical parameters for the measurements of the conductivity at a constant frequency were 1 Hz AC with an oscillating voltage of 1V. The oxygen partial pressure was controlled by mixing CO/CO_2, O_2/Ar or H_2/H_2O in different ratios by a gasmixer(9). The specimens were characterised by scanning electron microscopy (SEM). The crystal structure were determined by X-ray powder diffraction with Cr_{k_α} radiation.

Seebeck coefficient measurements

The specimens used for the electrical conductivity measurements were also used for Seebeck measurements. The specimens were modified by a polish treatment to remove the notches used in the electrical conductivity measurements. Each short end of the specimens were formed to a slightly round shape to get as good contact as possible with the thermocouples/ electrodes, which consisted of Pt / Pt+10%Rh. The Seebeck coefficient experiment was carried out by recording the voltage generated (ΔE) over the specimens under an applied temperature gradient (ΔT). The Pt-legs of the thermocouples were used as electrodes and the measured voltage was corrected for the Seebeck effect in the Pt-electrode wires(10). The Seebeck coefficient (Q) was calculated by

$$Q = - \frac{\Delta E}{\Delta T} \qquad [6]$$

For one specimen different temperature gradients were applied at constant oxygen partial pressure and average temperature to evaluate if the Seebeck coefficient was independent of the magnitude of the temperature gradient and to evaluate if there were any off-set voltage at origo due to small errors in the voltage or temperaure measurements. The results showed a straight line in a ΔE versus ΔT plot passing through origo within the error of the measurements with values of ΔT up to 30 °C.

EXPERIMENTAL RESULTS AND DISCUSSION

X-ray diffraction

The results from the X-ray diffraction of $NdCr_{1-x}Ti_xO_3$ showed for $x \geq 0.2$ a single phase of a distorted perovskite type structure (ABO_3). The crystal system is orthorhombic. Figure 2 shows the lattice parameters as function of the titanium content. The error in lattice parameters is calculated by the computer program CELLKANT(11). From figure 2 it can be seen that the lattice parameters vary up to Ti contents of about 20 %, for then to be approximately constant at higher contents. It is therefore concluded that the solubility of titanium is about 20% at 1500°C. This is also in agreement with X-ray diffraction spectra, which shows no peaks from the $Nd_2Cr_xTi_{2-x}O_7$ phase at 20 % titanium or less. Above

about 20 % titanium $Nd_2Cr_xTi_{2-x}O_7$ starts to form. This is a pyrochlore type structure ($A_2B_2O_7$), in this particular case of the monoclinic crystal system.

Electrical conductivity

In this study the electrical conductivity of four different specimens has been measured at 1000 °C and 1200 °C. At each temperature the electrical conductivity was measured as a function of oxygen partial pressure.

Oxygen partial pressure dependence

The results of the oxygen partial pressure dependence measurements of $NdCr_{1-x}Ti_xO_3$ at 1000 and 1200 °C are shown in figure 3. The results showed that the electrical conductivity at high oxygen partial pressure decreases with decreasing oxygen partial pressure with a slope of about 1/4 for then at intermediate oxygen partial pressures to go through a minimum. By a further decrease in the oxygen partial pressure the electrical conductivity starts to increase with a slope of -1/4. The minimum reflects a change from p-type conductivity at high p_{O_2} to n-type at low p_{O_2}. This corresponds to the region in figure 1 where the main ionic defect is $V_M^{''}$. From this survey plot it can be seen that at very low oxygen partial pressure the electrical conductivity changes more steeply than the predicted -1/4 dependence. This may be due to a phase transition or phase change at a distinct oxygen partial pressure. The phase transition may be due to formation of another phase with lower oxygen content.

Temperature dependence

The electrical conductivity has been measured as a function of the temperature at constant oxygen partial pressure. At $p_{O_2} = 0.21$ the activation energy is calculated to be in the range of 90-110 kJ/mol and at 10^{-11} atm to be in the range of 190-240 kJ/mol.

Seebeck coefficient

The Seebeck coefficient of two different specimens with composition $NdCr_{0.9}Ti_{0.1}O_3$ and $NdCr_{0.6}Ti_{0.4}O_3$ have been measured versus oxygen partial pressure at 1000°C. The results are shown in figure 4.

For $NdCr_{0.9}Ti_{0.1}O_3$ the results show that the Seebeck coefficient is positive at oxygen partial pressures higher than 10^{-4} atmospheres. In this region it is concluded that the electron holes are the major mobile defects. The observed decrease in the Seebeck coefficient by decreasing oxygen partial pressure is due to a beginning of a turnover from electron holes to electrons as the major mobile defects. For $NdCr_{0.6}Ti_{0.4}O_3$ the Seebeck coefficient was positive at oxygen partial pressure higher than 10^{-3} and increased with decreasing oxygen partial pressure. This is attributed to a decrease in electron hole concentration. At 10^{-3} atm oxygen partial pressure a sharp shift from positive to negative values in the Seebeck coefficient was observed. At intermediate oxygen partial pressure (10^{-5} to 10^{-10} atm) the Seebeck coefficient shows approximately a constant negative value. In this region the Seebeck coefficient is suggested to be influenced by the second phase in the specimen, $Nd_2Cr_xTi_{2-x}O_7$. At oxygen partial pressure lower than 10^{-10} the absolute value of the Seebeck coefficient increases with decreasing oxygen partial pressure. This is concluded to be due to an increase in the electron concentration.

In view of this Heikes (12) has developed a relation between the Seebeck coefficient and the fraction of hopping sites for a semi conductor following the small polaron hopping mechanism. The relation is expressed by

$$Q=\pm\frac{k}{e}\left(\ln\frac{1-x}{x}+\frac{\Delta S'}{k}\right) \qquad [7]$$

where Q is the Seebeck coefficient, k is the Boltzman constant, e is the elementary charge, x is the fraction of occupied hopping sites and $\Delta S'$ is the vibrational entropy associated with the local distortions around the polaron. The contribution by the $\Delta S'/k$ term to the Seebeck coefficient is less than 10 μV/K (13) and may therefore be regarded as insignificant and is therefore excluded in the calculations below . Inserting the measured Seebeck coefficients at different oxygen partial pressure in eq.7 the mole fraction of charge carrier can be calculated. The results are shown in figure 5.

The values at intermediate oxygen partial pressure is excluded due to interference by several types of charge carriers. For $NdCr_{0.9}Ti_{0.1}O_3$ at an oxygen partial pressure as low as 10^{-20} atm the electron concentration is still two decades below available hopping sites which correspond to the sum of the titanium and chromium sites. In other words the electron concentration corresponds to 10 % of the doping level at 10^{-20} atm oxygen partial pressure. The difference from a -1/4 slope is suggested to be due to too short equilibrium times. For $NdCr_{0.6}Ti_{0.4}O_3$ the concentrations of charge carrier concentrations is extrapolated to point where the electron and electron hole concentration are equal. From this point the electronic equilibrium constant (K_i) is calculated to be about $3\cdot10^{-10}$ at 1000 °C.

Knowing the electrical conductivity and the concentration of the main charge carrying species the mobility can be calculated. The mobility is calculated to be 25±2 10^{-3} $cm^2/Vsec$ for electron holes and for 16±6 10^{-3} $cm^2/Vsec$ for electrons.

CONCLUSIONS

The glycine/nitrate method has been found to be the most suitable method for preparing $NdCr_{1-x}Ti_xO_3$ powder due to the reduced preparation time, formation of the finale phase directly without formation of any intermediate products and finally due to less agglomeration of the powder.

The solubility of titanium in $NdCr_{1-x}Ti_xO_3$ has been found to be about 20%. The results from the electrical conductivity and Seebeck coefficient measurements showed a p-type conductivity at high p_{O_2} and a n-type conductivity at low p_{O_2}. At low oxygen partial pressures the concentration of electrons decreased by a slope of -1/4 with increasing oxygen partial pressure and at high oxygen partial pressure the concentration of electron holes increased by a slope of 1/4 with increasing oxygen partial pressure. The mobility of the electronic defects have been calculated at 1000 °C as well as the defect concentration as function of oxygen partial pressure. The result showed that the desirable defect situation where $[Ti_{Cr}^{\cdot}] = n$ may is not satisfied before an oxygen partial pressure as low as about 10^{-24} atm.

It is therefore concluded that Ti-doped $NdCrO_3$ is not suitable for use as an anode material in solid oxide fuel cells due to the low electrical conductivity in the region of

interest. On the other hand, a substitution of chromium fully or partly with another d-element metal may lead to a shift in the high electron concentration in direction of higher oxygen partial pressures. To evaluate these further experiments are necessary.

ACKNOWLEDGEMENTS

The present study was made possible through financial support from the Nordic Energy Research Program for Fuel Cells 1991-1994, funded by the Council of the Nordic Ministers.

REFERENCES

1 I. Barin and O. Knacke, "Thermochemical Properties of Inorganic Substances", Springer, Berlin (1973)
2 I. Barin, O. Knacke and O.Kubaschewski, "Thermochemical Properties of Inorganic Substances" - Supplement, Springer, Berlin (1977)
3 S. F. Palguev, V.K. Gilderman and V.I. Zemtzov, Ceramics International, 13, p.119 (1987)
4 A. K. Tripathi, J. Mater. Sci., 17, p.1595 (1982)
5 Developed by F.W. Poulsen, Materials Department, Risø National Labaratory, P.O. box 49, DK-4000 Roskilde, Denmark (1992)
6 N.P. Pechini (1967), US Patent 3330697
7 L.A. Chick, J.L. Bates, L.R. Pederson and H.E. Kissinger, Proc. First Int. Symp. on Solid Oxide Fuel Cells, ed. S. C. Singhal, The Electrochem. Soc. Proc. Vol 89-11, p.170 (1989)
8 Developed by T. Norby, Center for Materials Research, Gaustadallěen 21, N-0371 Oslo, Norway (1992)
9 T. Norby, Solid State Ionics, 28 - 30, p.1586 (1988)
10 N. E. Cusack and P.W. Kentall, Proc. Phys.Soc, 72, p.898 (1958)
11 Developed by N.O. Ersson, Chemical Institute, University of Uppsala (1981)
12 R.R.Heikes, "Thermoelectricity: Science and engineering" ed: R.R.Heikes and R. Ure, Interscience Publishers, New York (1961)
13 J.B. Goodenough, Mat. Res. Bull., 5, p.621 (1970)

Table I Colour and crystal structure before and after calcination of the oxide powder.

Compound	Colour	Crystal structure before calcination	Crystal structure after calcination
$NdCrO_3$	Green	Orthorhombic	Orthorhombic
$NdCr_{0.7}Ti_{0.3}O_3$	Green-yellow	Orthorhombic	Orthorhombic + monoclinic
$NdCr_{0.4}Ti_{0.6}O_3$	Green-yellow	Cubic	Orthorhombic + monoclinic

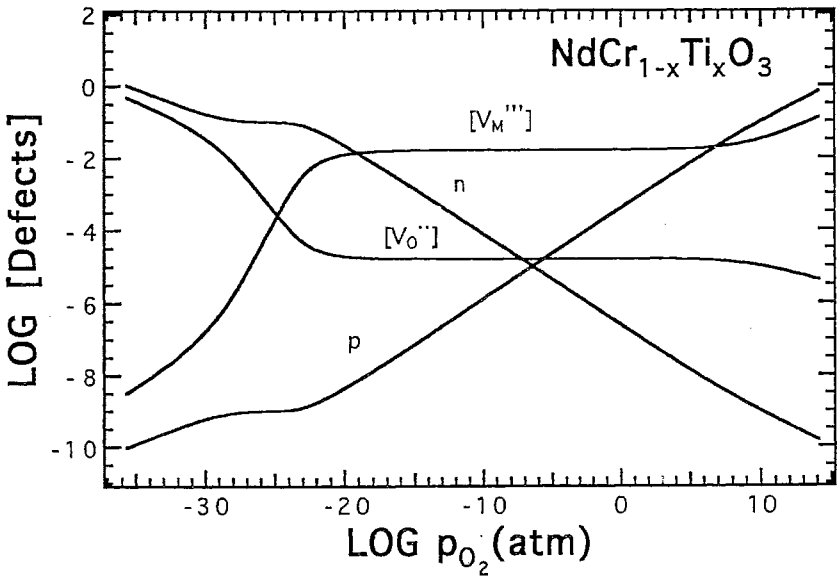

Figure 1 Kröger Vink diagram showing how the different concentrations of defects in $NdCr_{1-x}Ti_xO_3$ change with p_{O_2}. $K_i=10^{-10}$, $K_{VO}=3\ 10^{-2}$, $K_s=1.111\ 10^{-18}$ and x=0.1 have been used as input parameters.

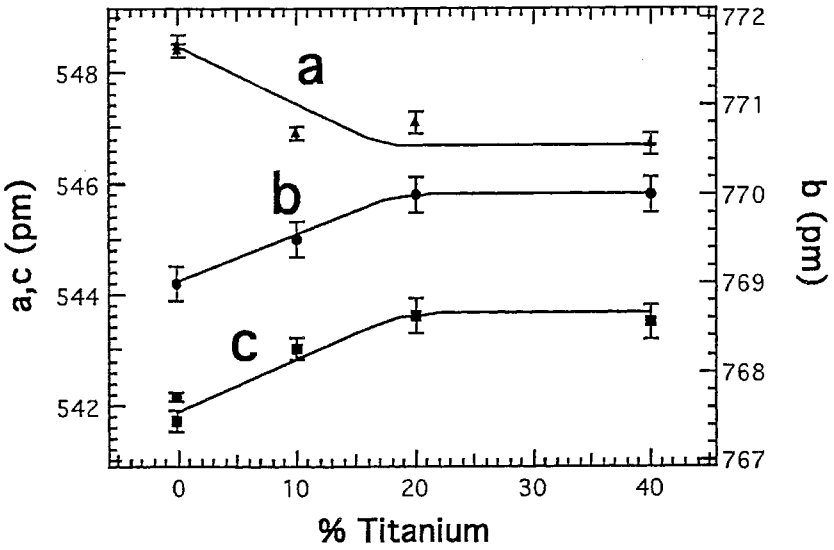

Figure 2 The lattice parameters for $NdCr_{1-x}Ti_xO_3$ as function of the titanium content. The crystal system is orthorhombic.

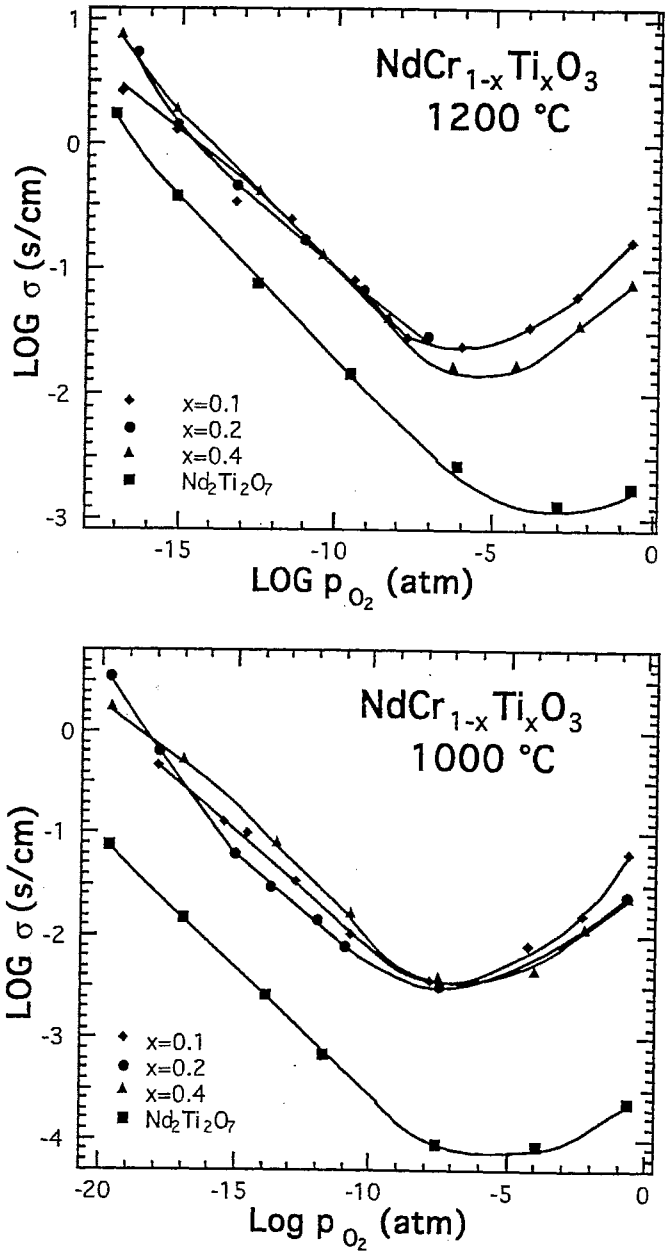

Figure 3 The electrical conductivity of $NdCr_{1-x}Ti_xO_3$ versus the oxygen pressure at 1000 and 1200 °C.

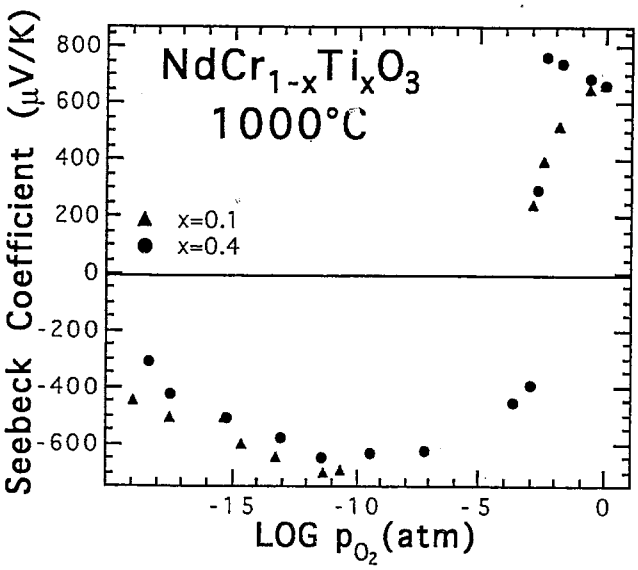

Figure 4 Seebeck coefficient of $NdCr_{0.9}Ti_{0.1}O_3$ and $NdCr_{0.6}Ti_{0.4}O_3$ at 1000 °C versus the oxygen partial pressure.

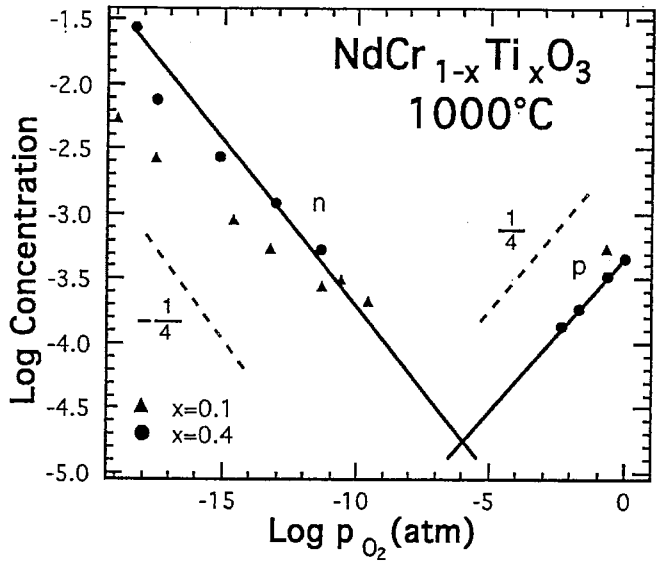

Figure 5 Concentration of electrons and electron hols on available hopping sites in $NdCr_{0.9}Ti_{0.1}O_3$ and $NdCr_{0.6}Ti_{0.4}O_3$ at 1000 °C versus the oxygen partial pressure.

A2.

F.W.Poulsen,; G. Ø. Lauvstad,.;R. Tunold,
Conductivity and Seebeck measurements on strontium ferrates.
Solid State Ionics **72** 47-53. (1994)

Solid State Ionics 72 (1994) 47–53
North-Holland

SOLID
STATE
IONICS

Conductivity and Seebeck measurements on strontium ferrates

Finn W. Poulsen
Materials Department, Risø National Laboratory, DK-4000 Roskilde, Denmark

Gro Lauvstad and Reidar Tunold
Department of Electrochemistry, The University of Trondheim, Norwegian Institute of Technology, N-7034 Trondheim, Norway

The Seebeck coefficient of nine strontium ferrate ceramics with the nominal compositions: $SrFe_yO_{3-x}$ (where y=0.909, 0.952, 1, 1.05, 1.10), and $Na_zSr_{1-z}FeO_{3-x}$ and $La_zSr_{1-z}FeO_{3-x}$ (where z=0.05, 0.1) were measured in air from 300–1000°C. The deficiency in oxygen stoichiometry, x, adjusts itself in air from approximately 0.15 to 0.35 in this temperature range. Most of the materials have reasonably high electronic conductivities, and some samples of lanthanum-doped ferrate reached conductivities of 50–90 S/cm at 25°C. The total spread in conductivity between the 9 samples was 4 decades at 25°C. Negative temperature coefficients for the total conductivity were observed above 5–600°C. The thermopowers (−5 to +120 μV/K) show similar (strong) temperature dependencies for all materials and increase with increasing temperature. The temperature dependency of conductivity and thermopower can be explained by the strong variation of oxygen content (hole concentration decreases with increasing temperature). A simple defect model for $SrFeO_{3-x}$ at high P_{O_2} was consistent with the observed oxygen partial pressure dependence of the conductivity at 800°C.

1. Introduction

Undoped $SrFeO_{3-x}$ is inherently oxygen deficient. When annealed under oxygen pressures in excess of 500 atm. the $SrFeO_3$ composition of the simple cubic perovskite structure is approached [1,2]. The oxidation state of +4 for all iron in the structure (as required in stoichiometric $SrFeO_3$) is thus difficult to reach. Various orthorhombic and tetragonal phases are found for $0.03<x<0.5$ (1). The end member formed for instance by heating in a N_2 atmosphere [1] to 1350°C: $SrFeO_{2.5}$ has the brownmillerite structure where equal numbers of Fe(+3) ions have 4−, respectively 6-fold coordination to oxygen [3]. The oxygen vacancies thus form an ordered structure in $SrFeO_{2.5}$ [3].

The objective of the present study was twofold: We wanted to identify compositions with high conductivity in the phase region near $Sr_1Fe_1O_{3-x}$, which might be used in the future as fuel cell electrodes, - secondly we wanted to establish a defect model for a material with large oxygen deficiency such as undoped $SrFeO_{3-x}$. Strontium doped lanthanum ferrates, $La_{1-z}Sr_zFeO_{3-x}$ with z=0.1 and 0.25, have been studied earlier by Mizusaki et al. [4]. These materials showed p and n-type conductivity at respectively high and low partial pressure of oxygen, the transition taking place at approximately $P_{O_2}=10^{-13}$–10^{-14} atm. (1000°C). The decrease of the Seebeck coefficient of $LaFeO_3$ above 440°C has been claimed to be due to a transition to n-type conduction [5]. However, the electrical properties of undoped $LaFeO_3$ is very sensitive to the exact La/Fe ratio as demonstrated by Mizusaki et al. [6].

2. Experimental

2.1. Synthesis

The glycine method was used for fabrication of the perovskite powders [7]. $Sr(NO_3)_2$ and $Fe(NO_3)_3\cdot 9H_2O$ were dissolved in water in the proper ratio (with or without additions of $NaNO_3$ or $La(NO_3)_3\cdot 6H_2O$). The added glycine (67% of the amount required for conversion of the nitrate groups to N_2) initially acts as a complexing agent for the metal ions and as a gel former (by polymerisation).

When most of the water has evaporated a highly exothermic reaction between glycine and the nitrate groups will start at around 180°C. The powders were ground and pressed to cylinders (diameter 4–5 mm, length 20–35 mm) in a cold isostatic press at 3000 bar and then sintered in air at 1200°C for five hours. The cooling rate was 60°C/h.

2.2. Equipment for thermal and phase analysis

DTA in air (Netzsch, max temperature 1175°C, heating and cooling rate 10°C/min); TG in 8%H_2 in Ar (apparatus Perkin-Elmer TGA7), heating rate 1°/min.; max temperature 700°C. The loss of oxygen by heating in air was found gravimetrically by quenching samples equilibrated for eight hours at 1000°C. Conventional X-ray powder diffraction on flat powdered specimens (Cu Kα-radiation) was used.

2.3. Electrical measurements

Seebeck measurements were carried out on 15–30 mm long rods, placed between two Pt/Pt 10% Rh thermocouples. The samples were placed in the natural gradient of a tube furnace. Data logging was made by a HP 3421A data acquisition unit, connected via a GPIB to a PC. Correction for the absolute thermopower of Pt (approximately -10 to -21 μV/K from 300–1000°C) was done using the data of Cusack and Kendall [8]. For further experimental details see ref. [9]. Four-point dc conductivity measurements were made using Pt-painted current electrodes at the end of the sample and Pt wire contacts (separation 6.4 mm). Six different dc-currents in the range 23 μA to 23 mA were used (both directions). The average of 12 measurements at each temperature was used.

3. Results

3.1. General observations

All synthesised materials had X-ray diffraction patterns containing characteristic peaks of the $SrFeO_{3-x}$ phases, as reported by Takeda et al. [1]. The $SrFe_yO_{3-x}$ samples with $y \neq 1$ and the Na- doped samples contain secondary phases together with the perovskite phase. The experimentally obtained densities for the sintered specimens (Archimedean principle) were in the range 4.76–5.19 g/cm^3.

In DTA experiments endothermic transitions (261–292°C during heating) and exothermic transitions (277–309°C during cooling) were assigned to transitions from the low temperature, ordered perovskite structures ($Z > 1$) to the disordered cubic high temperature perovskite structure ($Z = 1$). No thermal events were detected in the temperature region of 500–700°C, where the total conductivity changes from having a positive temperature coefficient (low T) to a negative temperature coefficient (high T), see later. According to the phase diagram of Takeda et al. [1] the $SrFeO_{3-x}$ sample should be in the disordered perovskite phase at 1000°C with an oxygen content of 2.65.

3.2. Electrical conductivity

Fig. 1 shows the observed specific conductivity at 25°C of isostatically pressed and sintered rods of the 9 different compositions, cf. table 1. Duplicate and triplicate measurements on various samples from the same powder production are included. The RT conductivities were determined in a separate sample holder (4-point method) that did not allow variation of temperature. A high scatter in conductivity values for material of the same batch is observed, which we assign to differences in porosity, oxygen content, local porosity/cracks in specimens and variations in phase distribution. Some trends are, however, apparent: (1) Deviation of the Sr/Fe ratio from unity results in materials with lower conductivity; (2) mechanically weak samples result with excess Sr-content; (3) Na-doping on Sr-site gives materials with low conductivity, the lower the more Na. EDX analysis of sintered Na-doped samples indicated loss of Na from the surface of the specimens, in turn leading to B/A ratios > 1; (4) La-doping on Sr-site yields materials with high conductivity, increasing with La-content. One would expect that La-substitution on the A-site should reduce the amount of electron holes (and thereby decrease the conductivity) if the oxygen stoichiometry is not changed significantly by the substitution. The influence of Sr/Fe ratios $\neq 1$ is not easily predicted: the maximum concentration of metal vacancies on the A and B-site

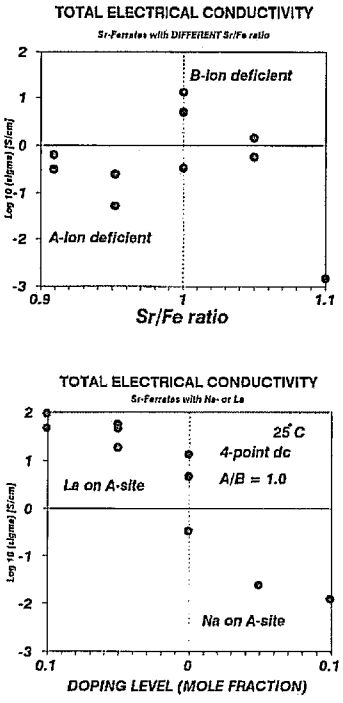

Fig. 1. Total electrical conductivity of strontium ferrates at room temperature measured by 4-point dc method: (upper part) conductivity of $SrFe_yO_{3-x}$ as function of the Sr/Fe ratio; (lower part) conductivity of Na- and La- substituted strontium ferrates (ions on A-site/B-site = 1.0).

is unknown, as is the nature of the secondary phases that will be exoluted.

Fig. 2 displays the temperature dependence of the total conductivity in an Arrhenius plot for $SrFeO_{3-x}$ (SF) and $Sr_{0.9}La_{0.1}FeO_{3-x}$ (SLF) in air and 9% H_2 in N_2, respectively. Activation energies (eV) are indicated. 0.1 eV is a quite usual value for the activation energy for small polaron hopping conductors. However, as discussed later (section 3.3), the concentration of charge carriers decreases at least a factor of 2 during heating, so the observed net activation energy is a sum of the "true" hopping activation energy and a (negative) term related to the decrease in concentration. The phenomenon of "a maximum

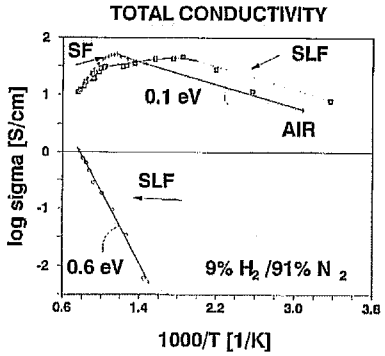

Fig. 2. Arrhenius plot of $SrFeO_{3-x}$ (SF) and $Sr_{0.9}La_{0.1}FeO_{3-x}$ (SLF) in air and 9% H_2. Activation energies (eV) are indicated.

conductivity" is thus observed in air, as is also reported for many manganese- and cobalt containing perovskites. The decrease in conductivity is certainly not due to a transition to a "metallic' type of conduction, as postulated in many publications, cf. section 4. Some contribution to the measured total conductivity from oxygen ion migration cannot be ruled out. The much larger activation energy found in reducing atmospheres is probably reflecting that the concentration of electrons increases with temperature, as evidenced by a decrease of the thermoelectric power upon heating in reducing atmospheres (see section 3.4). The relatively low conductivity of La-doped Sr-ferrate, i.e. just about 1 S/cm at 1000°C in reducing atmosphere sheds some doubt as to the use of these materials in anodes, unless the conductivity of the electrode can be increased by making a cermet or by doping the ferrate in a different manner.

Fig. 3 shows the conductivity of $SrFeO_{3-x}$ at 805 ± 3°C at different partial pressures of oxygen. The conductivity decreases with decreasing P_{O_2} range as expected for a *p*-type conductor. The intermediate P_{O_2} range was not experimentally accessible at the time of the experiments. At low P_{O_2} the conductivity starts to increase as expected for *n*-type conductors. The interpretation of the data is given in section 4.

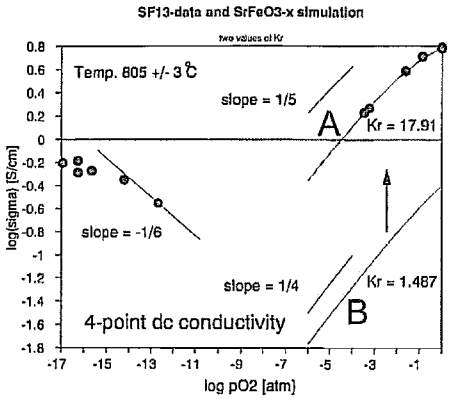

Fig. 3. Log σ (S/cm) versus log P_{O_2} at 805±3°C for $SrFeO_{3-x}$. The calculated conductivity due to electron holes is shown as curve a. Curve b, shown translated downwards, is calculated for a lower value of Kr, and also displays a slight curvature.

3.3. Oxygen content

The approximate oxygen content of $SrFeO_{3-x}$, when heated and cooled in air, was found from TG-analysis in dilute hydrogen. The weight stabilised at 700°C in dilute hydrogen. We assume following Takeda et al. [1], that this corresponds to $SrFeO_{2.500}$. The air annealed material is then calculated to be $SrFeO_{2.85}$. According to the phase diagram studies [1,2] this is on the borderline of the orthorhombic and tetragonal phase field at room temperature. The coexistence of several tetragonal/orthorhombic phases in the fabricated material is possible, since the X-ray powder patterns could not be matched with any of the individual phases: cubic $SrFeO_{2.97}$ ($Z=1$), tetragonal $SrFeO_{2.86}$ ($Z=16$) or orthorhombic $SrFeO_{2.73}$ ($Z=8$), described by Takeda et al. [1].

Strontium ferrate looses weight reversibly, when heated in air to 1000°C as is happening during the conductivity and Seebeck measurements: a weight-loss of 1.63%, corresponding to a change in oxygen content from 2.85 to 2.657 was determined. These values are slightly higher than 2.8 and 2.6, respectively, as read from the graphs of Takeda et al. [1].

3.4. Thermopower

The measuring cell can be represented by:

$$\begin{matrix} P_{O_2}/\text{Pt}/\text{strontium ferrate}/\text{Pt}/P_{O_2} \\ T_{hot} \qquad\qquad\qquad\qquad T_{cold} \end{matrix}$$

Thermal gradients of 20–30 K were employed. After correcting the measured thermopowers for the contribution of the Pt-lead wires all data sets more or less display the same general trends as shown in fig. 4.

Positive values are always observed above 450°C: All thermopowers increase with increasing temperature above this, some are reaching +120 μV/K around 1000°C in air. At lower temperatures small negative Seebeck coefficients are observed, but the values are admittedly quite sensitive to proper correction for the Pt contacts. A further general trend is that the higher the conductivity, the lower the measured thermovoltage. But these differences are small. The equilibrium time for obtaining stable readings were of the order of one hour. A $Sr_{1.1}FeO_{3-x}$ sample was exposed to 9% H_2 in Ar saturated with H_2O at RT ($P_{O_2} \sim 10^{-18}$ atm.). The observed thermovoltage changed to negative values in the course of minutes. Evidently the material changes to behave as an *n*-type conductor. After stabilisation the thermovoltage was approximately −700 μV/K at 300°C decreasing approximately linearly to −150 μV/K above 900°C. The sample could be redox cycled without mechanical disintegration and reproducible

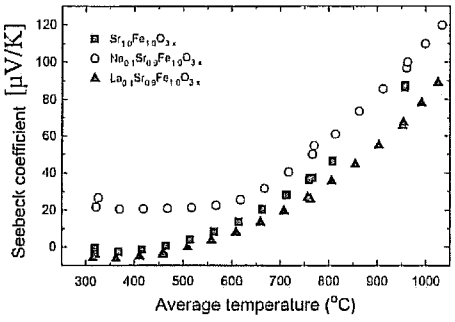

Fig. 4. Seebeck coefficients for three Sr-ferrates measured in air. Nominal compositions are given.

Table 1
Thermopower in air of 9 strontium ferrates materials. Values obtained by linear interpolation. The compositions are nominal. The $SrFeO_{3-x}$ samples with $Sr/Fe \neq 1$ and the Na- doped samples contain secondary phases in addition to the perovskite phase.

Nominal composition	Thermopower at 400°C (μV/K)	Thermopower at 900°C (μV/K)
$Sr_{1.0}Fe_{1.05}O_{3-x}$	+1.5	+71
$Sr_{1.0}Fe_{1.1}O_{3-x}$	+1.5	+71
$Sr_{1.0}Fe_{1.0}O_{3-x}$	−2	+70.5
$Sr_{1.05}Fe_{1.0}O_{3-x}$	−3.3	+73
$Sr_{1.1}Fe_{1.0}O_{3-x}$	−1.9	+65
$Na_{0.1}Sr_{0.9}Fe_{1.0}O_{3-x}$	+20	+81
$Na_{0.05}Sr_{0.95}Fe_{1.0}O_{3-x}$	0	+69.8
$La_{0.1}Sr_{0.9}Fe_{1.0}O_{3-x}$	−5	+53
$La_{0.05}Sr_{0.95}Fe_{1.0}O_{3-x}$	−5	+62.8

thermovoltages within 3 μV were obtained.

Table 1 summarizes the thermopower results at two temperatures.

4. Defect model for undoped $SrFeO_{3-x}$

The defect structure will be discussed using the Kröger–Vink notation. Since $SrFeO_{3-x}$ is highly oxygen deficient we rule out the possibility of having metal ion vacancies on the A-and B- site at the same time as found in "excess" stoichiometric materials such as "$LaMnO_{3.15}$". It is underlying the above assumption that $Sr/Fe = 1.0$. The major species on the perovskite lattice (cubic approximation) will be Sr and normal oxygen with invariant oxidation states plus oxygen ion vacancies. The nonstoichiometry (due to the redox chemistry of iron) can be described in several ways (Fe^{3+}/Fe^{4+} or $Fe^{3+}/h^{\cdot}$ etc.). Table 2 depicts four different approaches. The choice of parent compound to be used for description of $SrFeO_3$: (charges on A/B-sites being III/III or II/IV for the perovskite structure or II/III (brownmillerite), influences the formal charges given to the ions. Especially model D is problematic, since the charges on oxygen and oxygen ion vacancies on the extra sites are not easily defined. Model B will be tested below, since the other descriptions are dubious or not physically plausible. Models, including full charge dis-

Table 2
Defect model for $SrFeO_{3-x}$ at high P_{O_2}. At low P_{O_2} divalent Fe or e'-defects must be included. Various consequences of the models are described. Model B is in agreement with the obtained conductivity data at different P_{O_2}, cf. fig. 3.

Parent compound	A-site	B-site	O-site	delocalised	Remarks
Model A					
$A^{II}B^{IV}O_3$	$Sr^{\bullet}$	$Fe^{\bullet}(+4)$	$O_O^{\bullet}$, $V_O^{\bullet\bullet}$	e'	negative charge (e') to compensate for $V_O^{\bullet\bullet}$! Slope of $\log(e')$ versus $\log P_{O_2}$ is approx. −1/6.
Model B					
$A^{II}B^{IV}O_3$	$Sr^{\bullet}$	$Fe'(+3)$	$O_O^{\bullet}$, $V_O^{\bullet\bullet}$	h'	decreasing h' at increasing x, compensated by increasing $[V_O^{\bullet\bullet}]$ slope approx. +1/4
Model C					
$A^{III}B^{III}O_3$	Sr'	$Fe^{\bullet}$	$O_O^{\bullet}$, $V_O^{\bullet\bullet}$	h'	same equations as for model B
Model D					
$SrFeO_{2.5-x}$	$Sr^{\bullet}$	$Fe^{\bullet}(+3)$	$O_O^{\bullet}$, $V_O^{\bullet\bullet}$	h'	cf. text

proportionation of Fe(+4) into equal amounts of Fe(+3) and Fe(+5) have been used to explain Mössbauer spectra obtained at 4 K [11], but are also not likely to apply at high temperature, where fast exchange of electrons is dominating.

In model B, we put Fe(3+) on the B-site, where the structure "expects" a 4+ ion. The excess positive charge for oxygen stoichiometries above $SrFeO_{2.5}$ is assigned to the electron holes, h$^{\cdot}$. The electroneutrality condition and oxygen site balance read respectively: Model B:

$$[Fe'] = 1 = 2[V_O^{\cdot\cdot}] + h^{\cdot}, \quad 3 = [V_O^{\cdot\cdot}] + [O_O^*] .$$

Equilibration with the surrounding oxygen containing atmosphere is described by:

$$\tfrac{1}{2}O_2 + V_O^{\cdot\cdot} = O_O^* + 2h^{\cdot} ,$$

leading to:

$$Kr = \frac{[O_O^*]p^2}{[V_O^{\cdot\cdot}]P_{O_2}^{1/2}} = \frac{2(2.5+p/2)p^2}{(1-p)P_{O_2}^{1/2}} ,$$

where p is the concentration (in mole fractions) of electron holes ($p<1$) in one formula unit of ferrate.

The numerical value of Kr can be estimated from the known stoichiometry at 0.21 atm. of oxygen: Kr = 17.91 and 1.487 (atm.$^{-1/2}$) for $SrFeO_{2.84}$ (RT) and $SrFeO_{2.65}$ (1000°C), respectively. Using values for Kr in this range, it can be estimated that the $SrFeO_{2.5}$ stage of reduction will be reached in the pressure range 10^{-5} to 10^{-6} atm. of oxygen at 1000°C. The measured conductivity of different partial pressures of oxygen should scale with the hole concentration, p, if the ionic contribution to the conductivity is small. The cubic equation is easily solved for p at various oxygen pressures. Since the ferrate is highly nonstoichiometric there is no reason to expect "ideal" values for the slope of log σ versus log P_{O_2} (1/4 or 1/6). The calculated curve in fig. 3 matches very well the data. The limiting slope of the curve at low P_{O_2} is 1/4.

The scaling factor between calculated hole concentration and measured conductivity can be recalculated into a hole mobility. We obtain a value around 4×10^{-3} cm^2 V^{-1} s^{-1}, at 800°C, which is a quite reasonable value.

A defect model for $SrFeO_{2.5-x}$ in the low P_{O_2} range assuming introduction of electron defects, e', according to

$$O_O^* = V_O^{\cdot\cdot} + 2e' + \tfrac{1}{2}O_2(g)$$

predicts a log(σ) versus log P_{O_2} slope of $-1/6$ for small values of x. This is indicated in fig. 3. More data points are needed to verify the model. The decomposition of the brownmillerite structure to divalent iron compounds may start to proceed at low P_{O_2} values. The leveling off of the conductivity at low P_{O_2}, as seen on the left side of fig. 3 may be due to phase decomposition.

5. Interpretation of Seebeck-measurements

Our convention for defining the thermopower is:

$$Q = -(E_{hot} - E_{cold})/(T_{hot} - T_{cold}) .$$

For measurements, where the heterogeneous contributions of the electrode reactions can be neglected, one obtains that the sign of the majority charge carrier at low concentration conforms with the sign of the thermovoltage. The thermoelectric properties of perovskite structure manganites and chromites have recently been reviewed [10]. In cases, where the conducting material is a pure ionic conductor in the P_{O_2} range studied, such as for instance yttria-stabilized zirconia, one obtains large thermovoltages. In the latter case [9] the main contribution to the thermovoltage stems from the difference in entropy of gaseous oxygen at the two electrodes. Heikes formula, with the degeneracy factor $\beta = 1$, is used in the traditional approach for interpretation of thermoelectric measurements on narrow band semiconductors

$$Q = \pm k/e \cdot \ln[\beta(1-c)/c] .$$

Here c is the fraction of occupied sites (h$^{\cdot}$ concentration pr B-site). A straightforward application of Heikes formular ($\beta = 1$) predicts a shift in sign when c passes the value 0.5 although the material is a p-type conductor through the entire regime. The shift in sign should occur at stoichiometry corresponding to $SrFeO_{2.75}$, where $c=0.5$ or stated in chemical terms: $[Fe^{3+}] = [Fe^{4+}]$. As described in section 3.3 the oxygen content during a Seebeck measurement from room temperature to 1000°C changes from approximately 2.85 to 2.65, i.e. a change in sign (negative at low T) is predicted in the middle of this tem-

Table 3
Thermopowers of $SrFeO_y$ calculated from Heikes equation.

Oxygen stoichiometry: y, and fractional hole concentration, p.	Q for $\beta=1$ (μV/K)	Q for $\beta=2$ (μV/K)
2.65 ($p=0.3$) high temp. limit	+73	+132
2.84 ($p=0.68$) low temp. limit	−65	−5

perature range. Table 3 gives the low and high temperature values of the thermopower, calculated for two values of β.

As seen from table 3 the calculated thermopower using $\beta=2$ is in much better agreement with the experimental finding at low temperature (high hole concentration) than the value obtained using $\beta=1$. Conversely, using $\beta=1$ matches better with the observations at high temperature. We can find no theoretical explanation at present for these results. Goodenough [12] has commented that a change of the spin degeneracy over the measured temperature- and stoichiometry range cannot be ruled out.

A complication in the interpretation of the Seebeck measurements can also arise from oxide ion conduction in the sample.

Acknowledgement

GL wants to acknowledge financial support from the PUNG program, financed by the Norwegian Research Council and Norwegian industry, as well as The Council of the Nordic Ministers for a travel grant. E. Ahlgren, Risø, is thanked for experimental assistance with the Seebeck measurements; F.R. Müller, NTH, is thanked for assistance with powder preparation. Finally Dr. R. Ødegård, Statoil, is thanked for giving us the opportunity to make TG-measurements and Dr. R.W. Berg for critical comments on the paper.

References

[1] Y. Takeda, K. Kanno, T. Takada, O. Yamamoto, M. Takano, N. Nakayama and Y. Bando, J. Solid State Chem. 63 (1986) 237.
[2] J. Mizusaki, M. Okayasu, S. Yamauchi and K. Fueki, J. Solid State Chem. 99 (1992) 166.
[3] M. von-Harder M. and H.K. Müller-Buschbaum, Z. Anorg. Allg. Chem. 464 (1980) 169.
[4] J. Mizusaki, T. Sasamoto, W.R. Cannon and H.K. Bowen, J. Am. Ceram. Soc. 66 (1983) 247.
[5] K. Gaur, S.C. Verma and H.B. Lal, J. Mat. Sci. 23 (1988) 1725.
[6] J. Mizusaki, T. Sasamoto, W.R. Cannon and H.K. Bowen, J. Am. Ceram. Soc. 65 (1982) 363.
[7] L.A. Chick, J.L. Bates, L.R. Pederson, L.R. and H.E. Kissinger, Proc. First Intern. Symp. on Solid Oxide Fuel Cells, ed. S.C. Singhal, Proc. Vol. 98-11 (The Electrochem. Soc. NJ, 1989) p. 170.
[8] N. Cusack and P. Kendall, Proc. Phys. Soc. 72 (1958) 898.
[9] E.O. Ahlgren and F.W. Poulsen, Solid State Ionics XX-XX (1994) XXX.
[10] E.O. Ahlgren and F.W. Poulsen, Proc. 14th Risø Internat. Symp. (1993) (Risø Natl. Lab., Roskilde, 1993) p. 193.
[11] M. Takano, N. Nakanishi, Y. Takeda, S. Naka and T. Takada, Mat. Res. Bull. 12 (1977) 923.
[12] J.B. Goodenough, (1993) private communication.

A3.

F.W. Poulsen,
Method for calculating ionic and electronic defect concentrations in proton containing perovskites, J. Solid State Chem. **143**, 115-121. (1999)

Journal of Solid State Chemistry 143, 115–121 (1999)
Article ID jssc.1998.8092, available online at http://www.idealibrary.com on IDEAL®

Method for Calculating Ionic and Electronic Defect Concentrations in Proton Containing Perovskites

Finn Willy Poulsen

Materials Research Department, Risø National Laboratory, DK-4000 Roskilde, Denmark

Received July 15, 1998; in revised form November 7, 1998; accepted November 8, 1998

A general numerical method for calculation of concentrations of vacancies and ionic and electronic defects in solids in equilibrium with two gas pressures is presented. The method is applied to 5 at% B-site doped $SrCeO_3$ in equilibrium with oxygen and water vapor. The model includes protons and electronic defects, as well as cation vacancies on the *A* and *B* sites. The 10 concentrations in the model are determined uniquely by solving the linear and mass action law type equations in a rational sequence. No approximations or truncations of the equations are necessary. No information on the magnitude of the Schottky-equilibrium constant, K_s, controlling the population of cation vacancies is available. Limiting values of K_s were tested to illustrate suppression and enhancement of cation vacancy formation in perovskites. Deviations from Sieverts law are demonstrated. Deviation of the *A*/*B* ratio from unity has the same effect on the proton content as an increase of the dopant level. © 1999 Academic Press

Key Words: **Brouwer diagram; calculation; trial and error; protonic; electronic; defects; perovskite.**

INTRODUCTION

The traditional strategies for defect concentration calculations on doped, mixed conducting oxides rely on (i) omission of concentration terms from the electroneutrality equation for species of low concentration and (ii) assumptions for certain (high) concentrations of the host ions or oxygen vacancies, namely, that these are virtually independent of the partial pressure of oxygen. The analytical expressions one derives using these approximations are seldom of higher order than cubic. A typical approximative approach is employed in Ref. (1) for doped ceria. Approximation methods describe well the defect chemistry in regions of oxygen partial pressure, where predominantly *p*-type, predominantly ionic, or predominantly *n*-type behavior is observed. The procedure, however, fails to describe regions over one to three decades of oxygen partial pressure, where transitions from one defect type regime to the next take place. The approximation procedure becomes questionable with regard both to pedagogical value and to precision, when the defect chemistry of the solid is established by equilibration with two or more gases. Along the same line, Schottky-type equilibria involving more than two types of ions, such as the chemical equilibrium for perovskites associated with Eq. [7], are never considered in approximative solutions, since such third or higher order expressions in concentration are rather intractable to approximations. Nowotny and Rekas (2) recently modeled sub- and over stoichiometric (in oxygen) $(La,Sr)MnO_3$, but their solution is only valid under the restriction that $[V^{\cdot\cdot\cdot}_{La}] = [V^{\cdot\cdot\cdot}_{Mn}]$; i.e., it only applies to the case where the *A*/*B*-ratio equals unity. Commercial equation solving codes can in principle solve all defect, mass balance, and electroneutrality equations simultaneously by minimizing the residuals of the equations; see Ref. (3). The author's experience is that such codes often diverge or oscillate, since some of the partial pressures and concentrations are extremely small, while other concentrations simultaneously are large. Complete analytical expressions, obtained by substituting the linear equations into the nonlinear mass action law expressions will unavoidably lead to polynomials of high order in the unknown concentrations. An example of an exact defect description of a proton containing perovskite, resulting in a fourth degree polynomium, is presented by Bonanos and Poulsen in Ref. (4). However, as a general approach, the derivation of analytical, high order analytical expression (which would have to be solved by numerical means anyhow) appears therefore not to furnish a practical strategy.

The present procedure is general and calculates the concentrations in a stepwise manner, identifying the correct set of concentrations by a screening test. The partial pressure of oxygen, or alternatively of water vapor, corresponding to such a set of concentrations is finally calculated. This method was successfully used by us in 1993 on the *B*-site-doped perovskite $NdCr_{1-x}Ti_xO_{3+\delta}$ (5). We demonstrated in 1997 the applicability of the method to the more complex case of simultaneous presence of protonic, oxidic, and electronic defects in fluorite structure oxides (6). A similar mathematical principle was used by Spinolo and Anselmi-Tamburini in 1995 (7) to calculate defect concentrations in

0022-4596/99 $30.00

MO_2 oxides with interstitial cations having charges from 0 to +4. A more generalized treatment was given by Spinolo *et al.* in 1997 (8).

MATHEMATICAL FOUNDATION OF THE METHOD

(i) A model is formulated containing N different ionic and electronic species (neutral or charged); The Kröger–Vink notation (9) is used in the present paper. The word "species" means in the following any ion, neutral atom, electron- or electron hole defect and vacancy in the solid, including the proton attached to a lattice oxygen; cf. Table 1.

(ii) N independent equations are derived from mass balances, site balances, the electroneutrality condition, internal ionic and electronic equilibria, and finally equilibria between the solid sample and the gas atmosphere (typically equilibria with oxygen and/or water vapor). This set of equations is checked for presence of redundant equations (linear combinations of the other equations). Until this point we have followed a traditional route.

(iii) The calculation algorithm requires a species to be selected, the concentration of which will traverse several orders of magnitude, as the partial pressure of oxygen and/or water vapor is varied. It is a further functional requirement that the concentration of this species must vary monotonically with the gas pressure. At least four lattice species behave in this manner: There must exist a monotonic relation between the pO_2 of a gas in equilibrium with an oxide and the chemical potential of oxygen in the solid (and therefore also some monotonic relationship to the "chemical activity" of oxygen vacancies); similarly one can assume that the electron and electron hole concentrations bear a monotonic relationship to the reducing/oxidizing potential of the gas equilibrating with the solid. In the case of protonic and electronic defects in fluorite structure oxides, the electron hole concentration was most conveniently chosen as the running parameter. In the case of perovskites with inclusion of cation vacancies we use the oxygen vacancy concentration, $[V_O^{\bullet\bullet}]$ (see the following sections). For generality, let this species be named i, and let the concentration interval of interest for species i be min $< [i] <$ max. We will find solutions for all concentrations of the other species corresponding to a selection of values of $[i]$ in this interval. It is convenient to vary $[i]$ in logarithmic steps through the interval min $< [i] <$ max. By fixing one concentration within its physically possible interval, we have in effect added one (simple linear) equation to the set of N equations. We are therefore free to "avoid" one of the more problematic equations, which will typically be one of the high order mass action law expressions. An alternative way of explaining the basis of the present method is formulated as follows: In a series of physicochemical measurements on a nonstoichiometric oxide we normally consider temperature and partial pressure of oxygen as independent variables (controlled by the operator) and the concentrations as the dependent variables. The latter statement relates solely to a statistical treatment. From a computational point of view, however, one is free to select any two parameters as independent variables (here we choose one temperature, which in turn fixes all equilibrium constants and *one* concentration), if this makes the calculation simpler.

(iv) If the solid is in equilibrium with two different gasses, of pressure p_1 and p_2, respectively, we will identify solutions for discrete values of p_1 in the interval $p_{\min} < p_1 < p_{\max}$. Thus p_1 will be fixed for each trial and error calculation of the concentrations. A number of the N equations identified under (ii) are linear. By insertion of $[i]$ into these, we find some of the other concentrations. Substitution of the remaining linear equations into properly selected mass law expressions leads to quadratic equations, which are solved analytically. Eventually all concentrations are found by this procedure. What remains is to ensure that the concentrations are positive and below their maximum allowed magnitude (e.g., in crystals, a site cannot be more than 100% occupied). Invalid solution sets will disqualify themselves by containing one or more negative, complex, or too large positive roots among the calculated N concentrations. The approved set of concentrations are inserted into the equation having the highest order, which has not yet been employed (typically the equilibrium expression for reaction with oxygen). Thereby the corresponding $p_2 = pO_2$ is found.

TABLE 1
Simplest Realistic Defect Model for B-Site Doped $SrCeO_3$

A site	*B* site	O site	Delocalized
$Sr_A^{\times}$	$Ce_B^{\times}$	$O_O^{\times}$	$h^{\bullet}$
$V_A^{\prime\prime}$	Y_B	$V_O^{\bullet\bullet}$	$e^{\prime}$
	$V_B^{\prime\prime\prime}$	$OH_O^{\bullet}$	

Note. The dopant, Y, is assumed to be trivalent.

APPLICATION TO DOPED STRONTIUM CERATE

A- and/or *B*-site-doped perovskites can in principle exist in both an over- and an understoichiometric state depending on the redox properties of the *A* and *B* ions, temperature, and partial pressure of oxygen. The present model is made general in order to take account of this: in the overstoichiometric regime cation vacancies have to be assumed, as verified in doped and undoped $LaMnO_{3+\delta}$ by neutron diffraction (10) and oxygen content measurements (11). There is no room for interstitial oxygens in a perovskite structure. The model is furthermore made complete by including protonic species. Doped $SrCeO_3$ and, in more

recent years, also Sr- and Ca-zirconates have been intensely studied by Iwahara and co-workers (12,13) as a new class of high-temperature protonic conductors. Table 1 summarizes the species in the general model, using the Kröger–Vink notation with the ionic charges of Sr(II)Ce(IV)O_3 as the reference state. It requires 10 different "species" in the present model to describe fully the defect chemistry of $Sr_zCe_{1-x}Y_xO_{3-x/2\pm\delta}H_\varepsilon$. Protons are residing on lattice oxygens, $OH_O^\bullet$, in the present description. The site conservation equation [3] would have to be modified if protons were assigned an individual "life" as interstitial protons, $H_i^\bullet$.

The 10 independent equations, describing the system uniquely, are as follows. Note the special notation for concentrations of electronic defects: concentration of holes $[h^\bullet]$ is denoted 'p'; concentration of electrons $[e']$ is given by n in the equations below.

Site balances:

$$\text{Sr site} \quad [Sr_A^\times] + [V_A''] = 1 \qquad [1]$$

$$\text{Ce site} \quad [Ce_B^\times] + [Y_B'] + [V_B'''] = 1 \qquad [2]$$

$$\text{Oxide site} \quad [V_O^{\bullet\bullet}] + [O_O^\times] + [OH_O^\bullet] = 3. \qquad [3]$$

Mass balances:

$$[Ce_B^\times]/[Y_B'] = (1-x)/x \qquad [4]$$

$$A/B \text{ ratio} \equiv [Sr_A^\times]/([Ce_B^\times] + [Y_B']) = z. \qquad [5]$$

Electroneutrality condition:

$$2\cdot[V_A''] + [Y_B'] + 4\cdot[V_B'''] + n = 2\cdot[V_O^{\bullet\bullet}] + [OH_O^\bullet] + p. \qquad [6]$$

Mass action laws:

Schottky reaction for vacancy generation:

$$\text{nil} \leftrightarrow 3\,V_O^{\bullet\bullet} + V_A'' + V_B'''$$

$$\Rightarrow [V_O^{\bullet\bullet}]^3\cdot[V_A'']\cdot[V_B'''] = K_s. \qquad [7]$$

Internal electronic equilibrium:

$$K_i = n\cdot p \qquad [8]$$

Equilibria between the solid sample and the gas atmosphere:

$$\tfrac{1}{2}O_2\,(\text{gas}) + V_O^{\bullet\bullet} \leftrightarrow O_O^\times + 2h^\bullet$$

$$\Rightarrow K_{ox} = [O_O^\times]\cdot p^2/(pO_2^{1/2}\cdot[V_O^{\bullet\bullet}]) \qquad [9]$$

$$H_2O(\text{gas}) + V_O^{\bullet\bullet} + O_O^\times \leftrightarrow 2OH_O^\bullet$$

$$\Rightarrow K_w = [OH_O^\bullet]^2/(pH_2O\cdot[V_O^{\bullet\bullet}]\cdot[O_O^\times]). \qquad [10]$$

The solutions for the cation concentrations are not trivial when cation vacancies are included. The 10 equations group into 6 linear expressions and 4 nonlinear ones. An analytical expression in one of the concentrations could in principle be obtained by substitution; it would probably result in a polynomium of the 6′-9′ degree for this model. It is demonstrated below that the system of equations can be solved in a simple way, assuming a smart strategy is applied.

We want to carry out a calculation for known values of the four equilibrium constants, Eqs. [7]–[10], and for a known dopant level x and A/B ratio $= z$. We furthermore specify a number of pH_2O values, at which the calculation is required.

The stepwise calculation proceeds as follows: We assume a value for $[V_O^{\bullet\bullet}]$ and pH_2O.

By substituting Eq. [10] into Eq. [3] one obtains a quadratic equation in $[OH_O^\bullet]$ reading

$$[OH_O^\bullet]^2/([V_O^{\bullet\bullet}]\cdot pH_2O\cdot K_w) + [V_O^{\bullet\bullet}] + [OH_O^\bullet] - 3 = 0. \qquad [11]$$

Equation [11] is solved analytically.

$[O_O^\times]$ is then found from Eq. [3]:

$$[O_O^\times] = 3 - [V_O^{\bullet\bullet}] - [OH_O^\bullet]. \qquad [3']$$

The next task is to express $[V_B'']$ and $[V_B''']$ by $[Y_B']$ making use of Eqs. [1], [2], and [4] and to insert these in Eq. [7]. The resulting expression in $[Y_B']$ is still only of second order in $[Y_B']$:

$$(1 - z\cdot[Y_B']/x)\cdot(1 - [Y_B']/x) = K_s/[V_O^{\bullet\bullet}]^3. \qquad [12]$$

The positive (analytical) solution for $[Y_B']$ of Eq. [12] leads to

$$[V_A''] = 1 - z\cdot[Y_B']/x \quad \text{and} \quad [V_B'''] = 1 - [Y_B']/x \qquad [13,14]$$

The solutions for the host ions follow immediately from [1], [2]:

$$[Ce_B^\times] = 1 - [V_B'''] - [Y_B'] \quad \text{and} \quad [Sr_A^\times] = 1 - [V_A'']. \qquad [1',2']$$

At this point only the values of n, p and the corresponding pO_2 remain to be determined. In the electroneutrality equation [6], n can be replaced by K_i/p from Eq. [8]:

$$2\cdot[V_A''] + [Y_B'] + 4\cdot[V_B'''] + K_i/p = 2\cdot[V_O^{\bullet\bullet}] + [OH_O^\bullet] + p. \qquad [6']$$

Equation [6′] is again only a quadratic expression in p; all other terms have known numerical values. Equation [6′] is

solved for p. The electron concentration, n, is finally found from [8] as

$$n = K_i/p. \qquad [8']$$

So far we have not employed Eq. [9], since we initially "replaced" it by the linear equation $[V_O^{\bullet\bullet}]$ = an assumed numerical value. The three concentrations entering Eq. [9] define the partial pressure of oxygen corresponding to the set of 10 determined concentrations, assuming they all are within the physically possible range. We can thus accept the solution if the concentration of the ith species fulfils $0 < [i] < 1$ for $[Y_B^{\prime}]$, $[V_A^{\prime\prime}]$, $[V_B^{\prime\prime\prime}]$, $[Ce_B^{\times}]$, $[Sr_A^{\times}]$, n and p; and $0 < [i] < 3$ for $[V_O^{\bullet\bullet}]$, $[O_O^{\times}]$, and $[OH_O^{\bullet}]$. If the set of concentrations is accepted, we can insert $[V_O^{\bullet\bullet}]$, $[O_O^{\times}]$, and p into [9] and find the oxygen partial pressure that corresponds to the equilibrium concentrations. The calculation is next performed for a new value of $[V_O^{\bullet\bullet}]$. When $[V_O^{\bullet\bullet}]$ has covered the concentration interval of interest, we change to a new value of pH_2O and start all over again. The complete calculation of a three-dimensional Brouwer diagram (10 concentrations versus pH_2O and pO_2 for some 10×30 points in the pH_2O–pO_2 plane) took initially 20–30 s, programmed in primitive GWbasic and performed on a 486 PC. In a Pascal version the calculation takes less than 1 s. A printout of the program source code fills less than two A4 pages. An Excel spreadsheet version is available from the author.

DISCUSSION

General Performance of the Algorithm

The algorithm is built on three loops: in the outermost loop the program calculates for a set of Y-dopant concentrations and/or A/B ratios; for each doping level typically 6–12 pH_2O values are calculated, typically in the range 10^{-6} to 1 atm; in the innermost cycle 500–1000 steps of $[V_O^{\bullet\bullet}]$ in the interval $10^{-14} - 0.5$ are tested. The simulation thus stops at an oxygen content corresponding to the Brownmillerite composition $ABO_{2.5}$. In order to obtain satisfactory numerical precision, all variables in the algorithm must be declared as double precision variables. Some intuition is mandatory in order to find the right sequence in which the concentrations are calculated: very small concentrations should be calculated from mass action law expressions rather than from linear difference equations. A test, comparing the left-hand side and the right-hand side of the electroneutrality condition (Eq. [6]), reveals cumulative errors, which are usually around 10^{-14} to 10^{-18} atomic fraction.

Several features of the present procedure are evident: (i) simulations can be carried out to "dangerous" or "non-physical" high pressures; (ii) smooth transitions extending over several decades of pO_2 from one defect regime to the next are observed—this being in contrast to the "too straight" lines usually seen in hand-drawn Brouwer diagrams; (iii) very small, but finite stoichiometry deviations can be predicted. A few drawbacks of the present procedure must admittedly be exposed: (i) The calculated defect concentrations will result in a set of discrete oxygen pressures, the magnitude of which cannot be controlled; (ii) using logarithmic steps in $[V_O^{\bullet\bullet}]$ generates relatively few calculated points in those (intermediate) pO_2 regimes, where the oxygen stoichiometry varies little; however, Brouwer diagrams do not usually have unexpected features in such regions anyhow.

Defect schemes are often tested at the high and low extremes of oxygen partial pressures by plotting the logarithm of the measured total conductivity versus the logarithm of pO_2. The predicted slope, $\partial \log(\sigma)/\partial \log(pO_2)$, is traditionally derived from approximations to Eqs. [9] (in combination with Eqs. [8] at low partial pressures). For the doped perovskite structures one arrives at slopes of $+1/4$ and $-1/4$ (for the non-doped case $\pm 1/6$).

"Differentiated" Brouwer diagrams can easily be generated as output from the present simulations. $\Delta \log[i]/\Delta \log(pO_2)$ calculated between adjacent points is a sufficiently good approximation to $\partial \log[i]/\partial \log(pO_2)$ assuming calculated points lie close. Figure 5 shows such a plot. It is noted that deviations from the "magic" slopes occur for p and n at low pO_2. The region of $\partial \log[V_O^{\bullet\bullet}]/\partial \log(pO_2) = 0$ between 1 and 10^{-15} atm is the region of constant oxygen stoichiometry. The use of "differentiated" Brouwer diagrams is hereby advocated. The algorithm for this model system can, without modifications, be used to model perovskites, where protons have no or negligible solubility. This is achieved by setting $K_w \equiv 0$.

Actual Simulations

The equilibrium constants for $SrCe_{0.95}Yb_{0.05}O_{3\pm d}$ at 700°C, employed by Schober and Wenzl (14), were adjusted to the present definitions of the equilibrium constants. The values are $K_{ox} = 3 \cdot K_1 = 1.5 \times 10^{-5}$ (atm)$^{-1/2}$, $K_i = 10^{-11}$, and $K_w = 10$ (atm)$^{-1/2}$.

The present model is probably the first attempt to formulate a complete model for the defect chemistry of proton containing perovskites *including* cation vacancies. The factors controlling cation vacancy concentrations have therefore to be discussed in the following.

The inclusion of cation vacancies is described by a Schottky equilibrium (Eq. [7]). Cation vacancy formation will in general be favored by increasing temperature for entropic reasons; i.e., it is predicted that K_s increases with temperature. This is counteracted by the fact that oxygen vacancy formation via reaction [9] is probably also promoted by increasing temperature. A certain concentration of cation vacancies can in addition deliberately be imposed on the system by synthesis of materials with A/B ratios

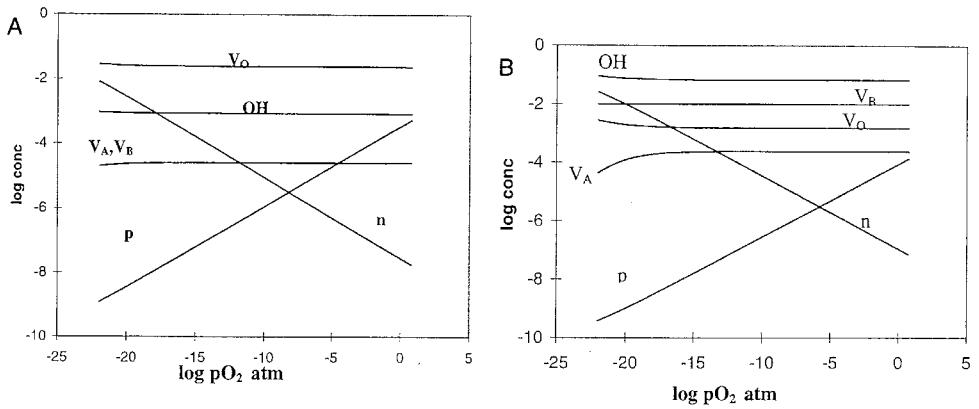

FIG. 1. Proton and other defect concentrations as function of pO_2, at 700°C. $K_s = 10^{-14}$, $K_{ox} = 1.5 \times 10^{-5}$, $K_i = 110^{-11}$, $K_w = 10$. Dopant level $x = 0.05$. (A) A/B ratio = 1.0 and $pH_2O = 10^{-6}$ atm; (B) A/B ratio = 0.99 and $pH_2O = 10^{-2}$ atm.

deviating from unity. Large concentrations of B-site vacancies are, however, probably not possible due to the high local charge on the B-site vacancy/ion. If a certain (as yet unknown) concentration is exceeded, breakdown of the perovskite structure will occur, resulting in formation of new phases. Equation (7) can thus be visualized as a sort of solubility product. Large concentrations of oxygen vacancies are possible, as in the disordered, high-temperature phase of $SrFeO_{2.5+d}$ (Brownmillerite structure at low temperature). In the latter material up to 17% of the oxygen sites are empty. Similarly, structures with large deficits of A ions can be derived from perovskites, e.g., WO_3, where there are no A ions needed at all to stabilize the structure.

Only a few reports have been found where the variation of the A/B ratio in perovskites with Ce on the B site has been addressed experimentally. Shima and Haile (15) investigated undoped and Gd-doped $BaCeO_3$, with A/B ratios ranging from 0.96 to 1.04. In some cases A-site-deficient-materials were obtained due to loss of BaO during the high-temperature treatment. Ahlgren *et al.* (16) studied the sintering and electrical properties of Y-doped $SrCeO_3$ with A/B ratios ranging from 0.990 to 1.005 (in steps of 0.005) and found that the best ceramic was obtained with $A/B = 0.995$. However, no information on the magnitude of K_s is available. Test calculations show that a value for $K_s = 10^{-20}$ or lower corresponds to a neglegible tendency to cation vacancy formation, while, for instance, $K_s = 3.2 \times 10^{-9}$ corresponds to coexistence of approximately 2 at % of $V_O^{\bullet\bullet}$, $V_A^{\Vert}$ and $V_B^{\Vert\Vert}$. Figure 1A shows a representative Brouwer diagram for a 5% Yb-doped strontium cerate at 700°C and a water partial pressure of 10^{-6} atm. The Schottky equilibrium, allowing formation of cation vacancies, has been included with $K_s = 10^{-14}$. The calculated cation vacancy concentrations are around 3×10^{-5} atomic fraction; the A- and B-site vacancy concentrations are equal, since the A/B ratio for this calculation is unity. The curves showing n- and p-type concentrations are symmetrical around a horizontal line passing through the point, where $n = p$ (at around $pO_2 = 10^{-8}$ atm). The proton content and $[V_O^{\bullet\bullet}]$ increase at low pO_2, which is more clearly illustrated in Figs. 2 and 3. The increase in protons at low pO_2 is a consequence of the increase in $[V_O^{\bullet\bullet}]$, giving room to more water uptake via reaction [10]. For a more detailed discussion of this effect, see Ref. (4). Figure 1B shows a calculation for the same values of equilibrium constants as in Fig. 1A, but the water

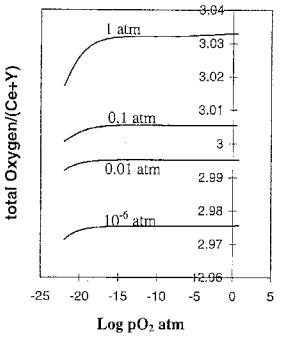

FIG. 2. Total oxygen content in a perovskite as function of partial pressure of oxygen for four water partial pressures in the range 10^{-6} to 1 atm. $K_s = 10^{-14}$, $K_{ox} = 1.5 \times 10^{-5}$, $K_i = 110^{-11}$, $K_w = 10$. A/B ratio = 1, dopant level $x = 0.05$.

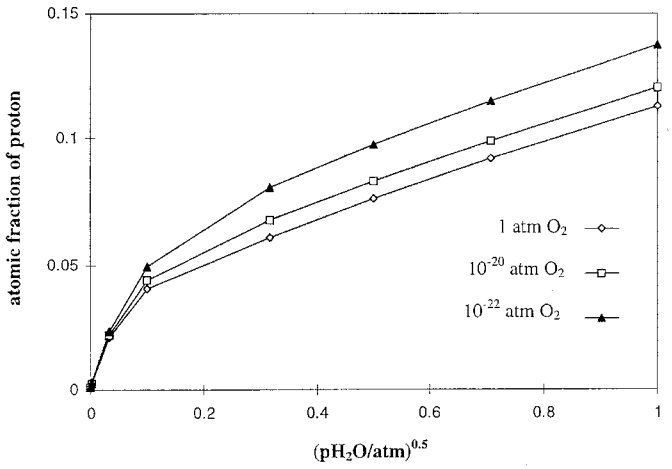

FIG. 3. Dependence of proton content (atomic fraction) on the square root of water partial pressure (atm) for three different oxygen partial pressures (atm). Values of equilibrium constants and composition are as in Fig. 2.

vapor pressure has been increased from 10^{-6} in Fig. 1A to 10^{-2} atm in Fig. 1B. At the same time the A/B ratio has been lowered to 0.99. Several things have happened: the proton concentration is now higher than the oxide ion vacancy concentration; the concentrations for the cation vacancies now follow two different curves—the B-site vacancy concentration is roughly a factor of 20 higher than the A-site vacancy concentration; and finally, the crossover pO_2, where $n = p$, has moved toward higher pO_2.

In situations far from saturation by protons, the proton content of the perovskite will sometimes follow the so-called Sieverts law, according to which the proton content is proportional to the square root of the partial pressure of water vapor. The law follows from Eq. [10], when one assumes $[V_O^{\bullet\bullet}]$ and $[O_O^{\times}]$ to be constant. In reality these two species are not constant in concentration, and the ratio of overall oxygen content to total amount of B ions does not have a general limiting value of $3 - [Y_B^{\prime}]/2$. The pO_2 region,over which in a thermogravimetric experiment one observes a constant weight, therefore cannot be used as a reference point unless one has supplementary information. Figure 2 illustrates the predicted overall stoichiometry for partial pressures of water from 10^{-6} to 1 atm. The proton content increases monotonically with increasing pressure. Only at the lowest water partial pressure of 10^{-6} atm does one find that the limiting oxygen content is close to $3 - [Y_B^{\prime}]/2 = 2.975$. Figures 3a and 3b in the paper of Schober and Wenzl (11) were supposed to illustrate this trend, but unfortunately show the results of a calculation corresponding to equilibrium constants different from those quoted in (11).

Figure 3 shows the protonic content as a function of the square root of the water partial pressure in the same range as in Fig. 2. Three deviations from "conventional" behavior are seen when cation vacancies are included in the defect model: (i) the proton content at high water partial pressure can exceed the doping level, here 0.05 atomic fraction; (ii) Sieverts law is obeyed only at very low partial pressure of water; (iii) a second linear regime in this square root plot is surprisingly also observed above 0.1 atm of pH_2O. Such an

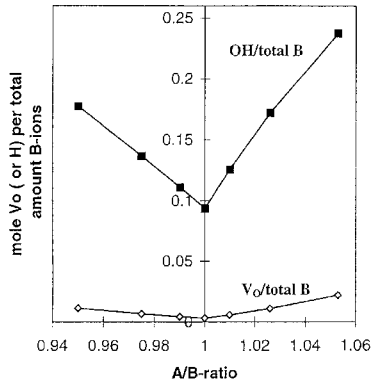

FIG. 4. Effect of A/B ratio on proton content and oxygen vacancy concentrations at $pH_2O = 1$ atm and 10^{-1} atm of pO_2; dopant level $x = 0.1$; $K_s = 0$. The concentrations have been normalized with respect to total amount of B ions in the solid.

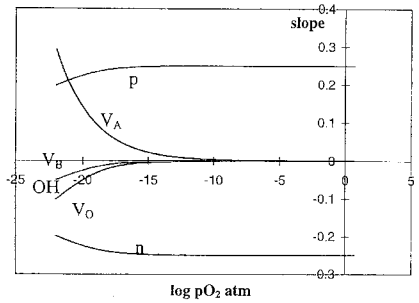

FIG. 5. Differentiated Brouwer diagram; data are the same as used for the generation of Fig. 1B. Slope is calculated for the various species, i, as $\delta \log[i]/\delta \log(pO_2)$.

observation could lead the experimenter to infer, by extrapolation to $pH_2O = 0$ atm, that the perovskite contains a certain amount (in the present case approximately 0.03 atomic fraction) of nonremovable protons.

Deviations of the A/B-ratio were finally modeled. Forcing the system to accomodate cation vacancies on either the A or B site has two effects: (i) The deficit of charge on the respective site has the same effect as if the system has been doped to a higher Y level. Fig. 4 shows the resulting concentrations of $[OH_O^\bullet]$ and $[V_O^{\bullet\bullet}]$ for A/B ratios in the range 0.950 to 1.053; (ii) The proton content is seen to increase as the A/B deviates from unity, the increase being approximately twice as strong for the B-ion-deficient regime. This is understandable since the ratio of the charges of $V_B^{|||}$ and $V_A^{|}$ is also equal to two. The equilibrium concentration of oxygen vacancies also increase slightly when the A/B ratio deviates from unity. The simulations furthermore show that materials with same doping level, but different A/B ratio, will, when compared at the same pO_2 and pH_2O, have very similar concentrations of hole carriers. Predictions and arguments based on isolated equilibria, such as the Schottky equilibrium, Eq. [7], in combination with Eq. [10] will inevitably lead to erroneous conclusions.

Extension to Other Defect Problems

Associates between oxygen vacancies and dopants/host ions were left out in the present treatment, due to complete ignorance regarding its importance in $SrCeO_3$-type materials. Test cases with strong association were examined by Schober and Wenzl (14). The present author will in the near future publish algorithms treating the following complex defect systems: (i) over- and understoichiometric perovskites such as $(La_{1-x}Sr_x)_yMnO_{3\pm\delta}$ with varying A/B ion ratios; (ii) Mg-doped $LiFeO_2$ (rock salt structure); (iii) defect association in doped and reduced ceria; and (iv) doped pyrochlore materials. At present the technique is being applied to modeling of the defect chemistry of the oxygen separation membrane material $Sr_4Fe_{6-x}Co_xO_{13\pm\delta}$ (17).

ACKNOWLEDGMENTS

The present work was started during the author's employment by The Nordic Energy Research Program for Fuel Cells, NEFP; continued under the Danish DK-SOFC projects; and completed with support and inspiration from the NEDO project on "Advanced Ceramics for Protonics, 1995–1998." Numerous fruitful discussions with N. Bonanos of Risø National Laboratory have assisted in the development of the present method.

REFERENCES

1. M. A. Panhans and R. N. Blumenthal, *Solid State Ionics* **60,** 279 (1993).
2. J. Nowotny and M. Rekas, *J. Am. Ceram. Soc.* **81**(1), 67 (1998).
3. T. Schober, W. Schilling and H. Wenzl, *Solid State Ionics* **86–88,** 653 (1996).
4. N. Bonanos and F. W. Poulsen, *J. Mater. Chem.* **9** (1999).
5. A. Holt, E. Ahlgren, and F. W. Poulsen, *in* "Proceedings, Third International SOFC, Honolulu" (S. C. Singhal and H. Iwahara, Eds.), Vol. 93–94, p. 562. The Electrochemical Society, Pennington, NJ, 1993.
6. F. W. Poulsen, *in* "Proceedings of Third International Symposium on Ionic and Mixed Conducting Ceramics, JECS-Meeting, Sept. 1997, Paris" (M. Mogensen and T. A. Ramanarayanan, Eds.), paper # 2179 1998.
7. G. Spinolo and U. Anselmi-Tamburini, *Ber. Bunsenges. Phys. Chem.* **99,** 87 (1995).
8. G. Spinolo, U. Anselmi-Tamburini, and P. Ghigna, Z. *Naturforschung A* **52,** 629 (1997).
9. F. A. Kröger and H. J. Vink, *in* "Solid State Physics" (F. Seitz and D. Turnball, Eds.), p. 307. 1956.
10. B. C. Tofield and W. R. Scott, *J. Solid State Chem.* **10,** 183 (1974).
11. I. G. Krogh Andersen, E. Krogh Andersen, P. Norby and E. Skou, *J. Solid State Chem.* **113,** 320 (1994).
12. H. Uscida, H. Yoshikawa, T.Esaka, S. Ohtsu, and H. Iwahara, *Solid State Ionics* **36,** 89 (1989).
13. H. Iwahara, T. Yajima, T. Hibino, K. Ozaki, and H. Suzuki, *Solid State Ionics* **61,** 65 (1993).
14. T. Schober and H. Wenzl, *Ionics* **1,** 311 (1995).
15. D. Shima and S. M. Haile, *Solid State Ionics* **97,** 433 (1997).
16. E. O. Ahlgren, J. R. Hansen, N. Bonanos and F. W. Poulsen, *in* "Proceedings 17th Risø Symposium on High Temperature Electrochemistry" (F. W. Poulsen *et al.*, Eds.), p. 161 Roskilde, Denmark, 1996.
17. F. W. Poulsen and K. Wiik, in preparation.

A4.

Bonanos, N.; Poulsen, F.W., ***Considerations of defect equilibria in high temperature proton-conducting cerates***. J. Mater. Chem. **9**, 431-434. (1999)

JOURNAL OF Materials CHEMISTRY

Considerations of defect equilibria in high temperature proton-conducting cerates

Nikolaos Bonanos* and Finn Willy Poulsen

Materials Research Department, Risø National Laboratory, DK-4000, Roskilde, Denmark. E-mail: nikolaos.bonanos@risoe.dk; finn.willy.poulsen@risoe.dk

Received 3rd July 1998, Accepted 10th November 1998

Acceptor doped perovskites such as strontium cerate form a variety of point defects through reaction with surrounding gases at high temperature, namely protons by dissolution of water vapour, electron holes by dissolution of oxygen and electrons by loss of oxygen. The defect equilibria can be described by three equilibrium constants coupled with electroneutrality and site conservation constraints. This work describes a numerical solution of these equations for arbitrary oxygen and water vapour partial pressures, without the need to neglect minority defects. It further examines the charge compensation mechanisms that dominate under the different regimes and their implications for transport properties.

1 Introduction

1.1 Background

Doped alkaline earth cerate and zirconate perovskites exhibit proton conduction at elevated temperatures[1–4] due to dissolution of water vapour and the formation of mobile protons. In such systems, an equilibrium arises between four types of point defects, namely oxide ion vacancies, protons, electrons and electron holes. The defect equilibria have been described for both vanishing[4,5] and finite[6,7] concentrations of free electrons, but these treatments have not taken into account a constraint namely, that of conservation of oxygen sites.

The present work describes a numerical solution of the complete set of defect equations, including this constraint. The solutions, presented in the form of two- and three-dimensional graphs of defect concentrations *versus* water vapour and oxygen partial pressures, are used to illustrate the dominant transport properties under various conditions and acceptor dopant concentrations. In common with earlier work,[4–7] this treatment ignores the Schottky defect equilibrium for which, in any case, the equilibrium constant is not available. The errors resulting from this omission will be negligible for heavily doped systems at temperatures low in comparison to their melting point, namely for typical perovskite proton conductors such as $SrCe_{0.95}Yb_{0.05}O_{2.975}$ or $BaCe_{0.90}Yb_{0.10}O_{2.95}$ at temperatures of 1200 °C or lower.

1.2 Definition of defect equilibria

Consider a system $AB_{1-y}M_yO_{3-y/2\pm\delta}$ where A and B are parent cations of valence 2 and 4 respectively and M is a trivalent cation substituting on the B-site. The following point defects and normal lattice oxygen are defined using the Krőger-Vink notation.[8]

Substitutional cation:	M_B'
Oxide ion vacancy:	$V_O^{\cdot\cdot}$
Proton (interstitial):	$H_i^{\cdot}$
Electron hole:	$h_i^{\cdot}$
Electron:	e'
Normal oxygen	$O_O^{\times}$

We now consider the following three defect reactions with their associated equilibrium equations. Dissolution of water vapour, with the generation of protons:

$$H_2O+V_O^{\cdot\cdot}\rightarrow O_O^{\times}+2\,H_i^{\cdot} \quad (1a)$$

$$[H_i^{\cdot}]^2=K_{II}\,P_{H_2O}\,[V_O^{\cdot\cdot}]\,[O_O^{\times}]^{-1} \quad (1b)$$

Dissolution of oxygen, with the generation of electron holes:

$$1/2\;O_2+V_O^{\cdot\cdot}\rightarrow O_O^{\times}+2\,h_i^{\cdot} \quad (2a)$$

$$[h_i^{\cdot}]^2=K_h\,P_{O_2}{}^{1/2}\,[V_O^{\cdot\cdot}]\,[O_O^{\times}]^{-1} \quad (2b)$$

Loss of oxygen, at low partial pressure, with the generation of electrons:

$$O_O^{\times}\rightarrow V_O^{\cdot\cdot}+2\,e'+1/2\;O_2 \quad (3a)$$

$$[e']^2=K_e\,P_{O_2}{}^{-1/2}\,[O_O^{\times}]\,[V_O^{\cdot\cdot}]^{-1} \quad (3b)$$

The above defect concentrations must satisfy the electroneutrality condition, namely:

$$2\,[V_O^{\cdot\cdot}]+[H_i^{\cdot}]+[h_i^{\cdot}]-[e']-[M_B']=0 \quad (4)$$

and also the anion site conservation condition, which for a perovskite is as follows:

$$[V_O^{\cdot\cdot}]+[O_O^{\times}]=3 \quad (5)$$

In the above, P_{H_2O} and P_{O_2} are independent variables, $[M_B']$, K_{II}, K_h and K_e are system and temperature dependent parameters and $[V_O^{\cdot\cdot}]$, $[H_i^{\cdot}]$, $[h_i^{\cdot}]$ and $[e']$ are the required solutions. The exciton equilibrium equation $[e'][h_i^{\cdot}]=K_{ex}$ is not explicitly used, but is implicit in the above, since it can be derived by multiplication of eqn. (2b) and (3b). In another formulation,[6] where the exciton equilibrium is included, (3b) is omitted. The above set of defect equations, and indeed more complex defect schemes involving cation vacancies, can be solved using an alternative, stepwise method proposed recently.[9] This uses the mathematical device of treating $[V_O^{\cdot\cdot}]$ as an independent variable and P_{O_2} as a dependent variable. As a result, however, that method cannot provide solutions at predefined values of oxygen partial pressure, leading to difficulties in the presentation of three-dimensional surface plots.

1.3 Solution of the analytical defect equation

Combining eqn. (5) with (1), (2) and (3) consecutively and taking square roots gives:

$$[H_i^{\cdot}]=K_{II}{}^{1/2}\,P_{H_2O}{}^{1/2}\,x \quad (6)$$

$$[h_i^{\cdot}]=K_h{}^{1/2}\,P_{O_2}{}^{1/4}\,x \quad (7)$$

$$[e']=K_e{}^{1/2}\,P_{O_2}{}^{-1/4}\,x^{-1} \quad (8)$$

$$\text{where } x=\{[V_O^{\cdot\cdot}]/(3-[V_O^{\cdot\cdot}])\}^{1/2} \quad (9)$$

in which case: $[V_O^{\cdot\cdot}]=(3x^2)/(x^2+1)$ (10)

inserting eqn. (6)–(8) into the electroneutrality eqn. (4) and rearranging, yields:

$$\beta x^4+(6-[M_B'])\,x^3+(\beta-\alpha)\,x^2-[M_B']\,x-\alpha=0 \quad (11)$$

$$\text{in which } \alpha=K_e^{1/2}P_{O_2}^{-1/4} \quad (12)$$

$$\text{and } \beta=K_H^{1/2}P_{H_2O}^{1/2}+K_h^{1/2}P_{O_2}^{1/4} \quad (13)$$

After solving eqn. (11), x is inserted into eqn. (6)–(8) and (10) to give the required defect concentrations. Eqn. (11) is quartic and, therefore, has an analytic solution, but, in practice it was found easier to implement a Newton–Raphson iterative solution, see for example ref. 10. If eqn. (11) is written in the form $f(x)=0$, the Newton–Raphson formula (14) gives the $(i+1)$th iteration of x in terms of the ith iteration.

$$x_{i+1}=x_i-f(x_i)/f'(x_i) \quad (14)$$

$$\text{where } f(x)=\beta x^4+(6-[M_B'])\,x^3+(\beta-\alpha)\,x^2-[M_B']\,x-\alpha \quad (15)$$

$$\text{and } f'(x)=4\beta x^3+3(6-[M_B'])\,x^2+2(\beta-\alpha)\,x-[M_B'] \quad (16)$$

The initial guess for x was provided by solving a quadratic equation (17) obtained under the assumptions $[e']=0$ and $x\ll 1$, the latter assumption allowing eqn. (10) to be simplified to $[V_O^{\cdot\cdot}]=3x^2$.

$$6x^2+\beta x-[M_B']=0 \quad (17)$$

$$\text{thus } x=\{-\beta+(\beta^2+24\,[M_B'])^{1/2}\}/12 \quad (18)$$

This solution is an excellent approximation for the full quartic model in the high-P_{O_2} regime, where the electron concentration is indeed negligible and the oxygen vacancy concentration never exceeds $[M_B']/2$. By using this initial guess, convergence was obtained within about ten iterations. To be on the safe side, fifteen iterations were used and the self-consistency of all solutions was checked by verifying electroneutrality.

2.3 Choice of simulation inputs

The purpose of this work is to focus on an interesting set of conditions, *i.e.* where several defects coexist in non-negligible concentrations. Therefore, wide ranges of partial pressure were chosen without concern as to their physical realisability, namely 10^{-8}–10^{8} atm for P_{H_2O} and 10^{-30}–10^{10} atm for P_{O_2}. The input parameters for the model are given in Table 1. For some typical perovskite proton conductors, values of K_H are available from thermogravimetric studies (Table 2), so K_H was assigned a realistic value for a rare earth doped cerate perovskite at 600–800 °C. Equilibrium constants K_h and K_e were set to values consistent, within about an order of magnitude, with those used by other authors.[7] The doping level, $[M_B']$, was held constant at 0.10, unless otherwise stated.

3 Results and discussion

The calculated concentrations for the four defects of interest are shown in Fig. 1(a) as a Brouwer diagram for a fixed P_{H_2O} of 10^{-2} atm. Over a wide range of P_{O_2}, the ionic defects (oxide ion vacancies and protons) have constant concentrations: $[V_O^{\cdot\cdot}]=0.028$; $[H_i^{\cdot}]=0.044$, corresponding to a water uptake of almost half the saturation value. The electronic defects behave as minority carriers. As shown in Fig. 1(b), the electroneutrality errors in these calculations are consistently 10^{-16} or less and are no doubt the result of rounding off errors in the calculation of x.

Fig. 2 shows the same defect concentrations as three-dimensional plots calculated for a logarithmically spaced grid of P_{O_2} and P_{H_2O}. In certain partial pressure ranges, the oxide ion vacancy and proton concentrations have plateaus which may be associated with intrinsic compensation regimes. For oxide ion vacancies [Fig. 2(a)] the plateau occurs at $[V_O^{\cdot\cdot}]=0.05$, determined by the simplified electroneutrality condition $2[V_O^{\cdot\cdot}]\approx[M_B']$. The latter limit is valid for very low proton uptake, *i.e.* very low water partial pressures. For the protons the plateau occurs at $[H_i^{\cdot}]\approx 0.10$, corresponding to the condition $[H_i^{\cdot}]\approx[M_B']$. These regimes are well understood and experimentally accessible in real systems. For the holes, a plateau corresponding to $[h^{\cdot}]\approx[M_B']$ was expected at very high P_{O_2}, but this was not found in the parameter space covered. Instead, the hole concentration increased monotonically with increasing P_{O_2} and decreasing P_{H_2O} [Fig. 2(c)]. For the acceptor doped system modelled, no intrinsic compensation regime is expected for electrons and indeed their concentration increases monotonically with increasing P_{H_2O} and decreasing P_{O_2} [Fig. 2(d)]. Outside the extrinsic regimes, more complex compensation conditions apply. When both P_{H_2O} and P_{O_2} are low, the vacancy concentration rises according to the condition $2[V_O^{\cdot\cdot}]\approx[M_B']+[e']$. Conversely, at low P_{H_2O} and high P_{O_2}, oxygen is dissolved in the solid and the vacancy concentration

Table 1 Input parameters used for the simulation study

Description	Symbol	Value
Doping level for trivalent ion on B-site	$[M_B']$	0.10[a]
Equilibrium constant for proton formation	K_H	20 atm^{-1}
Equilibrium constant for hole formation	K_h	10^{-5} $atm^{-1/2}$
Equilibrium constant for electron formation	K_e	10^{-17} $atm^{1/2}$

[a] Valid for all simulations except those shown in Fig. 3, in which $[M_B']$ has been varied.

Table 2 Experimental equilibrium constant K_H for selected perovskite proton conductors[a]

Compound	T/°C	K_H/atm^{-1}	Ref.
$BaCe_{0.95}Gd_{0.05}O_{2.975}$	600	26	11
$BaCe_{0.95}Nd_{0.05}O_{2.975}$	600	13	12
$BaCe_{0.95}Nd_{0.05}O_{2.975}$	900	3	12
$(Ba_{0.98}Gd_{0.02})(Ce_{0.87}Gd_{0.13})O_{2.945}$	800	20[b]	13

[a] The original literature values were based on models defining $[O_O^{\times}]\leqslant 1$. To reconcile these with the present site conservation equation, according to which $[O_O^{\times}]\leqslant 3$, the quoted literature values have been multiplied by a factor of 3. [b] Single crystal material; value interpolated from data supplied by authors.

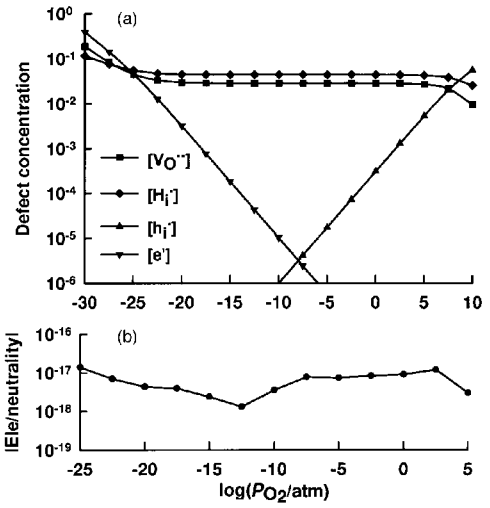

Fig. 1 (a) Brouwer diagram of defect concentrations in a perovskite proton conductor for the case $[M_B']=0.1$ and $P_{H_2O}=10^{-2}$ atm. (b) Electroneutrality errors for the calculations.

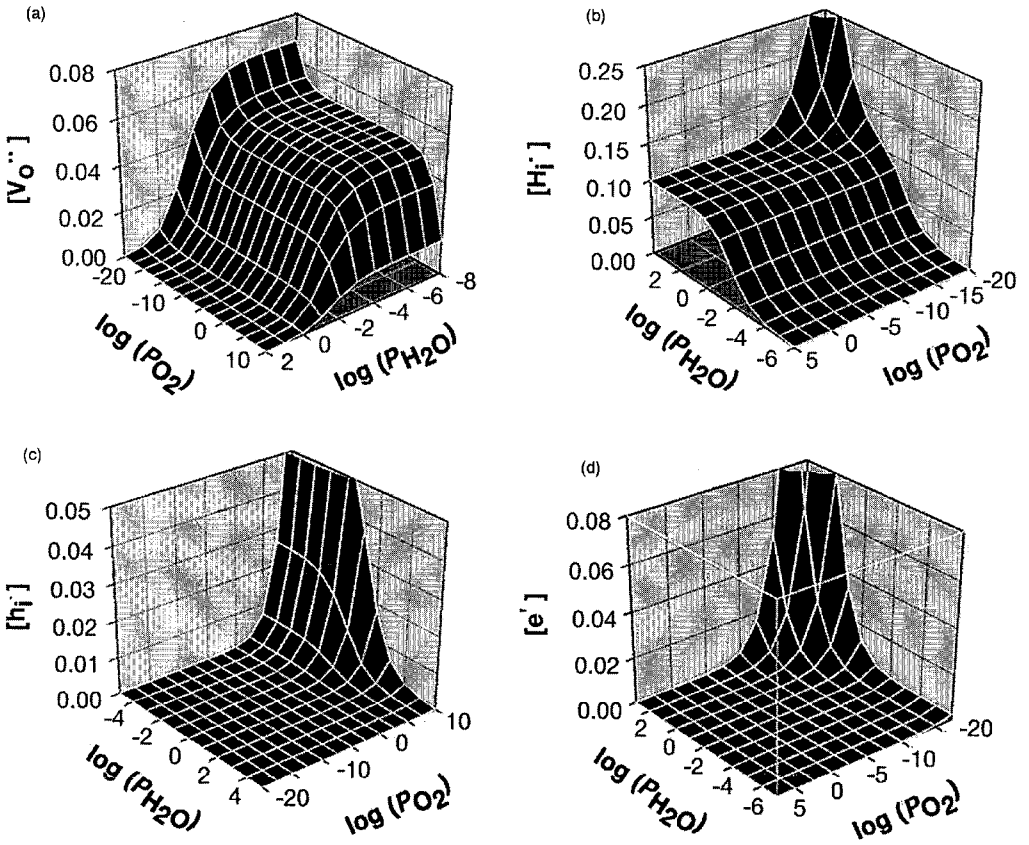

Fig. 2 Defect concentrations for a logarithmically spaced grid of P_{O_2} and P_{H_2O} for the case $[M_B']=0.1$. (a) oxide ion vacancies, (b) protons, (c) holes and (d) electrons. Partial pressures are in atm. The plateaus visible in (a) and (b) correspond to intrinsic charge compensation regimes.

falls, a situation that may be described by the condition $2[V_O^{\cdot\cdot}]+[h_i^{\cdot}]\approx[M_B']$.

Fig. 3 shows the four defect concentrations of interest as a function of dopant concentration for a fixed water vapour pressure of 10^{-2} atm. For vacancies and protons [Fig. 3(a)] and for holes [Fig. 3(b)] the calculations were performed for $P_{O_2}=1$ atm and for electrons [Fig. 3(c)] for $P_{O_2}=10^{-20}$ atm. As shown in Fig. 3(a), the concentrations of the ionic defects have different curvatures and $[V_O^{\cdot\cdot}]$ and $[H_i^{\cdot}]$ cross over at $[M_B']=0.20$, as well as in the trivial case $[M_B']=0$. It is interesting that for the realistic value of K_H used, the quantity $[H_i^{\cdot}]-[V_O^{\cdot\cdot}]$ is maximum at $[M_B']=0.075$; *i.e.* at this doping level protons dominate most strongly over vacancies. This may be linked to the empirical fact that, in this type of compound, pure protonic conductivity is achieved at doping levels of around 5%.[1 4] The concentrations of vacancies and protons are almost independent of the equilibrium constants K_h and K_e, provided these are both much lower than K_H, as is the case in the present simulations.

The electronic defects behave as expected but, in view of the uncertainty over K_h and K_e, their main use here is for showing qualitative trends. Thus $[h_i^{\cdot}]$ increases with doping level [Fig. 3(b)] in a manner similar to $[H_i^{\cdot}]$. As shown in Fig. 3(c), calculated for low oxygen partial pressure conditions, the electron concentration decreases with acceptor doping.

Fig.4 shows the P_{O_2} dependence of $[e']$ and $[H_i^{\cdot}]$, for the case $[M_B']=0.1$ and $P_{H_2O}=10^{-2}$ atm. For most of the simulated P_{O_2} range, electrons are minority carriers and $[e']$ is proportional to $(P_{O_2})^{-0.25}$ [Fig. 4(a)] and $[H_i^{\cdot}]$ is constant [Fig. 4(b)]. However, at $P_{O_2}<10^{-20}$ atm, the slope of $\log([e'])$ *versus* $\log(P_{O_2})$ begins to fall and $[H_i^{\cdot}]$ increases rapidly. Inspection of the output data files for this regime indicated an effective electroneutrality condition $2[V_O^{\cdot\cdot}]+[H_i^{\cdot}]-[e']-[M_B'']\approx 0$. Over the whole P_{O_2} range, the data in Fig. 4(b) is described by the power law $[H_i^{\cdot}]=a+b(P_{O_2})^{-0.15}$. Assuming a constant proton mobility, in these circumstances, the protonic conductivity would have an oxygen partial pressure dependence that might suggest that it is *n*-type electronic. This effect, which, to the authors' knowledge has not been pointed out before, might explain some discrepancies in the reported conduction mechanisms of proton conducting perovskites, as discussed below.

Acceptor doped $SrCeO_3$ and $BaCeO_3$ have been described as partial *n*-type electronic conductors due to an increase in conductivity at low partial pressures of oxygen.[14 16] On the other hand, in hydrogen-rich atmospheres, these compounds are found to retain high protonic transport numbers, as demonstrated by their ability to pump hydrogen electrochemically.[15] The above simulations show that, under strongly reducing conditions, the concentrations of protons and electrons can both be significant. Which carrier dominates the conductivity will depend on the relative magnitude of their mobilities; obviously, if the electrons had a much lower mobility, the protons would dominate. Therefore, a reliable identification of the conduction mechanism cannot be made

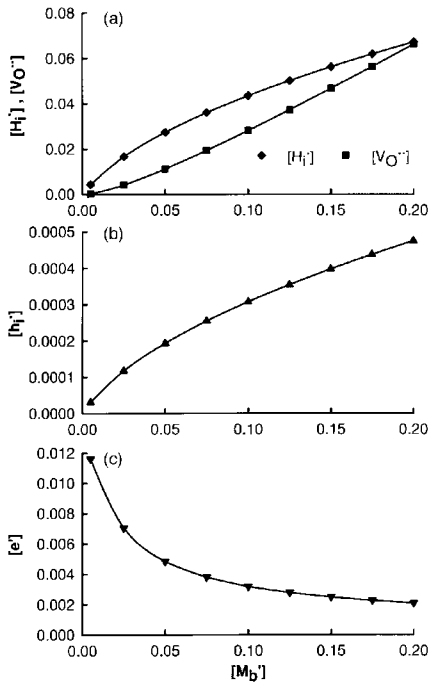

Fig. 3 Defect concentrations in a perovskite proton conductor as a function of acceptor dopant concentration calculated for a fixed P_{H_2O} of 10^{-2} atm. (a) Oxide ion vacancies and protons for $P_{O_2}=1$ atm; (b) holes for $P_{O_2}=1$ atm; (c) electrons for $P_{O_2}=10^{-20}$ atm.

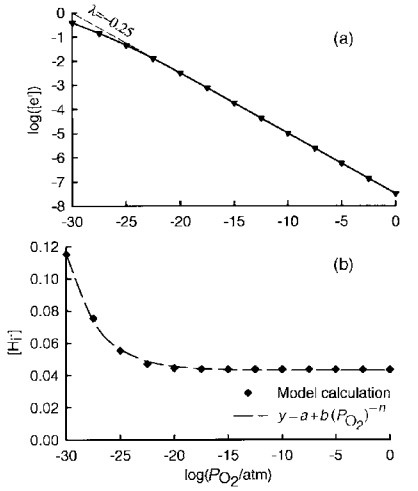

Fig. 4 Oxygen partial pressure dependence of the concentrations of (a) electrons and (b) protons in a perovskite proton conductor for $[M_B']=0.1$ and $P_{H_2O}=10^{-2}$ atm. At $P_{O_2}<10^{-20}$ atm the slope $\log([e'])$ *versus* $\log(P_{O_2})$ changes. Over the whole range, the concentration of protons follows a power law, plotted as a solid line.

on the basis of conductivity alone, but should be supplemented by electrochemical determinations, such as concentration cells studies or the faradaic transport of oxygen and/or hydrogen.

If the temperature dependence of the equilibrium constants is known, the above solution can be easily applied to thermogravimetric data; the sample weight can be calculated from the oxygen stoichiometry, $3-[V_O^{\cdot\cdot}]$, and proton concentration. It can also be used to model the total conductivities, provided the mobilities of the charge carriers are known. Considering the iterative nature of the solution, it is difficult to imagine using the full model to obtain equilibrium constants by fitting to conductivity data, but approximate solutions, such as the quadratic one described, can and have been used, see for example ref. 5.

4 Conclusions

The concentration of ionic and electronic defects in a perovskite proton conductor was obtained by numerical solution of a quartic equation involving three equilibrium constants, the doping level and the partial pressures of water vapour and oxygen. In certain ranges of partial pressure, the concentrations of vacancies and protons follow simple electroneutrality conditions such as $2[V_O^{\cdot\cdot}]\approx[M_B']$ or $[h_i^{\cdot}]\approx[M_B']$, corresponding to extrinsic doping regimes. Simulation of the low oxygen partial pressure regime shows that the protonic concentration varies with P_{O_2}, potentially giving rise to confusion with *n*-type electronic conductivity. The total electrical conductivity can be modelled if the charge carrier mobilities are known.

5 Acknowledgements

Yang Du and K.-D. Kreuer are acknowledged for supplying data on water vapour equilibrium constants, M. Mogensen, T. Norby and B. C. H. Steele are thanked for useful discussions and B. Zachau-Christiansen is thanked for a critical reading of the manuscript. This work was supported by the Materials Research Department, under the fundamental Defect Chemistry project and by the New Energy Development Organisation (NEDO) of Japan under the project *Advanced Ceramics for Protonics*, led by Professor H. Iwahara.

References

1 H. Iwahara, T. Esaka, H. Uchida and N. Maeda, *Solid State Ionics*, 1981, **3/4**, 359.
2 H. Iwahara, Proc. Intl. Conference on advanced materials (ICAM 91), Symposium A2: Solid State Ionics, Strasbourg, 27–31 May 1991, Ed. M. Balkanski, T. Takahashi and H. L. Tuller, Intl. Union of Materials Research Societies, Amsterdam, 1992, 575.
3 H. Iwahara, *Advanced Ceramics for Protonics*, in *High Temperature Electrochemistry, Ceramics and Metals*, Proc. 17th Risø Intl. Symposium on Materials Science, ed. F. W. Poulsen, N. Bonanos, S. Linderoth, M. Mogenson and B. Zachau-Christiansen, Risø National Laboratory, Roskilde, Denmark, 1996, Sept. 2–6.
4 H. Uchida, H. Yoshikawa and H. Iwahara, *Solid State Ionics*, 1989, **35**, 229.
5 Y. Larring and T. Norby, *Solid State Ionics*, 1997, **97**, 523.
6 T. Schober and H. Wenzl, *Ionics*, 1995, **81**, 111.
7 T. Schober, W. Schilling and H. Wenzl, *Solid State Ionics*, 1996, **86–88**, 653.
8 F. A. Kröger, and H. J. Vink, *Solid State Physics*, ed. F. Seitz and D. Turnbull, Academic Press, New York, vol. 3, pp. 307–435.
9 F. W. Poulsen, *J. Solid State Chem.*, 1999, in press.
10 S. Barnet and T. M. Cronin, *Mathematical Formulae for Engineering and Science Students*, Bradford University Press, 1971, p. 45.
11 J. F. Liu and A. S. Nowick, *Solid State Ionics*, 1992, **50**, 131.
12 A. S. Nowick and Du. Yang, *Solid State Ionics*, 1995, **77**, 137.
13 K-D. Kreuer, Th. Dippel, Yu. M. Baikov and J. Maier, *Solid State Ionics*, 1996, **86–88**, 613.
14 N. Bonanos, *J. Phys. Chem. Solids*, 1993, **54**, 867.
15 I. Kosacki and H. L Tuller, *Solid State Ionics*, 1995, **80**, 223.
16 E. O. Ahlgren, J. R. Hansen, N. Bonanos, F. W. Poulsen and M. Mogensen, *Electrical characterisation of* $SrCe_{0.95}Y_{0.05}O_{3-\delta}$, in *High Temperature Electrochemistry, Ceramics and Metals*, Proc. 17th Risø Intl. Symposium on Materials Science, ed. F. W. Poulsen, N. Bonanos, S. Linderoth, M. Mogenson and B. Zachau-Christiansen, Risø National Laboratory, Roskilde, Denmark, 1996, Sept. 2–6.

Paper 8/05150J

A5.

F. W. Poulsen, ***Defect chemistry modelling of oxygen-stoichiometric, vacancy concentrations and conductivity of*** $(La_{1-x}Sr_x)_yMnO_{3+d}$, Solid State Ionics **129** 145- 162. (2000)

ELSEVIER

Solid State Ionics 129 (2000) 145–162

SOLID STATE IONICS

www.elsevier.com/locate/ssi

Defect chemistry modelling of oxygen-stoichiometry, vacancy concentrations, and conductivity of $(La_{1-x}Sr_x)_yMnO_{3\pm\delta}$ ☆

Finn Willy Poulsen*

Materials Research Department, Risø National Laboratory, DK-4000 Roskilde, Denmark

Received 5 June 1999; received in revised form 2 September 1999; accepted 27 November 1999

Abstract

Two precise algorithms are devised for the calculation of defect concentrations in A-site acceptor doped ABO_3 perovskites. The two models contain nine species including cation vacancies on the A- and B-site. The small polaron model is based on three redox levels of the B-ion. A large polaron model, based on delocalised electrons, electron holes and all B-ions being trivalent is given in Appendix A. The sequential mathematical method allows us to calculate the high temperature oxygen partial pressure dependent properties of $(La_{1-x}Sr_x)_yMnO_{3\pm\delta}$ in a unified manner irrespective of the type of defect regime. Simulations are shown for a pO_2 span from 10^{-30} to 10^{5} atm. The three required equilibrium constants for $(La_{1-x}Sr_x)_yMnO_{3\pm\delta}$ had to be changed significantly from values given in literature in order to match the observed stoichiometry span. The main results shown are calculated by the small polaron model containing only ionic species – the B-ion may be Mn'_B (Mn^{2+}), $Mn^{\times}_B$ (Mn^{3+}), and $Mn^{\cdot}_B$(Mn^{4+}). The A/B-ratio = y greatly influences the oxygen stoichiometry, oxygen ion vacancy- and cation vacancy concentrations and the total conductivity. Calculations are given for the range $0.87 \le y \le 1.13$ for a Sr doping of 10% at 1000°C. The defect model can simultaneously describe the observed stoichiometry and conductivity dependence on pO_2, if the electronic mobility is decreased by up to 50% at $pO_2 < 10^{-10}$ and $pO_2 > 10^{2}$ atm.

Keywords: Conductivity; Defect modelling; LSM; Non stoichiometry; Perovskite; Sequential algorithm

1. Introduction

Oxides with the perovskite structure receive much attention at present due to the observation of both interesting electrical (superconductive, catalytic, oxygen cathode reduction-, piezo-), combined electromagnetic (colossal magneto resistive-), and mixed electronic–ionic conduction properties. Manganites of the type $(M_{1-x}M'_x)_yMnO_{3\pm\delta}$ are among the prime targets in the ongoing research. The A-site ions of interest are M=La, Nd, Y; and M′=Sr, Ca.

The idea of describing the redox chemistry of $La_{1-x}Sr_xMnO_{3\pm\delta}$ (LSM) in terms of coexistence of several oxidation states of Mn has gradually evolved via the work of H.U. Anderson and co-workers in the period 1989–90 [1–3] and by van Roosmalen and Cordfunke in 1991–94 [4–7]. Kofstad and Petrov [8] showed in 1993 that the pO_2 dependence of the conductivity and stoichiometry of LSM cannot be

☆ Dedicated to the memory of Professor Per Kofstad, University of Oslo.

*Fax: +45-46-77-5758.

E-mail address: finn.willy.poulsen@risoe.dk (F.W. Poulsen)

0167-2738/00/$ – see front matter
PII: S0167-2738(99)00322-7

explained by a simple model including manganese in the two oxidation states +3 and +4, but their model, on the other hand did not allow stoichiometries below $O_{tot}/Mn=(3-x/2)$. Kofstad and co-workers further addressed the crystallography, oxygen diffusion and defect chemistry of the cobalt substituted LSM: $La_{1-x}Sr_xCo_{1-z}Mn_zO_{3\pm\delta}$ in three publications [9–11]. Nowotny and Rekas [12] modelled in 1998 the high temperature (1000–1200°C) defect chemistry of (La,Sr)MnO_3 based on the presence of three oxidation states of manganese, Mn'_B, Mn^x_B and $Mn^{\cdot}_B$ (manganese +2, +3 and +4). The span in pO_2 covered in [12] was 10^{-20} to 1 atm. The oxidation states are populated in various proportions depending on temperature, partial pressure of oxygen and Sr-doping [12]. Three equilibrium constants, one for oxidation of the compound by oxygen, a dismutation reaction between the three oxidation states of Mn, and a Schottky reaction for vacancy formation, respectively, were extracted from literature data, where the main sources of data are found in references [1–7,13,14]. Two major conclusions were given in Ref. [12]: (i) There seems hardly to be evidence for cluster formation between Mn'_B and oxygen vacancies; and (ii) if one maintains hypothesis # (i) and the 3-oxidation state model, one is forced to accept equilibrium constants which vary with the strontium content.

No quantitative defect concentration calculations have so far treated LSM's with A/B-ratios different from unity. The mathematical approach of Nowotny and Rekas is only feasible under the assumption that the cation vacancy concentrations on the A- and B-sites are identical, i.e. their algorithm is only valid for the case $A/B\equiv 1$. There is a strong need to be able to model oxygen stoichiometry in A- or B-site deficient perovskites. Diffusion- and sintering mechanisms, as well as electrical- and magnetic properties and possibly electro-catalytic properties can then be modelled. In the case of $(La_{1-x}Sr_x)_vMnO_{3\pm\delta}$, the interest relates both to high as well as low temperature properties. LSM is the state of the art choice for an air electrode (cathode) in solid oxide fuel cells. The defect concentrations are bound to depend on the electrochemical polarisation of an LSM-electrode: An increase in oxygen vacancy concentration with polarisation of an LSM-cathode appears to be responsible for the improved performance of LSM-cathodes with increasing cathodic overpotential.

The oxygen vacancy concentration is of vital importance for the oxygen diffusion in LSM and possibly of equal importance for the oxygen reduction kinetics on LSM. Cathodes are often fabricated with an excess of Mn in order to reduce the reactivity between LSM and the solid electrolyte YSZ [15]. Reaction results in formation of the highly resistive phases $SrZrO_3$ and $La_2Zr_2O_7$ [16,17]. A typical formulation contains 15% Sr doping on the La-site and a nominal excess of manganese of 10 atomic %. Some of the excess manganese will be present as Mn_3O_4/Mn_2O_3 in the cathode [18], but the remaining is dissolved in the perovskite leading to an A-site deficient material, i.e. $[V'''_A]>[V'''_B]$. The low temperature magnetic properties of LSM's vary with the oxygen stoichiometry of the material, which has been equilibrated at high temperature. Variation of the colossal magnetoresistive (CMR) effect of variously doped lanthanum manganites can possibly also be analysed by defect chemistry models as the present ones. Ref. [19] gives an up to date review on magnetic properties including CMR of LSM.

The present mathematical approach for calculating defect concentrations was first presented late 1992 at a Nordic workshop on mixed conducting oxides [20] and later applied in 1993 to the defect concentration calculations on the pO_2 driven p- to n-transition in $NdCr_{1-v}Ti_vO_{3\pm\delta}$ [21]. In 1997 the method was used to model the simultaneous presence of electronic and protonic defects in doped zirconia and thoria [22]. A recent paper [23] on B-site doped $SrCeO_3$ describes a model with simultaneous presence of protons, oxide ion- and cation-vacancies and electronic defects. Ref. [23] also gives arguments for the applicability of the mathematical method. Spinolo and Anselmi-Tamburini suggested in 1995 [24] a similar mathematical method to calculate defect concentrations in MO_2 oxides with interstitial cations having charges from 0 to +4. A general treatment was given by Spinolo et al. in 1997 [25], however without application to actual oxides.

This paper is hopefully written in a tutorial way, in the sense that problems are presented, procedures are developed that enable us to treat these problems, and we experience how far one can get by these tools. Since the defect chemistry and conduction mechanism in LSM are still controversial issues, several questions are left open for the scientists of the next millennium to crack.

2. Defect chemical model for nonstoichiometric $(La_{1-x}Sr_x)_yMnO_{3\pm\delta}$

The acceptance criterion for a defect model being a good model for a given doped oxide, is that several (hopefully all) properties can be predicted as function of partial pressure of oxygen, pO_2. The data to be modelled may be the observed oxygen stoichiometry, total electrical conductivity, Seebeck coefficient (thermoelectric power), lattice parameter variation, and magnetic properties. Here we will restrict our interest to the oxygen stoichiometry and total electrical conductivity variation of LSM. The measurements of Kuo, Koc et al. [1–3] on 10% Sr doped LSM at 1000°C are given in Fig. 1 (calculated curves are commented on later). The challenge to the defect model is to account for: (i) over- and sub stoichiometry, (ii) why the total conductivity is independent of pO_2 in the range $1-10^{-8}$ atm, and finally (iii) why the conductivity curve starts to decrease at $pO_2 \approx 10^{-8}$ atm, while the stoichiometry curve first starts to go significantly below $Ox/Mn=3$ at $pO_2 \approx 10^{-12}$ atm.

The oxygen content per Mn in $(La,Sr)MnO_{3\pm\delta}$ can achieve values both greater and smaller than 3.

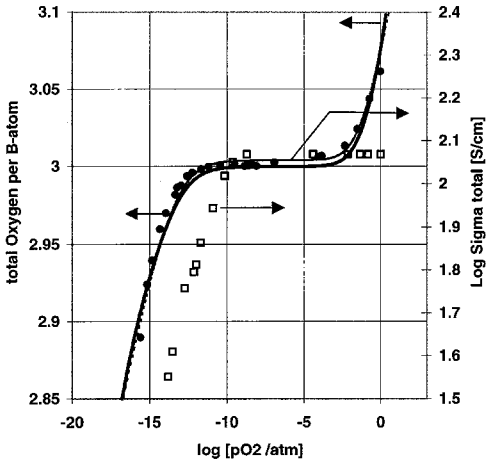

Fig. 1. Total conductivity, □, and oxygen stoichiometry, ●, at 1000°C of $(La_{0.9}Sr_{0.1})_{1.00}MnO_{3\pm\delta}$ based on measurements of Kuo et al. [1,2]. The model calculations are based on the large polaron model with equilibrium constants as given in Table 2, case #3. Thick line: Calculated stoichiometry; thin line: Calculated conductivity.

Negative deviations from 3 are explained by the presence of oxide ion vacancies and reduced manganese species, e.g. divalent Mn. Positive deviations *cannot* be explained by interstitial oxygen. The pioneering neutron diffraction study of Tofield and Scott in 1974 proved the presence of cation vacancies [26]. Careful classical chemical analyses by Krogh Andersen at al. of LSM's, annealed in different atmospheres, also indicate overstoichiometry of air synthesised LSM's [27], whereas annealing in standard nitrogen with a pO_2 in the range $10^{-2}-10^{-3}$ atm gives a material with $\delta \approx 0$.

The need to incorporate cation vacancies is mandatory for single phase perovskites, where the total content of A-site ions is different from the total content of B-site ions, e.g. when syntheses are made, where y differs from unity in $(La_{1-x}Sr_x)_yMnO_{3\pm\delta}$.

At least nine different species are required in order to explain the span of δ-values observed experimentally. The A-, B- and O-site 'inhabitants' are shown in Table 1 and the model may be described as a 'narrow band/small polaron/localised charge' description. An alternative model based on delocalised electrons, delocalised electron holes and all manganese as Mn_B^x, is given in Appendix A. This model is also based on nine species and could be named a 'large polaron' or band-like model.

Three assumptions underlie the present calculation method:

Assumption 1. The model involves only the nine species defined in Table 1, i.e. there is no Mn_B' on the A-site, no interstitial oxygen, and association between defects is neglected. The latter case has been treated by van Hassel et al. [29]. The electronic states of Mn_B', Mn_B^x and $Mn_B^{\cdot}$ are not specified in

Table 1
Simplest chemical defect model for $(La_{1-x}Sr_x)_yMnO_{3\pm\delta}$. The Sr-dopant is assumed to be divalent. Kröger–Vink-notation [28] is used with $La(+3)Mn(+3)O_3$ as the reference state. The 'chemical' equivalents of the manganese species are shown in parentheses. Table A.1 of Appendix A displays the alternative electron/electron hole description of LSM

A-site	B-site	O-site
La_A^x	Mn_B^x (Mn^{3+})	O_O^x
Sr_A'	Mn_B' (Mn^{2+})	$V_O^{\cdot\cdot}$
V_A'''	$Mn_B^{\cdot}$ (Mn^{4+})	–
–	V_B'''	–

terms of high spin or low spin states and possible changes in the electronic configurations with temperature are not considered.

Assumption 2. Measure for relative concentrations: We use (occupancy number)×(number of equivalent sites)/mol ABO_3 as a measure of the activity of a given species at a given temperature. From a crystallographical point of view there are two different types of oxygen sites in orthorhombic LSM. From an energetic point of view we ought to distinguish between these, but this would complicate the treatment. From the above definition it follows that the relative concentration of species on A- and B-sites cannot exceed 1, and the oxygen and oxygen vacancy relative concentrations cannot exceed 3. We also neglect the effect of small variations in sites/cm^3 following from the changes in lattice parameters as the oxygen content varies, or when the larger Sr^{+2} ion substitutes for La^{+3}. As the oxygen/total metal = $O_{tot}/M_{B,tot}$ content exceeds 3, the number of unit cells in the system increases, leading to a macroscopic expansion of the sample; at $O_{tot}/M_{B,tot}=3.06$ there are roughly 2% more unit cells in the sample than at $O_{tot}/M_{B,tot}=3$.

Assumption 3. Ideality of the chemical system: Instead of introducing activity coefficients we use Sr-concentration dependent equilibrium constants, as extracted form the literature by Nowotny and Rekas [12]. One can further argue that activity coefficients be concentration independent for a given Sr-doping, since the 'ionic strength' in the perovskite is very high; the oxide ion concentration is of the order of 77 mol/l.

A set of nine independent equations containing the nine concentrations of the different species will now be identified. The set will contain the global electroneutrality principle Eq. (1), a number of site balances, Eqs. (2)–(4) and mass conservation requirements, Eqs. (5) and (6), and finally some mass action law expressions, Eqs. (7)–(9). Care must of course be taken to avoid redundant equations among the equations. The nine equations required for a complete description of LSM with the species given in Table 1 are:

Principle of electroneutrality:

$$2[V_O^{\cdot\cdot}] + [Mn_B^{\cdot}] = [Mn_B'] + [Sr_A'] + 3[V_A'''] + 3[V_B'''] \quad (1)$$

A-site balance:

$$[La_A^x] + [Sr_A'] + [V_A'''] = 1 \quad (2)$$

B-site balance:

$$[Mn_B'] + [Mn_B^x] + [Mn_B^{\cdot}] + [V_B'''] = 1 \quad (3)$$

O-site balance:

$$[O_O^x] + [V_O^{\cdot\cdot}] = 3 \quad (4)$$

Metal contents:

$$[La_A^x]/[Sr_A'] = (1-x)/x \quad (5)$$

$$\{[La_A^x] + [Sr_A']\}/\{[Mn_B'] + [Mn_B^x] + [Mn_B^{\cdot}]\} = y \quad (6)$$

Eqs. (5) and (6) allow for A-site doping and deviation of the A/B-site occupation ratio from 1, respectively.

Schottky-reaction for vacancy formation: nil $\Leftrightarrow$ 3 $V_O^{\cdot\cdot} + V_A''' + V_B'''$, leading to the mass action expression

$$K_s = [V_O^{\cdot\cdot}]^3 \cdot [V_A'''] \cdot [V_B'''] \quad (7)$$

Comparison of the definitions of Nowotny and Rekas [12] with the present (simpler) definition of K_s leads to the following identity

$$K_s \text{ (present work)} \equiv K_r^3/K_2 \text{ (Nowotny and Rekas)} \quad (7')$$

Eq. (7) controls the geometrical/physical stability of the perovskite, and secures that high concentrations of both oxygen ion vacancies and metal ion vacancies do not coexist. If the latter were to occur, the crystal would collapse by annihilating the excess of partly filled unit cells; or it would decompose; or exolute new phases.

Redox reaction involving oxygen from the gas phase:

$$Oo^x + 2Mn_B^{\cdot} \Leftrightarrow V_o^{\cdot\cdot} + 2Mn_B^x + 1/2O_2(gas) \quad (8)$$

$$K_r = \frac{[Mn_B^x]^2 \cdot [V_O^{\cdot\cdot}] \cdot pO_2^{1/2}}{[Mn_B^{\cdot}]^2 \cdot [O_O^x]}$$

$[atm^{1/2}]$

Eq. (8) controls the chemical stability of the perov-

skite, and K_r has the same definition as in the work of Nowotny and Rekas [12].

All non-stoichiometric solid oxides can release/take up oxygen, which can be described by expressions analogous to Eq. (8). The equilibration reaction may be written either with different oxidation states of the reducible ion as above, or with creation of electrons, as in Eq. (A.8) proceeding from right to left, alternatively with consumption of electron holes. In the present chemical model, redistribution of electronic charges is represented by a disproportionation equilibrium between three oxidation states of manganese, in solution chemistry sometimes called a dismutation reaction:

$$2Mn_B^x \Leftrightarrow Mn_B' + Mn_B^{\cdot} \text{ leading to} \quad (9)$$

$$K_i = \frac{[Mn_B'] \cdot [Mn_B^{\cdot}]}{[Mn_B^x]^2}$$

K_i has according to Nowotny and Rekas (Fig. 10 of Ref. [12]) a weak negative temperature dependence for undoped $LaMnO_3$, whereas for $x=0.1$ to 0.2 there is virtually no temperature dependence. Equilibrium (8) in combination with equilibrium (9) can be said to furnish a sort of redox buffer capacity to a perovskite over extended regions of pO_2: If $[Mn_B^{\cdot}]$ in LSM is lowered due to reaction (8) proceeding to the right, more $[Mn_B^{\cdot}]$ will be formed via reaction (9).

3. Analytical solutions to determine the defect concentrations

An analytical expression in one of the unknown concentrations would result in a polynomial of a high degree in concentration and the expression will contain the six system- and/or temperature dependent parameters x, y, pO_2, K_s, K_i, and K_r. Especially Eq. (7), which in itself is of 5th order in concentration, adds to the complexity of the analytical expression. It would require some hours of work to find this analytical expression, even when taking advantage of symbol manipulation software. The problem is of course trivial from a mathematical point of view. Appendix B offers an exact analytical expression for the case $x=0$ and A/B-ratio=1, resulting in a polynomial of 12th degree in $[V_O^{\cdot\cdot}]$. From the mathematical investigations by the Norwegian mathematician Niels H. Abel in the 1820s, we know that general analytical solutions to high order polynomials are not possible at and above the level of quintic polynomials [30]. Assuming that we have obtained an analytical expression of high order, we must resort to numerical methods in order to find the *one and only* physically meaningful root. We may use Newton–Raphson iteration based on the analytical derivative or a numerical approximation of the derivative as for example done by Bonanos and Poulsen for $SrCe_{1-x}Y_xO_{3-\delta}$ [31]. An alternative procedure would be to solve all equations simultaneously by using Mathematica, Eureka or similar software packages. The disadvantage and occasional failure of the latter procedures have been mentioned earlier [23].

4. The present numerical method

Mathematical descriptions of a chemical system at equilibrium will yield only one physically acceptable solution – otherwise the chemical system will oscillate between two or more states or be chaotic. We will rely on this theorem in the following. Further justification of the present method is found in [23,24].

One assumes values for the three equilibrium constants, the dopant level x and A/B-ratio y; we then assume a physically possible value for the $[V_O^{\cdot\cdot}]$ concentration – the rest of the concentrations can then be found by linear or at most quadratic equations as shown below. Finally we check the 'healthiness' of the obtained result, e.g. (1) the concentrations must all be positive, and (2) they must not exceed the available number of sites in a perovskite lattice. If the calculated concentrations pass criteria (1) and (2), then one can calculate the corresponding equilibrium oxygen partial pressure from Eq. (8). In a computer programme one steps $[V_O^{\cdot\cdot}]$ from a low value, 10^{-20} to 0.5 and starts saving the data, when condition (1) and (2) are fulfilled. In spread sheet programming one creates a long column (some 500 cells long) full of stepped values for $[V_O^{\cdot\cdot}]$; the other concentration columns are calculated one by one from this column. The sequential calculation of concentrations proceeds as follows: By manipulation

with Eqs. (1)–(6), one can express the various defect concentrations by the oxygen vacancy concentration:

$$[V_O^{\cdot\cdot}] = \text{test value in the interval } 10^{-20} \text{ to } 0.5 \qquad (5')$$

$$[O_O^x] = 3 - [V_O^{\cdot\cdot}]$$

Eqs. (2), (3) and (6) inserted into Eq. (7) leads to a quadratic equation in $[V_B'''']$, which has only one physical (positive) solution:

$$[V_B'''']^2 - [V_B''''] \cdot (y-1)/y - K_s/\{y \cdot ([V_O^{\cdot\cdot}])^3\} = 0 \qquad (7')$$

Then follows immediately that

$$[V_A''''] = 1 - y + y \cdot [V_B''''] \qquad (10)$$

$$[Sr_A'] = x \cdot (1 - [V_A'''']) \qquad (11)$$

$$[La_A^x] = [Sr_A'] \cdot (1-x)/x \qquad (12)$$

$[Mn_B']$ and $[Mn_B^{\cdot}]$ can be expressed by $[Mn_B^x]$ by using Eqs. (1) and (3)

$$[Mn_B'] = 1/2 \cdot (T_1 - [Mn_B^x]) \qquad (13)$$

$$[Mn_B^{\cdot}] = 1/2 \cdot (T_2 - [Mn_B^x]) \qquad (14)$$

where

$$T_1 = 1 - 4[V_B''''] - 3[V_A''''] - [Sr_A'] + 2[V_O^{\cdot\cdot}] \qquad (15)$$

and

$$T_2 = 1 + 2[V_B''''] + 3[V_A''''] + [Sr_A'] - 2[V_O^{\cdot\cdot}] \qquad (16)$$

The expressions for $[Mn_B']$ and $[Mn_B^{\cdot}]$ are inserted into Eq. (9) leading to a quadratic equation in $[Mn_B^x]$:

$$[Mn_B^x]^2 \cdot (4K_i - 1) + (T_1 + T_2) \cdot [Mn_B^x] - T_1 \cdot T_2 = 0 \qquad (17)$$

All concentrations entering the T_1 and T_2 terms have numerical values at this point, $[Mn_B^x]$ is thus also calculated numerically, using the smallest of the positive roots. Finally $[Mn_B']$ and $[Mn_B^{\cdot}]$ are found from Eqs. (13) and (14). All equations but Eq. (8) have been employed so far. A set of nine concentrations has been found, and there are no more mathematical degrees of freedom. If the nine concentrations are all positive and below their respective limiting values, we have found the only physical solution. Only one specific partial pressure of oxygen can correspond to this situation. Insertion of the determined concentrations of $[Mn_B']$, $[O_O^x]$, $[Mn_B^x]$ and $[V_O^{\cdot\cdot}]$ in Eq. (8) thus defines the pressure that corresponds to the nine concentrations. The oxygen stoichiometry is calculated as $[O_O^x]/[Mn_{tot}]$. The calculation is then repeated with a new test-value of $[V_O^{\cdot\cdot}]$.

5. Results

5.1. General remarks on the model calculations.

As shown in Section 4, *all* chemical equilibria, leading to the mass action law expressions Eqs. (7)–(9), are taken into account at *all* partial pressures of oxygen in the present treatment and no approximations were made to the equations. The simulations are normally made for an interval of $[V_O^{\cdot\cdot}]$ from an arbitrarily chosen lowest limit, say 10^{-20} up to 0.5, which means that solutions are created for over-stoichiometric LSM's down to a hypothetical phase with $[O_O^x]/[Mn_{tot}] = 2.5$. Solutions are normally generated for a very wide pO_2 span, at least from 10^5 down to 10^{-30} atm. The full span is shown graphically in several of the following figures, although LSM's with 10–20% Sr doping *are not* stable below say $pO_2 \approx 10^{-16}$ atm at 1000°C, see Sections 5.2 and 5.3. The numerical precision of the present method is probed by checking the error in the electroneutrality condition, Eq. (1). The precision is determined entirely by the computer, computing language, and/or definitions of single or double precision and/or the quality of spread sheet used. The precision is in other words *not* determined by the mathematical procedure or approximations. The difference between the left hand side and right hand side of the electroneutrality condition is always better than 10^{-17} relative concentration units, i.e. the present method is far more precise than solutions based on approximations, where concentrations of the order of 10^{-6} or lower are neglected in the linear site-, mass-, and/or electroneutrality equations. Section 5.6 and Appendix A will discuss how to calculate the electronic and total electrical conductivity.

As the test value for $[V_O^{\cdot\cdot}]$ is most conveniently stepped logarithmically through its parametric space, one obtains relatively few (widely spaced) calculated points in regions of pO_2, where the stoichiometry curve is flat. After an initial calculation one can insert more narrowly spaced values of $[V_O^{\cdot\cdot}]$ in these regions in a second (and final) calculation sequence. The calculation speed of the present sequential method is impressive: Calculation and plotting of all concentrations at 500 different pO_2's, which is equivalent to solving 500 sets of equations with nine equations in each set, takes less than 0.4 s in an Excel spread sheet on a 200 MHz Pentium.

The interplay between equilibrium oxygen partial pressure, magnitude of equilibrium constants, temperature, Sr-doping and the A/B-ratio will be illustrated and discussed in Sections 5.2–5.6. The equilibrium constants used in the following were initially taken from Nowotny and Rekas [12], converted into units of atmospheres, and modified according to the present definition of the Scottky reaction, Eqs. (7) and (7′). Table 2 gives representative values of the equilibrium constants used for the various graphs.

The defect scheme in Table 1, the nine equations with nine concentrations, and the algorithm represent a 'universal' description for all $A(III)B(III)O_3$ perovskites doped with a divalent dopant on the A-site: With properly chosen equilibrium constants, the model describes any concentration–pO_2 relationship for perovskites, whether they remain electronic insulators with or without ionic conduction, exhibits a typical p- to n-type transition [21] or remain p-type at all pO_2's, such as lanthanum chromites [32]. In a study of the defect chemistry in pyrochlore oxides $A_2B_{2-x}Mf_xO_{7\pm\delta}$ [33] we give typical regimes for four equilibrium constants leading to different types of majority carrier behaviour in pyrochlores.

The three equilibrium constants for LSM may in principle be obtained by fitting the calculated weight curve (TG) as function of pO_2 to the observed one, assuming the oxygen content is known on an absolute scale. However, the quality of present TG-data is not sufficient to allow a reliable determination of the three constants. At the same time the variation of the observed conductivity as function of pO_2 must also match the predicted one, following from the same model, cf. Section 5.6. The non-linear least squares problem consists of adjusting three equilibrium constants and three electrical mobility constants: m_{43}, $m_{23}$and μ_{ion} in Eqs. (24)–(26). It is shown in Section 5.6 that a model with concentration independent mobilities can (unfortunately) *not* describe the observed conductivity versus pO_2 behaviour (minor variations of the mobilities will do the job, cf. Fig. 10).

5.2. Presence of one, two or three oxidation states of Mn and the pO_2 stability limit

Fig. 2 shows the effect of the equilibrium constant $K_i=[Mn_B']\cdot[Mn_B^{\cdot}]/[Mn_B^x]^2$ of Eq. (9), which is controlling the charge distribution on the three oxidation states of Mn. The calculation assumes a Sr doping of $x=0.20$ and $A/B=1$. The values of K_i, relevant for LSM with 10–20% Sr at 1000°C, are in the range $2\cdot10^{-3}$ to $2\cdot10^{-2}$. Calculations of defect concentrations with realistic equilibrium constants for LSM are shown in Figs. 1, 5 and 6 and are commented on in detail in Section 5.3 and 5.4. For

Table 2
Equilibrium constants for small (SP) and large polaron (LP) model of LSM, 10% Sr doping 1000°C

Case #, model	K_s	K_r/atm $^{1/2}$	K_i	Remarks
Case 1, SP, Figs. 4 and 9	$7.57\cdot10^{24}$	$9.3\cdot10^{7}$	$1.58\cdot10^{3}$	Ref. [12]
Case 2, SP, Figs. 5, 6 and 11	$1.5\cdot10^{27}$	$2\cdot10^{8}$	$4\cdot70^{2}$	Good fit to stoichiometry
Case 3, LP, Figs. 1 and 10	10^{26}	10^{11}	10^{2}	Bad fit to conductivity
Case 4, SP, Figs. 7 and 8	$6.59\cdot10^{25}$	$2\cdot10^{5}$	$1.58\cdot10^{3}$	

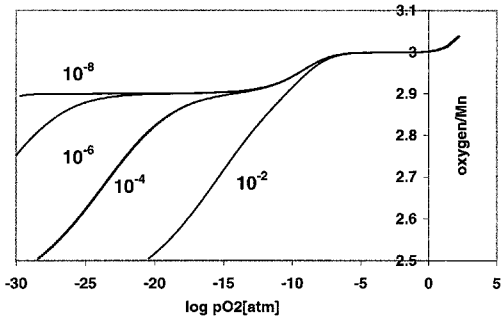

Fig. 2. Variation of O_{tot}/Mn ratio in $(La_{0.8}Sr_{0.2})_{1.00}MnO_{3+\delta}$ with pO_2 according to small polaron model. The composition is calculated at 510 different pO_2 values for each value of $K_i = [Mn'_B]\cdot[Mn^{\cdot}_B]/[Mn^{x}_B]^2$. K_i values are indicated in the graph. K_i around 10^{-3} is representative of LSM's, whereas $K_i \leq 10^{-6}$ apply to systems, where only two oxidation levels are found (+4/+3). Equilibrium constants $K_s = 2\cdot10^{-23}$ and $K_r = 2.5\cdot10^{-4}$ atm$^{1/2}$ are valid for 1000°C.

all values of K_i in Fig. 2 one observes over-stoichiometry at oxygen pressures higher than 1 atm. This behaviour is therefore determined exclusively by the values of K_s (strongest influence) and K_r (minor influence). For all values of K_i, where $K_r < 1[\text{atm}^{1/2}]$, one generally observes an extended region in pO_2, where the oxygen/Mn ratio is very close to 3.0.

Depending on the value of K_i, however, there may be a second plateau on the oxygen/Mn versus pO_2 curve at an oxygen/Mn ratio around 3−1/2(dopant level), in the present case at 2.90. The combination of the actual values of the equilibrium constants for LSM is such that this second level in the stoichiometry–(TG) curve is smeared out (invisible). The absence of a second stoichiometry plateau is therefore coincidental, and *not* indicative of any special type of defect chemistry going on in LSM.

The magnitude of K_i is the main parameter, which determines whether one, two or all three oxidation states of the B-ion are present: $K_i \approx 10^{-2}$, respectively 10^{-4}, lead to situations, where $[Mn'_B] \approx [Mn^{\cdot}_B]$ at $pO_2 = 10^{-11}$, respectively 10^{-14} atm. In both cases all three oxidation states are important. For very small values, $K_i \leq 10^{-6}$, there are hardly any divalent B-ions present. $[Mn'_B]$ exceeds 0.1 only at extremely low pO_2 (below 10^{-25} atm). For $K_i \leq 10^{-8}$ there is no divalent Mn present ever. The tetravalent B-ion is stable down to $pO_2 \approx 10^{-7}$ atm, where reduction to trivalent manganese starts. When $K_i < 10^{-11}$ and the equilibrium constant for incorporation of oxygen from the gas phase, $K_r \geq 10^{5}$ [atm$^{1/2}$], one arrives at a situation, where the B-site ion remains trivalent at all experimentally accessible pO_2's. Such a material, when A-site doped, would potentially be in the ionic regime throughout the entire pO_2 range. For materials, where the activation barrier for moving oxygen from a filled to a vacant oxygen site is 1.5 eV or lower, one should expect the material to be a reasonable good oxygen ion conductor.

Thermogravimetric studies of LSM's usually stop at $pO_2 \approx 10^{-13}$–10^{-16} atm [1–7,13,14]. LSM reduced in hydrogen is a mixture of three phases: La_2O_3, SrO, and MnO, sometimes including a less well defined ternary Sr–La oxide. The decomposition pressure increases with temperature. Other perovskites, such as $SrFeO_3$ can be reduced to the Brownmillerite composition, $Sr_2Fe_2O_5$, which at high temperature has disordered oxygen vacancies [34,35]. LSM may be structurally unstable at low pO_2 due to the fact that large concentrations of divalent Mn cannot be accommodated on the B-site in a La-perovskite. The effective ionic radii [36] for the Mn ions in octahedral coordination ($CN = 6$) are: Mn^{+2}: 0.67(LS) 0.83(HS); Mn^{+3}: 0.58(LS) 0.645(HS) Mn^{+4}: 0.53 Å (LS), where LS/HS refer to low or high spin. The ionic radii of the O^{-2}, La^{+3} and Sr^{+2} ions, the latter ones with $CN = 12$ are: $r_O = 1.40$ Å, $r_{La} = 1.36$ Å and $r_{Sr} = 1.44$ Å. Goldschmidt's [37] tolerance factor, $t = (r_A + r_O)/(\sqrt{2}(r_B + r_O))$, is plotted in Fig. 3 as a function of the average oxidation state of Mn. It is noted that t gets considerably below 1, when LSM is reduced. The concentration curves for $[Mn'_B]$ and $[Mn^{\cdot}_B]$ in Figs. 4–6 cross at $pO_2 \approx 10^{-15}$ atm, which is close to the stability limit. It is then argued that the lower pO_2 stability limit for LSM is defined by the pO_2, at which the Mn^{2+} concentration exceeds the Mn^{4+} concentration.

5.3. Defect concentrations in LSM at 1000°C

Fig. 4 shows the Brouwer diagram for a 10% Sr doped LSM, calculated for the 'ideal' case A/B = 1. The equilibrium constants were calculated from the regression expressions in Ref. [12], which correlate

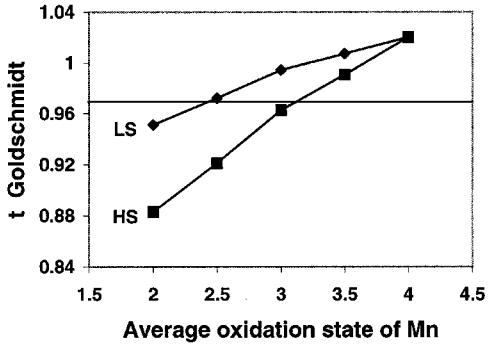

Fig. 3. Goldschmidt's tolerance factor t for hypothetical perovskites $La_{0.8}Sr_{0.2}MnO_3$ as function of the average oxidation state (and thereby different average ionic radius) of the Mn ion. Ionic radii were used for low spin (LS) and high spin (HS) states of Mn. The weighted average of the La and Sr radii was used. A full occupancy of the oxygen sites is assumed.

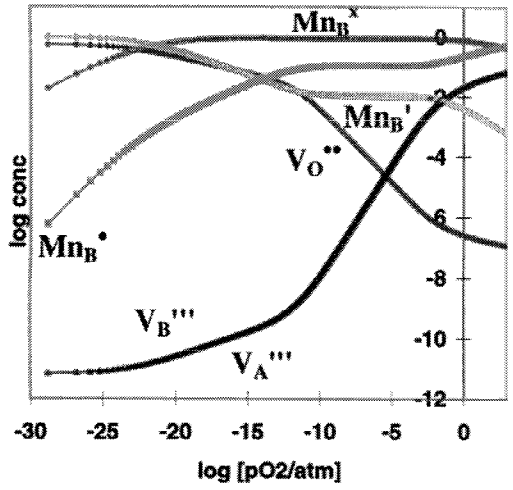

Fig. 4. Calculated Brouwer diagram for $(La_{0.9}Sr_{0.1})_{1.00}MnO_{3\pm\delta}$ at 1000°C from small polaron model. A/B-ratio=1, equilibrium constant due to Nowotny and Rekas [12], Case #1 of Table 2.

the three constants with the Sr-doping level in the range 0–20%. The relations are of the type $\log(K) = a + x_{Sr} \cdot b$ giving $K_s = 7.57 \cdot 10^{-25}$, $K_i = 1.58 \cdot 10^{-3}$ and $K_r = 9.3 \cdot 10^{-7}$ [atm]$^{1/2}$. There are no physical solutions for the set of nine concentrations at $pO_2 > 2 \cdot 10^{7}$ atm, where the $[Mn_B']$ concentration

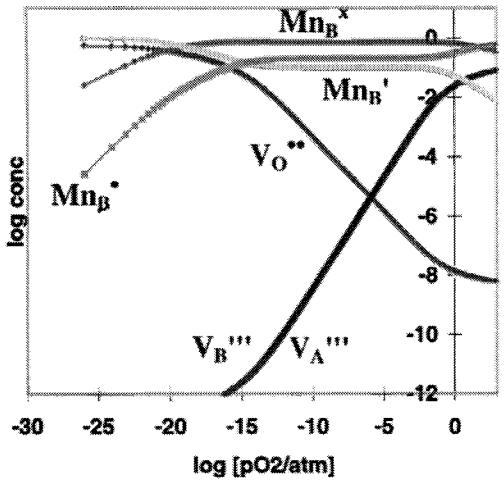

Fig. 5. Calculated Brouwer diagram for $(La_{0.9}Sr_{0.1})_{1.00}MnO_{3\pm\delta}$ at 1000°C from small polaron model. A/B-ratio=1, equilibrium constants adjusted by FWP to match known stoichiometry. Case #2 of Table 2.

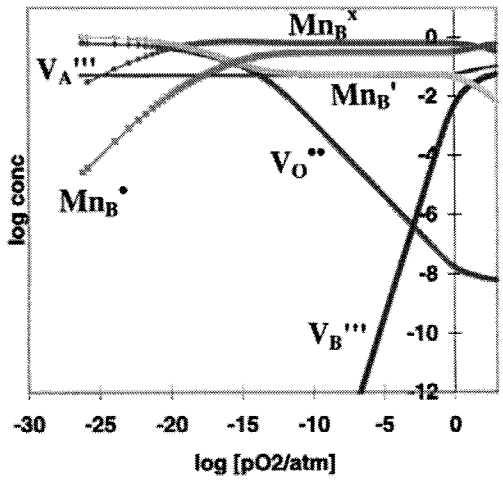

Fig. 6. Calculated Brouwer diagram for $(La_{0.9}Sr_{0.1})_{0.95}MnO_{3\pm\delta}$ at 1000°C from small polaron model. A/B-ratio=0.95, equilibrium constants as in Fig. 5.

goes negative, i.e. all manganese is in oxidation state +4 and the sample can of cause not be oxidised any further. Similarly, there is a lower limit: No physical solutions exist for $pO_2 < 10^{-26}$ atm in the small

polaron model for the above mentioned values of the equilibrium constants. Below this pO_2-limit the $[Mn_B^{\cdot}]$ concentration goes negative, at the time where all manganese has been reduced to +2 at $O_{tot}/Mn \approx 2.5$. Defect models (even very simple ones) predict via the site- and mass-balances the ultimate phase boundaries as seen above. When the model calculation further includes the mass law expressions we also get to know at what pO_2 the limit is reached.

Fig. 4 and the corresponding calculation of Nowotny and Rekas, Fig. 14 of Ref. [12], are qualitatively similar apart from the highest three decades in pO_2. The latter discrepancy is discussed below. The similarities and common conclusions of the two calculations are the following: (i) Divalent Mn is only 5.4% or less of the total Mn content, above $pO_2 \approx 10^{-12}$ atm, i.e. the chemistry of LSM can by and large be explained just by the presence of the two highest oxidation states of Mn above this pressure. This greatly facilitates the discussion; (ii) cation vacancies on the A- and B-site are of equal concentrations (trivial for A/B = 1), but become significant only above 10^{-3} atm of oxygen.

The two ways of calculation differ from each other in the high pO_2 range: (i) The concentrations curves for $[Mn_B^{x}]$ and $[Mn_B^{\cdot}]$ stay complete flat approaching 1 atm in [12] whereas a clear curvature comes out of the present (more precise) calculation; (ii) The cation vacancy concentrations at 1 atm following from Nowotny are 0.018, whereas the present method yields roughly 0.021 using the same constants; (iii) the present numerical method finds the oxygen stoichiometry, O_{tot}/Mn, at the two pO_2 extremes: $3.064 = O_{tot}/Mn$ in air, and $2.936 = O_{tot}/Mn$ at $pO_2 = 10^{-15}$ using Nowotny and Rekas constants [12]. This is to be confronted with reality, where one can read from Fig. 1, based on the measurements of [1–3] that $O_{tot}/Mn = 3.05$ in air, and 2.89 at $pO_2 = 10^{-15}$ atm. Nowotny and Rekas' calculations reproduces this satisfactorily in Fig. 2 of Ref. [12]. The discrepancy between what is found here and in [12], using the same equilibrium constants must lie in the approximations done in [12] for the under-, respectively over-stoichiometric situation, possibly amplified by the problem of where to use one and when to use the other algorithm of Table 6 of [12]. The fitted equations to the doping and temperature dependence of the equilibrium constants in [12] do have fairly large uncertainties [38].

Fig. 5 shows the Brouwer diagram, again for a 10% Sr doped LSM, A/B = 1.0 but with the equilibrium constants adjusted, such that the calculated oxygen stoichiometry at 1 and 10^{-15} atm fit better at the two pO_2 values with the experimental ones of Kuo et al. [1,2] at 1000°C. Fig. 6 shows the more realistic situation of a Mn excess LSM cathode material with A/B = 0.95 as used in an SOFC. The case $A/B \neq 1$ is further discussed in Section 5.5. Fig. 1 shows the calculated oxygen content curve and calculated conductivity versus pO_2 based on the large polaron model of Appendix A. There is no clear plateau in the predicted stoichiometry curve around $O_{tot}/Mn = 2.95$, as explained in Section 5.2. Neither the small- nor the large polaron model describe the actual curve shape at $pO_2 > 10^{-2}$ atm particularly well. A 5th order polynomial can describe the stoichiometry curve in Fig. 1 quite well. Refinement of the three equilibrium constants by non-linear least squares minimisation of Σ(observed–calculated stoichiometry)^2, did not lead to any better fit, than was obtained by a manual trial and error procedure. In addition, one observes a discrepancy between observed and calculated shapes of the conductivity curve for values of the equilibrium constants where the stoichiometry curve is fairly well reproduced. This is commented on in Section 5.6. Summarising: The two models describe the *main* features of the pO_2 dependence of the stoichiometry but not the details at high pO_2.

5.4. Change of defect concentrations in LSM-cathodes with polarisation

Many solid state electrochemists and SOFC-R&D teams have reported that LSM cathodes show an improved performance, i.e. a lower polarisation resistance during oxygen reduction over the first periods of minutes to hours until a steady state is reached [39]. At very long times, exceeding hundreds of hours, the cathode may deteriorate due to grain growth, formation of insulating phases, detachment from the solid electrolyte, or for other macroscopic reasons. Kleitz and co-workers have earlier reported that also a polarisation potential driven improvement can be observed [40,41]. Sörby et al.

[42] have similarly reported an in-situ synchrotron diffraction experiment on an LSM-cathode on YSZ (the oxygen ion conductor 8 mol % Y_2O_3 doped ZrO_2) under polarisation, where the lattice parameter shifted reversibly forth and back with the current density (0 to 200 mA/cm^2). The oxygen reduction can in principle proceed entirely at the gas/YSZ/LSM triple phase boundary, where LSM would serve entirely as a sink for electrons:

$$1/2O_2(\text{gas}) + V_O^{\cdot\cdot}(\text{YSZ}) + 2e'(\text{LSM}) \Rightarrow O_O^x(\text{YSZ}) \quad (18)$$

Alternatively the reduction can proceed on the surface of LSM, with a subsequent diffusion of the formed lattice O_O^x through the LSM lattice to the LSM/YSZ interface (and further on to the anode side of the fuel cell, where the final combination with hydrogen/protons yields water):

$$1/2O_2(\text{gas}) + V_O^{\cdot\cdot}(\text{LSM}) + 2e'(\text{LSM}) \Rightarrow O_O^x(\text{LSM}) \Rightarrow O_O^x(\text{YSZ}) \quad (19)$$

The two processes may operate in parallel, as analysed in detail by Svensson et al. [43,44]. In the present context it does not matter, whether reaction path (19) is operating on its own or in combination with Eq. (18) at a given overpotential, temperature and external oxygen pressure. The higher the current density, the lower will be the local oxygen partial pressure in the inner parts of the LSM cathode near the YSZ interface. A lowering of the pO_2 will increase the concentration of $V_O^{\cdot\cdot}$ in LSM, thereby promoting the oxygen reaction until a steady state is reached. The calculations shown in Figs. 4–6 can be used to put numbers on the increase in $V_O^{\cdot\cdot}$(LSM) upon polarisation. The oxygen vacancy concentration in un-polarised LSM in air at 1000°C is around $1.93\cdot10^{-8}$ for A/B=1 and $3.06\cdot10^{-8}$ for A/B=0.95. When polarised cathodically by 63 mV, corresponding to $pO_2=0.021$ atm (Nernst law) the vacancy concentration increases to the higher values of $4.06\cdot10^{-8}$ (A/B=1) and $9.2\cdot10^{-8}$ (A/B=0.95). The oxygen vacancy concentration increases by a factor of 2–3 upon polarisation, supporting the idea that the increased cathode performance with polarisation is linked to this phenomenon. It is on the other hand not surprising that the oxygen ionic conductivity and the diffusion coefficient for oxygen are very low, considering the very low concentration of vacant oxygen sites in LSM around ambient oxygen pressures.

5.5. Variation of properties with A/B-site population ratio

The *state of the art* SOFC cathodes are made with an excess of manganese in order to suppress formation of poorly conducting Sr- and La-zirconates via reaction with YSZ. The influence of deviations of the A/B ratio from unity was analysed at 1000°C for the case of 10% Sr-doping. Figs. 7 and 8 show the

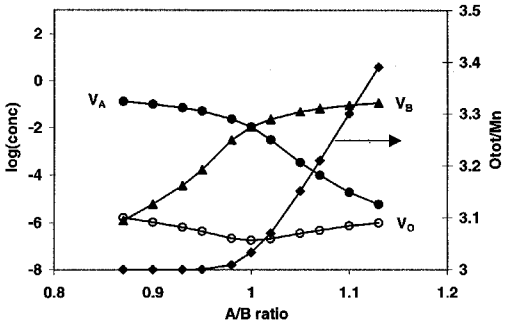

Fig. 7. Variation of cation vacancy concentrations and oxygen stoichiometry as function of the A/B-ratio for a 10% Sr doped LSM. Small polaron model. Equilibrium constants as case #4 in Table 2.

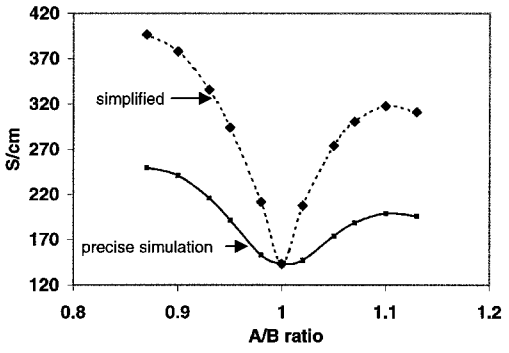

Fig. 8. Variation of total conductivity of 10% Sr doped LSM, small polaron model. Same equilibrium constants as in Fig. 7. The conductivity, predicted from Eqs. (20) and (21), based on simplifications, are shown for comparison.

variation of the calculated conductivity, cation vacancy- and oxygen vacancy concentration at $pO_2 = 0.21$ atm. Calculation of conductivity is treated in 5.6. Note that the variation of the oxygen vacancy concentration with A/B-ratio is hardly predictable by intuition. The variation of conductivity with the A/B ratio is shown on a linear axis in Fig. 8. It is easy to rationalise the trend qualitatively: Deficiency of either A- or B ions has the same effect as aliovalent doping with a hypothetical ion with zero absolute charge/valence on the respective site. The conductivity thus has a minimum at A/B = 1. The higher the A/B ratio is however, the fewer manganese sites/cm^3 there will be in the solid. We, therefore, predict a pronounced damping of the conductivity increase for A/B > 1.05.

It is illustrative at this point to show how much a solution obtained by approximation deviates from the accurate calculation. For the two cases, A/B < 1, respectively A/B > 1, we will for a while neglect the presence of cation vacancies on the 'opposite' cation lattice and only consider presence of the two highest oxidation states of manganese. For A/B < 1 we arrive at the approximate composition $[La_{1-x}Sr'_x]_y[V'''_A]_{(1-y)}[Mn^x_{(1-c)}Mn^{\cdot}_c]O_3$. This is solved for c using the electroneutrality condition leading to

$$\sigma = m_{34} \cdot [Mn^x] \cdot [Mn^{\cdot}] = m_{34} \cdot (3y - x \cdot y - 2) \cdot (x \cdot y + 3 - 3y) \quad (20)$$

For A/B > 1 the approximated composition is $[La_{1-x}Sr'_x]\ [Mn^x_{(1-c)}Mn^{\cdot}_c]_{1/y}[V'''_B]_{(1-1/y)}]O_3$ leading to

$$\sigma = m_{34} \cdot [Mn^x] \cdot [Mn^{\cdot}] = m_{34} \cdot (x \cdot y - 3 + 3y)/y \cdot (4 - x \cdot y - 3y)/y \quad (21)$$

Fig. 8 shows the respective branches of these two functions plotted together with the 'real' solution found by the algorithm. It is noticed that the approximations lying behind Eqs. (20) and (21) lead to exaggerations of the predicted conductivity – the chemical system is in reality much more buffered with respect to deviations of the A/B ratio from unity.

5.6. Predicting the electronic and ionic conduction in LSM

LSM exhibits electrical conductivity in the range from 1 to 250 S/cm going from room temperature to 1000°C. The conductivity increases with the amount of Sr-doping up to $x = 0.5$. The apparent activation energy for conduction, as derived from the slope of Arrhenius plots, is only a few tenth of an eV, and even apparent negative activation energies are observed at high temperature and high Sr-doping [1–7,13,14]. Specific conductivities well in excess of 5 S/cm can only be due to transport of electronic carriers. A very small fraction of the current may be carried by oxygen ions, which are able to move from occupied sites, O^x_O, to vacant ones, i.e. the higher the $[V^{\cdot\cdot}_O]$ concentration is, the higher the ionic conductivity we expect. Endo et al. have determined the oxygen ion conductivity in LSM in the pressure range 10^{-1}–10^{-3} atm oxygen at 800°C to be $5.9 \cdot 10^{-8}$ S/cm by the Hebb–Wagner technique [45], leading to an ionic transport number below $6 \cdot 10^{-10}$.

We believe that we can sum up the individual contributions from ionic and electronic carriers to find the total conductivity. For a model description of LSM based on electrons and electron holes, as given in the Appendix, the summation (Eq. (A.12)) contains three terms. Each term is a product of the numerical value of the charge of the carrier, the relative concentration of the carrier and a kind of mobility, μ, for that carrier. The chemical/small polaron model does *not* contain any free and mobile electrons nor are there any electron holes. The multi valent cations have a too high charge density to be able to jump through the lattice and thereby contribute to the measured conductivity. Cation diffusion/migration may occur over periods of hours/days in samples, which contain reasonable amounts of cation vacancies (over-stoichiometric samples or samples, where the A/B ratio $\neq 1$). Electrons must anyhow supply the conductivity, although they are not specifically mentioned in the model. A donor ion may deliver an electron, which is then received by an acceptor ion. The electron transport (polaron conduction) in LSM can be formulated as a charge transfer

reaction (hopping), where an electron is transferred from a manganese ion, in one oxidation state, to a neighbour manganese in a higher/lower oxidation state, possibly via an oxygen ion:

$$\underset{\text{site 1}}{Mn_B^{\cdot}} + \underset{\text{site 2}}{Mn_B^{x}} \overset{O_O^x}{\Leftrightarrow} \underset{\text{site 1}}{Mn_B^{x}} + \underset{\text{site 2}}{Mn_B^{\cdot}} \quad (22)$$

$$\underset{\text{site 3}}{Mn_B^{\prime}} + \underset{\text{site 4}}{Mn_B^{x}} \overset{O_O^x}{\Leftrightarrow} \underset{\text{site 3}}{Mn_B^{x}} + \underset{\text{site 4}}{Mn_B^{\prime}} \quad (23)$$

In Eqs. (22) and (23) one electronic charge has passed from site 2 to site 1, respectively from site 3 to site 4, reading from left to right. Neighbouring manganese ions are approximately 3.8–4 Å apart, which is a too large distance to travel in one jump. Orbitals of oxygen and manganese overlap, since the structure is not truly ionic. What is depicted in Eqs. (22) and (23) is nowadays described as a 'double exchange mechanism' [46].

Transfer of two electrons simultaneously (e.g. as a Cooper pair) at high temperature is very unlikely, if not forbidden. In order to find the conductivity contribution from electron transfers, such as in Eqs. (22) and (23), one applies rate theory, which tells us that the probabilities for the respective reactions to occur are proportional to the product of the concentrations of the reactants:

$$\sigma_{43} = m_{43} \cdot [Mn_B^{\cdot}] \cdot [Mn_B^{x}] \quad (24)$$

$$\sigma_{23} = m_{23} \cdot [Mn_B^{\prime}] \cdot [Mn_B^{x}] \quad (25)$$

Here the subscripts signify transfer from tetra- to trivalent Mn, respectively from divalent to trivalent manganese (and vice versa). The proportionality constants, m_{43} and m_{23} [and m_{ion} in Eq. (26)], are specific conductivities normalised to relative concentrations, i.e. they contain the mobility, a conversion factor from relative concentrations to particles/cm^3 and the elementary charge.

The oxygen ionic contribution to conductivity is found by the same argument as above, i.e. the probability for an oxide to jump is proportional to the product of concentrations of vacant and occupied oxygen sites:

$$\sigma_{ion} = m_{ion}|-2| \cdot [V_O^{\cdot\cdot}] \cdot (3 - [V_O^{\cdot\cdot}]) \quad (26)$$

The charge transferred per oxide ion hop is -2, as written inside the numeric sign in Eq. (26). The total calculated conductivity is the sum of the three types of contributions:

$$\sigma_{tot} = \sigma_{43} + \sigma_{23} + \sigma_{ion} \quad (27)$$

The ionic contribution will be a monotonically increasing function of $[V_O^{\cdot\cdot}]$ in the stoichiometry range down to oxygen/Mn$\geq$2.5. The electronic contributions, on the other hand, may pass through maxima at certain pO_2's, where the concentration products in Eqs. (24) and (25) have a maximum. Porat et al. [47] have indeed observed a maximum in the electronic conductivity in the temperature range 600–1000°C in a 2% manganese doped pyrochlore structure $Gd_2Ti_2O_7$. This finding was interpreted in terms of the product of Mn(+3)×Mn(+4) having a maximum value in the pO_2 range 10^{-12}–10^{-8} atm. Fig. 9 shows the calculated stoichiometry and conductivity of 10% Sr doped LSM. The contributions from charge transport via Eqs. (22) and (23) are set equal in this calculation by equating $m_{43} = m_{23} = 1000$. The conductivity at high pO_2 has only a weak pO_2 dependence – the product $[Mn_B^{\cdot}] \cdot [Mn_B^{x}]$ is

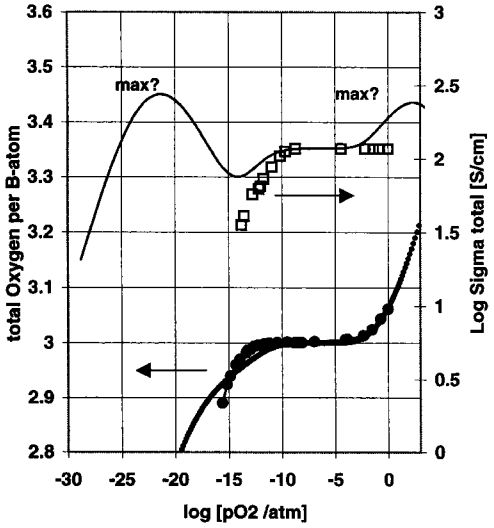

Fig. 9. Predicted maxima and minima in conductivity outside stability limits of LSM predicted from small polaron model. The maxima follow from Eqs. (24) and (25). Case #1 of Table 2.

virtually constant; at 10^{-10} atm the conductivity decreases with an approximate slope $=\partial\log\sigma/\partial\log(pO_2)\approx 0.14$. This is in accordance with the experiments [1,2].The *calculated* conductivity continues through a minimum and increases again until a maximum is predicted at a pO_2 of 10^{-22} atm. The minimum is below and the following maximum far below the stability limit of LSM, and are thus not experimentally accessible. It is clear from Figs. 4–6 that the product $[Mn_B^{\cdot}]\cdot[Mn_B^{x}]$ never passes through a maximum below $pO_2\approx 10^{-17}$ atm, which however would be the case for the product $[Mn_B^{\prime}]\cdot[Mn_B^{x}]$, *had* LSM been stable in this pO_2 interval. A maximum in conductivity at high pO_2 has not yet been reported. More measurements at oxygen pressures above 1 atm are required to test the theory. If the electronic conductivity at high pO_2 is described as p-type (Appendix A) the increase in conductivity is proportional with $p=[h^{\cdot}]$, which predicts a slightly steeper increase than for a conductivity scaling with the product $[Mn_B^{\cdot}]\cdot[Mn_B^{x}]$.

Figs. 1 and 10 show the observed and predicted conductivity based on the large polaron model. It is seen that the predicted conductivity is higher than the observed one both at high and low pO_2. The predicted conductivity can be tuned to follow the experimental one by gradually lowering the mobility somewhat in the two pressure extremes. The normalised mobility, represented in Fig. 10, needs only to be lowered by 50% at low pO_2 and by 33% at high

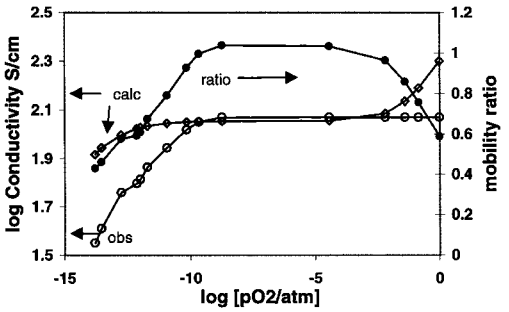

Fig. 10. Observed and calculated conductivity from the large polaron model and their ratio in terms of a relative mobility. The calculated conductivities have been normalised, in a way that they become equal to the observed one in the pO_2 range from 10^{-5} to 10^{-2} atm. Case #4 of Table 2.

pressure to account for the observed conductivity dependence. It is finally puzzling that the bell shaped curve of the mobility versus log pO_2 has a maximum, where also the calculated thermodynamic enhancement factor:

$$W=\partial\log(\text{activity})/\partial\log(\text{concentration}) \propto\partial\log(pO_2)/\partial\log[O_O^{x}] \quad (28)$$

will have a maximum. One can only speculate on a possible interpretation of this incidence.

5.7. Variation of stoichiometry with Sr-doping

There is extended solid solution formation between the two end members in the pseudo-binary system $LaMnO_3$–$SrMnO_3$. The ability to form overstoichiometric phases appears to decrease going from lanthanum towards strontium. Fully stoichiometric $SrMnO_3$ is stable in air only up to 1035°C, above which temperature substoichiometric $SrMnO_{3-\delta}$ is formed [48]. δ approaches 0.5 at 1800°C. Heating at 1000°C under 70 atm of oxygen pressure did not change the diffraction pattern, indicating likewise the unwillingness of $SrMnO_3$ to go overstoichiometric [48]. Krogh Andersen et al. [27] annealed a series of LSM's with $0\leq x\leq 0.5$ at 1100°C in air and nitrogen, and the samples were given the opportunity to take up further oxygen during a slow cooling of samples in the furnace. Fig. 11 shows their oxygen content determinations as function of Sr-doping level. It is seen that the ability to form overstoichiometric LSM's in air disappears at $x>0.27$–0.3. The nitrogen annealed LSM's were all stoichiometric, irrespective the Sr-level [27]. In stoichiometric $La_{0.7}Sr_{0.3}MnO_3$ the average oxidation state of manganese is +3.3, which apparently is the higher limit in the La-rich end of the system. Calculation of the stoichiometry at 1, 0.21 and 10^{-4} atm using the equilibrium constants, case #3 in Table 2, are shown for comparison in Fig. 11. The defect model clearly predicts the observed levelling off of the overstoichiometry with increasing Sr-doping.

6. Conclusions and outlook

When the defect equations for a given perovskite defect model, including a Schottky reaction, are

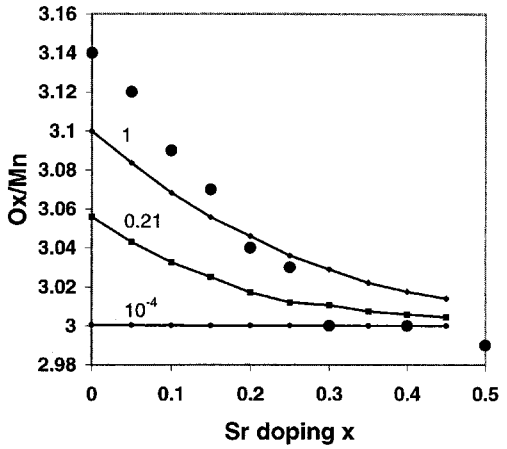

Fig. 11. Calculated stoichiometry of LSM's at 1000°C as function of Sr-doping at three oxygen pressures [atm]. A/B=1, equilibrium constants as in case #3. Key: Full curves are calculated, full spheres are stoichiometry of LSM's slowly cooled in air from 1100°C (Krogh Andersen et al. [27]).

combined by substitution and subsequent factorisation, one obtains polynomials of the 12th degree or higher. Searching for analytical expressions does not pay off at this level of complexity. The present mathematical approach offers a sequential solution of the defect equations, with the minor drawback that the defect concentrations are calculated at pO_2's, which are not coinciding with a set of experimental pO_2's.

Neither the small (chemical), nor the large polaron model for LSM can simultaneously account for the observed oxygen stoichiometry and conductivity variations, maintaining the mobilities to be concentration independent. The two models were both found equally applicable in describing the main features of the pO_2 dependence of LSM's stoichiometry.

Defect modelling of pyrochlore structure oxides [33] and oxygen separation materials of the type $Sr_4Fe_{6-x}Co_xO_{13\pm\delta}$ are under way, using the same sequential technique. The inclusion of association of defects will be demonstrated in a forthcoming paper on doped ceria. Also, a general algorithm was developed early 1999 for a perovskite system, with dopants on both the A- and B-site. One dopant is assumed to be redox stable, the other dopant is allowed to have two possible redox states (in addition to the overall n- and p-type pO_2 dependent properties of the host lattice).

The mathematical approach, which was demonstrated in the present paper, has both pedagogical and scientific value. The former because the algorithm, coded into a spread sheet, gives instant visualisation of the impact of doping, change in A/B-ratio and magnitude of the equilibrium constants. The latter, since this method does not rely on approximations of the electroneutrality condition, as traditionally employed (by need) in construction of Brouwer diagrams. Furthermore it is a useful tool to predict the properties of perovskites outside their stability limits. Spread sheet versions (Excel) of the above mentioned algorithms are available from the author by e-mail.

Acknowledgements

This study was in part made possible through a research grant to FWP by 'Nordisk Energiforskningsprogram for brændselsceller' (Fuel Cell programme, 1991–1998, under The Nordic Energy Research Programme) and via FWP's engagement under the Danish fuel cell programme DK-SOFC. The author further thanks Dr. Nicholaos Bonanos, Dr. Mogens Mogensen and Dr. Eivind Skou for valuable discussions and proof reading. Prof. J. Nowotny, University of New South Wales, Australia is thanked for clarifying several aspects relating to his pioneering LSM-modelling. Finally, the author remembers many joyful and instructive discussions with late professor Per Kofstad, without whom my understanding of defect chemistry of oxides would still have been embryonic.

Appendix A. Hole/electron description of LSM

Table A.1 describes the model. The concentration of holes [$h^{\cdot}$] is denoted p, and the concentration of electrons [e'] is given by n in the nine equations following from this model:

Principle of electroneutrality:

Table A.1
'Large polaron' defect description of an A-site acceptor doped perovskite $[A(III)_{1-x}Mf(II)_x]_1B(III)O_{3\pm\delta}$ with delocalised electrons and electron holes

A-site	B-site	O-site	Delocalized
La_A^x	Mn_B^x	O_O^x	$h^{\cdot}$
V_A'''	V_B'''	$V_O^{\cdot\cdot}$	e'
Sr_A'	–	–	–

$$2[V_O^{\cdot\cdot}] + p = n + [Sr'] + 3[V_A'''] + 3[V_B'''] \quad (A.1)$$

A-site balance:

$$[La_A^x] + [Sr_A'] + [V_A'''] = 1; \quad (A.2)$$

B-site balance:

$$[Mn_B^x] + [V_B'''] = 1 \quad (A.3)$$

O-site and mass balances:

$$[O_O^x] + [V_O^{\cdot\cdot}] = 3; \quad (A.4)$$

$$[La_A^x]/[Sr_A'] = (1-x)/x; \quad (A.5)$$

$$[Mn_B^x]/\{[La_A^x] + [Sr_A']\} = 1/y \quad (A.6)$$

Schottky-reaction for vacancy formation:

$$K_s = [V_O^{\cdot\cdot}]^3 \cdot [V_A'''] \cdot [V_B'''] \quad (A.7)$$

Redox reaction with oxygen: $O_O^x \Leftrightarrow 2e' + V_O^{\cdot\cdot} + 1/2O_2$ leading to

$$K_r = n^2 \cdot [V_O^{\cdot\cdot}] \cdot pO_2^{1/2}/[O_O^x] \quad (A.8)$$

The balance (creation/annihilation) between holes and electrons is given by the reaction:

$$nil \Leftrightarrow e' + h^{\cdot}, \text{ leading to the mass action law } K_i = n \cdot p \quad (A.9)$$

Note that there is in the present model no built-in mathematical restrictions on how large the n and p concentrations can be. This is in contrast to the limits put on the concentrations of reduced and oxidized manganese in the small polaron/chemical model: $[Mn_B']$ and $[Mn_B^{\cdot}]$ must be below 1 in relative concentration units due to the site conservation condition Eq. (3).

The algorithm for calculating all concentrations proceeds as follows: By manipulation with Eqs. (A.1)–(A.7) one can express the various defect concentration by the oxygen vacancy concentration:

$$[O_O^x] = 3 - [V_O^{\cdot\cdot}] \quad (A.5')$$

$$[V_A'''] \cdot (y-1) - y \cdot K_s/[V_O^{\cdot\cdot}]^3 = 0 \quad (A.6')$$

$$[V_B'''] = 1 - 1/y + [V_A'''] \quad (A.10)$$

One guesses a value of $[V_O^{\cdot\cdot}]$ in the interval 0.5–10^{-20} and calculates the concentrations in Eqs. (A.5'), (A.6') and (A.10). The electroneutrality equation combined with Eq. (A.9) gives a quadratic equation in n:

$$n^2 + n \cdot \{x(1-[V_A''']) + 3[V_B'''] + 3[V_A'''] - 2[V_O^{\cdot\cdot}]\} - K_i = 0 \quad (A.11)$$

$$p = K_i/n \quad (A.9')$$

The equilibrium oxygen pressure is finally calculated from Eq. (A.8). The solutions for $[La_A^x]$, $[Sr_A']$ and $[Mn_B^x]$ are trivial, and found from Eqs. (A.2), (A.3) and (A.5). It is seen that the algorithm following from a description based on n and p, instead of three individual oxidation's states of the B-ion (chemical model in bulk of paper), is simpler/shorter from a mathematical point of view. The chemical model and the electron model in principle predict different stoichiometry versus pO_2 relationships. The difference resides in the different mathematical relationships in Eq. (9) respectively Eq. (A.9), combined with the fact that $[Mn_B^x]$ in chemical model is *not* independent on pO_2. However from an experimental/curve-fitting point of view the two models may in practice be indistinguishable.

The calculated total conductivity is the sum

$$\sigma_{tot} = |-1| \cdot n \cdot \mu_n + |1| \cdot p \cdot \mu_p + |-2| \cdot [V_O^{\cdot\cdot}] \cdot (3 - [V_O^{\cdot\cdot}]) \cdot \mu_{ion} \quad (A.12)$$

Appendix B. Analytical solution for undoped $LaMnO_{3\pm\delta}$

The exact analytical expression to be solved for the delocalised electron model of Appendix A for undoped $LaMnO_{3\pm\delta}$, was obtained by proper substitution into the electroneutrality equation [Eq. (A.1)]

$$2[V_O^{\cdot\cdot}] + K_i K_r^{1/2} pO_2^{1/4} \{[V_O^{\cdot\cdot}]/(3 - [V_O^{\cdot\cdot}])\}^{1/2} = \{(3 - [V_O^{\cdot\cdot}])/[V_O^{\cdot\cdot}]\}^{1/2} K_r^{-1/2} pO_2^{-1/4} + 6\{K_s [V_O^{\cdot\cdot}]^{-3}\}^{1/2} \quad \text{(B.1)}$$

This equation was derived under the simplifying restriction that La/Mn=1.0, i.e. $[V_B'''] \equiv [V_A''']$. A close inspection of Eq. (B.1) reveals that it is a polynomial in $[V_O^{\cdot\cdot}]$ of the 12th order. The polynomial describing the general situation allowing the A/B-ratio to deviate from unity will at least be 15th order in the unknown concentration $[V_O^{\cdot\cdot}]$!

References

[1] J.H. Kuo, H.U. Anderson, D.M. Sparlin, J. Solid State Chem. 83 (1989) 52.
[2] R. Koc, H.U. Anderson, S.A. Howard, D.M. Sparlin, in: S.C. Singhal (Ed.), Proc. First Int. Symp. on Solid Oxide Fuel Cells, Vol. PV 89-1, Electrochem. Soc, NJ, 1989, p. 220.
[3] J.H. Kuo, H.U. Anderson, D.M. Sparlin, J. Solid State Chem. 87 (1990) 55.
[4] J.A.M. van Roosmalen, E.H.P. Cordfunke, J. Solid State Chem. 93 (1991) 212.
[5] J.A.M. van Roosmalen, E.H.P. Cordfunke, R.B. Helmholdt, H.W. Zandbergen, J. Solid State Chem. 110 (1994) 100.
[6] J.A.M. van Roosmalen, E.H.P. Cordfunke, J. Solid State Chem. 110 (1994) 109.
[7] J.A.M. van Roosmalen, E.H.P. Cordfunke, J. Solid State Chem. 110 (1994) 113.
[8] P. Kofstad, A. Petrov, in: F.W. Poulsen et al. (Ed.), Proc. 14th Risø Symposium on High Temperature Electrochemical Behaviour of Fast Ion and Mixed Conductors, Roskilde, Denmark, 1993, p. 287.
[9] A.N. Petrov, V.I. Voronin, T. Norby, P. Kofstad†, J. Solid State Chem. 143 (1999) 52.
[10] O.F. Kononchuk, T. Norby, P. Kofstad, Phase Transitions 58 (1996) 145.
[11] A.N. Petrov, O.F. Kononchuk, A.V. Andreev, V.A. Cherepanov, P. Kofstad, Solid State Ionics 80 (1995) 189.
[12] J. Nowotny, M. Rekas, J. Am. Ceram. Soc. 81 (1998) 67.
[13] K. Kamata, T. Nakajima, T. Hayashi, T. Nakamura, Mat. Res. Bull. 13 (1978) 49.
[14] H. Kamata, Y. Yonemura, J. Mizusaki, H. Tagawa, K. Naraya, T. Sasamoto, J. Phys. Chem. Solids 56 (1995) 943.
[15] M.J.L. Østergaard, C. Clausen, C. Bagger, M. Mogensen, Electrochim. Acta 40 (1995) 1971.
[16] F.W. Poulsen, N. van der Puil, Solid State Ionics 53–56 (1992) 777.
[17] G. Stochniol, E. Syskakis, A. Naoumidis, J. Amer. Ceram. Soc. 78 (1995) 929.
[18] B. Zachau-Christiansen, T. Jacobsen, S. Skaarup, SOFC-V. in: U. Stimming, S.C. Singhal, H. Tagawa, W. Lehnert (Eds.), The Electrochemical Soc. Proc. Vol. 97-40 (1996) 795.
[19] A.S. Alexandrov, A.M. Bratkovsky, J. Phys.-Conden. Mat. 11 (1999) 1989.
[20] F.W. Poulsen, in: F.W. Poulsen, E. Ahlgren, A. Holt (Eds.), Proc. of the Nordic Workshop on High Temperature Electrode Materials, Oct 26–27, Roskilde, Denmark, 1992, p. 6.
[21] A. Holt, E.O. Ahlgren, F.W. Poulsen, in: S.C. Singhal, H. Iwahara (Eds.), Proc. 3rd Int. Symp. Solid Oxide Fuel Cells, Honolulu, USA, May 16–21, Vol. 93–4, 1993, p. 562.
[22] F.W. Poulsen, in: T.A. Ramanarayanan (Ed.), Proc. of Third Int. Symp.on Ionic and mixed Conducting Ceramics. Paris, August 31–September 5, 1997, Vol. 97–24, 1998, p. 448, (Figures were left out by a mistake in the printing process).
[23] F.W. Poulsen, J. Solid State Chem. 143 (1999) 115.
[24] G. Spinolo, U. Anselmi-Tamburini, Ber. Bunsenges. Phys. Chem. 99 (1995) 87.
[25] G. Spinolo, U. Anselmi-Tamburini, P. Ghigna, Z. für Naturforschung A 52 (1997) 629.
[26] B.C. Tofield, W.R. Scott, J. Solid State Chem. 10 (1974) 183.
[27] I.G. Krogh Andersen, E. Krogh Andersen, P. Norby, E. Skou, J. Solid State Chem 113 (1994) 320.
[28] F.A. Kröger, H.J. Vink, in: F. Seitz, D. Turnball (Eds.), Solid State Physics, 1956, p. 307.
[29] B.A. van Hassel et al., Solid State Ionics 66 (1993) 295.
[30] N.H. Abel, in: B. Holmboe (Ed.), Oeuvres Completes, Cristiania, Oslo, Norway, 1839.
[31] N. Bonanos, F.W. Poulsen, J. Mater. Chem. 9 (1999) 431.
[32] J.D. Carter, M.M. Nasrallah, H.U. Anderson, J. Mat. Sci. 31 (1996) 157.
[33] F.W. Poulsen, M. Glerup, P. Holtappels, Solid State Ionics, Proceedings of SSI 12, 2000 (accepted).
[34] Y. Takeda, K. Kanno, T. Takada, O. Yamamoto, T. Takano, N. Nakayama, Y. Bando, J. Solid State Chem. 63 (1986) 237.
[35] F.W. Poulsen, G. Lauvstad, R. Tunold, Solid State Ionics 72 (1994) 47.
[36] R.D. Shannon, Acta Crystallogr. A32 (1976) 751.
[37] Goldschmidt, V.M., Det Norske Videnskaps-Akademi, I. Matem.-Naturvid. Klasse (1926). No2.
[38] Nowotny, J., personal communication (1999)
[39] Y. Jiang, S. Wang, Y. Zhang, J. Yan, W. Li, J. Electrochem. Soc. 145 (1998) 373.
[40] A. Hammouche, E. Siebert, M. Kleitz, A. Hammou, in: S.C. Singhal (Ed.), Proc. First Int. Symp. on SOFC, The Electrochem. Soc, Pennington, NJ, 1989, p. 265.
[41] E. Siebert, A. Hammouche, M. Kleitz, Electrochim. Acta 40 (1995) 1741.

[42] L. Sörby, F.W. Poulsen, H.F. Poulsen, S. Garbe, J. Thomas, in: Proc. of EPDIC V, Parma 1997, Materials Science Forum, Vol. 278–281, 1998, p. 408.
[43] A.M. Svensson, S. Sunde, K. Nisancioglu, J. Electrochem. Soc. 144 (1997) 2719.
[44] A.M. Svensson, S. Sunde, K. Nisancioglu, J. Electrochem. Soc. 145 (1998) 1390.
[45] A. Endo, M. Ihara, H. Komiyama, K. Yamada, Solid State Ionics 86–88 (1996) 1191.
[46] J.S. Zhou, J.B. Goodenough, Phys. Rev. Lett. 80 (1998) 2665.
[47] O. Porat, M.A. Spears, C. Heremans, I. Kosacki, H.L. Tuller, Solid State Ionics 86–88 (1996) 285.
[48] T. Negas, R.S. Roth, J. Solid State Chem. 1 (1970) 409.

A6.

Shanwen Tao, Finn Willy Poulsen, Guangyao Meng and Ole Toft Sørensen,
High-temperature stability of the oxygen-ion conductor $La_{0.9}Sr_{0.1}Ga_{0.8}Mg_{0.2}O_{3-x}$
J. Materials Chemistry, **10**, 1-6. (2000)

JOURNAL OF Materials CHEMISTRY

High-temperature stability study of the oxygen-ion conductor $La_{0.9}Sr_{0.1}Ga_{0.8}Mg_{0.2}O_{3-x}$

Shanwen Tao,*†[a,b] Finn Willy Poulsen,[b] Guangyao Meng[a] and Ole Toft Sørensen[b]

[a]*Department of Materials Science and Engineering, University of Science and Technology of China, Hefei, Anhui, 230026, China*
[b]*Materials Research Department, Riso National Laboratory, DK-4000 Roskilde, Denmark*

Received 9th May 2000, Accepted 30th May 2000
Published on the Web 13th July 2000

$La_{0.9}Sr_{0.1}Ga_{0.8}Mg_{0.2}O_{3-x}$ (LSGM) has been prepared by a complexing sol–gel process and characterised by X-ray diffraction, thermogravimetric-differential thermal analysis (TG-DTA) and conventional weight analysis. The room-temperature structure is orthorhombic, space group *Pnma*, with $a=5.5340(14)$, $b=5.5074(22)$, $c=7.8003(31)$ Å. After heating at 1000 °C, the lattice parameters of LSGM shift a little, and La_4SrO_7 and $SrLaGaO_4$ separate from the parent phase, which may further affect other properties. The weight change of LSGM at 750 °C is insignificant and the phase is also stable after heating at 750 °C in a hydrogen atmosphere for a total of 132 h. Defect chemistry modelling supports the view that LSGM is not single phase at 1000 °C.

1 Introduction

Because of their high oxygen-ion conductivity, $LaGaO_3$-based perovskites substituted on the A and B sites, such as $La_{0.9}Sr_{0.1}Ga_{0.8}Mg_{0.2}O_{3-x}$ (LSGM), are considered to be promising alternatives to replace yttria-stabilized zirconia (YSZ) currently used in solid oxide fuel cells (SOFCs).[1–7] The mechanical properties[8] and creep behavior[9] of Sr- and Mg-substituted $LaGaO_3$ have also been reported. But as an applicable electrolyte for fuel cells, it must fulfil many other requirements, such as thermal and chemical stability, mechanical strength, density, thermal and chemical compatibility with the electrode and interconnector materials, with thermal and chemical stability the primary consideration.[10] It is supposed that Sr- and Mg-substituted $LaGaO_3$ is chemically stable over a broad range of oxygen partial pressures because the electrical conductivity remains almost unchanged in the P_{O_2} range between 10^{-23} and 1 atm at 850[1] and 800 °C.[5] However, these measurements can only indirectly demonstrate the possible stability of the materials. Thermal analysis and X-ray diffraction (XRD) phase analysis are more direct methods to study the thermal and chemical stability at high temperatures.

Generally, $La_{0.9}Sr_{0.1}Ga_{0.8}Mg_{0.2}O_{3-x}$ might be expected not to react readily with the strong oxidizing agent O_2 and the strong reducing agent H_2. However, several perovskite oxides react with CO_2 and H_2O.[11,12] It is possible that doped $LaGaO_3$ might react with CO_2 or H_2O, which usually exist under the operating conditions of SOFCs fuelled with H_2, CO or CH_4. There is also a possibility that secondary phases may separate from the doped $LaGaO_3$ when kept at high temperature for a long time. Furthermore, Djurado and Labeau[13] recently reported that secondary phases formed when sintering the material for longer than 6 h at 1500 °C. The amount of secondary phases formed in a reducing atmosphere was much larger than in an oxidizing atmosphere. This observation causes some doubt as to the long-term stability of LSGM.[13] Recently, Yamaji *et al.*[14] reported the instability of $La_{0.9}Sr_{0.1}Ga_{0.8}Mg_{0.2.85}$ at 1000 °C in a humidified reducing atmosphere because of the sublimation of gallium components such as Ga_2O and formation of $La(OH)_3$. In the present paper, we attempt to determine the thermal and chemical stability of $La_{0.9}Sr_{0.1}Ga_{0.8}Mg_{0.2}O_{3-x}$ at high temperature by thermal and weight analyses as well as room temperature X-ray diffraction phase analyses of heat-treated materials. The data obtained from conventional weight analyses were also analysed by a defect model given by Poulsen and Bonanos.[15,16]

2 Experimental

The powder of composition $La_{0.9}Sr_{0.1}Ga_{0.8}Mg_{0.2}O_{3-x}$ was prepared by using the same complexing sol–gel process which has been described elsewhere.[17] Calculated amounts of La_2O_3 and Ga_2O_3 were first dissolved in dilute HNO_3 to get a solution. Appropriate amounts of $Sr(NO_3)_2$ and $Mg(NO_3)_2{\cdot}6H_2O$ were then added and dissolved in the solution according to the formula $La_{0.9}Sr_{0.1}Ga_{0.8}Mg_{0.2}O_3$. This solution was carefully dried at 80 °C to remove the excess HNO_3 and water solvent. An appropriate amount of ethylene glycol was then added to the mixed nitrates and refluxed at 80 °C for 12 h to form a sol. A gel was formed after heating the sol at 120 °C. After pre-firing the gel on an electrical heating plate and calcining above 1200 °C, the Mg- and Sr-doped $LaGaO_3$ powder formed.

X-Ray diffraction was carried out with white Cu radiation on a STOE 0-0 reflection diffractometer. The energy dispersive Kevex detector was tuned to the Cu-Kα energy (8.04 keV). Lattice parameters were refined with the Visual X^{POW} software from STOE. Simultaneous thermogravimetry and differential thermal analyses (TG-DTA) were carried out on the as-prepared doped $LaGaO_3$ powders using a thermal analyser (Netzsch STA 429). The samples were heated from room temperature (around 20 °C) to 1200 °C at a heating rate of 2 °C min^{-1} and cooled to 100 °C at 5 °C min^{-1} in various atmospheres. The conventional weight analyses were carried out *in situ* after heat treatment in a tube furnace under various atmospheres. The purge gas flow rate was 50 ml min^{-1}. Humidity was measured by a dewpoint meter (DEWLUXE), from MCM, UK.

†*Present address*: School of Chemistry, University of St Andrews, St Andrews, Fife, Scotland, UK KY16 9ST. E-mail: st21@st-andrews.ac.uk.

DOI: 10.1039/b003890n

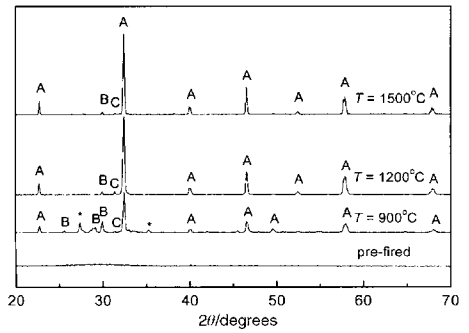

Fig. 1 X-Ray diffraction patterns of the pre-fired gel and the gel sintered at the temperatures indicated for 5 h. A, B and C indicate diffraction peaks due to $LaGaO_3$, La_4SrO_7 and $SrLaGaO_4$, respectively. * denotes unidentified peaks.

3 Results and discussion

3.1 Preparation of doped $LaGaO_3$

The X-ray diffraction patterns of Sr- and Mg-doped $LaGaO_3$ prepared by the sol–gel process and calcined at various temperatures are shown in Fig. 1. The pre-fired power is mainly composed of amorphous phases. These phases could be single or complex oxides decomposed from the organic precursors in the xerogel. When calcining the pre-fired powder at 900 °C for 5 h, the $LaGaO_3$ phase (orthorhombic, JCPDS card No. 24-1102) was mainly formed. Besides $LaGaO_3$, peaks of La_4SrO_7 were also observed as well as some unknown ones. The peak around $d=2.98$ Å belonging to $SrLaGaO_4$ is quite weak. Increasing the calcining temperature to 1200 °C, some peaks belonging to La_4SrO_7 disappear except the one around $d=2.85$ Å. The relative intensity of the peak for $SrLaGaO_4$ increases a little when calcining the sample at 1200 °C. The weak peaks of La_4SrO_7 and $SrLaGaO_4$ still exist in the powder although it is sintered at 1500 °C for 5 h. Similar to $LaGaO_3$, the phases La_4SrO_7 and $SrLaGaO_4$ are also thermodynamically stable between 900–1500 °C. In previous reports, these two impurity phases were also found in Sr- and Mg-doped $LaGaO_3$, when prepared by a solid state reaction.[2,7] Djurado and Labeau[13] have prepared Sr- and Mg-doped lanthanum gallate by solid state reactions and by an ultrasonic spray pyrolysis method. La_2O_3, MgO, $LaSrGa_3O_7$, $Sr_3Ga_2O_6$, $La_4Ga_2O_9$, $La_3Ga_5O_{12}$, $MgGa_2O_4$, La_2SrO_x and $LaSrGaO_4$ were found as second phase impurities in the synthesized samples. The impurity phases are strongly related to the preparation methods; various impurities appear when different methods are applied. The $La_{0.9}Sr_{0.1}Ga_{0.8}Mg_{0.2}O_3$ prepared by the method described in this paper contains only trace amounts of La_4SrO_7 and $SrLaGaO_4$ impurities.

3.2 TG-DTA analyses

TG-DTA was used to analyse the thermal and chemical stability of the $La_{0.9}Sr_{0.1}Ga_{0.8}Mg_{0.2}O_3$ powder obtained at 1500 °C. Fig. 2 shows the TG-DTA results in wet air. The wet air was obtained by passing dry air through water at 10 °C. During the equilibration process, the weight of the powder increased by 0.04 wt%. The colour of the powder did not change after the TG-DTA measurement. The TG-DTA results for the $La_{0.9}Sr_{0.1}Ga_{0.8}Mg_{0.2}O_3$ powder in an atmosphere containing 9% hydrogen and 91% nitrogen are shown in Fig. 3. In both figures an uncompensated baseline drift is observed, while only in Fig. 3 is a permanent weight loss observed. The weight change above 1000 °C can be attributed mainly to the loss of lattice oxygen and the sublimation of

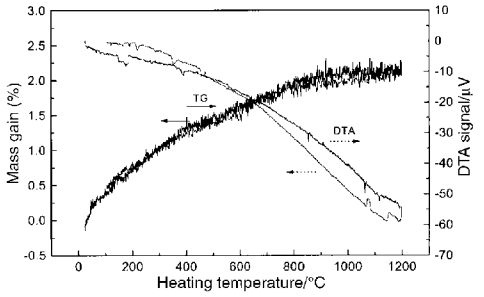

Fig. 2 TG-DTA traces of $La_{0.9}Sr_{0.1}Ga_{0.8}Mg_{0.2}O_{3-x}$ in wet air.

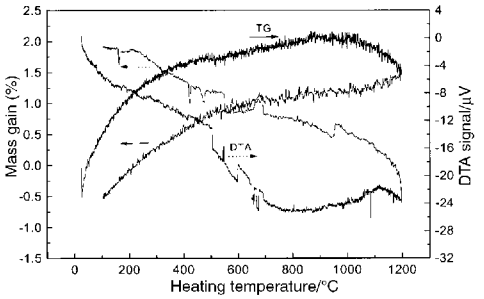

Fig. 3 TG-DTA traces of $La_{0.9}Sr_{0.1}Ga_{0.8}Mg_{0.2}O_{3-x}$ in 9%H_2 91%N_2.

gallium components, such as Ga_2O, at high temperature in a reducing atmosphere.[14] After the TG-DTA measurement in 9%H_2–91%N_2, the colour of the powder had changed from brown to grey.

In the Sr- and Mg-doped $LaGaO_3$, oxygen vacancies are introduced by substitution of Sr^{2+} for La^{3+} and Mg^{2+} for Ga^{3+} ions, according to the following:

$$x\mathrm{SrO}+(1-x)/2\mathrm{La_2O_3}+y\mathrm{MgO}+(1-y)/2\mathrm{Ga_2O_3}\Rightarrow \mathrm{La_{(1-x)}Sr_xGa_{(1-y)}Mg_yO_{3-x/2-y/2}} \quad (1)$$

It is clear from this formula that the doped compound should have a plateau in oxygen content corresponding to 2.85 oxide ions per formula unit in a large P_{O_2} range, if LSGM is assumed to be a pure or close to pure oxygen ion conductor. This corresponds to $[V_O^{\cdot\cdot}]\approx 0.15$. In the above, the formation of a small amount of second phases has been neglected.

The oxygen ion vacancies created are in equilibrium with atmospheric oxygen according to the following equilibrium equation, using K_h as defined in eqn. (7) and eqn. (10) below:

$$V_O^{\cdot\cdot}+1/2O_2\leftrightarrow O_O^{\times}+2h^{\cdot};\ K_h \quad (2)$$

In a hydrogen atmosphere, where the oxygen partial pressure is quite low, eqn. (2) will be displaced towards the left-hand side. The lattice oxygen in the $La_{0.9}Sr_{0.1}Ga_{0.8}Mg_{0.2}O_3$ will therefore combine with electron holes and oxygen will be released, resulting in a weight loss. In this case, the concentration of electron holes decreases. When the oxygen partial pressure is high, the main defects in $La_{0.9}Sr_{0.1}Ga_{0.8}Mg_{0.2}O_3$ are oxygen-ion vacancies and electron holes. The decrease of electron hole concentration in a reducing atmosphere might bleach the $La_{0.9}Sr_{0.1}Ga_{0.8}Mg_{0.2}O_3$ powder. On heating the grey $La_{0.9}Sr_{0.1}Ga_{0.8}Mg_{0.2}O_3$ powder at 750 °C for 12 h in air, it regained its initial brown colour. The endothermic effect above 500 °C on the DTA curve of Fig. 3 observed under a reducing atmosphere might be due to the release of lattice oxygen and sublimation of

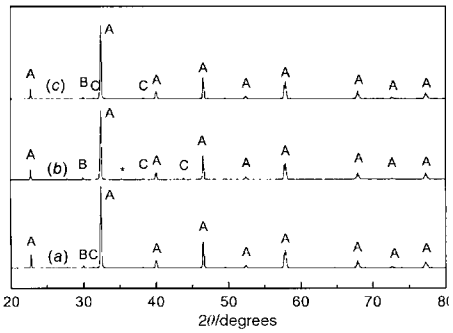

Fig. 4 X-Ray diffraction patterns of (a) $La_{0.9}Sr_{0.1}Ga_{0.8}Mg_{0.2}O_{3-x}$ obtained at 1500 °C after 5 h, (b) $La_{0.9}Sr_{0.1}Ga_{0.8}Mg_{0.2}O_{3-x}$ after TG-DTA analysis in wet air up to 1200 °C and (c) $La_{0.9}Sr_{0.1}Ga_{0.8}Mg_{0.2}O_{3-x}$ after TG-DTA analysis in 9 mol%H_2 91 mol%N_2 up to 1200 °C. A, B, C and * indicate $LaGaO_3$, La_4SrO_7, $SrLaGaO_4$ and unidentified phases, respectively.

gallium components from the $La_{0.9}Sr_{0.1}Ga_{0.8}Mg_{0.2}O_3$ accompanied by weight loss. On the other hand, the weight change and thermal effects of the material in wet air (Fig. 2) were not significant.

Fig. 4 shows the X-ray diffraction patterns of the $La_{0.9}Sr_{0.1}Ga_{0.8}Mg_{0.2}O_3$ powders after the TG-DTA analyses in wet air and 9%H_2–91%N_2. For comparison, the pattern of $La_{0.9}Sr_{0.1}Ga_{0.8}Mg_{0.2}O_3$ powder before TG-DTA analyses is also shown. After the TG-DTA tests up to 1200 °C, new weak peaks of $SrLaGaO_4$ were found in the sample tested in both wet air and 9% hydrogen. For the sample which underwent TG-DTA analysis in wet air, an unknown peak was also observed. These observations indicate that $SrLaGaO_4$ or another impurity phase may separate from the $La_{0.9}Sr_{0.1}Ga_{0.8}Mg_{0.2}O_3$ phase at high temperature. In order to study the long-term stability of $La_{0.9}Sr_{0.1}Ga_{0.8}Mg_{0.2}O_3$ at high temperature in different atmospheres, conventional weight analysis was introduced for further investigation.

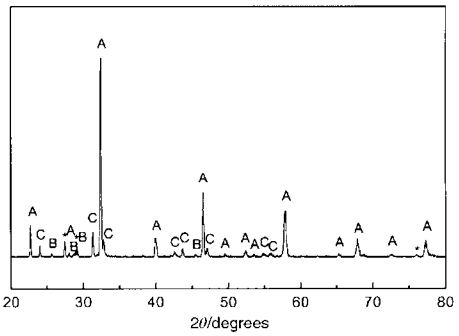

Fig. 5 X-Ray diffraction patterns of the samples after the weight analyses at 1000 °C. A, B, C and * indicate diffraction peaks due to $LaGaO_3$, La_4SrO_7, $SrLaGaO_4$ and unidentified phases, respectively.

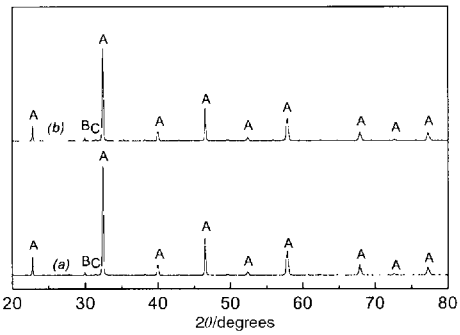

Fig. 6 X-Ray diffraction patterns of (a) $La_{0.9}Sr_{0.1}Ga_{0.8}Mg_{0.2}O_{3-x}$ obtained at 1500 °C, 5 h, and (b) $La_{0.9}Sr_{0.1}Ga_{0.8}Mg_{0.2}O_{3-x}$ after the weight analyses at 750 °C. A, B, C indicate diffraction peaks of $LaGaO_3$, La_4SrO_7 and $SrLaGaO_4$, respectively.

3.3 Conventional weight analyses

An alumina boat was heated at high temperature to remove the absorbed water and other impurities before weighing. Then $La_{0.9}Sr_{0.1}Ga_{0.8}Mg_{0.2}O_3$ powder was put into the boat, heated at 1000 °C overnight (12–14 h). After this, the furnace temperature was decreased to about 50 °C, the powder was removed and weighed immediately. The same powder was then heated in pure oxygen, nitrogen, hydrogen or 9%H_2–91%N_2, using the same process. The results of conventional weight analyses are shown in Table 1 and in Fig. 7. The weight changes in dry gases monotonically depend on the oxygen partial pressure. The weight increased in oxygen and decreased in nitrogen and hydrogen. These changes follow the trend predicted by eqn. (2), which is displaced under a different oxygen partial pressure. When heating the powder in wet

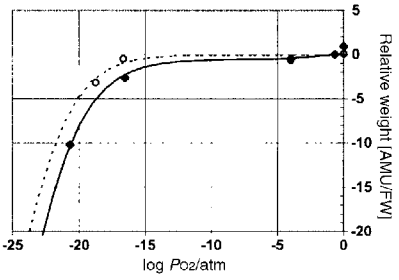

Fig. 7 Experimental and calculated relative weight at 1000 °C for two series of measurements at $P_{H_2O} = 8.4 \times 10^{-4}$ (dry, open symbols) and 6×10^{-3} atm (wet, filled symbols), respectively. The calculated weight curves were generated from $K_H = 1940$ atm^{-1}, $K_h = 11.0$ atm$^{-1/2}$, and $K_c = 4.5$ atm$^{1/2}$.

Table 1 Weight and colour change of $La_{0.9}Sr_{0.1}Ga_{0.8}Mg_{0.2}O_{3-x}$ in different atmospheres at 1000 °C overnight (12–14 h)

Atmosphere	O_2	Air	N_2	9%H_2 91%N_2	H_2
Weight in dry gas/g	0.6862	0.6836	0.6821	0.6761	0.6546
$(W_g - W_{air})/W_{air} \times 100$ (%)[a]	+0.38	0	−0.21	−1.10	−4.24
Colour	brown	brown	brown	grey	grey
Weight in wet gas (0.6 vol%H_2O)/g	0.6552	0.6550	0.6533	0.6536	0.6463
$(W_g - W_{air})/W_{air} \times 100$ (%)[a]	+0.03	0	−0.26	−0.21	−1.33
Colour	brown	brown	brown	grey	grey

[a] W_g is the weight of sample in different atmospheres. W_{air} is the weight of sample in dry and wet air respectively.

atmospheres, in general, the weight change is less significant than that in dry atmospheres; the mass loss is 4.24% in dry hydrogen but only 1.33% in wet hydrogen. The oxygen partial pressure is higher in wet hydrogen according to the equilibrium equation:

$$H_2O \leftrightarrow H_2 + 1/2O_2 \quad (3)$$

In this case, the oxygen partial pressure in wet oxygen is also a little lower than in dry oxygen. This significant mass loss cannot be explained by a displacement of eqn. (2) only. It can for the most part be attributed to the sublimation of gallium components in a reducing atmosphere. The weight of $La_{0.9}Sr_{0.1}Ga_{0.8}Mg_{0.2}O_3$ in dry oxygen increases by 0.38%, but by only 0.03% in wet oxygen.

After all these conventional weight analyses at 1000 °C listed in Table 1, the powder was tested by X-ray diffraction at room temperature (Fig. 5). It is obvious that the intensity of the La_4SrO_7 and $SrLaGaO_4$ peaks increase significantly. Three unidentified peaks also appear. The segregation of the impurities La_4SrO_7, $SrLaGaO_4$ and the unidentified phases from $La_{0.9}Sr_{0.1}Ga_{0.8}Mg_{0.2}O_3$ indicate that the material is unstable at 1000 °C. The instability of $La_{0.9}Sr_{0.1}Ga_{0.8}Mg_{0.2}O_3$ at 1500 °C has been demonstrated by Djurado and Labeau.[13] The segregation of degradation products may destroy the structure of $La_{0.9}Sr_{0.1}Ga_{0.8}Mg_{0.2}O_3$, decrease the concentration of oxygen-ion vacancies and further decrease the oxygen-ion conductivity.[18] In practice, the electrolyte has to be sintered at high temperature (usually above 1200 °C) when fabricating fuel cells. Therefore, the sintering of $La_{0.9}Sr_{0.1}Ga_{0.8}Mg_{0.2}O_3$ at higher temperatures for a long time needs to be avoided in the fabrication process.

The lattice constants of $La_{0.9}Sr_{0.1}Ga_{0.8}Mg_{0.2}O_3$ samples treated at different conditions are shown in Table 2. The impurity peaks were not included in the lattice parameter refinements. The cell volume after TG-DTA analyses up to 1200 °C in wet air and 9%H_2 is almost equal to that of the original $La_{0.9}Sr_{0.1}Ga_{0.8}Mg_{0.2}O_3$ powder because the heating time at high temperature is not enough to cause obvious phase separation. However, the cell volume of the sample after heating at 1000 °C for approximately 130 h is 238.39 Å^3, higher than the value 237.74 Å^3 for the original $La_{0.9}Sr_{0.1}Ga_{0.8}Mg_{0.2}O_3$ obtained at 1500 °C, which is attributed to the segregation of La_4SrO_7 and $SrLaGaO_4$ from the parent phase.

After being fabricated at higher temperatures, a fuel cell using $La_{0.9}Sr_{0.1}Ga_{0.8}Mg_{0.2}O_3$ as the electrolyte would usually operate at an intermediate temperature, *e.g.* 750 °C. Thus, the material was heated and weighed at 750 °C in dry and wet H_2 for a long time to determine its stability at intermediate temperatures. The results are listed in Table 3. The weight only decreases 0.06% after heating in dry hydrogen at 750 °C for 84 h. Compared to 4.24% in dry H_2 at 1000 °C in Table 1, it is insignificant. However, the weight increases 0.15% after heating at 750 °C in wet hydrogen for 48 h. Fig. 6(b) shows the XRD patterns of the sample after conventional weight analyses at 750 °C. The pattern is almost identical to the pattern obtained before the heat treatment [Fig. 6(a)]. The lattice parameters of the two samples are therefore unchanged within the standard deviation, as shown in Table 2. The phase segregation is insignificant at 750 °C. It is apparent that the material is relatively stable at this temperature. However, for a practical fuel cell that should run for several years, the long-term stability of $La_{0.9}Sr_{0.1}Ga_{0.8}Mg_{0.2}O_3$ would need to be further investigated.

3.4 Defect chemistry modelling

For the sake of generality we will consider a perovskite defect model, which can allow for variations in oxygen stoichiometry in LSGM, but also the possible presence of protonic defects. The argument for including protons is as follows: a systematic difference in weight was noticed between dry and wet atmosphere (see Fig. 7). Although LSGM has a transport number close to unity for oxygen ion,[1] and attempts to measure protonic conductivity in LSGM have so far failed,[19] non-conducting protons could still be present in LSGM.

The main volume fraction of the samples after heating to 1000 °C for 12–14 h is still a La–Ga-based perovskite phase, which has to account for some of the weight change observed, apart from the loss of Ga_2O by vaporisation under highly reducing conditions. The 10 weight measurements at 1000 °C, discussed in section 3.3, are, in principle, sufficient to determine the three equilibrium constants, describing the system, see eqn. (9–11) below. However, the weight data were not obtained *in situ*, nor by quenching. The extraction of three equilibrium constants from weight data obtained from equilibration at series of different P_{O_2} and P_{H_2O} pressures is demonstrated below.

A general defect description for a non-stoichiometric, proton containing perovskite, also including cation vacancies in $A_qB_{1-p}Mf_pO_{3\pm\varepsilon}$, was recently given by Poulsen.[15] In the present case we restrict our model to describe a perovskite with a ratio A/B = 1, and with no cation vacancies. The mathematical procedure of Bonanos and Poulsen,[16] originally developed for quantitative defect chemistry calculations on $SrCe_{1-p}Y_pO_{3-p/2\pm\delta}$, can directly be transferred to the $La_{1-x}Sr_xGa_{1-y}Mg_yO_{3\pm\varepsilon}$ case, since the dopants in both systems have a valence one lower than the respective host lattice ions. It is found that the mathematics are identical when setting $p = y + x$. The following quartic equation in concentration arises:

$$\beta \cdot u^4 + (6-p) \cdot u^3 + (\beta - \alpha) \cdot u^2 - p \cdot u - \alpha = 0 \quad (4)$$

where u substitutes for:

$$u = \{[Vo]/(3-[Vo])\}^{1/2} \quad (5)$$

$$\alpha = K_e^{1/2} \cdot P_{O_2}^{-1/4} \quad (6)$$

$$\beta = K_H^{1/2} \cdot P_{H_2O}^{1/2} + K_h^{1/2} \cdot P_{O_2}^{1/4} \quad (7)$$

where K_H and K_e are the K-values for eqn. (1a) and (3a) of ref. 16, respectively.

For a known atmosphere, P_{H_2O} and P_{O_2}, total dopant level, p, and assumed values of the three equilibrium constants, eqn. (4) can be solved by Newton–Raphson iteration using the analytical derivative of eqn. (4) and $u = 0.5$ as a starting value. The four defect concentrations of interest are then determined as:

Table 2 Lattice constants of $La_{0.9}Sr_{0.1}Ga_{0.8}Mg_{0.2}O_{3-x}$ samples treated under different conditions

	Sample				
Lattice constants	Obtained at 1500 °C	After TG-DTA analysis in wet air	After TG-DTA analysis in 9%H_2 91%N_2	After weight analysis at 1000 °C	After weight analysis at 750 °C
a/Å	5.5340(14)	5.5357(12)	5.5324(08)	5.5408(27)	5.5296(23)
b/Å	5.5074(22)	5.5069(18)	5.5070(11)	5.5150(28)	5.4991(47)
c/Å	7.8003(31)	7.7992(29)	7.8017(21)	7.8013(57)	7.8099(50)
Cell volume/Å^3	237.74(19)	237.76(16)	237.69(12)	238.39(34)	237.48(20)

Table 3 Weight and colour change of $La_{0.9}Sr_{0.1}Ga_{0.8}Mg_{0.2}O_{3-x}$ in different atmospheres at 750 °C

Atmosphere	Dry air, 12 h	Dry pure H_2, 84 h	Wet H_2 (0.6 vol%H_2O), 48 h
Weight/g	0.6764	0.6760	0.6774
$(W_g - W_{air})/W_{air} \times 100$ (%)[a]	0	−0.06	+0.15
Colour	brown	grey	grey

[a] W_g is the weight of sample in different atmospheres. W_{air} is the weight of sample in dry air.

$$[Vo] = 3 \cdot u^2/(u^2+1) \quad (4)$$

$$[H_i] = K_H^{1/2} \cdot P_{H_2O}^{1/2} \cdot u \quad (9)$$

$$[h^{\cdot}] = K_h^{1/2} \cdot P_{O_2}^{1/4} \cdot u \quad (10)$$

$$[e'] = Ke^{1/2} \cdot P_{O_2}^{-1/4} \cdot u^{-1} \quad (11)$$

The theoretical (calculated) relative weight change of one formula unit of perovskite, calculated in atomic mass units (AMU) is given by:

$$\Delta m_{calc} = \{16 \cdot (3 - [Vo]) + 1 \cdot [H_i]\}_{P_{H_2O}, P_{O_2}} - \{16 \cdot (3 - [Vo]) + 1 \cdot [H_i]\}_{ref} \quad (12)$$

where the calculated weight at $P_{H_2O} = 8.4 \times 10^{-4}$ atm (dry) or 6×10^{-3} atm (wet), and $P_{O_2} = 0.21$ atm are chosen as reference states. By using the non-linear least squares regression technique, values of the three equilibrium constants which minimise the residual $\Sigma(\Delta m_{calc} - \Delta m_{obs})^2$ can be searched for. Fig. 7 shows two theoretically generated weight curves for the dry and wet series, along with the experimentally observed relative weights. The best fit was obtained with the following equilibrium constants at 1000 °C: $K_H = 1940$ atm^{-1}, $K_h = 11.0$ atm$^{-1/4}$, and $K_e = 4.5$ atm$^{1/2}$. The estimated uncertainties for these parameters are about ±25%. The theoretically predicted weight curves, based on these values, apparently match the measurements quite well, apart from the measurement in 1 atm of oxygen, where the relatively large weight gain could not be accounted for.

However, other physical properties predicted from the three K-values are *not* physically acceptable. The predicted oxygen stoichiometries, O/(Ga + Mg), are 2.73 and 2.30 for the two most reducing measurements in wet and dry atmosphere, respectively. The latter oxygen content is far below what a perovskite requires. Also, the proton uptake amounts to 0.7 and 0.98 mol H per formula unit, respectively, which is far above any realistic level. It is apparent from the defect modelling that structural and other supplementary data are required along with the gravimetric data. Interpretation of the weight data alone would have led us to the false conclusion that doped $LaGaO_3$ becomes highly sub-stoichiometric and contains massive amounts of protons, even in moderately wet (0.6%H_2O) atmospheres. One possible reason for the higher weight in humid atmospheres than in dry ones could be the formation of oxyhydroxides or hydroxides, such as $La(OH)_3$ found by Yamaji *et al.*,[14] although these remained undetected in our samples. As described above, the modelling resulted in K-values predicting non-physical properties as well as unrealistic oxygen stoichiometries. The basic assumption for this modelling that the material is single phase does not hold.

4 Conclusions

The oxygen-ion conductor $La_{0.9}Sr_{0.1}Ga_{0.8}Mg_{0.2}O_3$ has been prepared by a sol–gel process. The weight of the materials is related to oxygen and water vapour partial pressure. At 1000 °C, the $La_{0.9}Sr_{0.1}Ga_{0.8}Mg_{0.2}O_3$ phase is unstable. The impurity phases La_4SrO_7 and $SrLaGaO_4$ separate from the parent phase, which may destroy the structure of the doped oxygen-ion conductor. Therefore, heating the materials at high temperature for a long time should be avoided. After heating the material at 750 °C in H_2 atmosphere for a total of 132 h, no phase change was detected, indicating that $La_{0.9}Sr_{0.1}Ga_{0.8}Mg_{0.2}O_3$ is relatively stable at intermediate temperatures. The question of the long term stability of $La_{0.9}Sr_{0.1}Ga_{0.8}Mg_{0.2}O_3$ at intermediate temperatures, however, still deserves further investigation before LSGM can be used as an electrolyte in fuel cells.

A general procedure for determining equilibrium constants for perovskites equilibrated in different water vapour and oxygen partial pressures is given. The present LSGM weight data could be modelled, but other non-physical properties follow from the equilibrium constants obtained. The modelling thereby supports the findings from X-ray diffraction that LSGM kept for long periods of time at 1000 °C is not single phase.

Acknowledgements

The authors are grateful to Dr Nikolaos Bonanos and Dorthe Lybye of the Materials Research Department, Risø National Laboratory, for advice and a critical reading of the manuscript. Thanks to Knud Jensen, Torben Strauss and Palle Jensen for data collection. One of the authors (S. Tao) would like to thank the Danida Fellowship Centre for financially supporting his work at Risø.

References

1 T. Ishihara, H. Matsuda and Y. Takita, *J. Am. Chem. Soc.*, 1994, **116**, 3801.
2 T. Ishihara, H. Matsuda and Y. Takita, *Solid State Ionics*, 1995, **79**, 147.
3 M. Feng, J. B. Goodenough, K. Q. Huang and C. Milliken, *J. Power Sources*, 1996, **63**, 47.
4 K. Q. Huang, M. Feng and J. B. Goodenough, *J. Electrochem. Soc.*, 1997, **144**, 3620.
5 P. N. Huang and A. Petric, *J. Electrochem. Soc.*, 1996, **143**, 1644.
6 T. Yamada, Y. Hiei, T. Akbay, T. Ishihara and Y. Takita, *Solid State Ionics*, 1998, **113–115**, 253.
7 T. Ishihara, T. Akbay, H. Furutani and Y. Takita, *Solid State Ionics*, 1998, **113–115**, 585.
8 J. Drennan, V. Zelizko, D. Hay, F. T. Ciacchi, S. Rajendran and S. P. S. Badwal, *J. Mater. Chem.*, 1997, **7**, 79.
9 J. Wolfenstine, P. Huang and A. Petric, *Solid State Ionics*, 1999, **118**, 257.
10 S. W. Tao, Z. L. Zhan, P. Wang and G. Y. Meng, *Solid State Ionics*, 1999, **116**, 29.
11 F. L. Chen, O. T. Sørensen, G. Y. Meng and D. K. Peng, *J. Mater. Chem.*, 1997, **7**, 481.
12 N. Bananos, K. S. Knight and B. Ellis, *Solid State Ionics*, 1995, **79**, 161.
13 E. Djurado and M. Labeau, *J. Eur. Ceram. Soc.*, 1998, **18**, 1397.
14 K. Yamaji, T. Horita, M. Ishikawa, N. Sakai and H. Yokokawa, *Solid State Ionics*, 1999, **121**, 217.
15 F. W. Poulsen, *J. Solid State Chem.*, 1999, **143**, 115.
16 N. Bonanos and F. W. Poulsen, *J. Mater. Chem.*, 1999, **9**, 431.
17 S. W. Tao, Q. Y. Wu, Z. L. Zhan and G. Y. Meng, *Solid State Ionics*, 1999, **124**, 53.
18 D. Lybye, F. W. Poulsen and M. Mogensen, *Solid State Ionics*, 2000, **128**, 91.
19 T. Norby, personal communication, 1999.

A7.

F.W. Poulsen, M. Glerup and P. Holtappels,
Structure, Raman spectra and defect chemistry modelling of conductive pyrochlore oxides, Solid State Ionics **135**, 595-602. (2000)

ELSEVIER

Solid State Ionics 135 (2000) 595–602

SOLID STATE IONICS

www.elsevier.com/locate/ssi

Structure, Raman spectra and defect chemistry modelling of conductive pyrochlore oxides

F.W. Poulsen*, M. Glerup, P. Holtappels

Materials Research Department, Risø National Laboratory, DK-4000 Roskilde, Denmark

Abstract

Mixed ionic–electronic conducting pyrochlore structure oxides, with Pr and Gd on the A site and Zr, Mn, Ce, Sn, In, Mo, and Ti on the B site, were characterised by X-ray powder diffraction and Raman spectroscopy. Mn and In have a solubility around $x = 0.1–0.2$ in $Pr_2Zr_{2-x}Mn_xO_7$ and $Pr_2Sn_{2-x}In_xO_7$, respectively. In the series $Pr_2M_{2-x}M'_xO_7$, where M=Sn, Zr and M′=In, Ce, we observe dopant–O_6 symmetrical stretch vibrations in addition to the host lattice modes. A defect model of a B site doped pyrochlore is developed with Pr^{3+} on the A site; Zr_B^x (Zr^{4+}), Ce'_B (Ce^{3+}), Ce_B^x (Ce^{4+}) on the B site; O_O^x and $V_O^{\cdot\cdot}$ on the O site, interstitial oxygens O_i'', and delocalised electrons and electron holes. Four mass action law expressions govern such a model. The defect model can rationalise why homo-valent doping, i.e. substitution of Zr(4+) by Ce(4+), can lead to an increase in ionic conductivity. The calculated Brouwer diagram for $Pr_2Zr_{1.6}Ce_{0.4}O_{7+\delta}$ is shown. This composition has a transition from mixed ionic p-type to presumably pure ionic conduction around $pO_2 = 10^{-7.5}$ atm. At $pO_2 < 10^{-15}$ atm the material gradually changes into the n-type regime. Typical magnitudes are finally given for the four equilibrium constants, leading to cases of pure p-type, p- to n-type and pure electrolytic behaviour of doped pyrochlores.

Keywords: Pyrochlore; Raman spectra; Defect model; Mixed conductor

1. Introduction

Oxides with the pyrochlore structure, $A_2B_2O_7$, furnish a host lattice suitable for incorporation of aliovalent dopants, interstitial oxygen, protons and electronic defects. The properties can possibly be tailored within wide limits by doping on the A and B site. Pyrochlore structure oxides have ipso facto attracted attention among the SOFC community. Initially, it was noticed that poorly conducting $La_2Zr_2O_7$ formed as a reaction product between yttria-stabilised zirconia and the $La_{1-x}Sr_xMnO_3$ cathode [1], giving rise to poor performance of the cathode. However, it has proven fruitful, via the work initiated by Tuller et al. [2–4], to search for new solid electrolytes and mixed conducting electrodes of the pyrochlore structure. Holtappels et al. present in these proceedings the electrical properties of a range of pyrochlore materials, with focus on their possible application as anodes in SOFC [5]. The defect chemistry of pyrochlores becomes somewhat complex to handle when the A and B site dopants are transition metal or rare earth ions with a choice between several oxidation states. Four chemical equilibria plus five linear equations originating

*Corresponding author. Fax: +45-46-77-5758.
E-mail address: finn.willy.poulsen@risoe.dk (F.W. Poulsen).

0167-2738/00/$ – see front matter
PII: S0167-2738(00)00417-3

from site, mass and electroneutrality restrictions are required for a full description, which is given in Section 3.3. Raman spectroscopy was chosen as a complimentary analytical tool to X-ray diffraction for two reasons. (1) In Raman spectra, oxygen–cation vibrations are expected to dominate the spectrum, whereas X-ray diffraction patterns are mostly influenced by the heavy metal ions. (2) Dopant–oxygen vibrations may be observed in addition to the vibrations of the host lattice. In the long term we must study and understand the phonon spectra of pyrochlores, since the electron transport through a pyrochlore lattice is likely to involve hopping via metal–oxygen bonds, assisted by lattice vibrations (phonons). Quantitative treatments of polaronic conduction in pyrochlores seem not to have been reported thus far. Raman spectra of doped pyrochlores, where the dopant is in its oxidised or fully reduced state will be presented in a forthcoming publication.

2. Experimental

The pyrochlores were prepared according to the mixed oxide method. Appropriate ratios of the oxides were milled, either by hand in a mortar, by ball milling or using a tumble miller, and then pressed into pellets and sintered at temperatures up to 1400°C in air or nitrogen diluted mixtures of hydrogen/water mixtures. Preparation details are described in full in Ref. [5].

X-ray powder diffraction was carried out with white Cu radiation on a STOE θ–θ reflection diffractometer. The energy-dispersive Kevex detector was tuned to the Cu Kα energy (8.04 keV). Lattice parameters were refined with the Visual X^{POW} software from STOE.

All Raman spectra were measured with a Bruker FRA-106 Raman module connected to a Bruker IFS 66 interferometer. The detector was a Ge diode detector working at liquid nitrogen temperature (77 K). The excitation source was a Nd:YAG laser with an excitation wavelength of 1064 nm at 75–200 mW. All spectra were corrected for the instrumental response. The spectrum of an incandescent lamp was recorded and divided by a calculated black body curve at 3200 K, the temperature assumed for the lamp. The measured NIR-FT-Raman spectra were divided by the resulting correction function. The resulting spectral resolution in the apodized spectrum is around 6 cm^{-1}. The spectra were measured at room temperature from polycrystalline sintered pellets of the pyrochlore materials.

3. Results and discussion

3.1. Structure and phase purity

Table 1 gives a survey of the synthesised pyrochlores, with information obtained from X-ray powder diffraction on lattice parameters and possible impurity phases, in cases where the solubility limits were exceeded. The cubic lattice constants are in the range 10.27 to 10.70 Å. In the archetype pyrochlore structure, $La_2Zr_2O_7$, the trivalent La ions are eightfold coordinated with A–O distances between 2.33 and 2.64 Å, while the tetravalent Zr cations have a near to perfect octahedral coordination by oxygen with a Zr–O distance of 2.09 Å [6]. $PrMnO_3$ and $PrInO_3$ were identified as impurity phases in $Pr_2Zr_{2-x}Mn_xO_{7\pm\delta}$ and $Pr_2Sn_{2-x}In_xO_{7\pm\delta}$. The Mn solubility limit in $Pr_2Zr_{2-x}Mn_xO_{7\pm\delta}$ is between $x = 0.1$ and 0.2. X-ray diffraction is relatively insensitive to the position and occupation of the oxygens on the 48f site, since the cations have high atomic numbers. Furthermore, the substitution of dopants into the lattice only reveals itself by a moderate change of the lattice parameter. The lattice parameters of the zirconates and stannates were seen to change in the predicted directions following known ionic radii. The Mn dopant is smaller than Zr, leading to contraction, and Ce is bigger than Zr, and In is bigger than Sn, leading to expansion. Measurements of the oxygen content of all the studied pyrochlores are underway, and will give the final answer as to the average oxidation state of the dopants in samples heat treated in air.

3.2. Raman spectra

Cubic pyrochlores, $A_2B_2O_6O'$, belong to the space group Fd3m (or O_h^7, No. 227), where $Z = 8$. The number of molecular units per primitive unit cell

Table 1
X-ray characterisation of pyrochlores. Standard deviation on lattice parameter is ±0.002 Å

Composition and sample ID	a_{cubic} (Å)	Impurity phase	Colour
$Pr_2Zr_2O_{7+\delta}$ (185-2s)	10.709		Brown
$Pr_2Mn_{0.1}Zr_{1.9}O_{7+\delta}$ (S0720)	10.6913	$PrMnO_3$[a]	Black
$Pr_2Mn_{0.2}Zr_{1.8}O_{7+\delta}$ (S0721)	10.6835	$PrMnO_3$	Black
$Pr_2Mn_{0.35}Zr_{1.65}O_{7+\delta}$ (S0722)	10.690	$PrMnO_3$	Black
$Pr_2Ce_{0.2}Zr_{1.8}O_{7+\delta}$ (S0723)	10.6824		Brown
$Pr_2Ce_{0.4}Zr_{1.6}O_{7+\delta}$ (S0724)	10.7145		Brown
$Pr_2Sn_2O_{7+\delta}$ (190)	10.599		Beige
$Pr_2In_{0.1}Sn_{1.9}O_{7+\delta}$ (204)	10.601		Brown
$Pr_2In_{0.2}Sn_{1.8}O_{7+\delta}$ (205)	10.605	$PrInO_3$[b]	Brown
$Pr_2In_{0.35}Sn_{1.65}O_{7+\delta}$ (206)	10.599	$PrInO_3$[b]	Brown
$Gd_2MoTiO_{7+\delta}$ (S0769)	10.2679–10.2703[c]		Black
$Gd_2Mo_{1.4}Ti_{0.6}O_{7+\delta}$ (198A)	10.281–10.2989[c]		Black

[a] Identified on the basis of one very small peak.
[b] A new perovskite.
[c] Variation between two batches.

is two. The corresponding factor group for the cubic pyrochlore is O_h. The site symmetry is D_{3d} for A and B ions, C_{2v} for the O ions and T_d for the O′ ion, which is in accordance with Ref. [7]. A factor group analysis was made based on the above assumptions, leading to the following predicted vibrational normal modes: Raman active modes, $1A_g+1E_g+4F_{2g}$; IR-active modes, $7F_{1u}$; inactive modes, $2F_{1g}+3A_{2u}+3E_u+4F_{2u}$; acoustic modes, $1F_{1u}$.

It was shown by Vandenborre et al. [8] that the force fields, determined in the case of Ti, Zr and Sn on the B site in three pyrochlore series, are essentially transferable from one pyrochlore series to another. Therefore, the assignment of the observed vibrational bands to the predicted symmetry species is done by comparison with these earlier results. In doped crystals the observation of extra Raman peaks may have at least three different explanations:

(i) the presence of impurity phases;
(ii) a breakdown of the selection rules, if the dopant and/or some of the host lattice ions are located in a lower symmetry and/or have a different coordination number than in the undoped crystal;
(iii) 'extra' observed modes from the dopant, given the same description as for the corresponding host lattice mode, but with a different force constant/mass involved.

The impurities observed by X-ray diffraction are of the perovskite or the fluorite structure, and the strongest features in their respective Raman spectra were not detected in the pyrochlore spectra. Since we only observe three to five well-resolved bands, there are no reasons to invoke off-centre modes at this level of qualitative evaluation of the spectra. We pursue the analysis along interpretation (iii), i.e. the local structure is, on average, preserved around the dopant ion.

Raman spectra were obtained at room temperature from three undoped and eight doped pyrochlores, including $La_2Zr_2O_7$ as a reference compound (Figs. 1 and 2); Table 2 gives Raman shifts for compounds which are not shown as spectra in Figs. 1 and 2.

In all the Raman spectra, three to five bands are observed and not six, as predicted by factor group analysis. This is, however, in good accordance with the literature [8]. The Raman spectra of $Pr_2Sn_{2-x}In_xO_{7\pm\delta}$, $x=0$, 0.1, 0.2, 0.35, are shown in Fig. 1. In the spectrum of undoped $Pr_2Sn_2O_7$, five bands are observed; when In is substituted at the B site of the lattice an additional band at 545 cm^{-1} appears. The area of the vibrational band at 545 cm^{-1} relative to the area of the band at 526 cm^{-1} increases with increasing In content. $PrInO_3$ was among the impurity phases identified by X-ray diffraction. However, this compound does not have any vibrational bands in the Raman spectrum in the

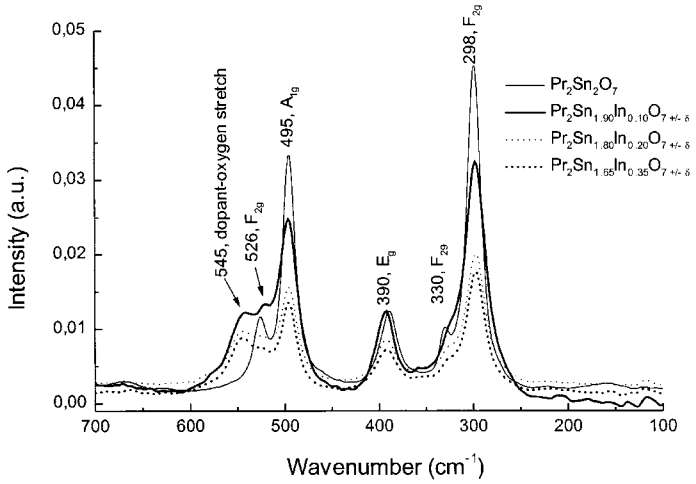

Fig. 1. Fourier transform Raman spectra at room temperature of $Pr_2Sn_{2-x}In_xO_{7\pm\delta}$, $x = 0.0$, 0.1, 0.2, 0.35.

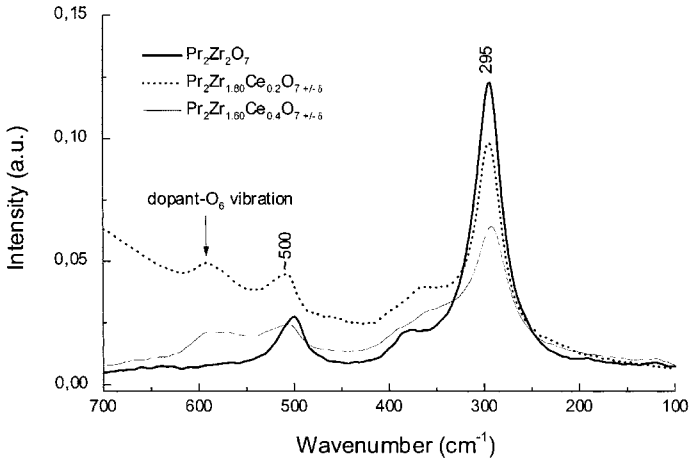

Fig. 2. Raman spectra of $Pr_2Zr_{2-x}Ce_xO_{7\pm\delta}$, $x = 0$, 0.2, 0.4, at room temperature.

range from 475 to 700 cm^{-1}. Consequently, the band at 545 cm^{-1} is assigned to the dopant–O_6 symmetrical stretch in the pyrochlore phase.

A similar trend is observed in the Raman spectra of $Pr_2Zr_{2-x}Ce_xO_{7\pm\delta}$, $x = 0.0$, 0.2, 0.4, shown in Fig. 2. The spectrum of $Pr_2Zr_2O_7$ only shows three distinct bands, which are due to an overlap of several of the vibrational bands. A new band is observed at around 590 cm^{-1} when Ce is introduced at the B site of the lattice. This new vibrational mode is likewise assigned to the Ce–O_6 symmetrical stretch vibration.

The observed frequencies for the Raman spectra of $Pr_2Zr_{2-x}Mn_xO_{7\pm\delta}$, $x = 0.1$, 0.2, 0.35, are given in Table 2. It can be seen from the X-ray data that

Table 2
Raman frequencies (cm $^{-1}$) and assignment for undoped and doped pyrochlore oxides. The numbers in parentheses are assumed values

$La_2Zr_2O_7$	$Pr_2(Zr_{1.90}Mn_{0.10})O_7$	$Pr_2(Zr_{1.80}Mn_{0.20})O_7$ [a]	$Pr_2(Zr_{1.65}Mn_{0.35})O_7$ [a]	Assignment
299	~300	~300	~300	F_{2g}
(299)	(~300)	(~300)	(~300)	F_{2g}
396	~370, very weak	~370, very weak	~370, very weak	E_g
494	500	~500	~500	A_{1g}
516	(~500)	(~500)	(~500)	F_{2g}

[a] A high content of impurities was observed by X-ray diffraction in these materials (cf. Table 1).

when $x = 0.2$ and 0.35 a noticeable amount of impurities is formed (cf. Table 1). These measured Raman spectra consists of very broad and not very distinct bands making it difficult to evaluate band positions and changes due to doping.

A linear relationship between the frequency of the A_{1g} vibration and the A ion radius with constant B ion radius has been described in previous studies [8]. However, the dependence of the A_{1g} vibration frequency on the B ion has thus far been explained by an increase in force constant when the atomic number increases. In the present study we noticed a second trend to the above by our observation of the dependence of the A_{1g} vibration on the size of the B ion. The larger the B ion radius (with the same A ion) the higher the observed A_{1g} vibrational frequency, indicating that the force constant has increased. This relationship is established by comparing the position of the A_{1g} vibrational frequency for $Pr_2Sn_2O_7$ and $Pr_2Zr_2O_7$ with the two B ion radii. The relationship can be used to explain the high vibrational frequency of the dopant–O_6 band compared to the Sn–O_6 vibrational band in In-doped $Pr_2Sn_2O_7$; the atomic weights are almost equal for In (115 g/mol) and Sn (119 g/mol), whereas the ionic radii differ significantly: $r(In^{3+}) = 0.800$ Å and $r(Sn^{4+}) = 0.690$ Å [9]. The same results are observed for Ce-doped $Pr_2Zr_2O_7$, but here both the ionic radii and the atomic weights differ. Therefore, it is concluded that the ionic radius is an important factor for the magnitude of the force constant and thereby the position of the A_{1g} vibrational band.

3.3. Defect modelling

A defect model for $Pr_2Zr_{2-x}Ce_xO_{7\pm\delta}$ was formulated in analogy to that of Tuller et al. [4] for $Gd_2Ti_{2-x}Mn_xO_{7\pm\delta}$. The model contains nine species: Pr_A^x (Pr^{3+}) on the A site; Zr_B^x (Zr^{4+}), Ce_B' (Ce^{3+}) and Ce_B^x (Ce^{4+}) on the B site; O_O^x and $V_O^{\cdot\cdot}$ on the O site; interstitial oxygens O_i''; and finally delocalised electrons and electron holes, n = [e′], p = [$h^{\cdot}$]. Inclusion of O_i'' in the model ensures that cases of oxygen over-stoichiometric pyrochlores (p-type) can be handled. Also, the displacement of normal oxygens into interstitial positions, see Eq. (3), is able to supply oxygen vacancies required for ionic conductivity. The concentrations are calculated from a set of nine equations: five linear equations from mass, site and electroneutrality conservation, and four mass action law expressions. Tuller et al. found a fifth-order polynomial in the electron density concentration and solved this numerically [4]. For a simulation of the Brouwer diagram the four equilibrium constants must have known values. The sequential algorithm for defect concentration calculation on perovskites [10] has been adjusted to the pyrochlore case. The calculation proceeds in a series of steps as follows (concentrations will be printed in *italics* as they stepwise assume numerical values; x is the B site dopant level in mol/formula unit).

A value of the electron concentration, $n = [e']$, is assumed in the interval 10^{-20} to 1. The hole concentration, p, is found from the intrinsic ionisation equilibrium:

$$p = K_i/n. \tag{1}$$

The reduced dopant $[Ce_B']$ concentration is found from

$$K_A = [Ce_B']/(n[Ce_B^x]) = [Ce_B']/(n(x - [Ce_B'])). \tag{2}$$

An expression for the interstitial oxygen concentration $[O_i'']$ is obtained from the anti-Frenkel equilibrium:

$$O_O^x \Leftrightarrow O_i'' + V_O^{\cdot\cdot}, \tag{3}$$

$$K_{\mathrm{AF}} = [\mathrm{O_i''}][\mathrm{V_O^{\cdot\cdot}}]/[\mathrm{O_O^x}], \quad (4)$$

which leads to

$$[\mathrm{O_i''}] = (7 - [\mathrm{V_O^{\cdot\cdot}}])K_{\mathrm{AF}}/[\mathrm{V_O^{\cdot\cdot}}]. \quad (5)$$

This expression for $[\mathrm{O_i''}]$ is inserted into the electroneutrality condition:

$$2[\mathrm{V_O^{\cdot\cdot}}] + p = [Ce_B'] + 2[\mathrm{O_i''}] + n, \quad (6)$$

resulting in a quadratic equation in $[\mathrm{V_O^{\cdot\cdot}}]$:

$$2[\mathrm{V_O^{\cdot\cdot}}]^2 - [\mathrm{V_O^{\cdot\cdot}}]([Ce_B'] + n - p - 2K_{\mathrm{AF}}) - 14K_{\mathrm{AF}} = 0. \quad (7)$$

$[\mathrm{V_O^{\cdot\cdot}}]$ is found analytically from the above quadratic, using the largest positive root. $[V_O^{\cdot\cdot}]$ now has a numerical value and we can therefore find $[\mathrm{O_i''}]$ from

$$K_{\mathrm{AF}} = [O_i''][V_O^{\cdot\cdot}]/(7 - [V_O^{\cdot\cdot}]).$$

Then

$$[O_O^x] = 7 - [V_O^{\cdot\cdot}]. \quad (8)$$

The solutions $[Pr_A^x] \equiv 2$ and $[Zr_B^x] \equiv 2 - x$ are trivial, since the model does not include cation vacancies. All nine concentrations have now been found.

The fourth mass law expression, describing the equilibration reaction with gaseous oxygen:

$$2\mathrm{e}' + \mathrm{V_O^{\cdot\cdot}} + \tfrac{1}{2}\mathrm{O_2} \Leftrightarrow \mathrm{O_O^x},$$

leading to

$$p\mathrm{O_2}^{1/2} \cdot K_{\mathrm{ox}} = [O_O^x]/\{n^2[V_O^{\cdot\cdot}]\}, \quad (9)$$

has not yet been employed. Only one physical value of the partial pressure of oxygen will correspond to the nine concentrations and the values of the four equilibrium constants. This is found by inserting the numerical values of $[O_O^x]$, n and $[V_O^{\cdot\cdot}]$ into Eq. (9).

Fig. 3 presents a Brouwer diagram for $\mathrm{Pr_2Zr_{1.6}Ce_{0.4}O_{7\pm\delta}}$. The equilibrium constants used for the generation of Fig. 3 have been chosen such that $\mathrm{V_O^{\cdot\cdot}}$ is supplied mainly by the anti-Frenkel equilibrium and not by reduction of the Ce dopant, which is first fully reduced around $p\mathrm{O_2} \approx 10^{-18}$ atm. The oxygen stoichiometries, $\mathrm{O_{tot}}$/[total amount of B] at $p\mathrm{O_2} = 10^{-25}$ and 1 atm, following from these equilibrium constants are 3.38 and 3.53, respectively, see Fig. 4, which also includes 14 experimentally determined $p\mathrm{O_2}$-dependent total conductivities [5].

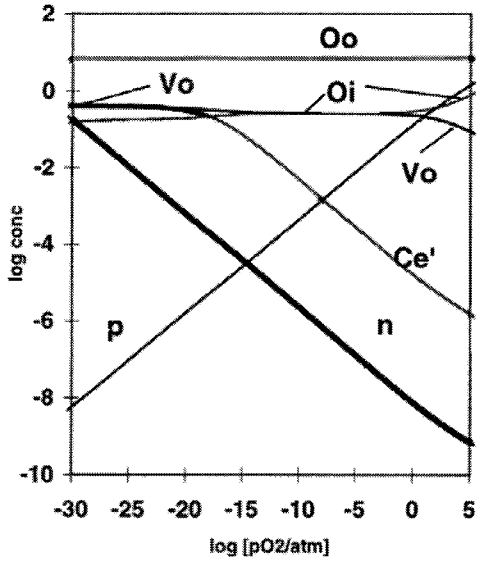

Fig. 3. Brouwer diagram for the defect concentrations in $\mathrm{Pr_2Zr_{1.6}Ce_{0.4}O_{7\pm\delta}}$. Equilibrium constants are shown in Table 3.

The total conductivity at 1000°C has a $(p\mathrm{O_2})^{1/4}$ dependence above $p\mathrm{O_2} = 10^{-7}$ atm, both for the experimental and predicted values. The standard interpretation of such behaviour is that the material is a p-type conductor above this pressure (still with a possible ionic contribution). The 1/4 slope of the p-type branch is indicative of the oxygen vacancy concentration being rather high and close to constant in the high $p\mathrm{O_2}$ range; see Eq. (9) in combination with $p \cdot n = K_{\mathrm{i}}$. Had the uptake of oxygen mainly been dominated by extra oxygens entering interstitial positions, $\mathrm{O_i''}$, one would expect a 1/6 slope in a $\log(\sigma)$ vs. $\log(p\mathrm{O_2})$ plot. At low $p\mathrm{O_2}$ one can envisage two kinds of n-type contributions to conduction [4]: (i) normal polaron n-type conduction scaling with n under very reducing conditions; and (ii) contributions from electron transfer between $\mathrm{Ce_B'}$ and $\mathrm{Ce_B^x}$ (via double exchange) scaling with the product of the two concentrations. The latter will only give a measurable contribution to the total conductivity when the Ce dopant concentration is high, and only at such values of $p\mathrm{O_2}$ where the two oxidation states coexist in comparable amounts. The individual conductivity contributions and the total

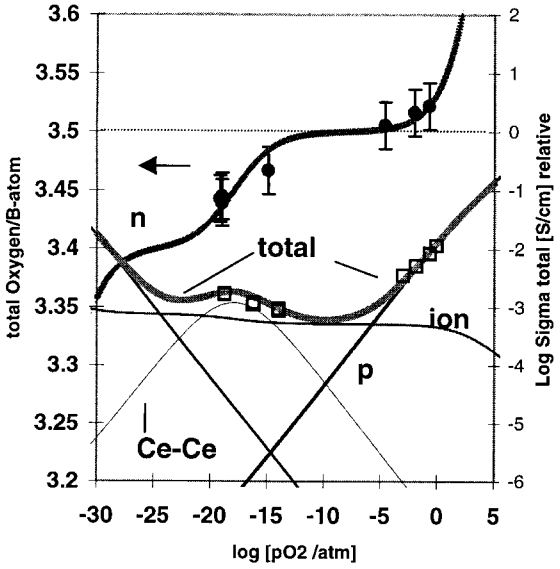

Fig. 4. Observed and calculated oxygen stoichiometry and conductivity for $Pr_2Zr_{1.6}Ce_{0.4}O_{7+\delta}$. Equilibrium constants for the simulation are shown in Table 3. Key: open symbols are the measured total conductivities; filled symbols are oxygen stoichiometries, normalised to $O_{tot}/M_{Ti}=3.5$ at 10^{-5} atm of O_2 [11].

conductivity are sketched in Fig. 4. Seven preliminary measurements [11] of the oxygen stoichiometry have been included in Fig. 4, and form the basis for the determination of the approximate equilibrium constants given in Table 3. It must be stressed that Figs. 3 and 4 only illustrate the applicability of the above algorithm, and we used qualitative guesses for the scaling factors for the various conductivity contributions (proportional to individual mobilities).

Three preliminary trends are revealed about the defect chemistry of pyrochlores from numerous Brouwer diagram simulations using the above algorithm. (i) Several sets of the four equilibrium constants exist, which reproduce an observed pO_2 dependence of the total conductivity — in fact the dependence can theoretically also be described as exclusively p-type throughout the pO_2 range above 10^{-10} atm. Table 3 gives representative sets of equilibrium constants leading to three types of behaviour: p-type, p- to n-type, and pure electrolyte

Table 3
Equilibrium constants for pyrochlore structure oxides

	K_I	K_A	K_{AF}	K_{ox} $(atm)^{1/2}$
$Pr_2Zr_{1.6}Ce_{0.4}O_{7+\delta}$. Constants used for generation of Figs. 3 and 4	10^{-9}	5×10^{3}	10^{-2}	0.5
p-Type 10^{-5}–10^{-25} atm over-stoichiometric above 10^{-7} atm ($x=0.3$)	10^{-9}	10^{3}	10^{-10}	10^{10}
p- to n-type transition at 10^{-12} atm ($x=0.1$)	10^{-8}	10^{-5}	10^{-10}	10^{3}
Pure electrolyte behaviour, $x=0.3$	10^{-12}	10^{12}	10^{-20}	10^{-3}

behaviour. (ii) Thermogravimetric data are required in order to answer questions concerning over- and sub-stoichiometry (K_{ox}, K_i) and the average oxidation state of the Ce dopant, determined by K_A. (iii) The equilibrium constant, K_{AF}, for the anti-Frenkel reaction, Eq. (4), can be changed gradually, such that there will be a smooth transition from an ordered pyrochlore defect model to a disordered fluorite structure oxide model.

4. Concluding remarks

Raman spectroscopy appears to be a fruitful characterisation method for doped pyrochlores, since individual Raman peaks are observed for the dopant–oxygen vibrations. In future experiments we will attempt to establish the oxidation state of dopants by Raman spectroscopy. On the other hand, it was found that Raman spectroscopy was relatively insensitive in the present case to the presence of impurity phases (at least when present below 5–10 vol%). Defect chemistry modelling will be developed further to assist our understanding of, and ability to predict, mixed conductivity in doped pyrochlores.

Acknowledgements

The authors express their gratitude for financial support from the DK-SOFC Programme and the Nordic Energy Research Programme (FWP), The Danish Research Academy (MG), and the EU-TMR Program under contract FMRX-CT97-0130 (PH).

References

[1] F.W. Poulsen, N. van der Puil, Solid State Ionics 53–56 (1992) 777.
[2] O. Porat, C. Heremans, H.L. Tuller, J. Am. Ceram. Soc. 80 (1997) 2278.
[3] O. Porat, M.A. Spears, C. Heremans, I. Kosacki, H.L. Tuller, Solid State Ionics 86–88 (1996) 285.
[4] H.L. Tuller, Solid State Ionics 94 (1997) 63.
[5] P. Holtappels, F.W. Poulsen, M. Mogensen, Solid State Ionics 135 (2000) 675.
[6] H.J. Deiseroth, H. Mueller-Buschbaum, Z. Anorg. Allg. Chem. 375 (1970) 152.
[7] R.A. McCauley, J. Appl. Phys. 51 (1980) 290.
[8] M.T. Vandenborre, E. Husson, J.P. Chatry, D. Michel, J. Raman Spectrosc. 14 (1983) 63.
[9] R.D. Shannon, Acta Crystallogr. A 32 (1976) 751.
[10] F.W. Poulsen, J. Solid State Chem. 143 (1999) 115.
[11] P. Holtappels et al. (in preparation).

A8.

Finn. W. Poulsen,
Speculations on the existence of hydride ions in Proton Conducting oxides, Solid State Ionics, **145**, 387-397 (2001)

ELSEVIER

Solid State Ionics 145 (2001) 387–397

SOLID STATE IONICS

www.elsevier.com/locate/ssi

Speculations on the existence of hydride ions in proton conducting oxides

Finn W. Poulsen *

Materials Research Department, Risø National Laboratory, DK-4000 Roskilde, Denmark

Received 25 September 2000; received in revised form 6 March 2001; accepted 6 April 2001

Abstract

The chemical and physical nature of the hydride ion is briefly treated. Several reactions of the hydride ion in oxides or oxygen atmosphere are given. A number of perovskites and inverse perovskites are listed, which contain the H^- ion on the oxygen or B-anion sites in the archetype ABO_3 system. H^- is stable with respect to oxide and halide anions but, among cations only with respect to oxides and halides of strongly electropositive metals such as alkaline, alkaline-earth and main group III metals. H^- is only stable in combination with transition metal ions of certain elements in their lowest positive oxidation state. Mixed oxide/hydride containing perovskites may thus exist. Steinsvik et al. have recently suggested a defect model for a perovskite including substitutional hydride ions on the oxygen site, $H_O^{\bullet}$, and protons associated with a lattice oxygen, $OH_O^{\bullet}$. The defect equations for this acceptor doped A(II)B(IV)O_3 model compound are solved without using the conventional Brouwer approximations. One case is presented where hydride formation is suppressed, and another case where it is promoted. Plots of concentration versus water and oxygen partial pressures show new interesting features; these are discussed.

Keywords: Stability; Defect modelling; Perovskite; Inverse perovskites; Proton; Hydride ion; Strontium titanate

1. Introduction

The hydride ion, H^-, has a similar size to the F^- and O^{2-} ion (Table 1). Hydride-containing compounds thus exist, which bear a direct structural resemblance to the corresponding oxides and fluorides. Perovskites analogous to ABO_3, but with H^- on the O-site of the $CsCaH_3$ type structure are now well established [1]. The International Centre for Diffraction Data (ICDD) data-base cites 7 cubic ($Pm\bar{3}m$) hydrides of this family, where the A-ion is Li^+, K^+ and Rb^+, and Be^{2+}, Mg^{2+}, Ca^{2-} or Ba^{2+} are on the B-site. Further, ICCD cites 14 perovskite-related orthorhombic (Pnma) trihydrides. An example of an inverse perovskite with the hydride/deuteride ion on the B-site is $Pd_3MnD_{0.7}$ [2], where D^- is surrounded by an octahedron of palladium ions.

A literature search for compounds containing both hydride and oxide ions finds few examples. Lanthanum hydride-oxide, LaHO, synthesised from $LaH_{2.5}$ and La_2O_3 at 900°C under hydrogen, appears to be a genuine mixed hydride-oxide [3]. Malaman and Brice [3] reported on its formation and deter-

* Fax: +45-46-77-5758.
E-mail address: finn.willy.poulsen@risoe.dk (F.W. Poulsen).

0167-2738/01/$ - see front matter
PII: S0167-2738(01)00935-3

Table 1
Characteristics of hydrogen in its three oxidation states

Bond lengths [10]
H_2: 0.74 Å, OH^-: 1.23–1.37 Å
H^-–O^{-2}: 2.75–2.99 Å in LaHO [3]
Ionic radii [11]
H^-: 2.08 Å in the free ion;
1.42 ± 0.09 Å in alkaline and earth alkaline hydrides
H^O: 0.3–0.37 Å
H^+: nucleus 1.5×10^{-5} Å [2]
F^-: 1.33 Å
O^{2-}: 1.40 Å
OH^-: 1.32–1.37 Å

Other ions of light elements and OH^- are shown for comparison.

mined its fluorite superstructure in 1984, with oxygen–hydrogen distances in the range 2.75–2.99 Å. This rules out the presence of 'normal' OH-groups, which have bond lengths in the range 0.97–1.37 Å (Table 1). LaHO is extremely hygroscopic and will liberate hydrogen in contact with H_2O [3]. The ICDD also reports some partially hydrided oxidic materials such as $Ti_xFeO_yH_{2.3-2.8}$, where $x = 2.3$ and $y = 0.2$ or 1 (ICCD #36-1385 and #36-1387) and $Al_3H_{4.8}O_{0.5}Zr$ [4]. These materials are also probably mixed hydride-oxides.

Two recent examples of stable hydride ions in oxides are given in the crystallographic papers by Huang and Corbett: $Ba_3(AlO_4)H$ (which is also an inverse perovskite with H^- on the B-site) and the $Ba_{21}Ge_2O_5H_{24}$ type compounds [5,6]. These materials can only be synthesised under extremely reducing conditions: the reactants BaH_2, BaO and Al_2O_3/GeO_2 are sealed under 1 atm of H_2 in a tantalum container and in the presence of metallic Ba. Experimental and theoretical studies of H^- ions in MgO, made by thermochemical reduction, have recently been reported by Monge et al. [7].

The impetus for the present study comes from the work of Steinsvik et al. [8]. They observe a change of sign of the EMF of a water vapour concentration cell with $SrTi_{1-x}Fe_xO_{3-x/2}$ as the membrane material at low pO_2 and 700–1000°C. It is alarming that this occurs at $pO_2 \sim 10^{-18}$ atm, where one would not expect hydride ions to be stable. A change of sign of the hydrogen species (from H^+ to H^-), could indeed result in the observed sign change of the EMF, but Steinsvik et al. [8] admit that alternative explanations must also be investigated. Gorelov et al. [9] have tentatively suggested that some peculiarities in conductivity data on doped $SrTiO_3$ may be explained by protons being transported as OH^- ions.

The existence of at least a few well-documented mixed hydride-oxide phases, as quoted above, leads us to assume that many more such compounds can exist.

The present speculative paper has two parts. First, some general properties and reactions of the hydride ion are described, along with some rules of thumb as to with which cations (oxidation states) the hydride ion may coexist. In the second part an exercise is performed: if hydride ions are assumed to be present in a perovskite structure oxide in some temperature–partial pressure regime, how would one then model their presence by conventional defect chemistry? Two model calculations on an acceptor doped $A(II)B(IV)_{0.8}Mf(III)_{0.2}O_{3-\delta}$ perovskite in equilibrium with both oxygen and water vapour are presented and discussed. Some hints as to how to calculate Brouwer diagrams for this rather complex defect model are given in Appendices A and B.

2. General behaviour of the H^- ion

Hydrogen gas, H_2, is not a very reducing substance, compared to the alkaline or earth alkaline metals or the hydride ion. In the electrochemical series (taken from aqueous chemistry [10]), the alkali metals span the range −3.02 V (Li,Cs) to −2.71 V (Na), the earth alkali metals lie in the range −2.9 V (Ba) to −1.70 V (Be). The estimated standard potential for the H^-/H_2 couple is −2.25 V versus the H_2/H^+ standard electrode (≡ 0 V). This is comparable to −2.37 V for Mg/Mg^{2+} making H^- one of the most powerful reducing agents known (citation from Ref. [10], p. 119). Many metal hydrides form easily, but this is more a result of the very electropositive nature of the metal from which the hydrides are made, along with a stabilising lattice energy, than a consequence of hydrogen being especially reducing.

Table 2
Two sets of equilibrium constants for perovskites containing protons and hydride ions

	K_i	K_O [atm$^{-1/2}$]	K_w [atm^{-1}]	K_H
Case 1: protons promoted, hydride ions suppressed (Figs. 1, 3 and 4)	10^{-11}	1.5×10^{-5}	10	10^{-20}
Case 2: protons suppressed, hydride ions promoted (Figs. 2, 5, 6 and 7)	10^{-11}	1.5×10^{-5}	10^{-6}	10^{-6}

The simulated Brouwer diagrams are all for an Fe-doping of $x = 0.2$.

The question of the stability of hydride ions in crystals can be restated as follows. Is the combination in a crystal of elemental Mg and a somewhat more noble metal ion, M^{z+}, in a high oxidation state a stable combination? The answer is generally 'no'. Irrespective of the external partial pressure with which the solid is equilibrated, an internal redox 'neutralisation' has a strong driving force, leading to Mg^{2+} and, for instance, $M^{(z-2)+}$.

Various properties of elemental hydrogen, hydride ion, the proton, OH^-, O^{-2} and F^- are given in Table 1. The electron configuration of H^-, $1s^2$, is identical to that of He; and the hydride ion is therefore colourless. Saline hydrides such as LiH and MgH_2 are sometimes not colourless, but greyish or darker, and this is a result of nonstoichiometry. The average ionic radius for H^- in alkali-hydrides and earth alkali hydrides is 1.42 Å, which is close to that of the oxide ion in sixfold coordination, 1.40 Å [11]. One of the more striking facts in Table 1 is that protons attached to an oxide ion, thus forming a hydroxyl ion, result in a shrinkage of the apparent ionic radius compared to O^{2-}, corresponding to an apparent negative radius of the proton.

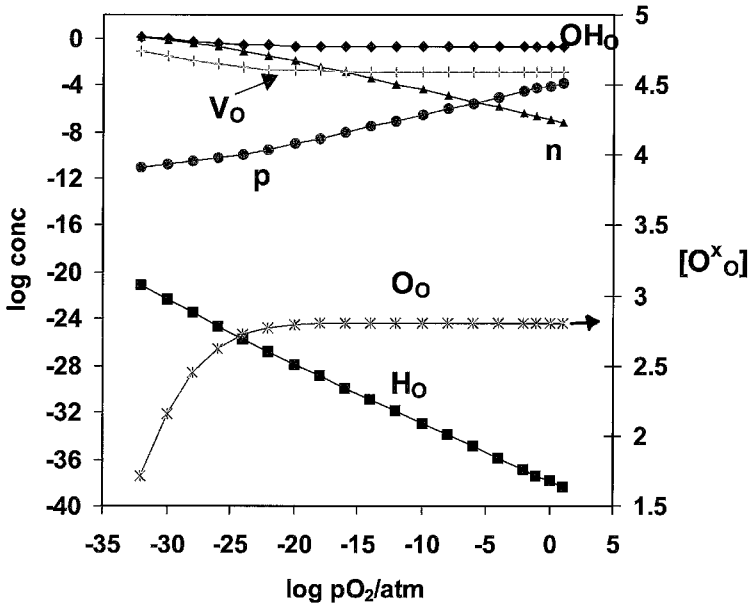

Fig. 1. Brouwer diagram for a perovskite containing protons, $OH_O^{\bullet}$, and oxygen vacancies, $V_O^{\bullet\bullet}$, as majority defects and hydride ions, $H_O^{\bullet}$, as minority defects. Equilibrium constants corresponding to case 1 of Table 2, $pH_2O = 1$ atm. Defect equation solved as in Appendix B.

Some examples of H^--consuming reactions, which will be strongly displaced to the right, are given below. The thermodynamic quantities ΔH_r and ΔS_r for these reactions will not be given.

$$2H^- + 1/2O_2 \Rightarrow H_2 + O^{2-} \quad (1)$$

$$H^- + O^- \Rightarrow O^{2-} + 1/2H_2. \quad (2)$$

Alternatively, using electron holes

$$H^- + h^\bullet \Rightarrow 1/2H_2. \quad (3)$$

Redox reactions with cations in high oxidation states, e.g.

$$2H^- + Pd^{4+} \Rightarrow H_2 + Pd^{2+} \quad (4)$$

or, involving a hypothetical hydride

$$'PdH_4' \Rightarrow H_2 + PdH_2. \quad (5)$$

We can conclude from the above cases and from general knowledge of Inorganic Chemistry (without explicitly proving it) that hydride ions are not stable in an oxidising environment, i.e. at high pO_2 and/or in the presence of cations in high oxidation states. This leaves only the cations of electropositive main-group metals, and transition-metals in their lowest positive oxidation states as candidate components of hydride-oxide systems. The existence of LaHO leads us to believe that H^- is also stable towards rare earth $+2$ and $+3$ cations. Among anions, we can choose between halide ions, X^-, and oxide ions. In the present context, it is thus improbable that trivalent iron and tetravalent titanium in $SrTi_{1-x}Fe_xO_{3-d}$ will coexist with H^- in the structure at $pO_2 = 10^{-18}$ atm [8].

What would be the maximum pO_2 at which H^- might exist in a crystal? This question is not easy to answer since, among other things, the stabilising lattice energy for a hydride ion in an oxide host lattice is at present unknown. If, for instance, we wish to form the mixed perovskite phase $SrTiO_{2.5}H_{0.5}$

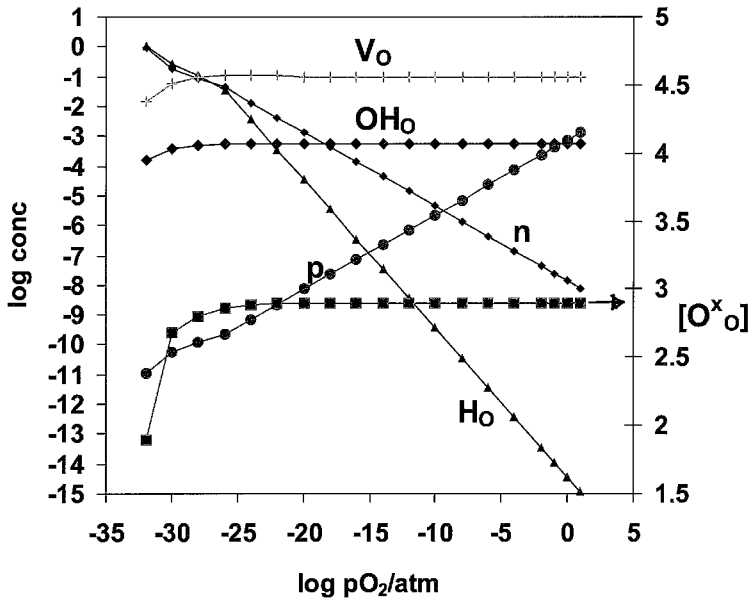

Fig. 2. Brouwer diagram for a perovskite containing protons, $OH_O^\bullet$ as minority defects ($[OH_O^\bullet] < 5.4 \times 10^{-4}$ mol fraction) and oxygen vacancies, $V_O^{\bullet\bullet}$, as majority defects. Hydride ions, $H_O^\bullet$, become majority defects below $pO_2 \approx 10^{-25}$ atm. Equilibrium constants corresponding to case 2 of Table 2, $pH_2O = 1$ atm. Defect equation solved as in Appendix B.

(where the average oxidation state of titanium is +3.5), it has to involve a redox reaction with oxygen, i.e.

$$1/4\,SrH_2 + TiO_2 + 3/4\,SrO \Leftrightarrow SrTiO_{2.5}H_{0.5} + 1/8\,O_2. \quad (6)$$

The problem of assessing the thermodynamics of this reaction from a Born–Haber cycle calculation is that the lattice energy of an analogous perovskite with hydride and oxide ions does not exist. In order to estimate the relative stability of hydrides versus oxides, Steinsvik et al. [8] take the oxidation of strontium hydride as an example

$$SrH_2(\text{solid}) + O_2(\text{gas}) \Leftrightarrow Sr(OH)_2(\text{solid}). \quad (7)$$

At the hypothetical temperature 1000°C, they estimate $\Delta H_r \sim -800 \pm 100$ kJ/mol and $\Delta S_r \sim -120$ J/K/mol. This leads to an equilibrium pressure of oxygen of $10^{-25.7}$ atm in contact with the two phases. Above this pressure, the hydride phase should be completely oxidised to $Sr(OH)_2$.

A second key question relating to the stability problem is the following: to what extent are the following equilibria displaced to the right?

$$H^- + H^+ \Leftrightarrow H_2(\text{gas}). \quad (8)$$

Rewriting this in two alternative ways

$$H^- + OH^- \Leftrightarrow O^{2-} + 1/2H_2 \quad (9)$$

or

$$H^- + H_2O \Leftrightarrow H_2 + OH^-. \quad (10)$$

In other words, can the positive and negative oxidation state of hydrogen coexist at some partial pressure in any significant concentration? We can here make an analogy to small band-gap semiconductors: relatively large concentrations of electrons and electron holes can coexist in the solid; likewise, the auto-dissociation of a molecule into a basic anion and an acidic cation can differ by several orders of magnitude in equilibrium constant. It is thus theoretically possible for H^- and H^+ to coexist, if this is favoured by the host lattice.

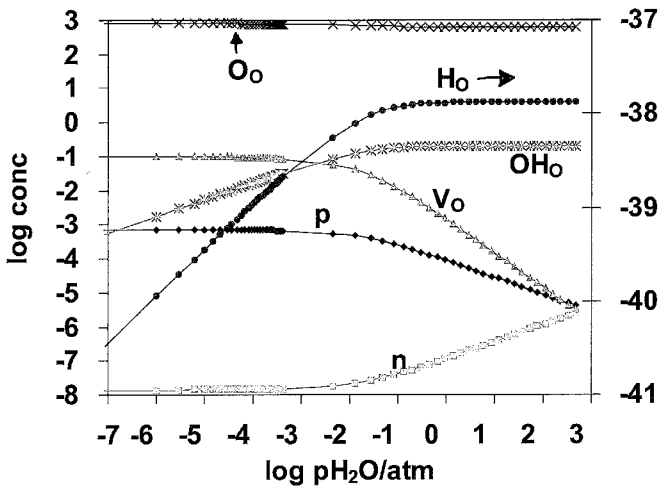

Fig. 3. Water partial pressure dependence of defect concentrations at $pO_2 = 1$ atm. Case 1. The left hand axis is linear for the oxygen concentration. Defect equations solved by the sequential procedure described in Appendix A.

3. A general defect model for protons and hydride ions in a perovskite

We will limit the treatment to a B-site doped perovskite, where cation vacancies are absent or can be neglected due to their very low concentration ($< 10^{-12}$ mol fraction). Protons will, in this model, be assumed to reside most of their time on a lattice oxygen ion, $OH_O^{\bullet}$. Because of their size, hydride ions can, if present, be assumed to occur as substitutional defects on the oxygen sub-lattice. Since the negative charge of H^- is one less than that of the oxygen ion, it becomes positively charged in K.V. notation, $H_O^{\bullet}$. In summary, we consider the following nine species in the lattice, taking $SrTi_{1-x}Fe_xO_{3-d}H_e$ as an example: O_O^x, $V_O^{\bullet\bullet}$, $OH_O^{\bullet}$, $H_O^{\bullet}$, Sr_A^x, Fe'_B, Ti_B^x, $h^{\bullet}$ and e'. Note that the iron dopant is forced to have a fixed +3 valency in this model; sub- and hyper-oxygen stoichiometry can be accounted for by electrons, e', and electron holes, $h^{\bullet}$, respectively.

This defect model has already been suggested by Steinsvik et al. [8], who construct a Brouwer diagram (log(conc) versus log pO_2) utilising conventional Brouwer approximations. A complete algorithm for a numerical solution to Brouwer diagrams in the log(conc)–log pH_2O plane is given in Appendix A, and exact numerical calculations of log(conc) versus log pO_2 plots will be outlined in Appendix B.

The nine equations describing the model system are:

$$\text{A-site: } Sr_A = 1 \tag{11}$$

$$\text{B-site: } Fe'_B + Ti_B^x = 1 \tag{12}$$

$$\text{O-site: } [O_O^x] + [V_O^{\bullet\bullet}] + [OH_O^{\bullet}] + [H_O^{\bullet}] = 3 \tag{13}$$

$$\text{Electroneutrality: } 2[V_O^{\bullet\bullet}] + [OH_O^{\bullet}] + [H_O^{\bullet}] + p = n + [Fe'] \tag{14}$$

$$\text{Mass: } Fe'_B = x. \tag{15}$$

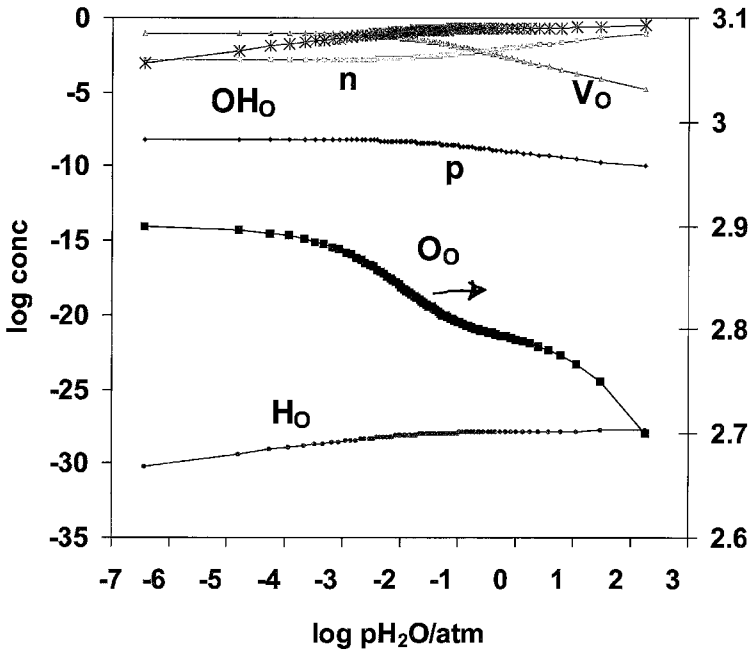

Fig. 4. Water partial pressure dependence of defect concentrations at $pO_2 = 10^{-20}$ atm. Case 1. Defect equations solved by the sequential procedure described in Appendix A.

The equations express site, electroneutrality and mass conservation.

Mass law expressions:

$$K_i = n \cdot p \text{ from nil} \Leftrightarrow h^{\bullet} + e' \quad (16)$$

$$K_O = p^2[O_O^x]/\left(pO_2^{1/2}[V_O^{\bullet\bullet}]\right)$$

$$\text{from } 1/2O_2(\text{gas}) + V_O^{\bullet\bullet} \Leftrightarrow 2h^{\bullet} + O_O^x \quad (17)$$

$$K_W = [OH_O^{\bullet}]^2/\left(pH_2O[O_O^x][V_O^{\bullet\bullet}]\right)$$

$$\text{from } H_2O(\text{gas}) + O_O + V_O^{\bullet\bullet} \Leftrightarrow 2OH_O^{\bullet} \quad (18)$$

$$K_H = [H_O^{\bullet}][O_O^x]/\left(n^2[V_O^{\bullet\bullet}][OH_O^{\bullet}]\right) \text{ from}$$

$$V_O^{\bullet\bullet} + OH_O^{\bullet} + 2e' \Leftrightarrow H_O^{\bullet} + O_O^x. \quad (19)$$

4. Simulation of Brouwer diagrams for perovskites containing hydride ions

Two limiting cases will be treated: a situation in which hydride ions are present only as a minority species, the concentration of which never exceeds 10^{-20} atomic fraction on the O-site; secondly, a situation where hydride-ion formation is promoted by changing the magnitude of the equilibrium constants K_w and K_H dramatically (see Table 2). In the latter case, the $H_O^{\bullet}$ concentration reaches unity, as does the electron concentration at low pO_2.

The author is well aware that the very low concentrations of certain species shown in Figs. 1–7 are not meaningful from a statistical thermodynamics viewpoint. The equilibrium constants have, however, been chosen such that clearcut behaviour of one or the other type result from the simulations.

Fig. 1 shows a calculation of defect concentrations for a case, where hydride-ions are present in a very small amount. They otherwise do not influence the defect chemistry of the perovskite. The slope of $\log[H_O^{\bullet}]$ versus $\log pO_2$ is $-1/2$. At the relatively high water partial pressure of 1 atm, the $[OH_O^{\bullet}]$ concentration saturates at 0.197 mol fraction ($\approx$ the

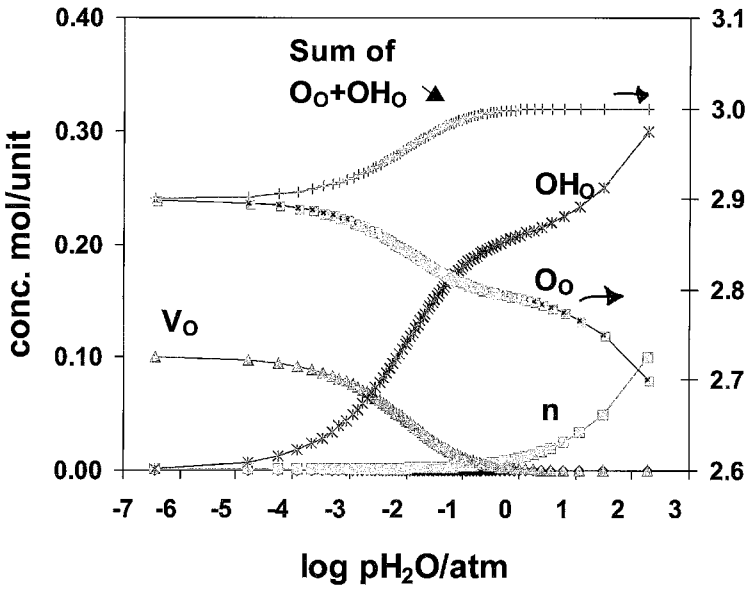

Fig. 5. Water partial pressure dependence of defect concentrations at $pO_2 = 10^{-20}$ atm. Case 1. Defect equations solved by the sequential procedure described in Appendix A. Same data as in Fig. 4, but plotting on linear axes and the p and $[H_O^{\bullet}]$ curves omitted because of their low concentrations ($\approx 10^{-8}$ and $\approx 10^{-27}$, respectively).

Fe-doping level $x = 0.2$). At $pO_2 < 10^{-18}$, there will be a slight increase of $[OH_O^\bullet]$, exceeding the doping level and compensated for by electrons.

Fig. 2 shows a defect situation where $[OH_O^\bullet]$ at $pH_2O = 1$ atm never exceeds 5.4×10^{-4}. The maximum $[OH_O^\bullet]$ concentration occurs around $pO_2 \approx 10^{-24}$ atm, where the $[V_O^{\bullet\bullet}]$ concentration has a weak maximum of 0.105 mol fraction. The maxima are so indistinct that they are barely detectable in log(conc) plots. Such behaviour has not, however, been reported previously for any defect model. It is an understandable outcome of the somewhat complex model, where four different species 'compete' for the same O-site in the lattice: O_O^x, $V_O^{\bullet\bullet}$, $OH_O^\bullet$ and $H_O^\bullet$. Slopes of n and p are $-1/4$ and $+1/4$, respectively. The hypothetical nature of the calculations is clear from the fact that solutions are found for perovskites with extreme stoichiometries: at $pO_2 = 10^{-30}$ atm the phase composition should be $SrTi_{0.8}Fe_{0.2}O_{1.8922}H_{1.0927}$ and with an electron concentration of 0.9226 per formula unit. Tetravalent Ti will certainly not be stable under such reducing conditions (both e′ and $H_O^\bullet$).

Figs. 3–6 show the defect concentrations as functions of the partial pressure of water, simulated with the same two sets of equilibrium constants. The defect situations at $pO_2 = 1$ and 10^{-20} atm are displayed. Figs. 3 and 4 show the case of hydride-ions as minority species, irrespective of the oxygen partial pressure. The slopes of the $OH_O^\bullet$- and $H_O^\bullet$ – curves are again $1/2$ at low p_{water}, and both $[OH_O^\bullet]$ and $[H_O^\bullet]$ saturate at $pH_2O > 0.1$ atm. In Fig. 3, the $OH_O^\bullet$ concentration reaches 0.2 mol fraction at high water pressure.

In Fig. 4, we see that the $OH_O^\bullet$ concentration at 100 atm H_2O approaches 0.3, i.e. higher than the Fe-doping concentration of 0.2. This is shown more clearly in Fig. 5, using linear concentration axes. The $OH_O^\bullet$ concentration exceeding 0.2 is possible, since approximately 0.1 mol fraction of electrons are also present. The shape of the $[OH_O^\bullet]$ versus log pH_2O plot has a rather interesting shape, with two types of region, one above and one below $[OH_O^\bullet] \approx 0.2$. This is just one of the consequences of the present defect model, and must *not* be interpreted as an indication of a two-site proton model [15].

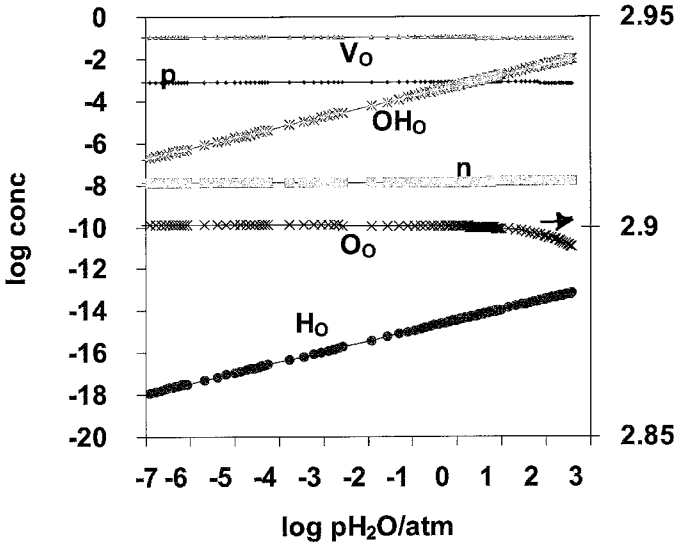

Fig. 6. Water partial pressure dependence of defect concentrations at $pO_2 = 1$ atm. Case 2. Defect equations solved by the sequential procedure described in Appendix A.

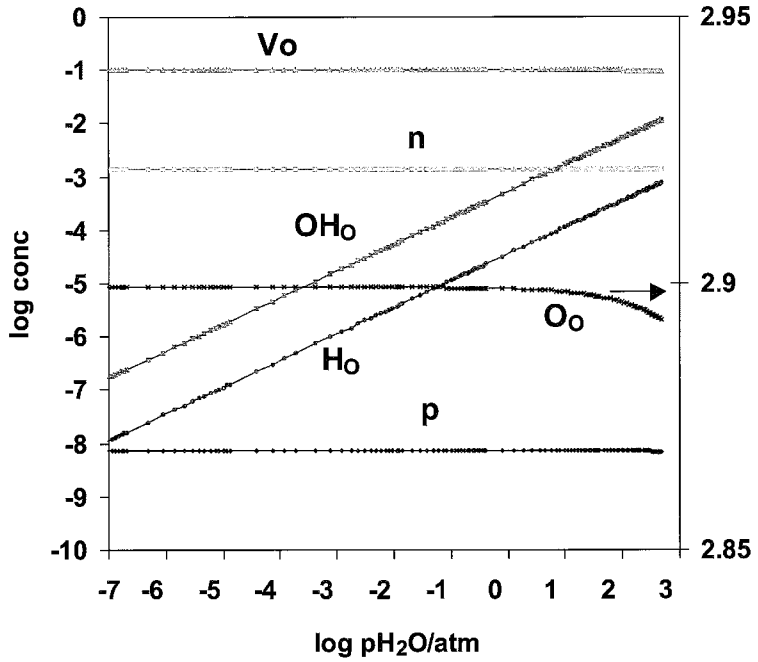

Fig. 7. Water partial pressure dependence of defect concentrations at $pO_2 = 10^{-20}$ atm. Case 2. Defect equations solved by the sequential procedure described in Appendix A. Note: the $[O_O^x]$ concentration is plotted on a linear axis.

Fig. 6 shows a situation where the material is p-type and the protonic content is 11 orders of magnitude higher than the hydride concentration, irrespective of the water activity. In Fig. 7, the material is n-type at $pO_2 = 10^{-20}$ atm, and the proton concentration is now only 10 times higher than the hydride concentration. It is seen in Figs. 6 and 7 that the $OH_O^\bullet$ and $H_O^\bullet$ concentrations both increase with increasing water partial pressure, and gradually replace O_O^x and $V_O^{\bullet\bullet}$. The two species can therefore coexist in fairly high concentrations according to the present defect model.

5. Final remarks

A literature review has ascertained that mixed hydride-oxide compounds exist. Perovskite and fluorite structures, which are known to be good host lattices for ionic conduction, may be formed to include hydride-ions, although only a limited number of cations are stable with respect to H^-. Synthesis work will be initiated in the near future. This group of materials will have no application in high temperature devices in wet atmospheres such as fuel cells, but their use as hydrogen sources in ambient temperature batteries cannot be ruled out. No estimate of the possible mobility of hydride ions has been attempted in the present paper. Spectroscopic and electrical methods need to be developed for characterisation of hydride ions and hydride-ion transport in oxides.

Acknowledgements

S. Steinsvik, Y. Larring and T. Norby of Oslo University are thanked for giving me access to their

paper on Fe-doped $SrTiO_3$ prior to publication. The Nordic Energy Research Programme for electrochemical energy conversion has made frequent consultations with the Oslo University group possible. The present study has been carried out in part under the INTAS-project #99-0636 on 'Hydrogen in oxide systems: fundamentals and promising applications'. Financial support from the DK-SOFC programme is finally acknowledged.

Appendix A. Solution of defect equations at specified pO_2

An analytical solution to the set of nine equations, Eqs. (11)–(19), becomes extremely complicated, if not impossible due to (i) the inclusion of four mass law expressions, and (ii) the presence of four different species on the O-site. The sequential method used to solve this system of equations by guessing of one of the concentrations is, however, surprisingly simple. More details on the application of the sequential technique are described for the protonic conductor $SrCe_{1-x}Y_xO_{3-\delta}$ in Ref. [12], La(Sr)$MnO_{3\pm\delta}$ [13] and pyrochlore structure oxides [14]. The method is based on solving the set of equations with one concentration as the independent variable and the remaining concentrations and pO_2 (or pH_2O) as the dependent variables. A value for the electron hole concentration, p, is assumed; from which follows $n = K_i/p$. The trivial solutions for the cation concentrations are: $[Sr_A] = 1$, $[Ti_B] = 1 - x$, and $[Fe'_B] = x$.

The unknown concentrations are now $[O_O]$, $[OH_O^\bullet]$, $[V_O^{\bullet\bullet}]$ and $[H_O^\bullet]$. By subtracting the electroneutrality equation and the oxygen site equation, Eqs. (13) and (14)

$$2[V_O^{\bullet\bullet}] + [OH_O^\bullet] + [H_O^\bullet] + p = n + [Fe'] = p/K_i + x \quad (A1)$$

$$[O_O^x] + [V_O^{\bullet\bullet}] + [OH_O^\bullet] + [H_O^\bullet] = 3 \quad (A2)$$

we obtain

$$[V_O^{\bullet\bullet}] + p - [O_O^x] = K_i/p + x - 3 \quad (A3)$$

or

$$[O_O^x] = [V_O^{\bullet\bullet}] + p - K_i/p - x + 3. \quad (A4)$$

This is inserted into the expression for K_O

$$K_O = p^2\{[V_O^{\bullet\bullet}] + p - K_i/p - x + 3\} / (pO_2^{1/2}[V_O^{\bullet\bullet}]) \quad (A5)$$

which then has only one unknown, $[V_O^{\bullet\bullet}]$, assuming that the partial pressure of oxygen is specified along with the electron-hole concentration p. Eq. (A5) is linear in $[V_O^{\bullet\bullet}]$ and is solved. It follows immediately that

$$[O_O^x] = K_O PO_2^{1/2}[V_O]/p^2 \quad (A6)$$

$$[OH_O^\bullet] = (3 - [O_O^x] - [V_O^{\bullet\bullet}]) / (1 + K_{II}n^2[V_O^{\bullet\bullet}]/[O_O^x]) \quad (A7)$$

$$[H_O^\bullet] = K_H n^2 [V_O^{\bullet\bullet}][OH_O^\bullet]/[O_O^x]. \quad (A8)$$

Finally, the equivalent partial pressure of water is calculated from Eq. (18).

The calculation is repeated for many values of p in the interval 10^{-20}–1. The numerical errors using this procedure can be estimated by checking the electroneutrality condition. Typically, the difference Σnegative charge $-\ \Sigma$positive charge is 10^{-16}–10^{-35}, i.e. essentially zero. The procedure was used to generate the data for Figs. 3–6.

Appendix B. Solution of the defect equations at specified pH_2O

The sequential solution method, as applied in Appendix A fails for the present case. The nine equations, Eqs. (11)–(19), were inserted into the equation solver program, EUREKA 1.0 from Borland International, and solved for one pair of (pO_2, pH_2O) values at a time. The programme finds the nine concentrations by a minimisation procedure, where the sums of the squares of the differences of left-hand and right-hand sides of the nine equations are minimised. Great care is required in specifying proper starting values for the unknowns. The numerical precision is comparable to the method in Appendix A. This procedure was used for generating Figs. 1 and 2.

References

[1] F. Gingl, T. Vogt, E. Akiba, K. Yvon, J. Alloys Compd. 282 (1999) 125–129.
[2] P. Onnerud, Y. Andersson, R. Tellgren, P. Nordblad, F. Bouree, G. Andre, Solid State Commun. 101 (1997) 433–437.
[3] B. Malaman, J.F. Brice, J. Solid State Chem. 53 (1984) 44–54.
[4] N. Clark, E. Wu, J. Less-Common Met. 142 (1988) 145–154.
[5] B.Q. Huang, J.D. Corbett, J. Solid State Chem. 141 (1998) 570–575.
[6] B.Q. Huang, J.D. Corbett, Inorg. Chem. 37 (1998) 1892–1899.
[7] M.A. Monge, R. Gonzalez, A.I. Popov, R. Pareja, Y. Chen, E.A. Kotomin, M.M. Kuklja, Defect Diffus. Forum 170 (1999) 1–11.
[8] S. Steinsvik, Y. Larring, T. Norby, Solid State Ionics 143 (2001) 103–116.
[9] V.P. Gorelov, V.B. Balakireva, N.V. Sharova, Russ. J. Electrochem. 35 (1999) 400–405.
[10] F.A. Cotton, G. Wilkinson, Advanced Inorganic Chemistry. Fifth edn., Wiley, NY, 1988.
[11] R.D. Shannon, Acta Crystallogr. A 32 (1976) 751–767.
[12] F.W. Poulsen, J. Solid State Chem. 143 (1999) 115–121.
[13] F.W. Poulsen, Solid State Ionics 129 (2000) 145–162.
[14] F.W. Poulsen, M. Glerup, P. Holtappels, Solid State Ionics 135 (2000) 595–602.
[15] B. Gross, St. Marion, K. Lind, D. Grambole, F. Herrmann, R. Hempelmann, Solid State Ionics 125 (1999) 107–117.

A9.

Marianne Glerup, Ole Faurskov Nielsen and Finn W. Poulsen

The structural transformation from the Pyrochlore structure, $A_2B_2O_7$, to the Fluorite structure AB_2, studied by Raman Spectroscopy and Defect Chemistry Modelling,

J. Solid State Chem. **160** (1): 25-32 (2001)

Journal of Solid State Chemistry **160**, 25–32 (2001)
doi:10.1006/jssc.2000.9142, available online at http://www.idealibrary.com on IDEAL®

The Structural Transformation from the Pyrochlore Structure, $A_2B_2O_7$, to the Fluorite Structure, AO_2, Studied by Raman Spectroscopy and Defect Chemistry Modeling

Marianne Glerup,*,[1] Ole Faurskov Nielsen,* and Finn Willy Poulsen†

** Department of Chemistry, University of Copenhagen, Universitetsparken 5, DK-2100 Copenhagen Ø, Denmark; and †Materials Research Department, Risø National Laboratory, Frederiksborgvej 399, DK-4000 Roskilde, Denmark*

Received November 9, 2000; in revised form March 7, 2001; accepted March 15, 2001; published online June 7, 2001

Pyrochlore oxides of the composition $Y_2Ti_{2-y}Zr_yO_7$, with $y = 0$, 0.3, 0.6, and 0.9, were studied using Raman spectroscopy. Doping with Zr^{+4}, a homovalent ion, gradually induces the material to undergo a structural change from the perfect pyrochlore structure to a defect pyrochlore structure and ends at an oxygen deficient fluorite structure with the formula $(Y, Ti, Zr)_1O_{1.75}$. Invoking the bigger Zr^{+4} ion on the Ti^{+4} site causes this structural transformation. We have also investigated highly Ti-doped YSZ ceramic samples, which all have an oxygen deficient cubic fluorite structure. These samples have formula units between $(Y, Ti, Zr)_1O_{1.675}$ and $(Y, Ti, Zr)_1O_{1.90}$. It is argued that a band observed at 750 cm^{-1} in both the Ti-doped pyrochlore samples and in the Ti, Y, Zr fluorite samples is due to oxygen in seven fold coordination around Ti. Local structures are accordingly observed by Raman in these samples. We finally report a Raman spectrum of orthorhombic Y_2TiO_5. A defect chemistry model has been formulated, which qualitatively describes the observed pyrochlore–fluorite structural transition.

INTRODUCTION

Perfect pyrochlore oxides, $A_2B_2O_7$, are cubic with two different types of oxygen ions. The A ion is coordinated to 8 oxygen atoms and the B ion is coordinated to 6 oxygen atoms. Neutron diffraction experiments on $Y_2Ti_{2-y}Zr_yO_7$ (1) has shown that when the Zr^{+4} concentration increases a third oxygen position will become occupied, corresponding to a defect pyrochlore structure. With $y = 0.9$ the oxide can be described as belonging to an oxygen defect cubic fluorite structure. The structural transformation is caused by the increase of the six-coordinated B-ion radius, $r(Ti^{+4}) = 0.605$ Å and $r(Zr^{+4}) = 0.72$ Å (2). Compounds with fluorite structures have the general formula AO_2, where the A ion is coordinated to 8 oxygen atoms. Cubic yttria-stabilized-zirconia (YSZ) materials with the fluorite structure have been studied for many years because of their application as an electrolyte for solid oxide fuel cells (SOFC) (3). In doped zirconias the average cation-oxygen coordination numbers are between 6 and 8. The highly doped Ti-YSZ oxides have also shown possibilities as an anode material for SOFC, because of the materials ability to act as a mixed conductor, i.e., an oxide ion conductor and electronic conductor (4, 9).

Cubic ZrO_2 and YSZ have in the $k = 0$ approximation only one allowed fundamental transition, F_{2g}, but in the Raman spectra of these compounds more bands are always observed (5, 16).

In this investigation we hope to increase the knowledge of the gradual structural transformation from a pyrochlore structure to the defect fluorite structure, and thus enhance our understanding of defect fluorite structures. To our knowledge it is the first time that Raman spectra of highly doped Ti-YSZ materials, the $Y_2Ti_{2-y}Zr_yO_7$ pyrochlores and Y_2TiO_5, are reported.

The complete ternary phase diagram for ZrO_2–$YO_{1.5}$–TiO_2 appears not to have been determined. We have tried to sketch a phase diagram in Fig. 1 from the published binary systems: ZrO_2–$YO_{1.5}$ (6) and TiO_2–ZrO_2 (7), and $YO_{1.5}$–TiO_2 (8) Also included in the figure are data from Kaiser *et al.* (9) on the composition range for cubic, fully stabilized zirconia with up to 20 mole% titania (shaded area). The broken lines indicate approximate limits for the solid solution ranges. The solid solution range around the pyrochlore composition $Y_2Ti_2O_7$ is only 2–3 mole% according to (8). The investigated compositions of the present work are marked by small filled squares and a star in Fig. 1. The composition $Y_{0.5}(Ti_{0.15}Zr_{0.35})O_{1.75}$ (marked with a star) lies well within the fluorite structure phase field, but also on the line for stoichiometric pyrochlore compositions starting

[1] To whom correspondence should be addressed. E-mail: marianne.glerup@risoe.dk.

0022-4596/01 $35.00

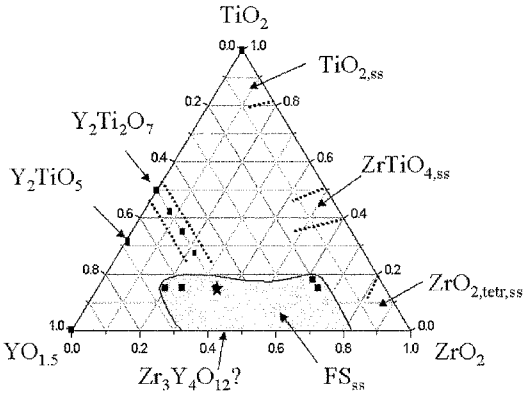

FIG. 1. Tentative ternary phase diagram for ZrO_2–$YO_{1.5}$–TiO_2 based on data in Refs. (6–9).

at $Y_2Ti_2O_7$. We initially asked ourselves the following crucial question: Will the Raman spectra of the pyrochlore series, moving from $Y_2Ti_2O_7$ toward the $Y_{0.5}(Ti_{0.15}Zr_{0.35})O_{1.75}$ composition gradually approach that of the disordered fluorite?

EXPERIMENTAL

Pyrochlore Materials

The ceramic samples were prepared by solid state synthesis (10). Ball milling was carried out of the oxides over night, followed by heating at 1400°C in air for 8 h. These procedures were repeated until single-phase materials were achieved. The following oxides were synthesized: $Y_2Ti_2O_7$, $Y_2Ti_{1.7}Zr_{0.3}O_7$, $Y_2Ti_{1.4}Zr_{0.6}O_7$, and $Y_2Ti_{1.1}Zr_{0.9}O_7$.

Fluorite Structures (Ti, Y) Doped ZrO_2

Preparation of the highly titania doped YSZ materials is described in Ref. (11) and the following compositions are investigated in this paper: $Y_{0.20}Ti_{0.15}Zr_{0.65}O_{1.90}$, $Y_{0.50}Ti_{0.15}Zr_{0.35}O_{1.75}$, $Y_{0.60}Ti_{0.15}Zr_{0.25}O_{1.70}$, and $Y_{0.65}Ti_{0.15}Zr_{0.20}O_{1.675}$.

Other Compositions

Y_2TiO_5 was made by solid state reaction between Y_2O_3 and TiO_2 at 1300°C, with three intermediate grindings and reheating. Laboratory grade (99.9%) rutile TiO_2 and cubic Y_2O_3 (Johnson–Matthey) were used.

X-Ray

X-ray powder diffraction was carried out on all the ceramic samples to check that the materials were single phase and to determine the lattice parameters. The X-ray diffraction experiments were done with white Cu radiation (1.2 kW) on a STOE θ–θ reflection diffractometer. An energy-dispersive Kevex detector was tuned to Cu$K\alpha$ (8.04 keV) with an energy window of 300 eV.

The structure analysis was carried out using the Rietveld program WinPLOTR (12).

NIR–FT–Raman

NIR–FT–Raman spectra were recorded on a Bruker model IFS 66 spectrometer equipped with a FRA 106 FT–Raman module using near infrared laser excitation (Nd:YAG, 1064 nm). A Ge detector, cooled to liquid nitrogen temperature, was used. All spectra were obtained in a 180° scattering configuration. The high-frequency detector cut-off was set at 3500 cm^{-1} (Raman shift), and a narrow band frequency filter removed the spectral features in the region from -100 to 84 cm^{-1} (Raman shifts). The laser output was 200 mW and the estimated spectral resolution was approximately 6 cm^{-1}.

VIS–Raman

The instrument used was a Dilor Z-24 Raman spectrometer equipped with a frequency-doubled Nd:YAG laser (532 nm). All spectra were measured in a 90° scattering configuration. Spectral width of 2.66 cm^{-1} and 200 mW laser power were used. All Raman spectra were recorded at room temperature.

RESULTS AND DISCUSSION

Phase Content

Unit cell parameters are given in Table 1, including fractional coordinates of the oxygens and occupancies for the four pyrochlore compositions obtained by Rietveld refinement. Vegard's law for the lattice parameter is perfectly obeyed. The trend in oxygen occupancy, as found in (1) could be confirmed by our X-ray data: the O(1) 48*f* position is gradually depopulated and the empty O(3) 8*b* position is being populated as the Zr content is increased, whereas the O(2) 8*a* position is kept fully populated. For the undoped pyrochlore, no refinement was made on the occupancies. For the doped compositions, the sum of the Zr and Ti was kept constant, but for the oxygen occupancies the refinement was done without restrictions, meaning that the sum of the oxygen content is not correct. A fully occupied position has by definition the occupancy = 1 in Table 1. The $\chi^2 = (R_{wp}/R_{exp})^2$ values for the fits in Table 1 were 3.1, 8.0, 6.1, and 16.0, respectively, for the compositions $y = 0$, 0.3, 0.6, and 0.9. The χ^2 values are rather large as expected for refinement on X-ray data obtained by a conventional powder diffractometer; however, the trends in both the

TABLE 1
Unit Cell Parameters for the Pyrochlore Samples

	$Y_2Ti_{2-y}Zr_yO_7$			
Site	$y = 0$	$y = 0.3$	$y = 0.6$	$y = 0.9$
a (Å)	10.0904	10.1385	10.1937	10.2367
	(0.0002)	(0.0003)	(0.0003)	(0.0003)
Y ion 16c (0,0,0)				
Occupancy	1.0000	1.0000	1.0000	1.0000
Ti ion 16d $(\frac{1}{2},\frac{1}{2},\frac{1}{2})$				
Occupancy	1.0000	0.8025	0.6516	0.4614
		(0.0096)	(0.0096)	(0.0118)
Zr ion 16d $(\frac{1}{2},\frac{1}{2},\frac{1}{2})$				
Occupancy	1.0000	0.1975	0.3484	0.5386
		(0.0096)	(0.0096)	(0.0118)
O(1) ion 48f $(x,\frac{1}{8},\frac{1}{8})$				
Occupancy	1.0000	0.9556	0.9259	0.9031
		(0.0175)	(0.0163)	(0.0175)
Fractional coordinate, x	0.4231	0.4189	0.4151	0.4100
	(0.0009)	(0.0006)	(0.0006)	(0.0008)
O(2) ion 8a $(\frac{1}{8},\frac{1}{8},\frac{1}{8})$				
Occupancy	1.0000	0.9777	0.9646	1.0008
		(0.0294)	(0.0282)	(0.0388)
O(3) ion 8b $(\frac{3}{8},\frac{3}{8},\frac{3}{8})$				
Occupancy	0.0000	0.0492	0.1303	0.3189
		(0.0236)	(0.0233)	(0.0357)

Note. The numbers in brackets are the standard deviations.

x coordinate and the occupancies were confirmed by starting with widely different starting values for these parameters.

The powder diffraction patterns of Y_2TiO_5 revealed that when cooled from 1300°C it has the orthorhombic structure described by Mummc and Wadsley (13) with 7-fold coordinated Y and 5-fold coordinated Ti. Samples cooled from 1550°C at ~100°C/h had very strong peaks from a high temperature disordered fluorite structure polymorph (7) with $a = 5.1496 \pm 0.0006$ Å, and only minor traces (<5%) of the low temperature phase were seen.

Factor Group Analysis and Expected Normal Modes

Cubic pyrochlores. Cubic pyrochlores, $A_2B_2O(1)_6O(2)$, belong to the space group ($Fd\bar{3}m$, O_h^7), no. 227, with $Z = 8$. The site symmetry is D_{3d} for A and B ions, C_{2v} for the O(1) ions, and T_d for the O(2) ion, which is in accordance with reference (14). Factor group analysis was made on the basis of the above site symmetries. The vibrational normal modes were predicted as follows, in accordance with (15)

$$\Gamma^{*2}_{\text{opt.}} = A_g^{(R)} + 3A_{2u}^{(i.a)} + E_g^{(R)} + 3E_u^{(i.a)} + 2F_{1g}^{(i.a)} + 7F_{1u}^{(IR)} + 4F_{2g}^{(R)} + 4F_{2u}^{(i.a)}$$

$$\Gamma_{\text{ac.}} = F_{1u}.$$

Raman active vibrations per set of ions were

A ion: *none*

B ion: *none*

O(1) ion: $A_g + E_g + 3F_{2g}$

O(2) ion: F_{2g}

Cubic fluorites. Cubic fluorites, AO_2, belong to the space group ($Fm\bar{3}m$, O_h^5), no. 225, where $Z = 4$. The site symmetry is O_h for the A ion and T_d for the O ion, the normal modes predicted are, in accordance with (16),

$$\Gamma_{\text{opt.}} = F_{1u}^{(IR)} + F_{2g}^{(R)}$$

$$\Gamma_{\text{ac.}} = F_{1u}$$

Raman active vibrations per set of ion are

A ion: *none*

O ion: F_{2g}.

Y_2TiO_5. Y_2TiO_5 belongs to the orthorhombic space group (*Pnma*, D_{2h}^{16}) no. 62 with $Z = 4$. The site symmetry is C_s for all the atoms: Y(1), Y(2), Ti(1), O(1), O(2), O(3), O(4), and O(5) according to (13).

The normal modes predicted are

$$\Gamma_{\text{opt.}} = 16A_g^{(R)} + 8A_u^{(i.a.)} + 8B_{1g}^{(R)} + 15B_{1u}^{(IR)} + 16B_{2g}^{(R)} + 7B_{2u}^{(IR)} + 8B_{3g}^{(R)} + 15B_{3u}^{(IR)}$$

$$\Gamma_{\text{ac.}} = B_{1u} + B_{2u} + B_{3u}.$$

Raman active vibrations per set of ion are

Y(1)-ion: $2A_g + B_{1g} + 2B_{2g} + B_{3g}$

and the same for the rest of the ions.

It is mentioned in Ref. (13) that Y_2TiO_5 could alternatively belong to the orthorhombic space group $Pn2_1a$, C_{2v}^9. The site symmetry for the ions would then be C_1 allowing all 93 normal modes to be active in the Raman spectrum. Since we only observe ~7 peaks in the spectrum we find it more likely that the low-temperature form of Y_2TiO_5 can be the more symmetric orthorhombic space group *Pnma*.

[2] (*) Denotes (R) Raman active, (IR) Infrared active, and (i.a.) inactive.

Reasons for Violation of the Selection Rules

More bands may be observed than predicted due to (i) a change of local symmetry or coordination numbers, e.g., from CN = 6 or 8 to CN = 5 or 7; (ii) a breakdown of the selection rules due to the presence of "foreign" atoms/ions allowing silent or IR-active modes to appear in the Raman spectrum, including combination tones with non-Raman active modes; (iii) allowance for $k \neq 0$ modes.

Gradual frequency changes, as the dopant level level is increased, may result from longer/shorter bond distances.

Spectra of Pyrochlore Samples

NIR-FT-Raman spectra of the undoped and doped pyrochlore oxides $Y_2Ti_2O_7$, $Y_2Ti_{1.7}Zr_{0.3}O_7$, $Y_2Ti_{1.4}Zr_{1.1}O_7$, $Y_2Ti_{1.1}Zr_{0.9}O_7$, and $Y_2Ti_{0.6}Zr_{1.4}O_7$ are shown in Fig. 2. The composition $Y_2Ti_{0.6}Zr_{1.4}O_7$ is more correctly described as a defect fluorite structure $(Y_{0.5}Ti_{0.15}Zr_{0.35})O_{2-0.5/2}$ and not as a pyrochlore structure. The above compositions are plotted in the same figure since they all lie on a straight line in the ternary phase diagram with the same oxygen content.

Raman frequencies for the undoped and doped pyrochlore oxides are shown in Table 2. The bands in the Raman spectra are tentatively assigned to symmetry species in Fig. 2 by comparing with previously published Raman spectra of pyrochlore oxides including $Y_2Ti_2O_7$ (17). The spectrum of single-crystal $Y_2Ti_2O_7$ in the I_{VV} geometry was shown Ref. (17), and therefore, the relative intensities are different from the intensities in the powder spectrum shown in the present work.

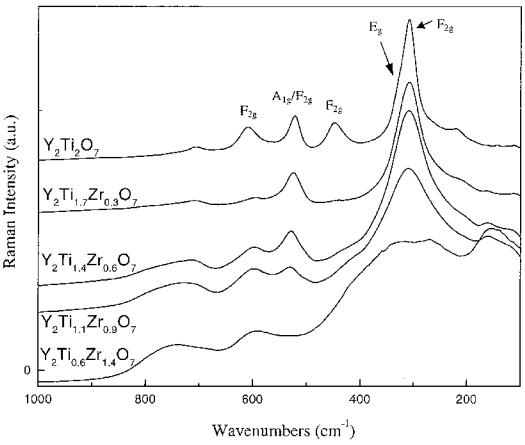

FIG. 2. NIR-FT-Raman spectra of the undoped and doped pyrochlore oxides: $Y_2Ti_2O_7$, $Y_2Ti_{1.7}Zr_{0.3}O_7$, $Y_2Ti_{1.4}Zr_{0.6}O_7$, $Y_2Ti_{1.1}Zr_{0.9}O_7$, and $Y_2Ti_{0.6}Zr_{1.4}O_7$.

TABLE 2
Observed Bands in the Raman Spectra for $Y_2Ti_{2-y}Zr_yO_7$

$Y_2Ti_2O_7$ (cm^{-1})	$Y_2Ti_{1.7}Zr_{0.3}O_7$ (cm^{-1})	$Y_2Ti_{1.4}Zr_{0.6}O_7$ (cm^{-1})	$Y_2Ti_{1.1}Zr_{0.9}O_7$ (cm^{-1})
221	~211	—	—
309	308	309	310
333	333	—	—
448	443	~420	~413
522	525	529	531
609	597	597	598
720	720	720	720
—	—	750	750

We can see from the factor group analysis made in this paper on pyrochlore structures that the cations do not contribute to the allowed fundamental transition, so doping with the Zr^{4+} ion on the *B* site will not directly influence the Raman spectra.

Although, it is observed that when Zr^{+4} is invoked in the structure, slight shifts of the vibrational frequencies are observed. Furthermore, the bands broaden and the peak intensities decrease.

In the Raman spectrum of the material with $y = 0.3$ the exact same peaks are observed as for the undoped pyrochlore oxide, but the $F_{2g} + A_{1g}$ band at ~309 cm^{-1} has broadened and the bands at 442 and 597 cm^{-1} have lost intensity. These trends are continually observed as the dopant concentration is increased. When $y = 1.4$ (a fluorite material) it looks like the F_{2g} and A_{1g} bands have split.

The neutron diffraction experiments (1) have shown that the occupancy of the O(2) position is unchanged up to $y > 0.9$. It is the occupancy at the O(1) site that is changing when the O(3) positions start to be occupied. A new band appears at 750 cm^{-1} as the dopant concentration reaches $y = 0.6$. It could look like a frequency shift of the 720 cm^{-1} band, but when the doping concentration is increased to 0.9 it is evident that it is actually a new vibrational band, which is observed. The band at 720 cm^{-1} is observed in all the Raman spectra presented in this work and has also been reported in undoped $Y_2Ti_2O_7$; it is assigned to be a combination band as was also argued in (17).

The broad band at ~750 cm^{-1} is therefore assigned to oxygen in a Ti–O_7 coordinated species. Although the average (*A* and *B*) cation–oxygen coordination number is 7 for all the compositions in the series, a shift occurs going from the perfect pyrochlore, where an equal amount of cations have, respectively, 6 and 8 coordination, in the case of disordered fluorites, where many—maybe not all cations —in reality have ~7 oxygen neighbors.

The band at 750 cm^{-1} is also observed for the highly Ti-doped YSZ but not in YSZ itself, see next paragraph, and here it is observed that the intensity of the band depends on

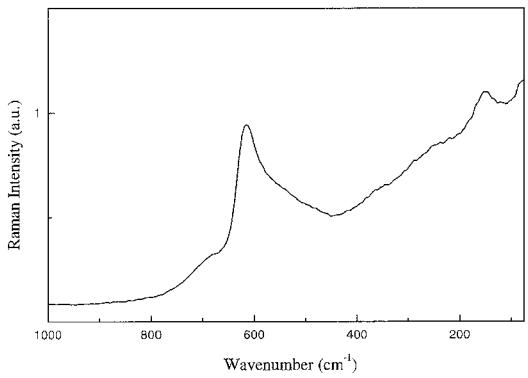

FIG. 3. NIR-FT-Raman spectrum of $Y_{0.18}Zr_{0.82}O_{1.91}$ (YSZ 10 mol%).

the Ti concentration. We conclude that the band is caused by a 1′ order vibrational transition and the reason for observing the band is that we observe local structures in the pyrochlore materials, which is in accordance with (15).

Fluorite Samples

Figure 3 shows the FT-Raman spectrum of a cubic 10 mol% yttria stabilized zirconia (10 mol% YSZ). The stoichiometric formula for this compound is $Y_{0.18}Zr_{0.82}O_{1.91}$. We observe no bands above 730 cm^{-1}, but also we observe more than the one allowed band predicted by factor group analysis. Figure 4 shows the VIS-Raman spectra of the highly doped Ti-YSZ samples. The composition $Y_{0.50}Zr_{0.35}Ti_{0.15}O_{1.75}$ was also shown in Fig. 2. A broad band with maximum at $\sim$745 cm^{-1} is observed. This is an additional proof for the 745 cm^{-1} bands belong to a Ti–O vibration. In these compounds, the cations have an average coordination to the oxygen on 7.6, 7.0, 6.8, and 6.7, respectively, going from high Zr content to low. The coordination number 7 corresponds directly to a disordered pyrochlore material.

The peak intensity at 620 cm^{-1} observed in the Raman spectra of Ti-YSZ and YSZ depends on the Zr^{+4} content, the band is very distinct when Zr > 0.60 w/w% but when Zr $\leq$ 0.35 w/w% it is not well resolved. This band is also observed in the 10 mol% YSZ sample. At the same time, the intensity for the peak at $\sim$490 cm^{-1} assigned to the F_{2g} mode for cubic ZrO_2 (18) decreases or disappears with decreasing Zr^{+4}-content, and is therefore not easily observable.

Previous studies of the Raman spectra of Ti-doped 8 mol% YSZ by Traqueia *et al.* (19) showed that two local structures were present, e.g., cubic and tetragonal. This is understandable since the Y-concentrations are lower than in the present study. The coexistence of the two local structures however could not be observed using X-ray diffraction. The authors correlated the band at 720 cm^{-1} to depend on the Ti^{+4} concentration and assigned the band to a $Ti-O_6$ octahedral vibration.

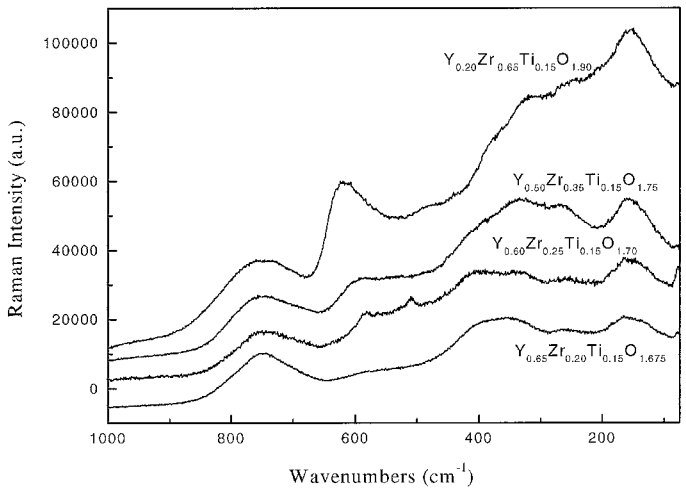

FIG. 4. VIS-Raman spectra of highly Ti-doped YSZ, e.g., $Y_{0.20}Ti_{0.15}Zr_{0.65}O_{1.90}$, $Y_{0.20}Ti_{0.18}Zr_{0.62}O_{1.90}$, $Y_{0.50}Ti_{0.15}Zr_{0.35}O_{1.75}$ (also shown in Fig. 2), $Y_{0.60}Ti_{0.15}Zr_{0.25}O_{1.70}$, $Y_{0.65}Ti_{0.15}Zr_{0.20}O_{1.675}$. The average oxygen coordination numbers are for the cations 7.6, 7.0, 6.8, and 6.7, respectively.

Spectrum of Y_2TiO_5

Pure orthorhombic Y_2TiO_5, was studied because it exhibits the unusual Ti–oxygen coordination number 5. In Fig. 5 we observe two high frequency modes at ≈ 860 and 730 cm^{-1}. In the five-fold coordination there is one quite short Ti–O bond of 1.78 Å and four longer bonds around 1.94 Å (13). Tentatively, we will assign the two peaks to strongly and less strongly bonded oxygen, respectively. The Ti–O separation in rutile is longer, 1.97 Å, resulting in an A_{1g} mode at 610 cm^{-1} (20). The Raman spectrum of Y_2TiO_5 cooled from 1550°C was very weak and had hardly any distinguishable peaks. This is in line with the X-ray data indicating that a supercooled disordered fluorite phase had been obtained.

Defect Chemistry Modeling of $Y_2Ti_{2-y}Zr_yO_7$ at Fixed pO_2

Below is described a first attempt to model an order–disorder transition by classical defect chemistry. The Kröger–Vink notation is used throughout (21). As seen in Table 3, the defect model is based on eight species. We assume that the model is valid for a pO_2 domain, where minor electronic defects, electron holes and electrons, and/or reduced cations, can be neglected. Also, in order to maintain simplicity, we assume that Ti always resides on the *B* site. We furthermore treat the two different oxygen sites in the pyrochlore structure, O(1) and O(2), as energetically equivalent. The O(3) on the 8*b* position will be modeled as interstitial oxygen, O_i''. The eight equations describing the interrelation between the eight concentrations are obtained

$$A\text{-site balance:}\quad [Y_A^x] + [Zr_A^\bullet] = 2 \qquad [1]$$

TABLE 3
Defect Model for a Pyrochlore with Simultaneous Disorder on the Cation and Oxygen Ion "Sublattices"

A site (16*c*)	*B* site (16*d*)	O sites (48*f*,8*a*)	O site (8*b*)
Y_A^x	Ti_B^x	O_O^x	O_i''
$Zr_A^\bullet$	Zr_B^x	$V_O^{\bullet\bullet}$	
	Y_B'		

Note. The site symmetries of the various sites are given as the Multiplicity and the Wykoff notation. The reference charges are + 3 for the *A* ion and + 4 for the *B* ion.

$$B\text{-site balance:}\quad [Zr_B^x] + [Ti_B^x] + [Y_B'] = 2 \qquad [2]$$

$$\text{O-site balance:}\quad [O_O^x] + [V_O^{\bullet\bullet}] = 7 \qquad [3]$$

$$\text{Mass balances:}\quad [Y_A^x] + [Y_B'] = 2 \qquad [4]$$

$$[Zr_B^x] + [Zr_A^\bullet] = y \qquad [5]$$

$$[Ti_B^x] = 2 - y \qquad [6]$$

Electroneutrality condition (EN):

$$[Zr_A^\bullet] + 2[V_O^{\bullet\bullet}] = 2[O_i''] + [Y_B']. \qquad [7]$$

The substitution of Ti by Zr is assumed to provoke disorder on the cation "sublattice" as well as a redistribution of oxygen between the "normal" sites in a pyrochlore structure and the vacant 8*b* positions. The defect model must therefore include a chemical equilibrium involving all

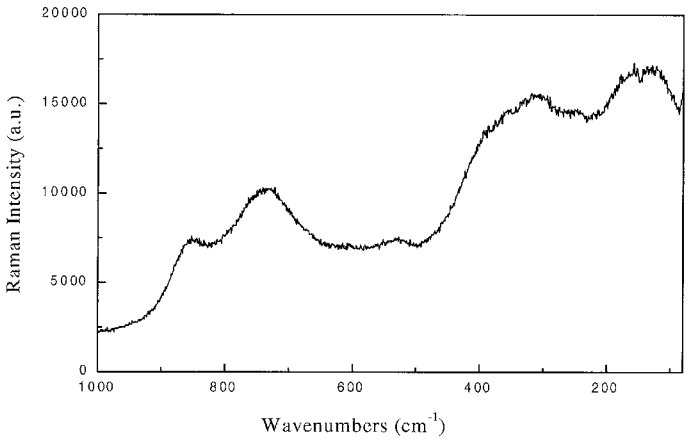

FIG. 5. VIS–Raman spectrum of the low-temperature orthorhombic form of Y_2TiO_5.

these species, i.e.,

$$Zr_B^x + Y_A^x + nO_O^x \Leftrightarrow Zr_A^{\bullet} + Y_B' + nV_O^{\bullet\bullet} + nO_i'' \qquad [8']$$

leading to the mass action law

$$K_{ex} = [Zr_A^{\bullet}] \cdot [Y_B'] \cdot [V_O^{\bullet\bullet}]^n \cdot [O_i'']^n / \{[Zr_B^x] \cdot [Y_A^x] \cdot [O_O^x]^n\}. \qquad [8'']$$

This mass law expression has been formulated for the general case, where n in principle can adopt both larger and smaller values than unity. In the following, we will only deal with the case $n = 7/8$. This choice leads to a statistical (complete) disorder on the cation and oxygen sites, respectively, for the hypothetical end member in the substitution series "$Y_2Zr_2O_7$" = $(Y/Zr)O_{1.75}$ (seven oxygens distributed on eight sites). It is in other words postulated that the (more complex) pyrochlore defect model can also describe the (simpler) case of a disordered fluorite. Using the linear mass-, site-, and electroneutrality equations [1–7], Eq. [8''] can be written as

$$K_{ex} = 64/49 \cdot [O_i'']^2 \, [O_i'']^{14/8} / \{(y - 8/7 \cdot [O_i'']) \cdot (2 - 8/7 \cdot [O_i'']) \cdot (7 - [O_i''])^{7/8}\}. \qquad [9]$$

The value of K_{ex}, leading to a statitical distribution, where $[O_i''] \equiv 7/8$, is then

$$K_{ex,\, y=2} = 1 \cdot 1 \cdot (7/8)^{7/8} \cdot (7/8)^{7/8} / \{1 \cdot 1 \cdot (49/8)^{7/8}\} = 0.1621. \qquad [10]$$

This value is close to the value of the anti-Frenkel constant,

$$K_{AF} = [O_i''] \, [V_O^{\bullet\bullet}] / [O_O^x] = 1/8, \qquad [11]$$

for a statistical distribution of the equilibrium $O_O^x \Leftrightarrow O_i'' + V_O^{\bullet\bullet}$ calculated in an earlier paper on the defect chemistry of the pyrochlore $Pr_2Zr_{1.6}Ce_{0.4}O_{7\pm\delta}$ (15). In the latter pyrochlore system there was only observed disorder on the oxygen "sublattice." For a known (or assumed) value of K_{ex}, one could choose to solve Eq. [9] for different values of the Zr-doping, y, by Newton–Raphson iteration. However, for the purpose of simulating the relationship

$$[O_i''] = f(y, K_{ex}), \qquad [12]$$

we can make the calculation much easier by inverting the problem to solve for the "inverse" relation

$$y = g([O_i''], K_{ex}). \qquad [13]$$

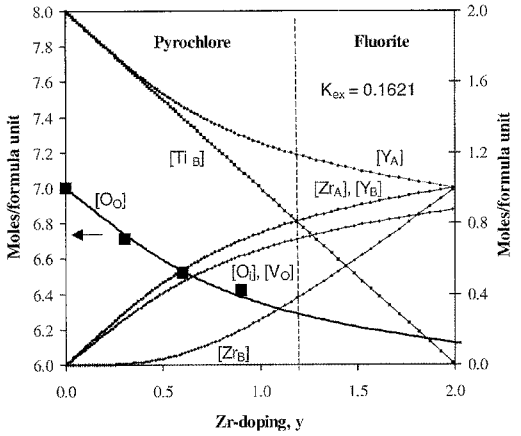

FIG. 6. Concentrations of defect species in pyrochlore $Y_2Ti_{2-y}Zr_yO_7$ at fixed pO_2. The equilibrium constant, $K_{ex} = 0.1621$, leads to complete disordering of oxygens and of Zr- and Y cations at the composition, $y = 2$. Kröger–Vink charges have been omitted in the figure. Filled symbols indicate the sum of oxygen on O(1) and O(2).

Rewriting Eq. [9] we find

$$y = 1/K_{ex} \cdot 64/49 \cdot [O_i'']^{30/8} / \{(2 - 8/7 \cdot [O_i'']) \cdot (7 - [O_i''])^{7/8}\} + 8/7 \cdot [O_i'']. \qquad [14]$$

Inserting values for $[O_i'']$ in the range $0 \le [O_i''] \le 7/8$ in Eq. [14] will deliver corresponding values of dopant levels, y. Figure 6 shows the distribution of ionic species as function of the doping level, using the statistical value for $K_{ex} = 0.1621$.

The approximate Zr-composition, $y \sim 1.2$, where the transition from pyrochlore to disordered fluorite structure occurs according to Kaiser *et al.* (9) has been marked by a vertical dashed line. Several features can be noticed from this calculation: (i) it is first observed that the concentration of the Zr-dopant on the A site, $[Zr_A^{\bullet}]$, rises much faster than the $[Zr_B^x]$ concentration; (ii) above $\approx y = 1.2$ most oxygen ions, which can be moved into the interstitial 8*b* position have done so; (iii) also passing $y = 1.2$, we come into a situation where there are more Y (originating from the A site) on the B site than Ti. All these trends are in line with the observed transition from an ordered pyrochlore to a disordered fluorite structure at a Zr-doping level around $y = 1.2$. Since the transition is a consequence of including the chemical equilibrium equation [8'] into the model, the transition must be gradual and not abrupt. This is qualitatively in agreement with the neutron study in (1), where

complete mixing of cations onsets at $y = 1.2$ and is complete at $y = 1.8$. Finally, the sum of oxygen on O(1) and O(2), according to the Rietveld refinement results in Table 1, is plotted for $y = 0$, 0.3, 0.6, and 0.9. We see that the model prediction mimics the oxygen occupancy found from X-ray quite well.

CONCLUSIONS

Raman spectroscopy shows a gradual change going from an ordered pyrochlore structure $Y_2Ti_2O_7$ to a disordered fluorite structure $Y_{0.5}(Ti_{0.15}Zr_{0.35})O_{1.75}$. A new Raman band, which cannot be predicted by conventional factor group analysis due to the disordered lattice, appears around 750 cm^{-1}, and was assigned to an increasing concentration of seven-coordinated Ti as the Zr doping level is increased. The band is absent in YSZ, which precludes that it could come from seven-coordinated Zr.

Defect chemistry modeling has succeeded qualitatively in rationalizing the smooth structural change.

ACKNOWLEDGMENTS

This study is part of the European TMR-project "Synthesis, Fabrication and Characterisation of Alternative Anodes for direct Methane Oxidation in SOFC's" (Contract FMRX-CT97-0130). Dr A. Kaiser is thanked for making the Ti-doped YSZ samples available to us. M.G. gratefully acknowledges the Danish Research Academy for funding. F.W.P. obtained financial support from the DK-SOFC programme. The Danish Natural Science Research Council and Haldor Topsøe A/S are thanked for funding the NIR-FT-Raman instrument within the Danish Materials Science Program.

REFERENCES

1. C. Heremans, B. J. Wuensch, J. K. Stalick, and E. Prince, *J. Solid State Chem.* **117,** 108–121 (1995).
2. R. D. Shannon, *Acta Cryst. A* **32,** 751–767 (1976).
3. S. P. S. Badwal, *Solid State Ionics* **52,** 23–32 (1992).
4. D. P. Fagg and J. T. S. Irvine, *Ionics* **4,** 61–71 (1998).
5. J. Cai, C. Raptis, Y. S. Raptis, and E Anastassakis, *Phys. Rev. B* **51,** 201–209 (1995).
6. H. G. J. Scott, *J. Mater. Sci.* **10,** 1527–1535 (1975).
7. A. V. Shevchenko, L. M. Lopato, I. M. Maister, and O. S. Gorbunov, Russ. *J. Inorg. Chem.* **25,** 1379–1381 (1980).
8. N. Mizutani, Y. Tajima, and M. J. Kato, *J. Am. Ceram. Soc.* **59,** 168 (1976).
9. A. Kaiser, A. J. Feighery, D. P. Fagg, and J. T. S. Irvine, *Ionics* **4,** 215–219 (1998).
10. P. Holtappels, F. W. Poulsen, and M. Mogensen, *Solid State Ionics* **135,** 675–679 (2000).
11. A. J. Feighery, J. T. S. Irvine, D. P. Fagg, and A. Kaiser, *Solid State Chem.* **143,** 273–276 (1999).
12. WinPLOTR, T. Roisnel, and J. Rodriguez-Carvajal, Laboratoire Léon Brillouin (CEA-CNRS), Beta version/Jan 99.
13. W. G. Mumme and A. D. Wadsley, *Acta Cryst. B* **24,** 1327–1333 (1968).
14. R. A. McCauley, *J. Appl. Phys.* **51,** 290–294 (1980).
15. F. W. Poulsen, M. Glerup, and P. Holtappels, *Solid State Ionics* **135,** 595–602 (2000).
16. N. Kjerulf-Jensen, R. W. Berg, and F. W. Poulsen, 2nd European Solid oxide fuel cell forum, proceedings, 6–18 May, 1996, Norway, Vol. 2, Edited by Bernt Thorstensen pp. 647–656.
17. M. T. Vandenborre, E. Husson, J. P. Chatry, and D. Michel, *J. Raman Spectrosc.* **14**(2), 63–71 (1983).
18. C. M. Phillippi and K. S. Mazdiyasni, *J. Am. Ceram. Soc.* **54,** 254–258 (1971).
19. L. S. M. Traqueia, T. Pagnier, and F. M. B. Marques, *Journal of the European Ceramic Society* **17,** 1019–1026 (1997).
20. M. Glerup, Ph.D. Thesis, University of Copenhagen (February, 2001).
21. F. A. Kröger, and H. J. Vink, *in* "Solid State Physics." (F. Seitz and D. Turnbull, Eds.), pp. 307–435, Academic Press In., New York, 1956.

A10.

Finn W. Poulsen and Martin Søgård,
Defect chemistry modelling of complex SOFC materials,
Proc. 5th European SOFC Forum, Lucerne 2002, Ed. Joop Huijsmans, 687-694. (2002)

Defect Chemistry Modelling of Complex SOFC Materials

Finn Willy Poulsen and Martin Søgård*
Materials Research Department
Risø National Laboratory
DK-4000 Roskilde, Denmark

Abstract

Electrodes, electrolytes, interconnects, protective coatings and auxiliary construction materials in SOFC's display a great variation in their defect chemistry. The defect models become increasingly more difficult to handle, when several dopants and host ions are present, which have a choice of several oxidation states. Oxygen stoichiometry data for $(La_{.6}Sr_{.4})_{0.99}Fe_{.8}Co_{.2}O_{3-\delta}$ at 1000 ^{O}C was modelled with five specified electronic states: a small polaron model describes better the data than a mixed model with 3 small polarons + holes and electrons. The sequential method of solving a set of defect equations is shown for $La_{2-x}Sr_xNiO_{4+\delta}$, with interstitial oxygens subject to the restriction that $\delta \leq 0.25$. A strategy for determining equilibrium constants based on least squares minimisation is outlined.

Introduction

Real SOFC-materials differ from model SOFC-compounds in several aspects. More elements are often present in a given phase, either as impurities or added on purpose. Further, cation exchange by inter-diffusion or chromium evaporation between adjacent electrolyte-/electrode/other layers, develop over the span of thousands of hours of operation. We will address complex defect systems in this paper. Simpler defect models apply to solids, where there are 1-3 types of host ions, 2-3 oxidation states, 1-3 types of dopant ions and only two species on the oxygen site: normal oxygen, O_O^x, and the oxygen vacancy, $V_O^{\bullet\bullet}$. The variation of the properties of the solid can be expressed as a function of the activity of one gas only, typically oxygen. The solution to these cases can often be obtained on a closed analytical form (3-5th degree polynomial). However, in many recent publications Brouwer approximations are still used precluding for instance that a pO_2 behaviour deviating from say a $pO_2^{1/4}$–law can be described. Also, by applying

* Student at Chemistry Department, South Danish University, Odense

Brouwer approximations, one looses the possibility to calculate theoretically the thermodynamic enhancement factor for chemical diffusion, $\partial\ln(a_O)/\partial\ln(c_O)$. The latter will reach infinity, if one assumes a constant oxygen vacancy concentration in a certain pO_2-range.
The analysis is taken one step further in what follows. By complex defect systems we understand solids exhibiting one or more of the features:

i) Anti-site cation disorder may take place, e.g. transition form ordered pyrochlore to disordered fluorite structure [1];
ii) More than three oxidation (electronic) states are present [this work);
iii) Schottky equilibrium in multinary systems, as in LSM [2,3,4]
iu) Mixed small and large polaron description, as in pyrochlores [5]
u) Frozen-in equilibria at lower temperature [6,7,8]
ui) Solid is in equilibrium with two or more gasses, as protons in perovskites [9]
uii) More than two different species competing for the same site, such as substitutional hydride ions in perovskites, [10]
uiii) Oxygen may distribute over both normal and interstitial sites, via a Frenkel reaction [present work]
ix) Associates are formed between defects and/or dopants, eventually leading to formation of higher clusters, as in doped urania [11].

The cases dealt with below incorporate phenomena of the type mentioned under ii), iu) and uiii).

2. Calculation of Brouwer diagrams for complex defect systems

The sequential way of solving sets of defect equations is demonstrated in paragraph 2.2, Table 1. For further details on this method see references [1,2,5,9,10]. It is our experience that models including e' and $h^\bullet$ do not require cumbersome substitutions, as will models based exclusively on localised charges (pure small polaron models). A third formalism for describing electronic equilibria, based on the Rigid Band Model, as employed by Lankhorst et al. [12] and Nowotny et al. [4] for perovskites, will be dealt with in a forthcoming study.

2.1 Generalised oxide defect model

Sasaki and Maier applied a general scheme to non-stoichiometric oxides in [7]. There are 16 different species in their model, distributed on 8 cation species, 6 species on oxygen sites, and delocalised electronic charges as e' and $h^\bullet$. Host lattice oxygen, host cations, and vacant interstitial oxygen site positions are not included as variables (they are assumed to be of high and practically constant concentration). The latter has the consequence that there is no site conservation equation for the oxygen-site, since a_{Oo} is assumed constant. In order to describe

the trapping of electrons on acceptors, donors, in oxygen vacancies and on the interstitial oxygens, 9 mass law expressions are in operation. A 10th equilibrium describes the Frenkel-type distribution of oxygen between normal and interstitial sites, in analogy to equation (8) of Table 1. The 11th mass-law expression describes the equilibration of the sample with the oxygen atmosphere, in analogy with equation (9) of Table 1. Upon substitution the authors arrive at an expression with $[h^{\bullet}] \equiv p$ as variable. The analytical expression, eq. (14) in ref. [7], was not further factorised, but appears to lead to an 8th degree polynomial in $[h^{\bullet}]$. The above described defect model is easily solved using the sequential method, - in which case one does not have to solve any equations of higher degree than quadratic (will be shown in a subsequent publication).
Defect models involving even more species appear now and then, e.g. the model of Lagerlöf and Grimes for Mg- and Ti-doped corundum contains 27 variable concentrations controlled by 24 mass law expressions!! [13].

2.2 $La_{2-x}Sr_xNiO_{4+\delta}$ of K_2NiF_4 structure

The title compound was discussed recently at the "3'rd Petite Workshop on the Defect Chemical Nature of Advanced Materials" in Geilo (N), 2002. Materials belonging to this class may find use as a cathode and oxygen separation membrane material. It was requested [14] that a defect model be developed including the limitation that the oxygen over-stoichiometry was limited to $\delta \leq 0.25$. In order to keep track of the number of available sites for interstitial oxygens one has to introduce one more species, - an uncharged species on the vacant interstitial oxygen site, V_i^x, as shown in equation (4) and (8) in Table 1.

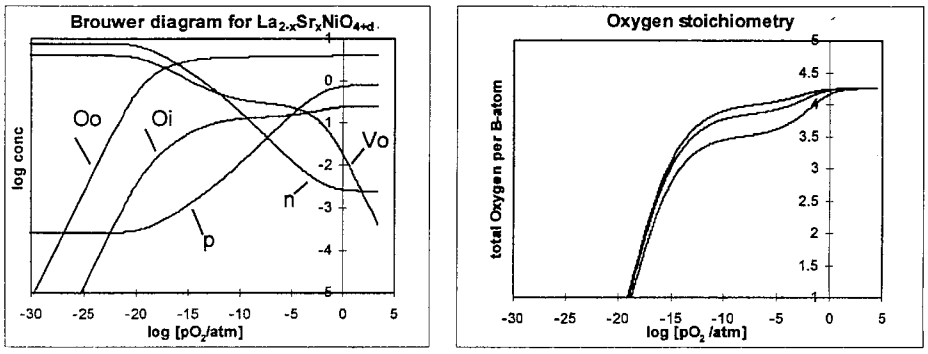

A B

Figure 1. Brouwer diagram (A) and total oxygen stoichiometry curves (B) for $La_{2-x}Sr_xNiO_{4+\delta}$ using the algorithm depicted in Table 1. (A): dopant level x = 0.3; K_i = 0.002; K_{oi} = 0.1; K_{ox} = 122 $atm^{-½}$; (B): Doping level in increasing order: x = 0, 0.3 and 1.0.

Having done this, the numerical solution is still straight forward, cf the R-H column of Table 1. Figure 1 A and B show a calculated Brouwer diagram and the corresponding total oxygen content curve. The equilibrium constants for reactions (7), (8) and (9) were chosen such that the simulated material becomes very oxygen deficient (unstable) at moderately low pO_2. The plateau's on the oxygen stoichiometry curves around 10^{-10} –10^{-5} atm are seen to obey the 4 - [Sr']/2 behaviour.

2.3 Defect models for $(La_{1-x}Sr_x)_sFe_{1-y}Co_yO_{3-\delta}$

Perovskite structure oxides with simultaneous doping on the A – and B-site are studied intensively. Typically they are made slightly A-site deficient, i.e. s<1, in order to reduce reactivity towards zirconia type electrolytes and/or H_2O or CO_2. Any defect model for this s <1 system must then include the species V_A'''. An A-site deficiency has three times the effect of acceptor-doping with a divalent element on the La-site. In the three models, investigated here, cation vacancies are not included on the B-site. This means that we do not consider a Schottky-equilibrium, neither can such models therefor cope with over-stoichiometry, $O/M_B > 3.0$.

We first applied a simple model by forcing all B-ions to have the same charge, i.e. +3 as in the reference compound $A(+3)B(+3)O_3$. Variations in the oxygen content of course is still rationalised by presence of varying amounts of e' and $h^\bullet$. This model is however too simple to explain the finer details of the oxygen stoichiometry versus pO_2 curve, cf. Figure 2. Two more complex defect models are described in Table 2. In chemical terms model 1 (23434) deals with five distinct oxidation states: Co+2, Co+3, Co+4, Fe+3, and Fe+4, whereas model 2 (np34) involves: Co+3, Fe+3, Fe+4, e', and $h^\bullet$. The defect equations are solved sequentially [15] in analogy with the $La_{2-x}Sr_xNiO_{4+\delta}$ case.

Plateau's in the oxygen stoichiometry curve (from TGA) are predicted at the following O/M_B ratios for model 1:

high pO_2:	$\Sigma O_{total}/\Sigma(\text{B-ions}) \leq 3$	(1)
intermediate pO_2:	$\Sigma O_{total}/\Sigma(\text{B-ions}) = 3 - s*x/2 - 3*(1-s)/2$	(2)
low pO_2:	$\Sigma O_{total}/\Sigma(\text{B-ions}) = 3 - s*x/2 - 3*(1-s)/2 - y/2$	(3)

The limiting stoichiometry at low pO_2 for model 1, with s = 0.99, x = 0.4 and y = 0.2 is then 3 – 0.313, as also confirmed by the modelling in Figure 2. For model 2, equation (3) is not in operation, since we put no restriction on further reduction of Fe3+ or Co2+ , which is the same as appreciating that $[e']_\infty = n$ can exceed y in $(La_{1-x}Sr_x)_sFe_{1-y}Co_yO_{3-\delta}$.

Table 1. Description of defect model for $La_{(2-x)}Sr_xNiO_{4+\delta}$		**Sequential solution of equations**
limitation: $\delta \leq 0.25$		Trivialities:
K_2NiF_4-type		$[Ni^x] = 1$
		$[La^x] = 2-x$
A-site: La^x , Sr'		$[Sr'] = x$
B-site: Ni^x		
O-site: O_o^x, $[V_o^{\bullet\bullet}]$		assume value for $[O_i'']$ in the interval
O-interstitial: O_i'' ,V_i^x		$0 \leq [O_i''] \leq 0.25$
delocalised: e' , h$^\bullet$		then $[V_i^x] = 0.25 - [O_i'']$
all together 9 unknown concentrations		
		from eq 2 inserted in eq (8)
equation	#	$K_{oi} = [O_i''] \bullet [V_o^{\bullet\bullet}]/([O_o^x] \bullet [V_i^x]) =$
		$[O_i''] \bullet [V_o^{\bullet\bullet}] / ((4-[V_o^{\bullet\bullet}]) \bullet [V_i^x])$
Site-conservation:		
$[La^x] + [Sr'] = 2$	1	solution for $[V_o^{\bullet\bullet}] =$
		$4K_{oi} \bullet [V_i^x] /([O_i''] \bullet (1+K_{oi}*[V_i^x]/[O_i'']))$
$[O_o^x] + [V_o^{\bullet\bullet}] = 4$	2	
		then $[O_o^x] = 4 - [V_o^{\bullet\bullet}]$
$[Ni^x] = 1$	3	
$[O_i''] + [V_i^x] = 0.25$	4	$[Sr']$, $[O_i'']$ and $[V_o^{\bullet\bullet}]$ are now known and can be inserted in eq (6) EN, also using eq. (7), and resulting in a quadratic in p
Mass:		
$[La^x] = 2-x$	5	
		$ap^2 + bp + c = 0$
Electroneutrality:		
$[Sr'] + 2[O_i''] + n = 2[V_o^{\bullet\bullet}] + p$	6	where $a = 1$, $b = 2[V_o^{\bullet\bullet}] - 2[O_i''] - [Sr']$,
Mass action laws:		and $c = -K_i$
nill = e' + h$^\bullet$		
		p is calculated using the positive root, and then $n = K_i/p$
$K_i = n \bullet p$	7	$O_{total} = [O_o^x] + [O_i'']$
$O_o^x + V_i^x = O_i'' + V_o^{\bullet\bullet}$		
$K_{oi} = [O_i''] \bullet [V_o^{\bullet\bullet}]/([O_o^x] \bullet [V_i^x])$	8	Finally the pO_2 in equilibrium with the above concentrations is calculated from equation (9)
$\frac{1}{2}O_2(g) + V_o^{\bullet\bullet} = [O_o^x] + 2h^\bullet$		
$K_{ox} = [O_o^x] \bullet p^2 / (pO_2(g)^{1/2} \bullet [V_o^{\bullet\bullet}])$	9	

Table 2. **Defect models for $(La_{1-x}Sr_x)_sFe_{1-y}Co_yO_{3-\delta}$**	1. Small polaron model (23434)	2. Mixed localised-delocalised model (np34)
Common species in the two models Reference state: $A(3+)B(3+)O_{3-\delta}$	A-site: La_A^x , Sr_A' , V_A''' O-site: O_O^x , $V_O^{\bullet\bullet}$ B-site: Co_B^x, Fe_B^x , $Fe_B^{\bullet}$	
Electronic charge at high/low pO_2	$Co_B^{\bullet}$, Co_B'	$h^{\bullet}$, e'
Limiting equation at low pO_2	$\Sigma O_{total}/\Sigma$(B-ions) = 3 - s*x/2 –3*(1-s)/2 –y/2	no limitation as to degree of sub-stoichiometry at low pO_2
Definition of equilibrium constants	K_{ox} = $[Co_B^x]^2[V_O^{\bullet\bullet}]pO_2^{½}/$ $([Co_B^{\bullet}]^2[O_O^x])$ K_{mix}= $[Co_B^{\bullet}][Fe_B^x]/([Co_B^x][Fe_B^{\bullet}])$ K_{Co}= $[Co_B^x]^2/([Co_B^{\bullet}][Co_B'])$	K_r = $[O_O^x]$ / $([V_O^{\bullet\bullet}]n^2pO_2^{½})$ K_{Fe} = $[Fe_B^{\bullet}]n/[Fe_B^x]$ K_i = np
Concentration chosen for solution of defect equations by the sequential method	$[Co_B^x]$	$[h^{\bullet}]$ = p or n

Depending on the magnitude of the equilibrium constants, the middle plateau may smear out and eventually become invisible. Figure 2 shows best fit of the two models to a data set with 26 determinations of the oxygen content at 1000 ^{O}C in the pO_2 range 0.21 – $10^{-9.5}$atm [15]. The low pO_2 branch of model 2 inevitably has a pronounced upward bend towards very large oxygen deficiencies. Our conclusion at present is that we find model 1 to be a better representation of what is going on than model 2.

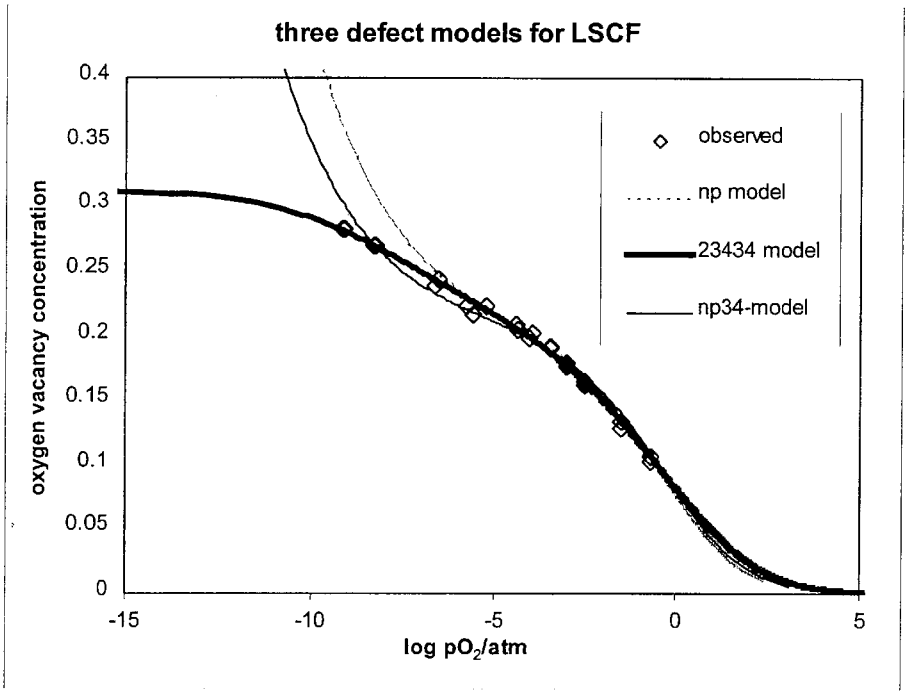

Figure 2. Defect modelling of $(La_{0.6}Sr_{0.4})_{0.99}Fe_{0.8}Co_{0.2}O_{3-\delta}$. Oxygen vacancy concentrations determined from TG. The adjusted equilibrium constants for the three cases were as follows: Model np: $K_{red} = 3 \cdot 10^{6}$ atm$^{-½}$, $K_i = 1 \cdot 10^{-3}$; Model 23434: $K_{ox} = 0.485$ atm^{½}, $K_{mix} = 0.604$, $K_{Co} = 180$; Model np34: $K_{red} = 9.98 \cdot 10^{6}$ atm$^{-½}$, $K_{Fe} = 9.98 \cdot 10^{-6}$, $K_i = 5 \cdot 10^{-4}$.

3. Determination of equilibrium constants by least squares minimisation

Traditionally, one would aim at searching for the minimum of either $\Sigma([O_O^x]_{obs} - [O_O^x]_{calc})^2$ or $\Sigma([V_O^{\bullet\bullet}]_{obs} - [V_O^{\bullet\bullet}]_{calc})^2$ by adjusting the two equilibrium constants in the model. The summation runs over the discrete pO_2 values, at which measurements were performed. One can however argue that determination of pO_2 is not always a trivial matter- and that this parameter is subject to larger errors than the stoichiometry, as determined from the weight. In other words, it is not clear which parameter should be selected as independent variable. The sequential method, for calculating defect

concentrations anyhow does not deliver calculated values at predetermined pO_2-values unless a subroutine/macro is taking care of that. Arguments of the above nature has led us to use $\Sigma(\log pO_{2,obs} - \log pO_{2,calc})^2$ at the experimentally determined vacancy concentrations for minimisation. The approximate magnitudes of the equilibrium constants are fairly easily found within half a decade by trial and error/the human eye, since the sequential way of calculating the defect concentrations delivers an almost instantaneous graphic output. Calculation of 1000 points on the stoichiometry curve takes a fraction of a second. The final step in the refinement is done by mapping the LSQ-sum in the 2D or 3D landscape of 2 or 3 equilibrium constants, respectively. A simple search then locates the parameters giving the lowest LSQ-sum.

Acknowledgements

The authors wish to thank the DK-SOFC project and NEFP (FWP), and the Oticon Foundation (MS) for financial support. Eivind Skou, South Danish University, Mogens Mogensen and Peter Vang Hendriksen, both at Risø, are thanked for valuable comments.

References

1. M. Glerup, O.F. Nielsen and F.W. Poulsen, J. Solid State Chem. **160**.(2001), 25- 32.
2. F. W. Poulsen, Solid State Ionics **129**(2000), 145-162.
3. J. Mizusaki, N. Mori, H. Takai, Y. Yonemura, H. Minamiue, H. Tagawa, M. Dokiya, H. Inaba, K. Naraya, T. Sasamoto and T. Hashimoto, Solid State Ionics **129** (2000) 163-17.
4. T. Bak, J.Nowotny, M. Rekas, and C.C. Sorrell, J. Phys. Chem. Solids **62** (2001) 731-735, and 736-742.
5. F.W. Poulsen, M. Glerup, P. Holtappels, Solid State Ionics **135** (2000), 595- 602.
6. J. Maier, Solid State Ionics **86** (1996) 55-67.
7. K. Sasaki and J. Maier, J. Appl. Phys., **86** (1999) 5422-5433
8. K. Sasaki and J. Maier, J. Appl. Phys., **86** (1999) 5434-5443.
9. F.W. Poulsen, J. Solid State Chem. **143** (1999), 115-121
10. F.W. Poulsen, Solid State Ionics **145** (2001), 387-3971
11. H.S. Kim, Y.K.Yoon, Y.W. Lee, J. Nucl. Mat. **226** (1995) 206-215
12. M.H.R. Lankhorst , H.M.J. Bouwmeester and H. Verweij, Solid State Ionics **96** (1997) 21-27.
13. K.D.P. Lagerlöf and R.W. Grimes, Acta Materialia **46** (1998) 5689-5700
14. T. Norby (2002), private communication
15. M. Søgård et al. (2002) to be published.